


For Reference

NOT TO BE TAKEN FROM THIS ROOM

Ex libris
UNIVERSITATIS
ALBERTAENSIS





Digitized by the Internet Archive
in 2024 with funding from
University of Alberta Library

<https://archive.org/details/Withers1977>

THE UNIVERSITY OF ALBERTA

RELEASE FORM

NAME OF AUTHOR ROBERT JOHN WITHERS

TITLE OF THESIS SEISMICITY AND STRESS DETERMINATION

..... AT MAN-MADE LAKES

.....

DEGREE FOR WHICH THESIS WAS PRESENTED PH.D.

YEAR THIS DEGREE GRANTED 1977

Permission is hereby granted to THE UNIVERSITY OF
ALBERTA LIBRARY to reproduce single copies of this
thesis and to lend or sell such copies for private,
scholarly or scientific research purposes only.

The author reserves other publication rights, and
neither the thesis nor extensive extracts from it may
be printed or otherwise reproduced without the author's
written permission.

THE UNIVERSITY OF ALBERTA

SEISMICITY AND STRESS DETERMINATION AT MAN-MADE LAKES

by



R. J. WITHERS

A THESIS

SUBMITTED TO THE FACULTY OF GRADUATE STUDIES AND RESEARCH
IN PARTIAL FULFILMENT OF THE REQUIREMENTS FOR THE DEGREE
OF DOCTOR OF PHILOSOPHY

IN

GEOPHYSICS

DEPARTMENT OF PHYSICS

EDMONTON, ALBERTA

SPRING, 1977

THE UNIVERSITY OF ALBERTA
FACULTY OF GRADUATE STUDIES AND RESEARCH

The undersigned certify that they have read, and
recommend to the Faculty of Graduate Studies and Research,
for acceptance, a thesis entitled
SEISMICITY AND STRESS DETERMINATION AT MAN-MADE LAKES
.....
.....
submitted by ROBERT JOHN WITHERS
in partial fulfilment of the requirements for the degree of
DOCTOR OF PHILOSOPHY in GEOPHYSICS

This work is dedicated to the memory of
Matthew Robert Withers.

ABSTRACT

Two related models are proposed to explain aspects of the connection between seismicity, water depth, loading history, and hydrologic conditions at an artificial lake. Both models involve fluid loads on layered half spaces. The response in each case is most rapidly determined with Fourier transform techniques. The models are laterally homogeneous, but in spite of this simplification predict a gratifying number of observed seismic features. A model of a load on an elastic half-space predicts many features, but does not provide time dependent predictions. A similar calculation for a permeable layered structure predicts that initial seismicity will occur directly beneath a reservoir during the first filling. However, the region most subject to seismicity changes in position and time as the lake depth varies and may be offset from the lake. The response of a permeable structure can be expressed as a product of two terms; one evaluated at the particular time of interest and the other a convolution integral containing the rate of change of depth.

Examples of the calculations for various loading histories are given in two and three dimensions. For a two dimensional lake model and an assumed filling history, it is shown that seismic risk is a function of time and position with respect to the lake. Maintaining a constant water depth

allows the region to stabilize slightly by permitting lobes of high pore pressure to diffuse away. It is also shown that a partial emptying and refilling sometime after the initial filling can cause extremely large stresses in the rock. In some instances it is felt that draining and refilling may cause an increase in the regional seismicity.

ACKNOWLEDGEMENTS

No work is ever done in isolation and there are many people I would like to thank for their assistance and encouragement during the time work was being done on this thesis.

I would like to thank my supervisor Dr. E. Nyland, firstly for suggesting this line of research and also for his support, suggestions and helpful discussions.

My colleagues and friends Mr. J. Bannister, Mr. T. Hughes, Dr. D. Oldenburg and Dr. J. H. Debeer have helped me both in my work and in making this period of my life enjoyable.

Dr. D. I. Gough and Wendy Gough have always been liberal with suggestions and have saved me a lot of time by opening their large files of data and information concerning lake seismicity. The Kariba bathymetry data they provided, had only been obtained after many hours of their hard work. In this respect I would like to thank C. Gold for modifying his thesis work for me so bathymetry reduction could be done quickly and efficiently on the computer.

Thesis production is an expensive time consuming task and I would like to thank Mrs. Ella Ritz and her staff at the Data Entry Service for their typing of the text, and Mrs. Lee Cech for her careful typing of the equations.

This work was done with the financial support of the

National Research Council of Canada. I would also like to thank the University of Alberta for their support in the form of a teaching assistantship. Without the full cooperation and assistance of the University of Alberta Computer Department, and their excellent facilities this work could never have been as extensively checked numerically.

I would like to thank my wife Barbara for her help and cooperation during this work and in the years leading up to it. Her assistance in the preparation of this thesis is greatly appreciated and I thank her for the many hours of proof reading and figure cutting she has done. Being the wife of a student is not easy and I apologise for the time that we have not had together due to the requirements of work. The encouragement given to me by my family is also appreciated.

TABLE OF CONTENTS

CHAPTER	PAGE
1. Background to the Study.	1
1.1 Introduction	1
1.2 The Seismicity	5
1.3 The Concept of Effective Stress	45
1.4 The Denver Earthquakes	51
1.5 The Rangely Experiments	58
2. The Three Dimensional Analysis of a Load on an Elastic Half Space.	64
2.1 Point Force Solutions	64
2.2 A Transform Solution of Boussinesq's Problem	71
2.3 An Example of Transform Techniques	89
2.4 Generalisation to Regular Loads	90
2.5 Generalisation to a Layered Half Space	98
3. Loading of a Reservoir on a Porous Elastic Fluid- Filled Halfspace.	111
3.1 Biot's Consolidation Equations	111
3.2 Solution of the Boundary Value Problem	117
3.3 Excess Fluid Pressure	121
3.4 Displacement	123
3.5 Effective Stress	124

3.6	Vertical Flow Velocity	127
3.7	Examples of Heaviside Loading in Two Dimensions	127
3.8	Examples of Time Dependent Loading	142
3.9	Layered Porous Elastic Half Space	156
4.	Extensions and Improvements of the Work	173
4.1	Pressure Dependent Effective Stress Laws	173
4.2	Variation of Permeability	175
4.3	Finite Element Analysis	178
4.3.1	Variational Equation	179
4.3.2	Finite Element Description	181
4.3.3	Possible Elements in Three Dimensions	185
4.4	An Introduction to Statistical Prediction	194
5.	Data Analysis and Interpretation	198
5.1	Conversion of Bathymetry to Regular Grid	198
5.1.1	Manual Integration	198
5.1.2	Digitising	198
5.1.3	Weighted Distance Techniques	200
5.1.4	Irregular Triangular Interpolation	201
5.2	Discussion of Results	207
5.3	Concluding Remarks	225
	Bibliography	233

LIST OF TABLES

Table	Description	Page
1.1a	Table of Large Dams	6
1.1b	Table of High dams	7
1.2	'b' values for aftershock sequences at lakes	31
1.3	Six Categories of Lake Seismicity and the lakes which fall into these groups.	41
5.1	Triangulation costs and statistics	206

LIST OF FIGURES

Figure	Page
1.1 Map of Lakes showing seismicity.	3
1.2 Epicentres for Southern Africa.	9
1.3 Epicentres at Kremasta, Greece.	11
1.4 Epicentres at Koyna, India.	14
1.5 Epicentres at Kariba, Rhodesia.	16
1.6 Epicentres at Nurek, USSR.	18
1.7 Epicentres at Oroville, California.	21
1.8 Epicentres at Hoover, U.S.A.	25
1.9 Positions of aftershocks at Koyna.	27
1.10 Waterlevel and seismic frequency at Kariba, Koyna, Kremasta and Vajont.	35
1.11 The Mohr circle and Coulomb failure criteria for different fault environments.	47
1.12 The number of observed earthquakes and well bottom pressure at Denver.	54
1.13 Number of earthquakes per month, and the water pressure at Rangely.	62
2.1 Observed and calculated roadbed deflection near Kariba.	67
2.2 Vertical displacement at several depths below a 1 bar load applied over a 284 km square.	81

2.3	Stresses at 13 km below a unit pressure applied to a 284 km square area.	83
2.4	Vertical deflection at several depths below a 1 bar load applied over a 100 km square.	85
2.5	Stresses at 10 km below a unit pressure applied to a 100 km square area.	87
2.6	Maximum shear stress, vertical deflection and shear planes 13 km below Lake Kariba.	91
2.7	Vertical deflections at several depths below Lake Kariba.	93
2.8	Maximum shear stress at several depths below Lake Kariba.	95
2.9	Configuration used for the layered half space model.	102
2.10	Vertical deflections below Lake Kariba on a layered half space compared to the elastic solution.	106
2.11	Vertical deflections below Lake Kariba on a layered halfspace.	108
3.1	Excess pressure and vertical deflection as a function of depth and time one year after rapid filling. Coupling is equal to zero.	130
3.2	Excess pressure and vertical deflection for full coupling as a function of depth.	134
3.3	Displacement, pressure and stress for change	

in the hydrologic parameter α .	137
3.4 Displacement, pressure and stress for change in the hydrologic parameter Q .	140
3.5 Excess pore pressure and vertical deflection for 0.25 coupling as functions of depth and time.	143
3.6 Hypothetic filling curve used in the time dependent solutions.	146
3.7 Pressure and consolidation at 3.75, 4.75 and 6.5 years for a two dimensional section.	149
3.8 Pressure, displacement and effective stresses in the horizontal and vertical directions at 3, 6 and 12 km depths.	152
3.9 Pressure, displacement and effective stress at several times below a two dimensional load.	154
3.10 Pressure, displacement and effective stress for a different loading rate.	157
3.11 Three dimensional section below Lake Kariba	160
3.12 Three dimensional section below Lake Nurek.	162
3.13 Three dimensional section below Lake Oroville.	165
4.1 Three dimensional tetrahedral finite element.	186
4.2 Serendipity and Lagrangian brick elements	188
4.3 Quartic shape functions	192

5.1	Triangular interpolation network and triangular co-ordinates.	202
5.2	The centre and radius of the Mohr circle at different times during filling.	210
5.3	Locus and instability of the Mohr circles.	213
5.4	Positions for which the locus of the Mohr circle are plotted.	215
5.5	Loci of Mohr circles at various positions.	218
5.6	Instability at different times.	223
5.7	Instability in thrust regions	226
5.8	Instability with different fluid constants	228

Chapter 1

Background to the Study

1.1 Introduction

The filling of large artificial lakes has often been associated with an an apparent increase in the seismicity of the region. This work will investigate the seismicity from the theoretical aspect of examining stresses produced in the rock by the application of a surface load - the lake. A mathematical approach has many difficulties, since the application of simplified theoretical models to the complicated Earth rarely leads to results which are conclusive in every case.

The literature on seismicity around lakes is extensive with the current activity directed toward the aim of being able to predict whether the filling of a certain lake will increase the region's seismicity. This is called the "predictive problem".

Perhaps the most important consequence of lake seismicity can be expressed in terms of the life and property damage which may occur near epicentres of magnitudes greater than 6 on the Richter scale, several of which have been detected close to large reservoirs. The descriptions of these earthquakes can be found in several

excellent review articles (See Simpson (1976), Gupta and Rastogi (1976)) and need no detailed documentation here. At Koyna (see Figure 1.1) 200 lives were lost and a large amount of property damage was caused by a magnitude 6.5 earthquake within 10 km of the lake. It is generally conceded that dam engineers can design structures to withstand extremely large earthquakes safely so the chances of a dam failure are minimal. They would however like to keep the cost down by knowing whether an earthquake is likely and, if so, its probable size. An assessment of the risk to the surrounding structures and population is also part of the predictive problem but is not discussed here.

Simpson (1976) has presented an excellent summary of the seismicity around reservoirs. What is obvious from his list of 'large' reservoirs is that not all of them are associated with earthquakes. The definition of a large reservoir given by the Commission On Large Dams is one that is deeper than 100 metres and contains a volume of approximately 1.2 billion cubic metres.

This thesis will concentrate on some of these 'large' dams since the weight and pressure head at the at the bottom of these is the greatest. Large dams also seem to be those most subject to noticeable seismic changes.

In the World Registry of Dams (I.C.O.L.D. 1973) there appear 275 dams with heights larger than 100 metres with a

Figure 1.1: A world map showing the positions of most of the lakes with significant seismic changes after filling. Rangely and Denver are sites where tests on the dependence of the seismicity on fluid pressure were conducted.



further 149 planned or being constructed. Of these 424, 93 are over 150 m and 38 have volumes in excess of 10 billion cubic metres. It is apparent that the size of dams, as well as their number, is rapidly increasing. The tallest is Nurek at 317 m high. Bratsk contains a volume of 169 billion cubic metres of water.

Table 1.1a (modified from Simpson (1976)) lists the largest dams and Table 1.1b the deepest. There appears to be no consistency between either the water depth or volume and the seismicity. This indicates that neither depth nor volume are in themselves sufficient to change the seismic pattern. Rothe (1973) has indicated that depth appears more important than the total volume and that the activity is greatest in reservoirs deeper than 100 metres. This is not evident from the tables 1.1a, 1.1b and the 100 m depth criteria now appears meaningless.

1.2 The Seismicity

In many cases lakes are situated in areas of relatively high tectonic activity. Even without the presence of the lakes, a large number of events can be expected. The problem of trying to separate parameters which indicate a change in the seismic level in the region before and after the filling is poorly treated in the literature. One problem to be considered is how far a seismic region extends. Gough and Gough (1970b) examined the seismic history for the area

TABLE 1a: HIGHEST DAMS

DAM NAME	LOCATION	DATE	SEIS- MIC	TYPE	DAM HGT m	RES. VOL. m ³ x10 ⁶
NUREK	USSR	72	*	ER	317	10400
GRANDE DIXENCE	SWITZERLAND	62		PG	285	400
INGURI	USSR	C		VA	272	1100
ROSSELLA	ITALY	65		TE	265	17
VAJONT	ITALY	61	*	HA	261	353
MICA	CANADA	74		TE	242	24670
SAYANSK	USSR	C		VA	242	31300
MAUVOISIN	SWITZERLAND	57		VA	237	180
OROVILLE	USA, CALIF	68	*	TE	236	4298
CHIRKEY	USSR	C		VA	233	2780
ESMERALDA (CHIVOR)	COLOMBIA	C75		ER	230	815
BORUCA	COSTA-RICA	P80		ER	227	6700
BHAKRA	INDIA	63		PG	226	9868
HOOVER (L. MEAD)	USA ARIZ.NEV	36		VA	221	36703
MRATINJE	YUGOSLAVIA	C		VA	220	880
CONTRA	SWITZERLAND	65	*	VA	220	86
PATIA	COLOMBIA	P		ER	220	11000
DWORSHAK DAM	USA, IDAHO	73		PG	219	4278
GLEN CANYON (POWELL)	USA, ARIZ.	64		VA	216	33305
TOKTOGUL	USSR	C		VA	215	19500
DANIEL JOHNSON	CANADA	68		MV	214	141851
AUBURN	USA, CALIF.	C		TE	210	2837
LUZZONE	SWITZERLAND	63		VA	208	87
KEBAN	TURKEY	74		ER	207	31000
HIGH MOUNTAIN SHEER	USA, IDAHO	P		VA	204	4
MOHAMAC REZA CHAH	IRAN	63		VA	203	3340
URANCANCHA	PERU	P		VA	203	701
ALMENDRA	SPAIN	70		VA	202	2649
ROSS HIGH	USA, WASH.	P		VA	201	4263
GRAND-MAISON	FRANCE	P		VA	200	205
RAZA CHAH KABIR	IRAN	73		VA	200	2900
KONDJILA	YUGOSLAVIA	P		VA	200	416

NOTATION - TYPE TE - EARTHFILL DATE - YEAR COMPLETED
 ER - ROCKFILL C - UNDER CONSTRUCTION
 PG - GRAVITY P - PROPOSED
 CB - BUTTRESS
 VA - ARCH
 MV - MULTI-ARCH

TABLE 1b: LARGEST RESERVOIRS

DAM NAME	LOCATION	DATE	SEIS- MIC	TYPE	DAM HGT m	RES. VOL. m ³ x10 ⁶
BRATSK	USSR	64		PG	125	169270
SAAD-EL-AALI (ASWAN)	EGYPT	70		ER	111	164000
KARIBA	RHODESIA	59	*	MV	128	160368
AKOSOMBO MAIN DAM	GHANA	65		ER	141	148000
DANIEL JOHNSON	CANADA	68		MV	214	141851
KRASNOYARSK	USSR	67		PG	124	73300
W.A.C. BENNETT	CANADA	67		TE	183	70309
ZEYA	USSR	C		PG	115	68400
SANMEN HSIA	CHINA	62		PG	107	65005
CABORA BASSA	MOZAMBIQUE	74		VA	171	63000
UST - ILIM	USSR	C		PG	105	59300
TANKIANGKOW	CHINA	62		PG	120	51000
HOOVER (L. MEAD)	USA ARIZ. NEV	36	*	VA	221	36703
LOUILOU	ZIARE	P		PG	137	35000
GLEN CANYON (POWELL)	USA, ARIZ.	64		VA	216	33305
SAYANSK	USSR	C		VA	242	31300
KEBAN	TURKEY	74		ER	207	31000
MICA	CANADA	74		TE	242	24670
KENNEY	CANADA	52		ER	104	22203
FURNAS	BRAZIL	62		ER	127	20860
TOKTOGAL	USSR	C		VA	215	19500
GURI	VENEZUELA	68		PG	106	17700
ITUMBIARA	BRAZIL	P79		ER/PG	106	17027
TAMAHARA	JAPAN	P		ER	116	16300
KOLYMA	USSR	C		ER	130	14600
TARBELA	PAKISTAN	75	*	TE/ER	143	13687
DICKEY	USA, MAINE	P		TE	105	13048
SAC SIMAO	BRAZIL	P		TE/PG	120	12500
MOSUL	IRAQ	P		ER	131	12500
BHUMIPHOL	THAILAND	64		VA/PG	154	12200
GRAND COULEE	USA, WASH	42		PG	168	11975
GORDON	AUSTRALIA	74		VA	140	11728
HSINFENGKIANG	CHINA	59	*	PG	105	11500
NAGARJUNA SAGAR	INDIA	C		TE	124	11315
PATIA	COLOMBIA	P		ER	220	11000
SOUAPITI	GUINEA	P		TE	121	11000
MANICOUGAN 3	CANADA	C75	*	TE	108	10423
NUREK	USSR	72	*	ER	317	10400

NOTATION -

TYPE	TE - EARTHFILL	DATE - YEAR COMPLETED
	ER - ROCKFILL	C - UNDER CONSTRUCTION
	PG - GRAVITY	P - PROPOSED
	CB - BUTTRESS	
	VA - ARCH	
	MV - MULTI-ARCH	

around Kariba but no events were found. However, when the seismicity for the whole of southern Africa is plotted, as shown in figure 1.2, two seismic areas become apparent on a feature passing through Kariba. One of these is near the reservoir with all the events occurring after the filling, and the other in the Okavango. In both areas there exist large quantities of surface water on a tectonic feature.

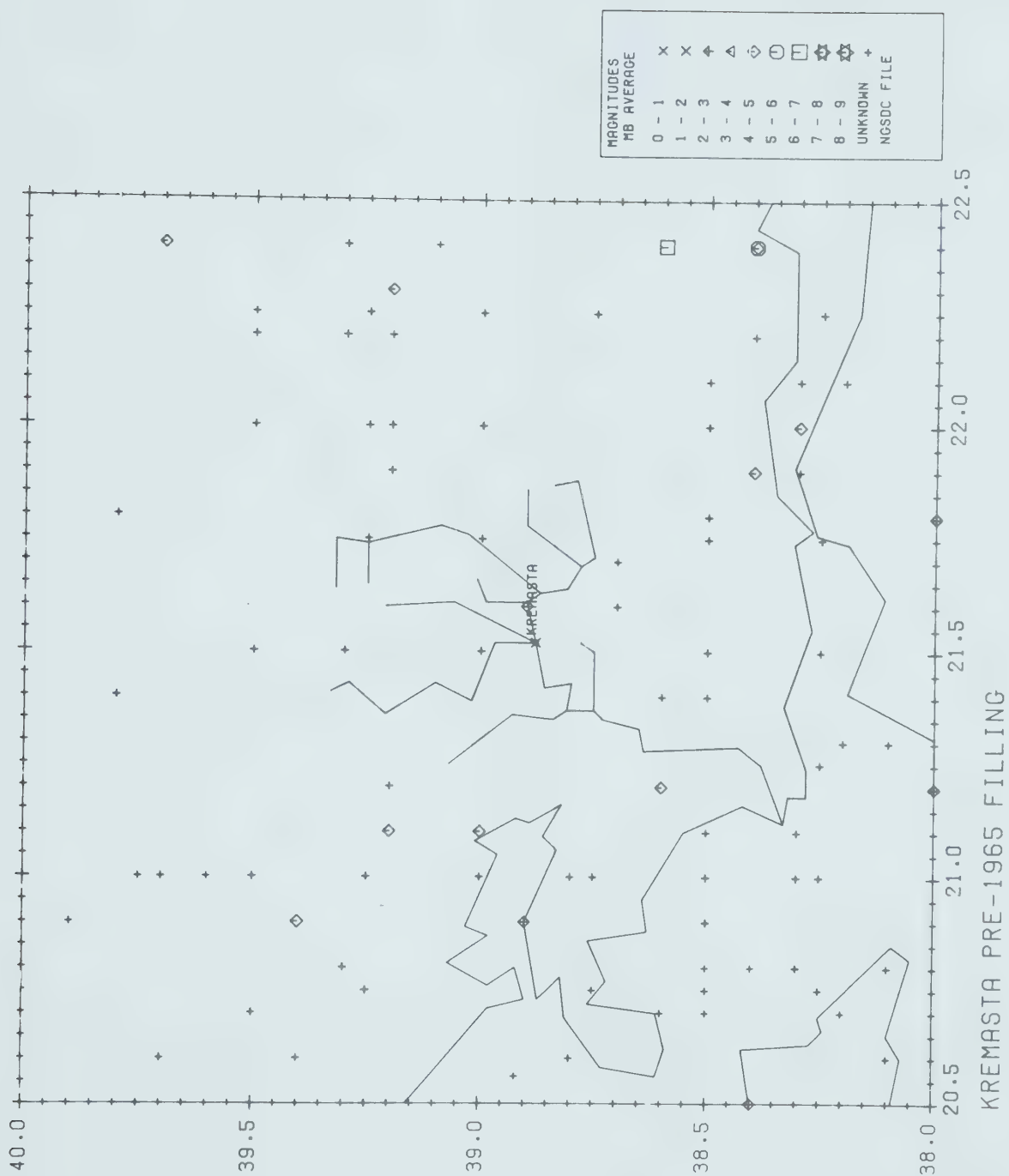
At the other extreme, Lake Kremasta was reported by Comninakis et. al. (1968) to show good correlation between the filling of the lake and the local seismicity. However, it is difficult to distinguish the epicentral distribution pattern before and after the filling using the same N.O.A.A. data bank. This is illustrated in figure 1.3.

If we examine the seismicity within an area subject to the same tectonic forces (earth forces causing large scale deformations) several observations can be made at lake sites. In many cases the epicentres are usually very close to the lake - within 25 km and often much closer. Local arrays often place many events directly under the lake. Several examples of the epicentral distribution of the larger (magnitude greater than 3) events at Koyna, Kariba, Nurek, Oroville and Hoover are shown in figures 1.4 to 1.8. The positions and magnitudes of these events were determined from teleseismic data and may differ from those determined by local networks. The difference in position was about 0.2 degrees at Koyna.

Figure 1.2: Epicentres plotted for Southern Africa from the N.O.A.A. Summary tape. Notice the linear pattern of events through Kariba and the Okavango Swamp to the south west. These are two areas where there is a large amount of ground water. The intense distribution of events near Pretoria is probably related to the Johannesburg mining activity.



Figure 1.3: Epicentres from the N.O.A.A. Summary tape for the Kremasta region in Greece with the coast line and drainage pattern. (a) shows the distribution up to and including 1965, and (b) shows the same data after filling in 1965. By comparing patterns, it is not obvious that a major change in the seismicity has occurred since filling. It should be emphasised that before 1965 fewer events were recorded and their magnitudes were generally unknown.



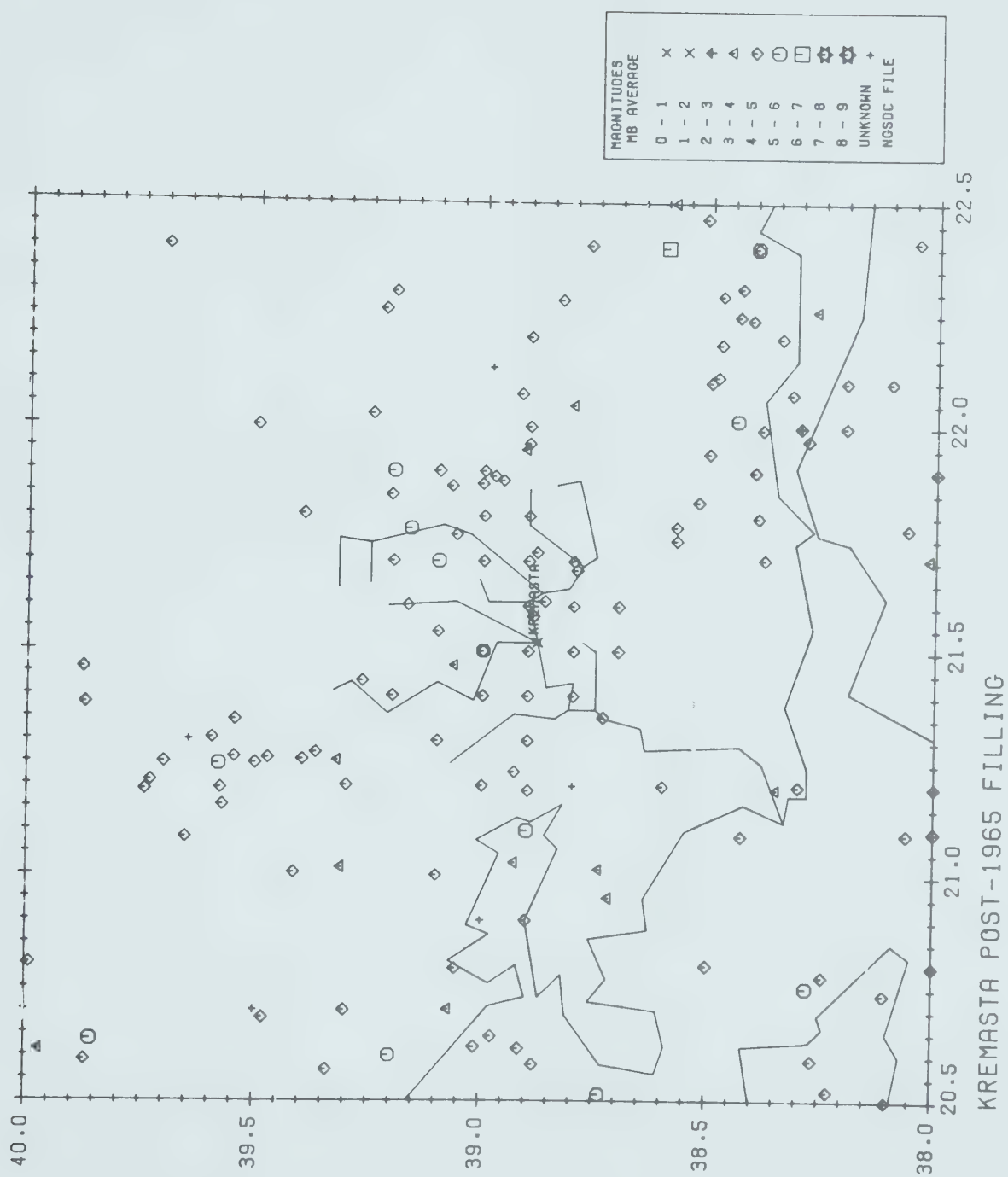


Figure 1.4: Epicentres determined near Koyna in India. All the events shown occurred after the completion of the reservoir. Uncertainties exist in the exact position of any event by up to one-tenth of a degree.



Figure 1.5: Epicentres from the N.O.A.A. Summary tape for the Kariba region in Rhodesia. All the events plotted in this region occurred after the completion of the reservoir. Notice the tight clustering of events at the deep end of the lake. Many more smaller events were observed by local stations but the smallest events plotted have magnitudes between 3 and 4 Mb.

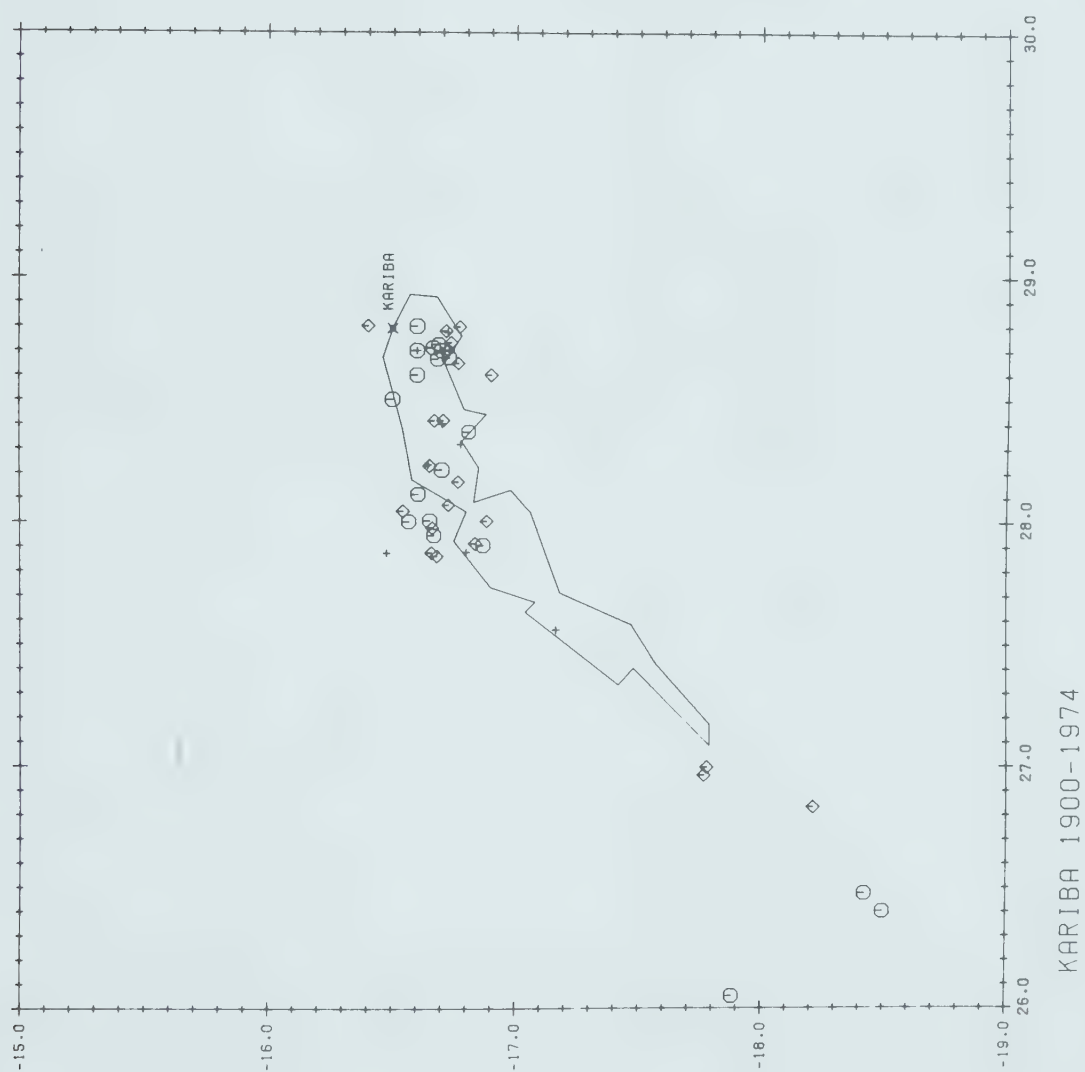
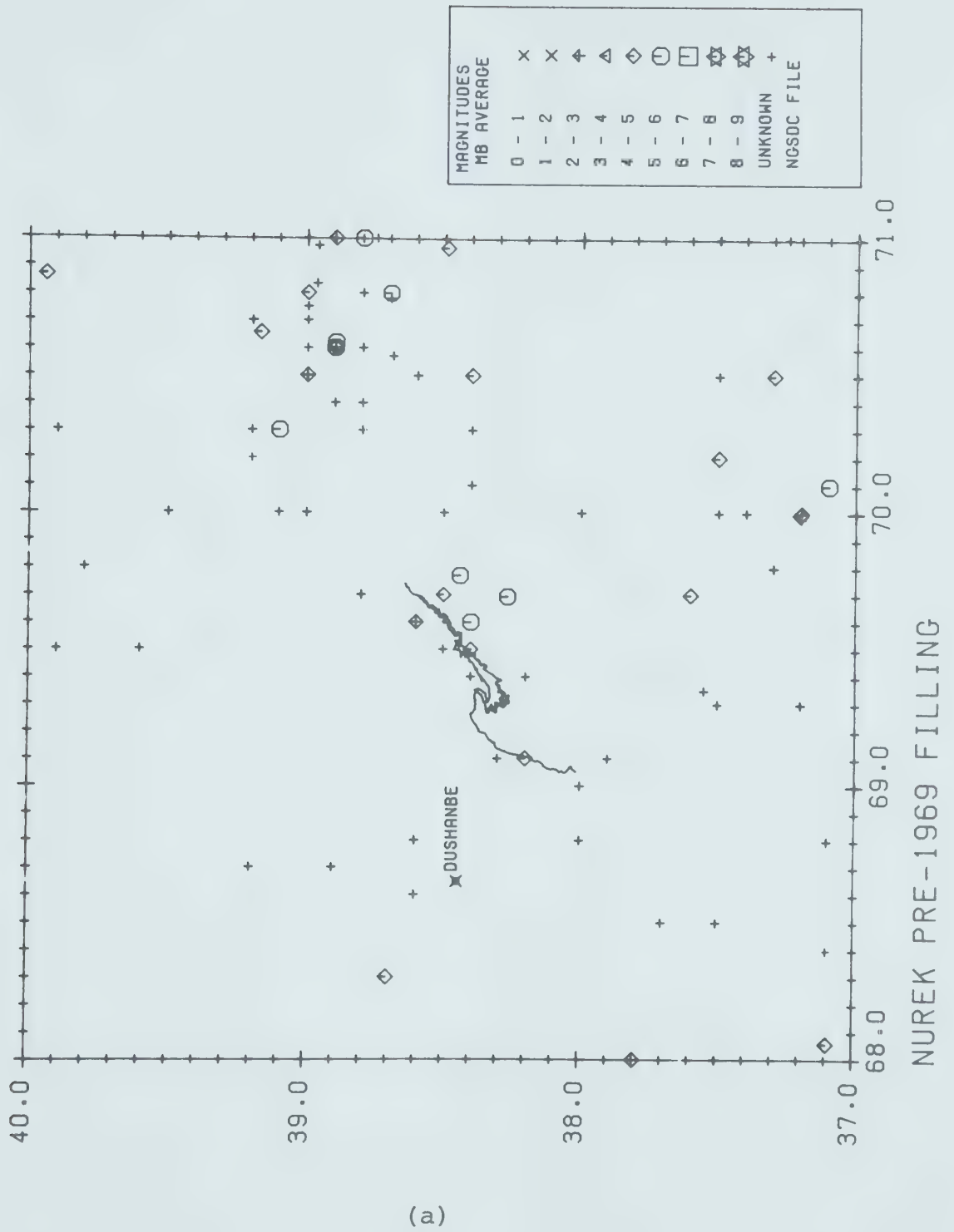


Figure 1.6: Positions and magnitudes of events recorded before (a), and after (b), impoundment at Nurek in the USSR. Several events are seen close to the lake both before and after filling and it is concluded that there is no significant change in tectonic activity. Local arrays have observed migration of microseismic events towards the lake.



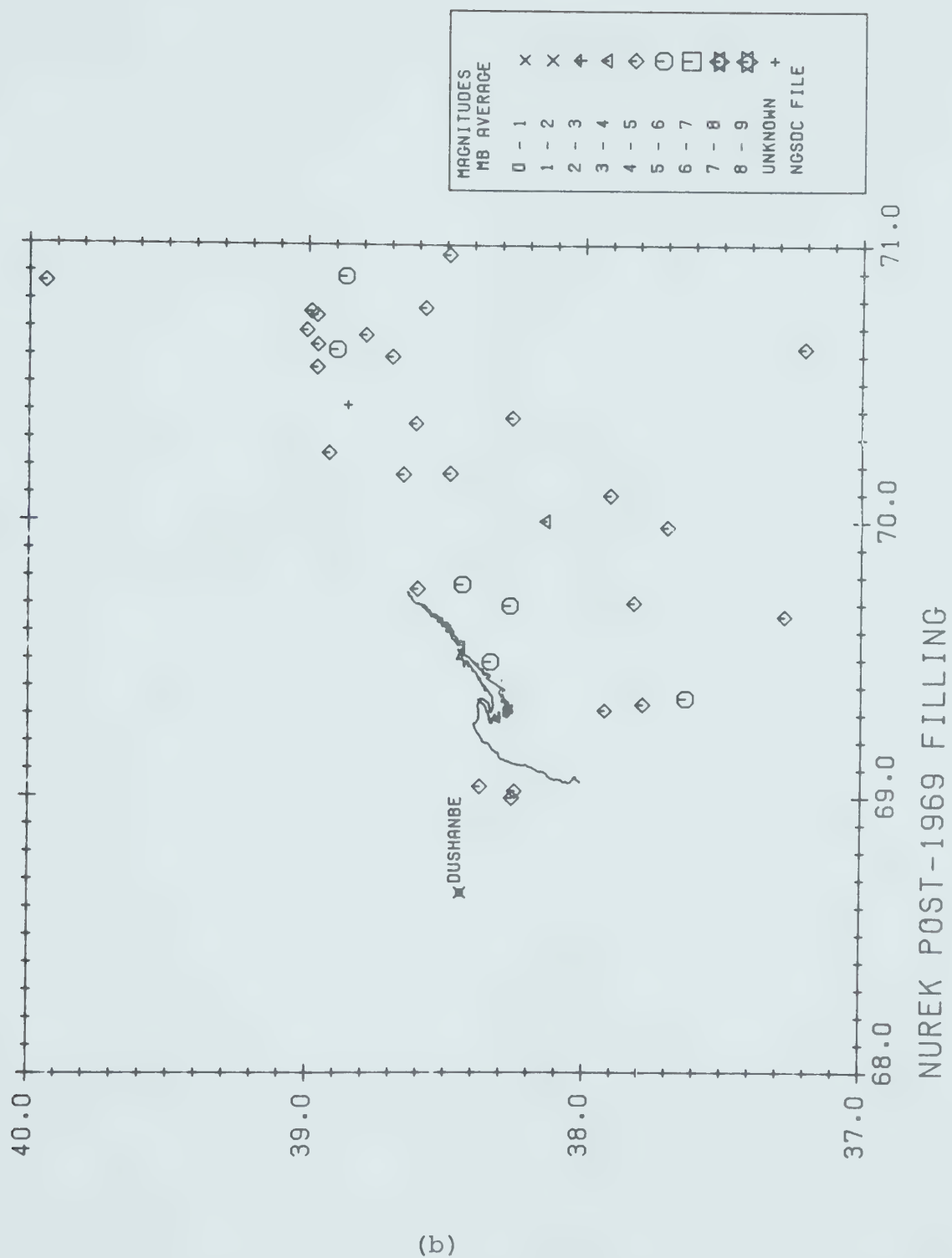
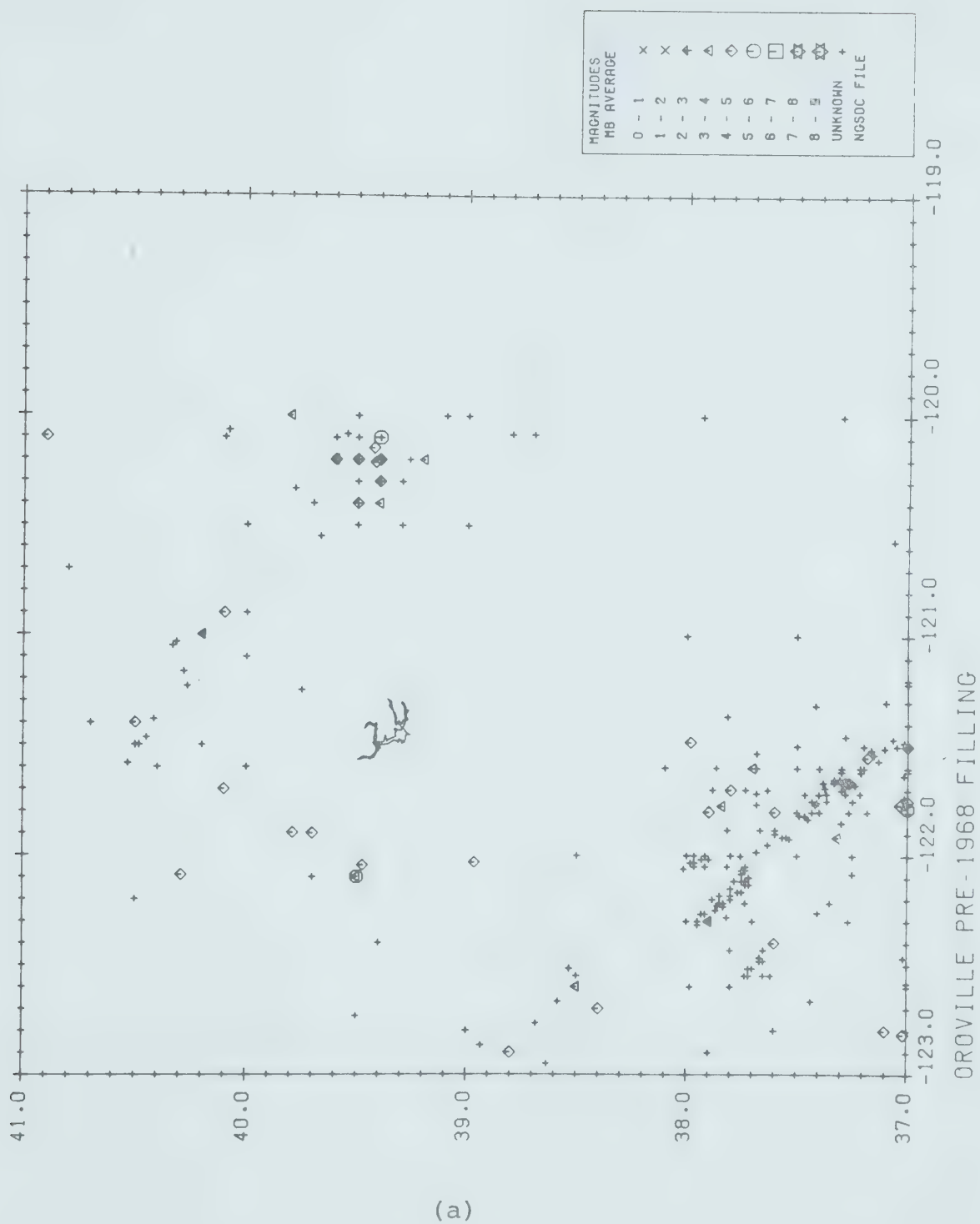


Figure 1.7: Epicentres near Lake Oroville in California up to and including 1968 are shown in (a). This shows a seismic gap within a 50 km radius of the lake. Since the filling of the lake, (b), the pattern has changed little. The position of the August 1975 magnitude 5.9 Mb event is shown by the star in (b).



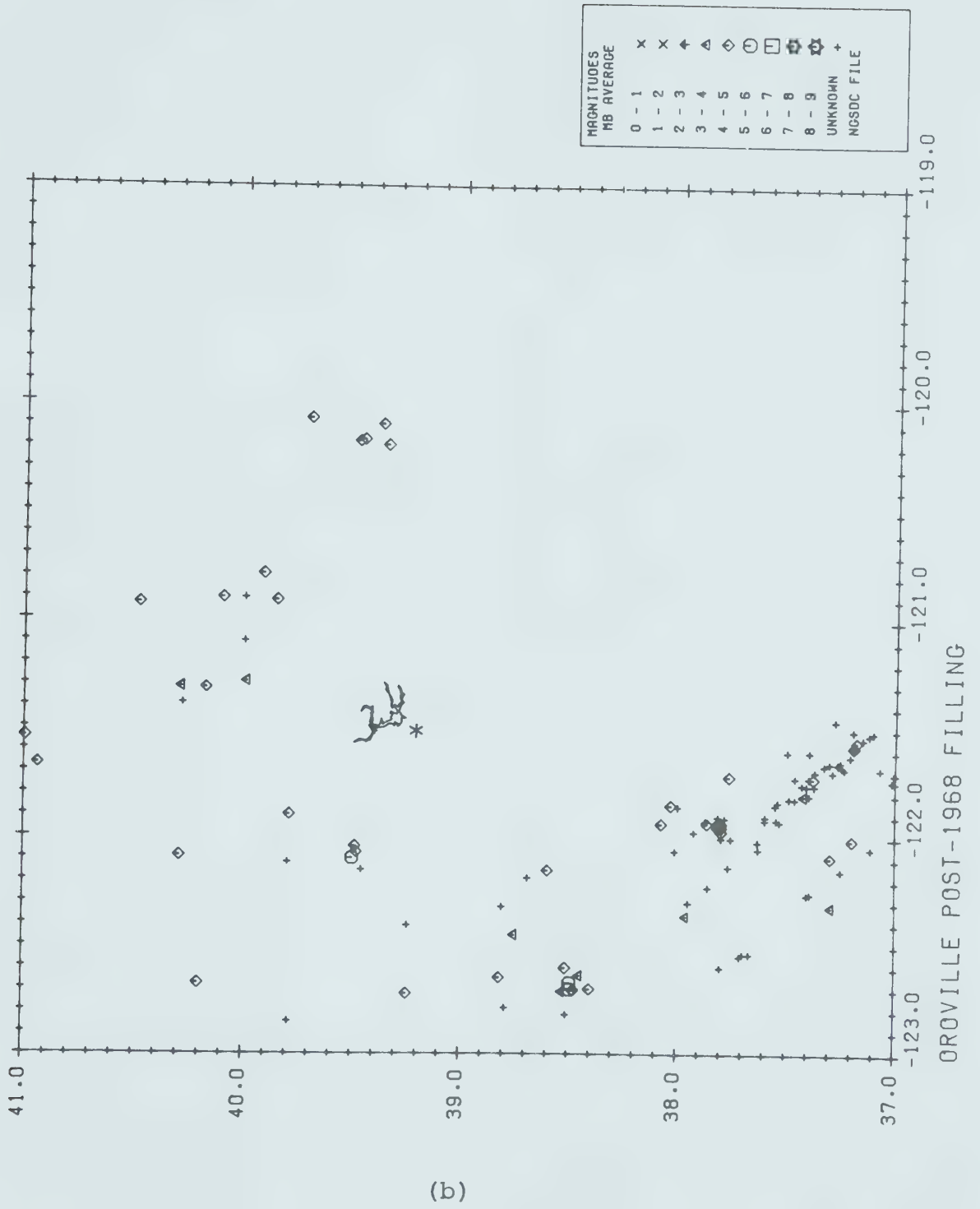
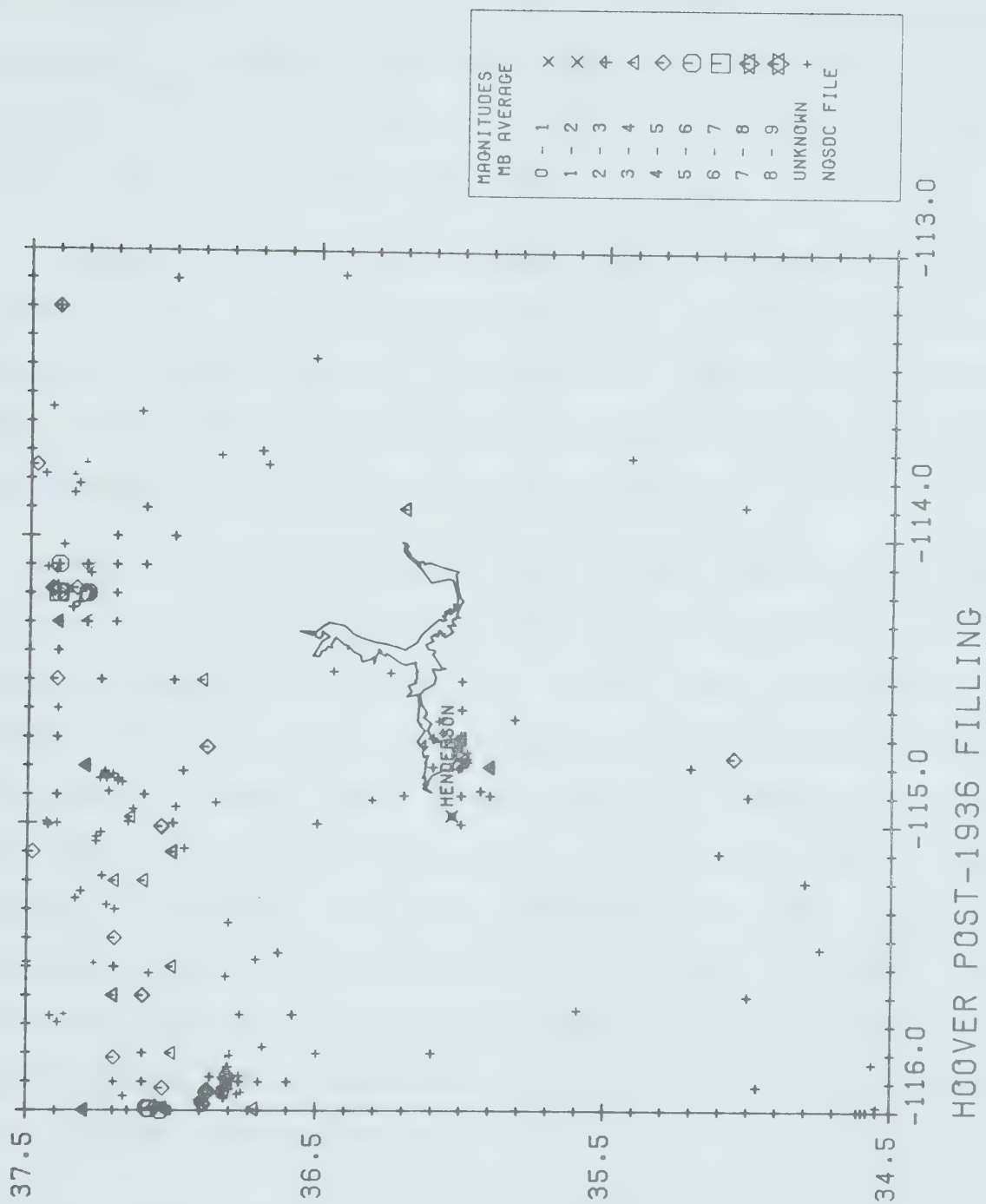


Figure 1.8: The earthquake epicentres at Hoover dam are shown since the filling in 1936. Before this, only two events of undetermined magnitude were observed in the far NE corner of the area. The small number of events before filling is probably only a consequence of the shortage of instrumentation at that time. A cluster of events is observed near the dam wall.



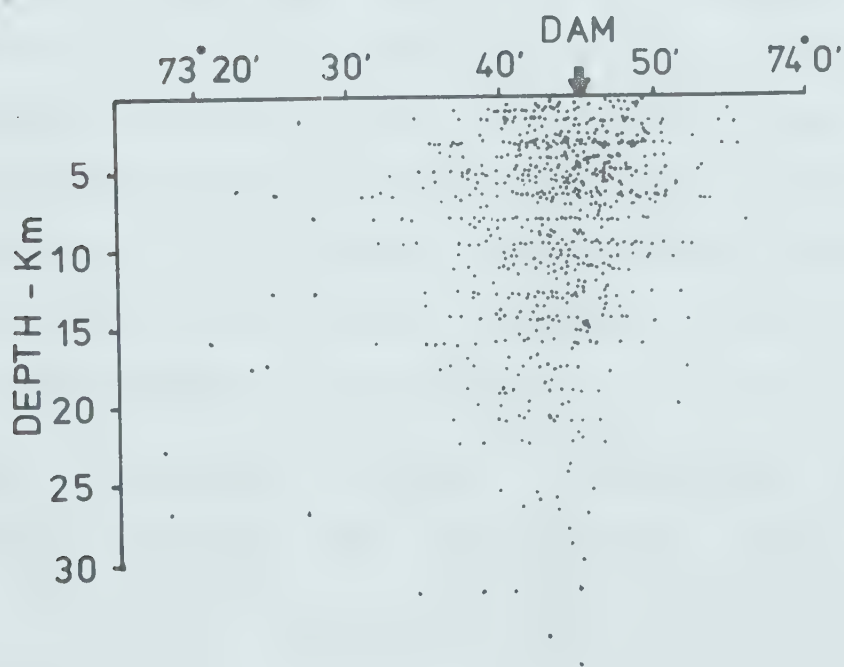
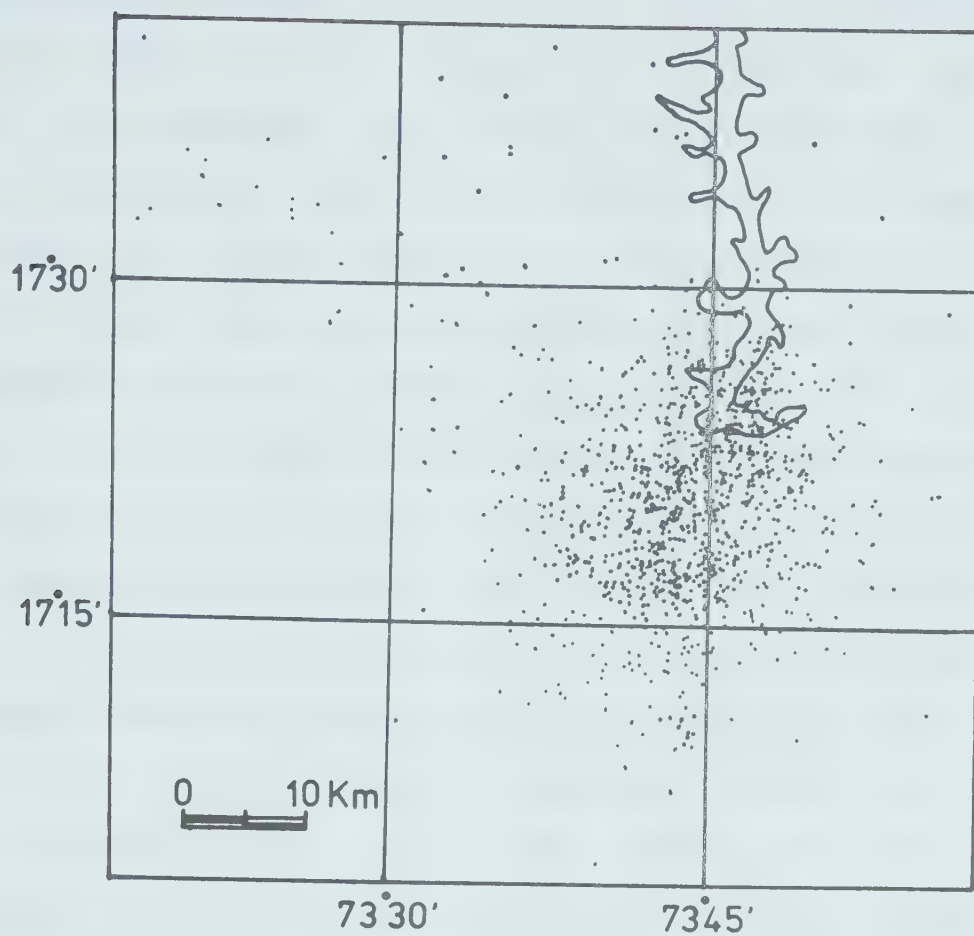
In only a few cases have depths been determined. Local observations and the teleseismic data all indicate that the hypocentres are shallow. Gupta et al (1970) have plotted positions determined from the local array at Koyna and the important results are shown in figure 1.9. The uncertainties in the determination are not given.

Figure 1.9 does serve to show that the bulk of the events occur less than 10 km deep but may extend to 30 km. They are limited laterally to within 10 km of the centre axis of the lake. Reports of noise (Simpson 1976) during the earthquakes is indicative of shallow events.

Migration of seismicity has also been observed at some lakes. Simpson (1976) and Soboleva and Mamadaliev (1976) have indicated the arrays of Nurek show a migration of events toward the lake. They propose a model in which the increased pressure head below the lake migrates away from the lake. The pressure changes are delayed behind the elastic deformation by the diffusion lag. The region of failure moves toward the lake in such a model. Inherent in this model is the assumption that the elastic load falls off more rapidly with distance than does the fluid pressure; this will be examined later.

The focal mechanisms (Sykes(1967,1970), Bufe et. al. (1976), Gough (1976) and an excellent article by Langston (1976)) observed at different lakes are consistent with

Figure 1.9: The array study at Koyna yielded the positions shown for the aftershocks. The events are clustering at the deep end of the lake and are relatively shallow. Most of the events were above 10 km deep and lay within 25 km of the lake.
(Modified from Guha et. al. (1974))



neighbouring tectonic faulting. At Kariba, Kremasta and Oroville normal dip-slip faulting is observed, while at Koyna, Hsinfengkiang and Hoover the mechanism was strike-slip. Jacob et. al. (1976) have reported a slight change in activity at Tarbela which is in a thrust faulting regime. Nurek has also had many small events in a thrust regime. The magnitudes of the main shocks near reservoirs have been as high as 6.5 at Koyna, 6.3 at Kremasta, 6.1 at Hsinfengkiang and so on down. There would appear to be no upper limit to the magnitude since recent work suggests that the lake acts only as a trigger. The magnitude is then only limited by the stresses available in the region. The fact that there have been only a few events of magnitude greater than 6 near lakes can be explained in two ways. Firstly, the lake has to be placed in a suitably highly prestressed region; and secondly, the larger events are less frequent than the smaller ones. Some authors feel that the magnitude of the main shock is limited since the anomalous stresses due to the lake are localized and the rupture length of a large earthquakes is hundreds of kilometers. This argument ignores the possibility of a locally induced rupture extending into an area in which there exist sufficient stresses for the fracture to continue to propagate.

The magnitude-frequency distribution of most earthquakes sequences follow the empirical rule

$$\text{Log } N = A - bM$$

where N is the number of shocks of magnitude greater than or equal to M . 'A' and 'b' are constants determined for the region. The constant A is uncertain since it depends on the sampling time and is subject to a large error, so only the 'b' value is usually used. Values of 'b' have been reported from 0.5 to 1.5, but it usually lies between 0.7 and 1.0 for tectonic regions. The 'b' value observed at many lakes is given in Table 1.2 derived from the data given in Gupta and Rastogi (1976). It can be seen from this that the 'b' value for after-shock sequences at lakes is about 1. They are on the high end of the normal range and usually higher than the 'b' value for the region. The foreshock 'b' values are larger than those of the after-shocks.

The lake seismicity also has a large M/M_0 value where M is the magnitude of the mainshock and M_0 the magnitude of the largest aftershock. M/M_0 values range from about 0.6-0.9. Gupta and Rastogi conclude the normal situation is one where large 'b' corresponds to a small M/M_0 ratio and smaller 'b' with a larger M/M_0 value. This is in contrast with the situation at reservoirs where large 'b' values are calculated with large M/M_0 , (Papazachos (1974)).

Little reliance should be placed on seismic parameters as they are difficult to determine accurately. The comparison of 'b' values with historic 'b' values is always meaningless. For example, it seems impossible to compute 'b' values for long periods while the means of detection are

TABLE 2: SEISMIC OBSERVABLES MEASURED AT LAKES MODIFIED FROM GUPTA AND RASTOGI (1976)

Region and Period	Main Shock Magnitude M	Largest Aftershock Magnitude Mo	b	Magnitude Range for b	M/Mo	Number of Earthquakes
Lake Mead 1941-1942	5.0	4.4	1.40	2.0 - 4.0	0.88	536
Monteynard 25/4/63-13/11/57	4.9	4.5	0.72	1.1 - 3.1	0.92	57
Mangla	3.5	3.3	0.96	2.5 - 3.5	0.94	--
Kariba aftershocks 23/9/63-27/12/68	6.1	6.0	1.02	2.0 - 5.8	0.98	1114
Kariba foreshocks 8/6/59-23/9/63	--	--	1.18	2.0 - 4.0	--	291
Africa Region 1/1/63-30/6/66	--	--	0.53	3.2 - 5.6	--	43
Kremasta aftershocks 5/2/66-30/11/66	6.2	5.5	1.12	2.0 - 5.6	0.89	2580
Kremasta foreshocks 1/9/65-5/2/66	--	--	1.41	2.0 - 4.2	--	740
Kremasta region	--	--	0.64	-- --	--	--
Koyna aftershocks 10/12/56-27/6/69	6.0	5.2	1.09	3.0 - 5.2	0.83	422
Koyna foreshocks 10/9/64-13/9/67	--	--	1.87	2.8 - 3.7	--	51
Indian Peninsula	--	--	0.47	4.0 - 7.0	--	52

changing. The 0.47 'b' value for the Indian Peninsula has been taken from data covering 300 years and I fail to see its significance in a comparison to a 'b' value computed by a modern seismic array. The Peninsula data was published by Gubin (1969).

It is my conclusion that the calculation of 'b' and M/M_0 values is only useful in observing possible trends. Caution should always be taken in comparing seismic 'lumped observables' from one area with another, and then expecting the averages to apply to a third.

The correlation between the water level and seismic frequency has been published by many authors (see Gupta and Rastogi (1976)). Hagiwara and Ohtake (1972) give typical results at Kurobe and show the highest correlation (0.41) exists, in their case, with a lag of less than one month.

The stresses produced by changes of water pressure in the rock affect the total stress. Two contradictory models can be examined depending on the rock's water content. If the rock is dry the water will not affect the stresses until after it has diffused into the rock. In this situation the rock deforms elastically, with the water effects occurring at a later time. If the rock is saturated, the pressure changes are transmitted through the connecting pores over the area affected by the load. This initial pressure change is rapid in the neighbourhood of the source of the change.

The pressure gradients established cause diffusion which relaxes the gradients. The relaxation takes place after the loading, with the rate governed by the rock permeability. The rock is assumed to contain water in the work that follows. Since dams usually confine pre-existing rivers it is a reasonable assumption that there already existed ground water and that it extended to significant depths.

Reservoirs are usually quite large, and may be tens of kilometers wide by several hundred long. For this reason the hydrologic regimes should be examined in an attempt to fully describe the conditions in the rock before the reservoir is filled. Large quantities of water may be transported by these regimes and the water pressure may differ substantially from the hydrostatic head. In some areas the water pressure will be larger, and at others the pressure smaller than hydrostatic. These large scale features are not well known since they are usually not reported in the open literature on lake seismicity. Obviously hydrology is as important as the tectonic stresses, but since no data is available at the reservoir scale it has been ignored in the examples. It is possible to generalise the mathematical theory presented later to include these effects.

One would assume the changes in seismicity would occur with the level changes and the later diffusion processes. at later times. Small foreshocks change the drainage pattern and hence the diffusion times required for fluid transfer so

correlations between lake level and seismicity may become confused at later times. The best correlations are usually seen during the first filling and several examples of this are shown in figure 1.10. The positions of most events are poorly known, and this particularly applies to the depth determination. At Vajont large scale slumping occurred, and since the depth is unknown several processes may be causing the detected activity.

It is not obvious from these diagrams whether the seismicity is related to the increased water level or the rate of change of level. Both are related to the water level and, in diffusion processes, the rate of change of pressure is an important factor.

Gough and Gough (1970) have indicated the desirability of using energy radiated, as well as frequency, in all correlations since this gives the correct weighting to the larger events. In the examination of induced seismicity the strain released is proportional to the square root of the energy (Richter (1958), p368). The energy radiated is closer to the cause-effect mechanism than are the readjustments shown by the seismic frequency.

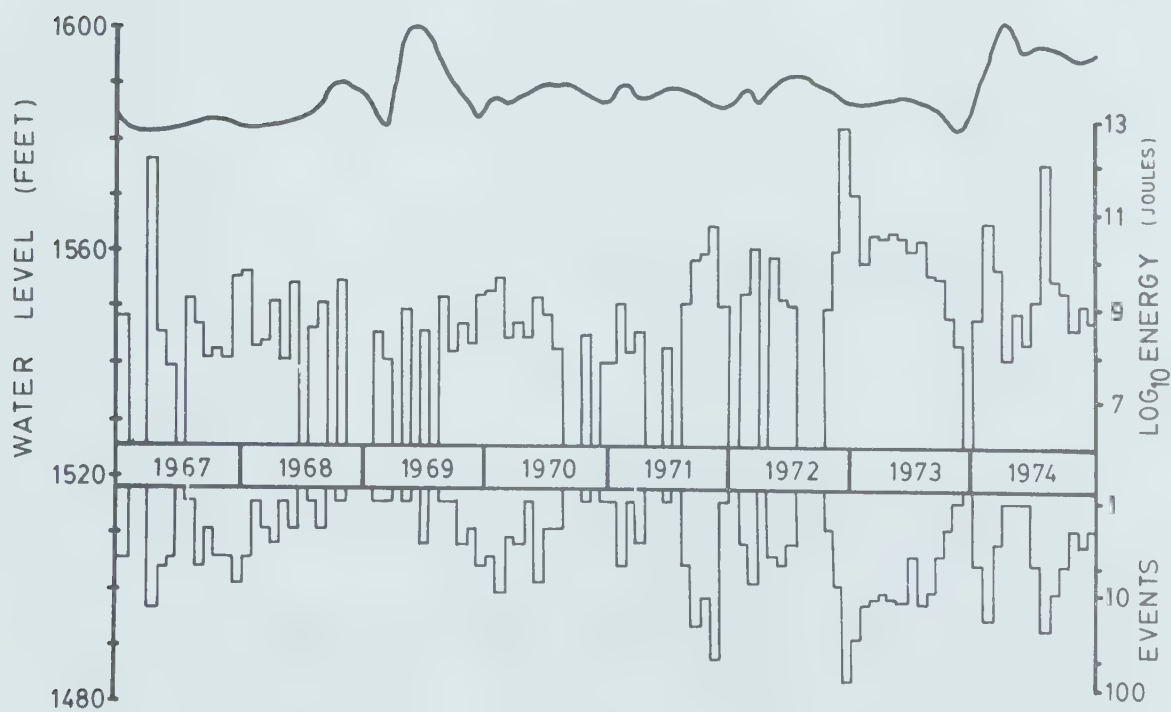
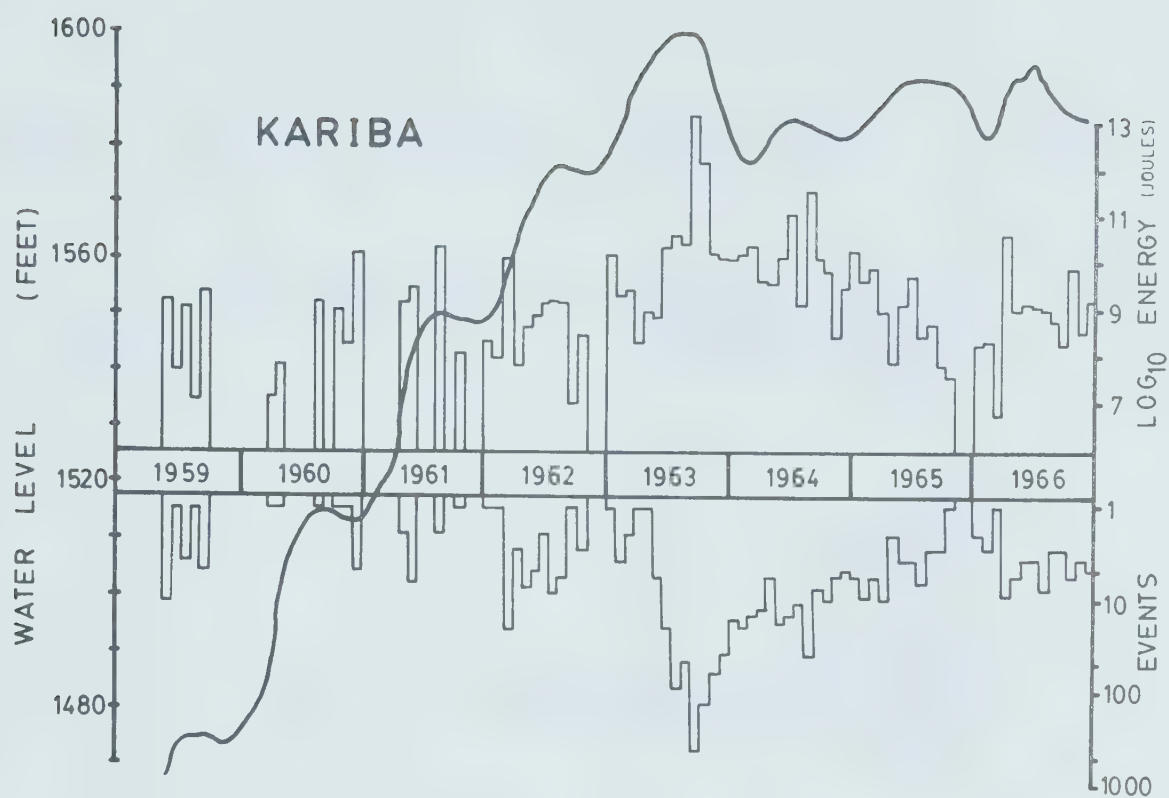
It will be shown later that it is possible to relate the stress produced in the rock by the lake with the water depth, the rate of change of pressure head, and the time the pressure head is maintained. The correlations between the

Figure 1.10: (a) Water level, frequency of events and energy radiated at Kariba are plotted as a function of time. The energy radiated is strongly dependent on the largest event within each of the four week periods. (Modified from Gough and Gough (1970b))

(b) Histogram of the number of events and lake depth at Vajont in Italy. In October 1963 a large mass of rock slid into the lake causing great damage. (From Galanopoulos 1966)

(c) Seismic activity and water depth at Kremasta for 15 day periods. A sudden increase in activity is noted when the rate of filling was increased. (From Galanopoulos (1966))

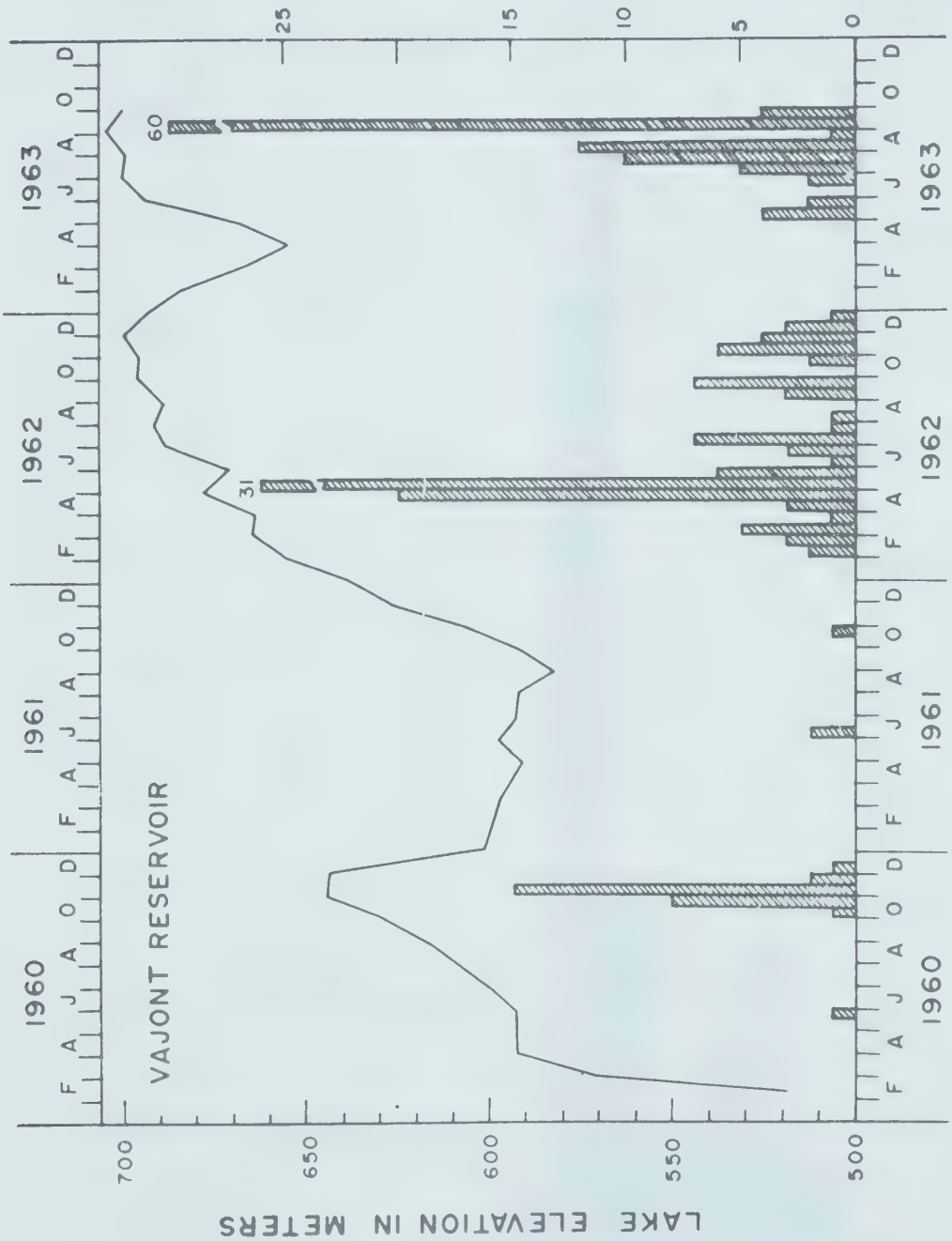
(d) Flow hydrographs, water level and seismic frequency are shown at Koyna. The frequency increases about three months after the water level increased. In 1967, the pattern is confused, and on December 10 a magnitude 6.5 event was detected.

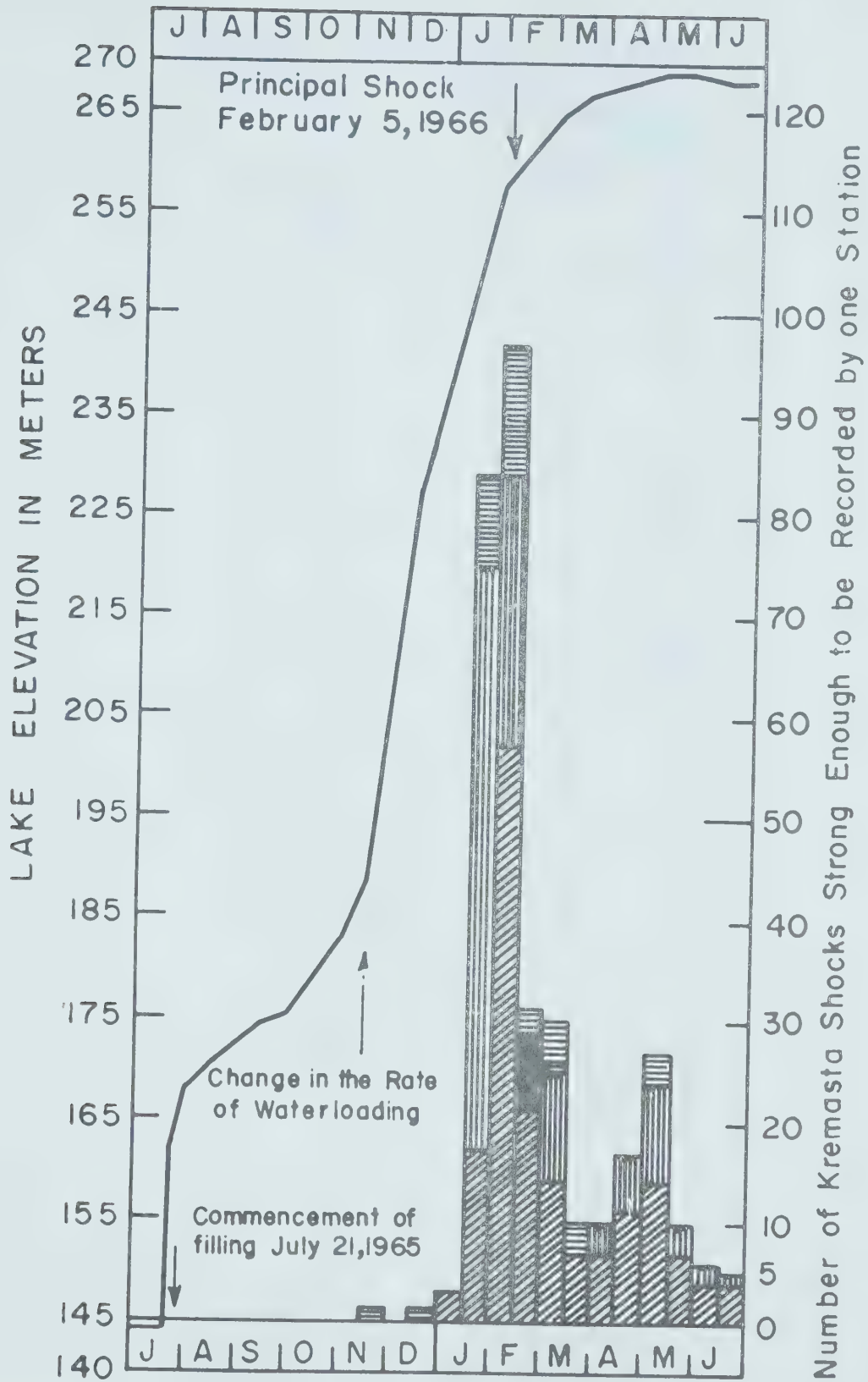


(a)

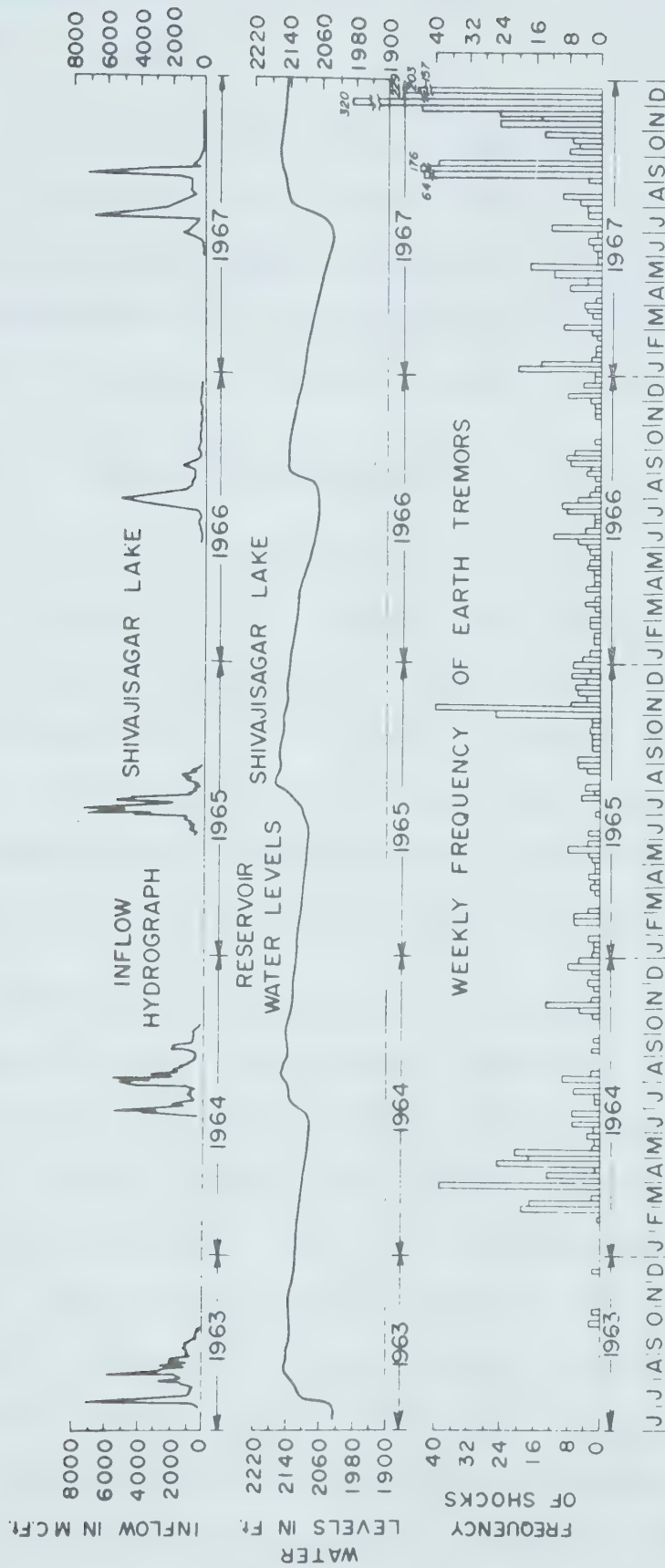
NUMBER OF RECORDED LOCAL EARTHQUAKES PER 15 DAY PERIOD

(b)





(c)



(d)

seismic frequency and lake level shown in figure 1.10 are not always as obvious.

The study of the seismicity is primarily concerned with changes in seismicity and Simpson (1976) has suggested the use of six categories. These are listed in table 1.3. It must be remembered that there are many times more lakes with no noticeable seismicity than are listed in table 1.3.

(a) Major Induced Earthquakes

Koyna, Kremasta, Hsinfengkiang, Kariba, Hoover and Marathon are placed in the category where there is a major change in the seismicity around the reservoir with a fully developed sequence of fore and after shocks. The case is quite clear at Koyna and Kariba where the N.O.A.A. Summary Tape and other research indicate that there were no events in the neighbourhood of the lake prior to filling.

At Kremasta good correlations are observed between the smaller events and the water depth. However, as shown in figure 1.3, the epicentral magnitudes and distribution of the larger events before and after filling are not significantly different. The area was obviously close to failure and it is not clear whether the event was statistically likely to have occurred regardless of the presence of the lake. Oroville could be included in this category but the case for lake induced seismicity in this instance is less clear. Unlike the other cases where events

TABLE 3: RESERVOIR INDUCED CHANGES IN SEISMICITY

Dam Name	Location	Height of Dam (m)	Volume of Reservoir (x10 ⁶ m ³)	Year of Impounding	Year of Largest Earthquake	Magnitude or Intensity
MAJOR INDUCED EARTHQUAKES						
Koyna	India	103	2780	1964	1967	6.5
Kremasta	Greece	165	4750	1965	1966	6.3
Hsinfengkang	China	105	10500	1959	1962	6.1
Oroville	U.S.A.	236	4295	1968	1975	5.9
Kariba	Rhodesia	128	160368	1959	1963	5.8
Hoover	U.S.A.	221	36703	1936	1939	5.0
Marathon	Greece	63	41	1930	1938	5.0
MINOR INDUCED EARTHQUAKES						
Benmore	New Zealand	118	2100	1965	1966	5.0
Monteynard	France	155	240	1962	1963	4.9
Kurobe	Japan	186	199	1960	1961	4.9
Bajina-Basta	Yugoslavia	89	340	1966	1967	4.5-5.0
Nurek	U.S.S.R.	317	10400	1969	1972	4.5
Clark Hill	U.S.A.	67	2500	1952	1974	4.3
Talbingo	Australia	162	921	1971	1972	3.5
Keban	Turkey	207	31000	1973	1974	3.5
Jocassee	U.S.A.	133	1430	1972	1975	3.2
Vajont	Italy	261	61	1961	1963	V
Grandval	France	88	292	1959	1963	V
Canalles	Spain	150	678	1960	1962	
CHANGES IN MICROEARTHQUAKE ACTIVITY						
Kamafusa	Japan	46	45	1970		<2.5
Pieve de Cadore	Italy	112	68	1949		2.0
Grancarevo	Yugoslavia	123	1280	1967		1.0-2.0
Hendrik-Verwoerd	S. Africa	88	5954	1970		<2.0
Schlegeis	Austria	130	129	1971		<0.0

TABLE 3: CONTINUED

Dam Name	Location	Height of Dam (m)	Volume of Reservoir (x10 ⁶ m ³)	Year of Impounding	Year of Largest Earthquake	Magnitude or Intensity
TRANSIENT CHANGES IN SEISMICITY						
Oued Fodda	Algeria	101	228	1932		
Camarilles	Spain	44	40	1960	1961	3.5
Piasta	Italy	93	13	1965	1966	VI-VII
Vougians	France	130	605	1968	1971	4.5
Contra	Switzerland	220	86	1965	1965	
DECREASED ACTIVITY						
Tarbela	Pakistan	143	13687	1974		
Flaming Gorge	U.S.A.	153	4647	1964		
Glen Canyon	U.S.A.	216	33305	1964		
Anderson	U.S.A.	72	110	1950		
OTHER POSSIBLE CASES						
Shasta (U.S.A.)						Parambikulam (India)
San Luis (U.S.A.)						Sharavathi (India)
Palisades (U.S.A.)						Ukai (India)
Clark Canyon (U.S.A.)						Ghirni (India)
Kerr (U.S.A.)						Mula (India)
Cabin Creek (U.S.A.)						
Rocky Reach (U.S.A.)						

were observed soon after the initial filling, little activity was detected at Oroville until a few months before the major event. The time lag between the initial filling and the main event is the longest of the cases (about 7 years). There may be some connection between the drawdown just before the main event and its onset. The seismicity at Oroville is summarised in a paper by Bufe et. al. (1976).

(b) Minor Induced Earthquakes

Simpson lists 12 cases where earthquakes of approximate magnitudes 3 to 5 have occurred and these are listed in table 1.3. In areas where prefilling activity was known the inclusion of Nurek, Monteynard, Bajura-Basta, Vajont and Benmore in the table 1.3 is based on increased activity coincident with the filling. At Talbingo and Kurobe prefilling instrumentation has shown that for 10 years prior to construction no earthquakes of the size measured after filling were detected.

(c) Changes in Micro Earthquake Activity

At the six reservoirs shown in table 1.3 instrument with sufficient sensitivity were available to detect an increase in activity below a magnitude of 2.5. A lack of instrumentation at other sites would indicate that this may be a more widespread phenomenon than the data would suggest.

(d) Transient Changes in Seismicity

Simpson places five reservoirs in this category which have been associated with activity which began after impounding but which has since stopped or decreased. These are listed in table 1.3. Rothe' (1970) has suggested that hydraulic or crustal adjustments account for the seismicity at Oved Fodda and Camarillas. At Contra the activity stopped after the water level was lowered. The seismicity occurred after a rapid emptying and filling of the reservoir at Vouglans.

These cases are very difficult to predict, but they indicate that the stresses were at a critical level and the region was close to failure before the lake was filled.

(e) Decrease in Activity after Filling

As reported earlier, Jacob et. al. (1976) have indicated a decrease in activity at Tarbela reservoir during the initial stages of filling. This reservoir has only just been impounded so the change in seismicity may be a transient phenomenon related to the initial filling. This decrease is expected by the simple elastic models shown in figure 1.11.

(f) Possible Cases of Reservoir Related Seismicity

There are a number of cases of increased activity near reservoirs where there is insufficient data to show a clear cause-effect relation. Simpson lists several in this

category, however they are of little use in assessing the risk at a particular dam site.

1.3 The Concept of Effective Stress

The introduction of large amounts of water into the rock below the reservoir affects the stress pattern in a manner opposite to that due to the stress changes due to the weight alone. Laboratory studies of fracture and deformation of fluid filled rock (Handin et. al. (1963), Knutson and Bohor (1963), Nur and Byerlee (1971), Garg and Nur (1973), Robinson (1959), and many others) have shown that the concept of effective stress proposed by Terzaghi (1923) and later supported by Hubbert and Rubey (1959), describes the behaviour of fluid filled rock. The effective stress is found by adding the fluid pressure, multiplied by a constant, to the applied stress. It must be remembered that pressure has the sign convention of an applied tensile load since it tends to expand the solid.

$$\sigma_{\text{eff}} = \sigma_{\text{applied}} + \alpha P$$

There is considerable discussion on the value of α (Nur and Byerlee (1971), Garg and Nur (1973)) but for most rocks and engineering applications, acceptable results are obtained when the constant equals one. α may be less for extremely high or low porosity and may depend on the stress. A description of the variation of α is given in section 4.1.

The Mohr circle representation best describes how the

pressure affects the stability condition in different faulting environments. In these diagrams the normal stress is plotted against the shear stress with a circle drawn centred on the average of the maximum and minimum principal stress and radius equal to half the difference. The radius, relative to the principal stress axes, is called the maximum shear stress. Diagram 1.11a shows a Mohr circle with F_1 the largest principal stress and F_3 the smallest. The envelope of Mohr circles at failure under moderate stresses has the form of a straight line

$$\tau = C + \sigma_n \text{ TAN } \phi$$

where τ , is the shear strength of the rock

ϕ , is the angle of shear resistance

σ_n , is the normal effective stress on the plane of failure

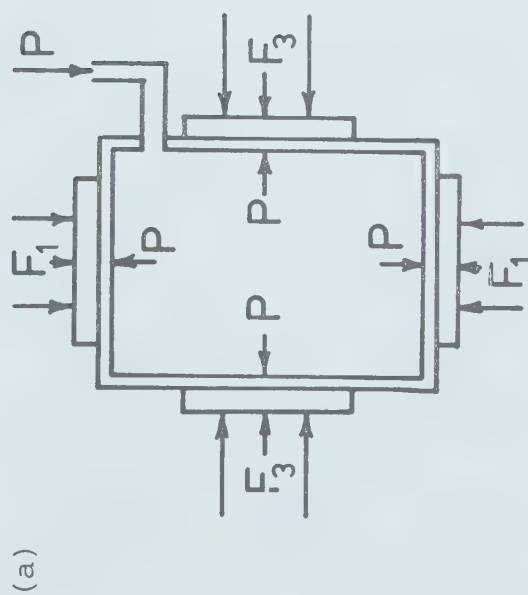
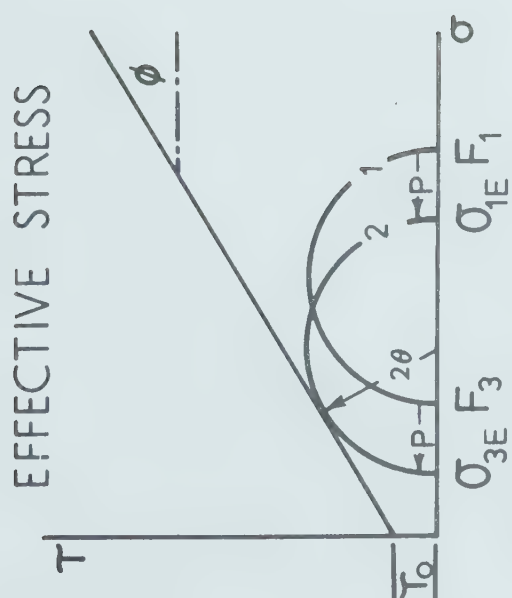
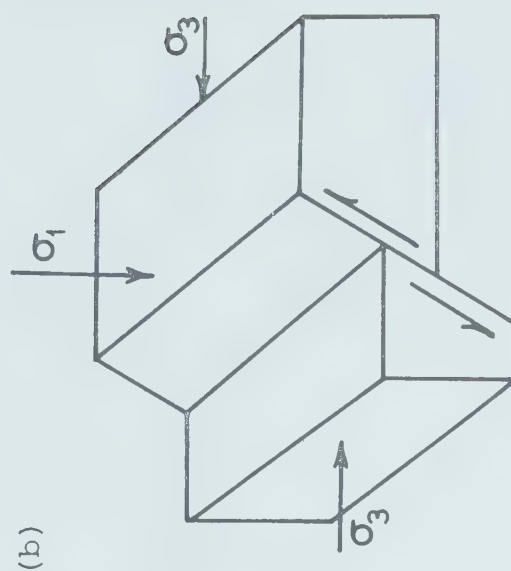
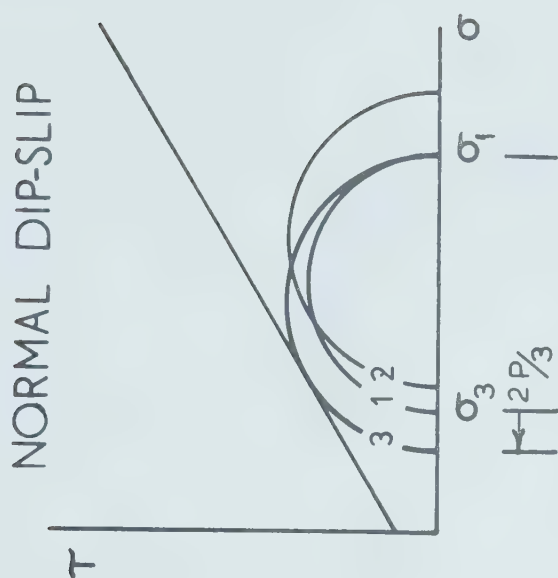
C , is the apparent cohesion, and is the shear strength of the material under zero normal pressures

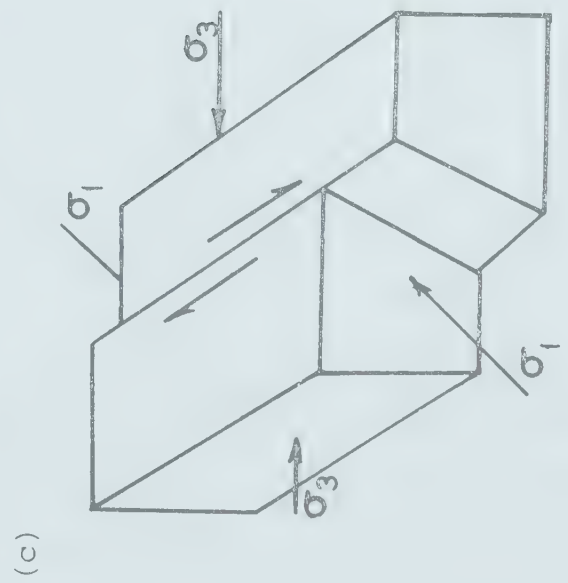
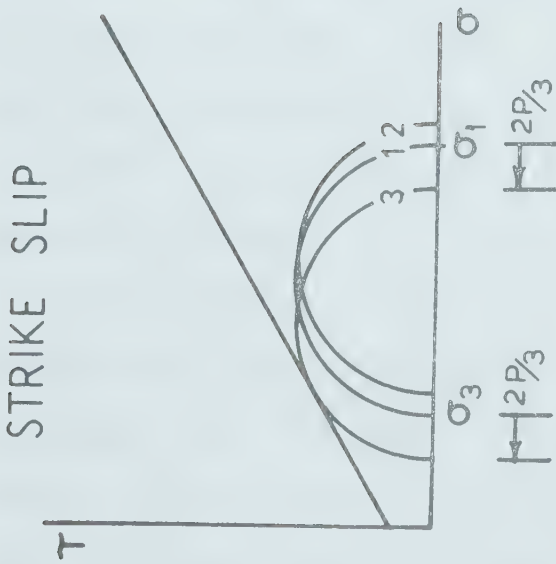
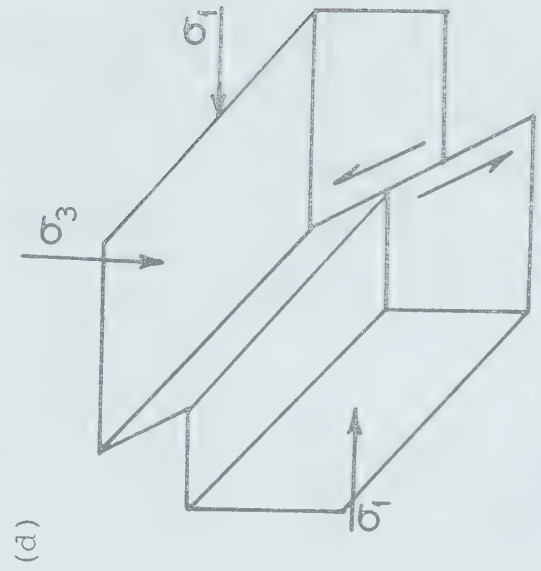
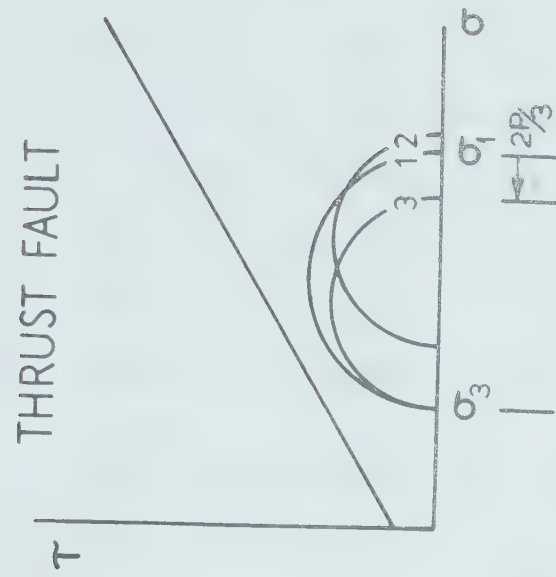
C varies considerably and may vary from zero in a fractured sample to several hundred bars in an intact sample. In a large scale geological situation fractures would usually be present and C is small, and thus the rock has little or no tensile strength. $\text{TAN } \phi$ is the coefficient of friction along the failure plane. As angle ϕ lies between 25° and 45° then the coefficient of friction is between 0.47 and 1.0 but is usually around 0.6 ($\phi=30^\circ$).

The failure envelope is found by triaxial testing of dry samples. Under extremely high confining pressures the

Figure 1.11: This illustrates the Mohr circle and Coulomb failure concepts. In the jacketed sample under compressive loads F_1 and F_3 the Mohr circle (in the absence of fluid) is shown by the circle labelled '1'. Increasing the fluid pressure moves the failure circle to position '2'. When the Mohr circle touches the Coulomb failure envelope, failure will occur along a plane at an angle θ to F_3 . The effective stresses σ_{1E} , σ_{3E} are shown by the final circle position, '2'.

The largest principal stress is σ_1 and the smallest σ_3 in each of the three fault conditions shown (b), (c), (d). The Mohr circles due to these principal stresses are labelled '1'. Application of a vertical load, P , moves the circles to position '2' in a dry condition. The horizontal stresses are affected by $0.3P$ due to Poisson effects. If fluid is introduced into the faults at pressure P the circles move to the left to positions '3'. The movement of the Mohr circles from initial to final positions are shown. In normal dip-slip and strike-slip faulting the area is made less stable by the application of the load and water pressure. Thrust fault regions are stabilised.





shear stress exhibits a decreasing dependence upon the confining pressure as the failure mechanism changes from intercrystalline slip to intracrystalline slip.

Knowing the form of the envelope, the plane of failure can be predicted from the point the Mohr circle is tangent to it. Failure will occur on a plane θ from the plane of F_3 in the two dimensional case. The angle 2θ is measured from the axis of increasing σ anticlockwise to the point the Mohr circle is tangent to the failure line.

The introduction of fluid, water in the case of reservoir loading, into a dry sample under compressional loads F_1, F_3 , moves the Mohr circle by the amount of fluid pressure applied to the jacketed rock towards the failure envelope.

The effect of a lake load on an area and the introduction of the water pressure head into different faulting environments is shown in figure 1.11. In each of the faults σ_1 , is the largest and σ_3 the smallest of the tectonic stresses. The Mohr circle before the lake is loaded is shown by circles labelled '1'. In normal faulting σ_1 is vertical but is horizontal for strike slip and thrust faulting. The addition of the weight of the water at the surface increases the vertical stress by $P = \sigma gh$. An increased vertical stress also increases the horizontal stresses by Poisson effects by an amount $P\nu/(1-\nu)$ where ν is Poisson's

ratio. If ν is a typical 0.25, then increasing the vertical stress by P increases the horizontal stresses by $0.3 P$. The circles '2' represent the combined effects of the tectonic stresses and the weight of the water. If the water is introduced into the fault region at the full pressure head, the stress circles are moved towards the failure envelope. The stresses are now effective stresses as the fluid affects all stresses equally. The final positions are shown by circles labelled '3'.

The introduction of a fluid load onto a normal dip-slip fault or a strike slip fault moves the region closer to failure. Thrust faulting areas are stabilised by the same argument as the Mohr circle '3' is smaller and thus is further from the failure envelope.

The arguments presented here are for idealised situations but the conclusions should apply to real faulting. In a realistic situation the effect of the load diminishes with the distance from the lake and the surface water head is not necessarily the same as that near the fault. These effects will be examined later. The arguments appear consistent with the observed faulting. Near reservoirs faulting has always been normal dip-slip or strike-slip except at Nurek and perhaps Tarbela.

1.4 The Denver Earthquakes

The Denver disposal well of the Rocky Mountain Arsenal was the first clear example of earthquakes caused by the action of man. D.M. Evans (1966) called attention to a correlation between the volume of fluid injected into the well and the number of earthquakes detected at a nearby observatory. The events were up to magnitude 4 on the Richter scale and their proximity to Denver City was cause for concern. The well had been drilled through 3700 m of sedimentary rocks and finished in fractured Precambrian granitic gneiss. During the drilling it was found that the water pressure was at least sixty bars below normal hydrostatic head.

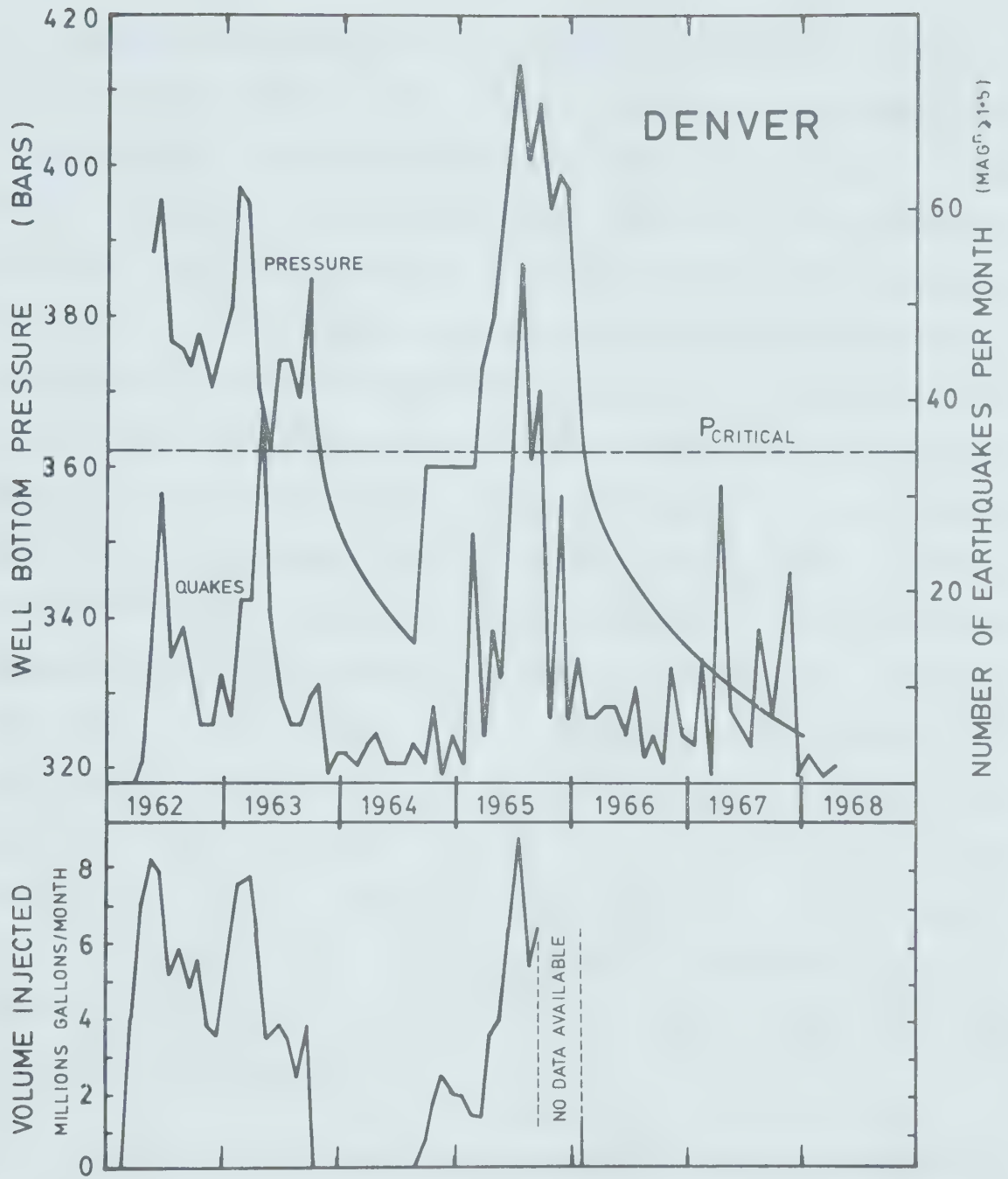
In March 8, 1962, $1.6 \times 10^4 \text{ m}^3$ of fluid waste was injected into the well with a maximum injection pressure of about 38 bars. Earthquakes were detected shortly after pumping commenced. The well was then shut down from September 1963 until March 1964. Until March 1965 injection was maintained at essentially a hydrostatic head and a monthly average of $9.1 \times 10^3 \text{ m}^3$ was added. To increase the discharge, the pumping pressures were raised to 70 bars and pumping was suspended in 1966 owing to public concern. The earthquakes continued at a varying rate of from 4 to 71 events per month with a magnitude 5.0, the largest of the series, occurring on 10 April 1967. From a plot of magnitude against the logarithm of the frequency this event was not unexpected since the relationship was still linear. On 9

August another large magnitude 5.3 event occurred, followed by a magnitude 5.1 event on 26 November. These events were significant in that they were not expected from the linear relation between \log -frequency and magnitude obtained from the earlier recordings. This indicated a dramatic change in the pattern of activity. Since 1967 the number of events has decreased and no more large events have occurred. The well pressure, frequency and volume of waste injected are plotted as a function of time in figure 1.12.

The U.S.G.S., the US Army Corps of Engineers and the Colorado School of Mines examined the seismicity near the Rocky Mountain Arsenal. A search of the historic records revealed no evidence of seismic activity before the well injection in March 1962 similar to that which has occurred since 1962. From a network of arrays of seismometers they concluded the epicentres lay within an elliptic zone 10 km by 3 km which encloses the disposal well. The focal mechanisms are consistent with right-lateral strike slip on vertical faults at N60W parallel to the major axis of the ellipse.

Healey et. al. (1968) deduced from the mechanisms that the energy released must have been stored in the basement as elastic strain of tectonic origin. There are two reasons for this conclusion. Firstly, the magnitude-frequency relation is similar to that of southern California, which is a similar tectonic region, and secondly, because the radiation

Figure 1.12: The number of earthquakes per month and the well bottom pressure were plotted for Denver. The critical pressure determined from hydrofracturing tests is also shown. The seismic frequency increases when the pressure is above P critical. Between 1963 and 1965 the number of earthquakes decreased significantly while the pressure was below the critical pressure.
(Modified from Healy et al (1968))



patterns suggest a zone of vertical fractures existed with a northwest trend prior to the injection of the fluid. These have now been observed in cored samples.

A model was proposed by Healey et. al. (1968) to explain the faulting in terms of effective stress. The triggering of the region must have been a result of the fluid injection. In strike-slip faulting the largest and smallest principal stresses are horizontal. The pressure required to start fluid injection was found to be 362 bars. Above this value the injection rate increased remarkably so at 362 bars the cracks open to fluid flow. One can conclude from this that the minimum principal stress, σ_3 , must have been 362 bars which is 93 bars above the initial fluid pressure in the well. The pore pressure before injection was calculated to be 269 bars by observing the rate of pressure fall-off with depth after pumping was ceased. The intermediate stress, σ_2 , is due to the weight of fluid and rock. At 3671 metres, σ_2 is 830 bars for saturated sedimentary rock of weight 0.226 bar/metre. The largest principal stress, σ_1 , is necessarily at least 830 bars. At the time faulting was initiated the water pressure was measured at 389 bars.

If $\sigma_1 = 830$ bars, $\sigma_3 = 362$ bars and $P_o = 269$ bars, the effective shear and normal stresses on a plane at 60° to σ_3 will be $\tau = 203$ bars and $\sigma_n = 210$ bars respectively. The angle of 60° was chosen since this is typically measured

in laboratory fracture tests. For a rock of frictional coefficient of 0.6, τ_0 , the cohesive strength would have to be at least 82 bars.

During injection when the fluid pressure was 389 bars, τ would again be 203 bars (independent of the fluid pressure) and $\sigma_n = 90$ bars. The frictional term $\sigma_n \tan \phi$ is smaller by 69 bars indicating faulting would occur in a rock with a τ_0 value of 151 bars or less. Brace (1974) has shown the strength of rock decreases as the sample dimension increases. The fracture strength of quartz diorite decreases by a factor of five over two orders of magnitude change in the sample dimension while coal's strength decreased by a factor of ten. The cohesive strength of sound rocks is around 500 bars so 150 bars may not be an unrealistic cohesive strength.

An alternative to this model was also suggested by Healey et. al.. If the fractures already existed, then rather than failure occurring by the opening of new fractures, old cracks may have been reopened. Brace (1974) also discusses this question and points out that stresses and stress drops associated with brittle fracture are generally much higher than those required for stick-slip faulting. Pre-existing faults nearly always occur in seismic areas and at Denver suitable fractures were observed in cored samples.

If 362 bars reopened the fractures, then the normal stress σ_n on them was 362 bars. The least principal stress can be computed from the Mohr circle to be

$$\sigma_3 = \frac{2\sigma_n - \sigma_1(\cos(2\alpha) + 1)}{(1 - \cos(2\alpha))} = 206 \text{ bars}$$

σ_1 was 830 bars and α was again chosen to be 60° . If the fluid pressure was raised to 362 bars the Mohr circle is tensile for angles up to about 60° . Rocks have a low tensile strength of only about 50 bars so pre-existing faults could easily open. Faulting would cease when the pressure has dropped sufficiently by permeating along the faults. This explanation of the failure was favoured by Healey et. al.. The results of the injection at Denver indicates a connection between fluid injection and induced seismicity. The later chapters of this thesis will try to examine the effect more quantitatively. The concept of effective stress has also been shown to be consistent with the failure observed.

1.5 The Rangely Experiments

The proximity of the Denver well to populated areas made it impossible to conduct experiments on earth stresses there. An opportunity to do the experiments came at Rangely, Colorado where waterflooding of an oilfield has apparently triggered small earthquakes. A paper by Raleigh et. al. (1975) summarizes the results of the tests on fluid pressure

and the application of effective stress.

The oilbearing Weber Sandstones are 350 m thick and lie at a depth of 1700 m. The Paleozoic sandstones and limestones lay beneath the Weber formation with the crystalline basement at 3000 m. The drainage pattern is aligned along a structure trending N30E. The Weber sandstone has an average porosity of 12% and a permeability of 1 millidarcy.

Hydrofracturing tests were conducted in oil wells to determine the in-situ stresses. This technique is well described by Hubbert and Willis (1957) and Morgenstern (1962). The water pressure is increased until the tensile strength of the rock is exceeded in a packed off section of the well. At this critical pressure, the breakdown pressure, fluid flows into the rock and the pressure drops. The pump is then stopped and the fluid pressure drops until the pores close and the fluid pressure drop flattens. This is the instantaneous shut-in pressure and is equal to the normal stress acting across the fracture.

At Rangely the least principal stress, σ_3 , equal to the shut-in pressure, was found to be 314 bars. The breakdown pressure, P_f , was 328 bars and the initial water pressure, P_o , was measured to be 162 bars. The maximum principal stress, σ_1 , can be found from:-

$$P_f = T + 3\sigma_3 - \sigma_1 - P_o$$

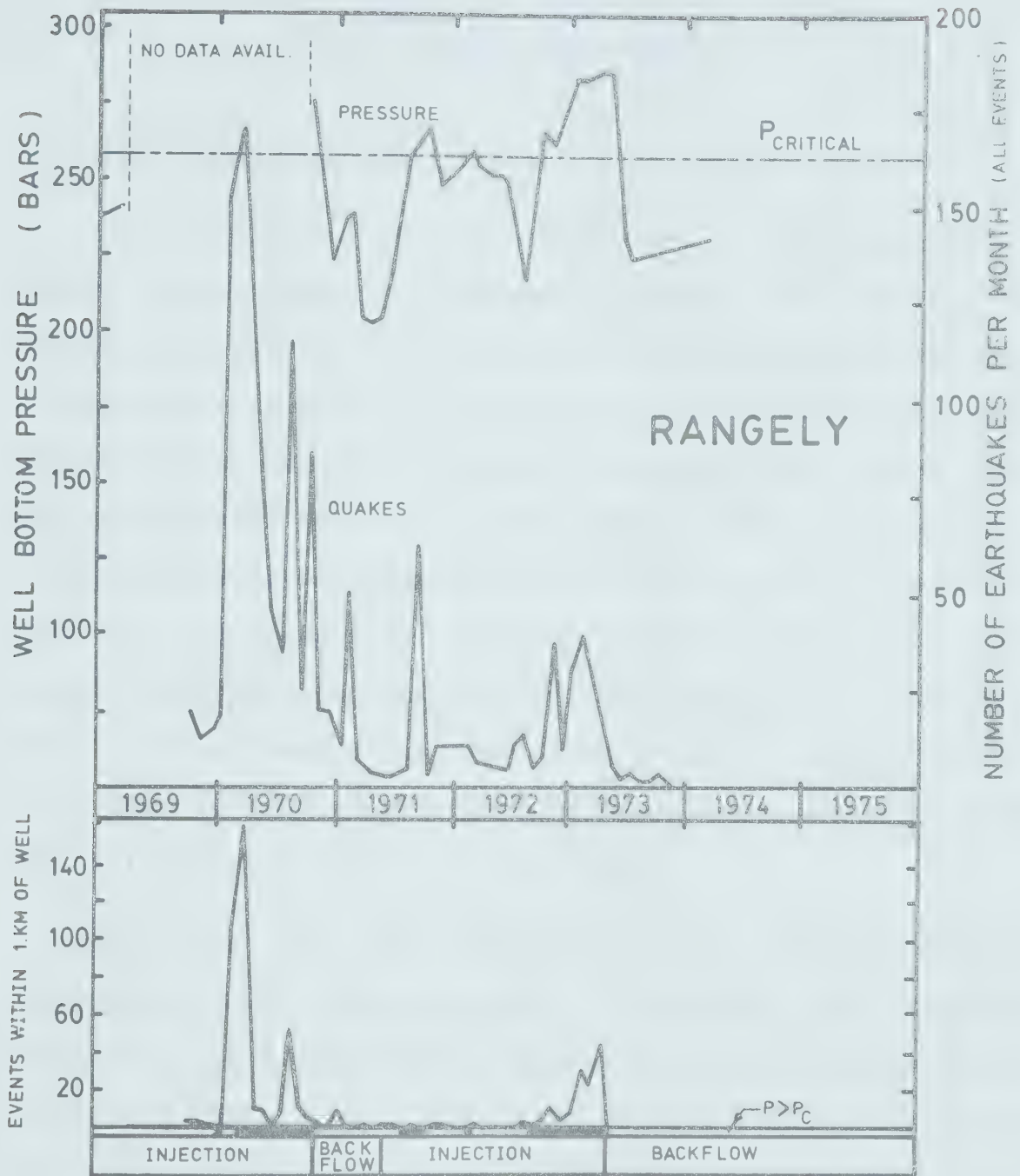
where T is the tensile strength measured in the laboratory to be around 100 bars. From this formula $\sigma_j = 552$ bars. The intermediate vertical stress in this strike-slip region equals the overburden pressure of 427 bars. The coefficient of static friction for Weber sandstone is 0.01. The tectonic stresses were resolved along the plane of faulting determined by the focal solutions of nearby earthquakes to give shear and normal stresses of 72 bars and 342 bars respectively. The critical pressure required to initiate fracturing using these values is $P_c = 257$ bars.

To test if the critical pressure is correct the pressure at the bottom of four wells was raised to between 235 and 275 bars between October 1969 and November 1970. There were 900 events in this period, 367 of them within 1 km of the wells. The wells were then sealed until 1971 and the pressure dropped in one hole from 275 to 203 bars. The number of events/month dropped from an average of 28 in the previous year to 1 event/month. In May 1971 injection was restarted. In well FEE-69, the pressure was raised to 265 bars and the activity remained low at 1 event/month. Due to production charges at other parts of the oilfield the drainage pattern was altered at this time. A booster pump was required to raise the pressure to about 275 bars. Between October 1972 and January 1973 with the pressure between the critical 257 bars and 275 bars, the monthly average rose to 6 events/month. Between January and March

1973 with the pressure about 280 bars, monthly average rose sharply to 26 events/month. Backflow was initiated in May 1973 and no events have occurred within one kilometer since that day. A summary of the result is shown in figure 1.13.

The consequence of the work described in this chapter are two-fold. It is clear that the presence of water certainly has an affect on induced seismicity and the effective stress concept has been shown to be sufficient to describe the triggering situation. It is on this basis that we approach the problem of seismicity at lakes. From the conclusions made it is necessary to propose a model which will explain the observed seismic features. The first model which will be introduced is one in which the weight of the water in the lake acts as a vertical surface load on an elastic layered half space. The second, and more important, is one in which the weight of the water acts on a permeable layered medium. The relation between these models and the available data is discussed.

Figure 1.13: The number of earthquakes per month and reservoir pressure are plotted at Rangely. The critical fluid pressure is shown. Notice a decrease in seismic activity when the well pressure was below the critical level. (Modified from Raleigh et. al. (1975))



Chapter 2.

The Three Dimensional Analysis of a Load on an Elastic Half Space

2.1 Point Force Solutions

The calculation of the response of a non-gravitating elastic half space to surface pressure is called the "Boussinesq" problem. It avoids the complications introduced by including the action of water in the rock and is a good starting point for the stress calculations which follow. The water is assumed to be a passive surface load. It is treated as if it were an equivalent block of ice applying a vertical load to the surface of a perfectly elastic half space. The elastic behaviour is justified since, as will be derived later, deflections are of the order of 10 cm over distances of 10 km: a strain of the order of 10^{-9} cm/cm. This is well within the elastic limit of most rocks.

Solutions of Boussinesq problems are common, and most engineering texts give examples, (Timoshenko and Goodier 1970) and a good treatment of geophysical problems was given by Farrell (1972). The application to lake loading was first done by Gough and Gough (1970 a,b) at Kariba. They represented the lake as 1302 point forces equal to the average pressure over rectangles 2.2x2.3 km. A considerable effort was necessary to determine these forces and a

description of attempts to find an easier method is given in a later section.

The stresses and displacements for a point force $\cdot F(0,0,0)$ at a point $P(x,y,z)$ are given by:

$$\sigma_x = \sigma_\theta \sin^2 \theta + \sigma_r \cos^2 \theta$$

$$\sigma_y = \sigma_r \sin^2 \theta + \sigma_\theta \cos^2 \theta$$

$$\sigma_z = \sigma_z$$

$$\tau_{xy} = (\sigma_r - \sigma_\theta) \sin \theta \cos \theta$$

$$\tau_{xz} = \tau_{rz} \cos \theta$$

$$\tau_{yz} = \tau_{rz} \sin \theta$$

and the vertical deflection:

$$w = \frac{F}{2\pi Y} \left\{ \frac{(1+\nu) z^2}{R^3} + \frac{2(1-\nu^2)}{R} \right\} \quad -2.1$$

where:

$$\sigma_r = \frac{F}{2\pi} \left(\frac{1-2\nu}{r^2} \left(1 - \frac{z}{r} \right) - \frac{3r^2 z}{R^5} \right)$$

$$\sigma_z = - \frac{3F}{2\pi} \frac{z^3}{R^5}$$

$$\sigma_\theta = \frac{F(1-2\nu)}{2\pi} \left(- \frac{1}{r^2} + \frac{z}{r^2 R} + \frac{z}{R^3} \right)$$

$$\tau_{rz} = - \frac{3F}{2\pi} \frac{rz^2}{R^5}$$

These are derived in Timoshenko and Goodier (1970) and are used by Gough and Gough. In these equations:

$$R^2 = x^2 + y^2 + z^2$$

$$r^2 = x^2 + y^2$$

$$\tan \theta = y/x$$

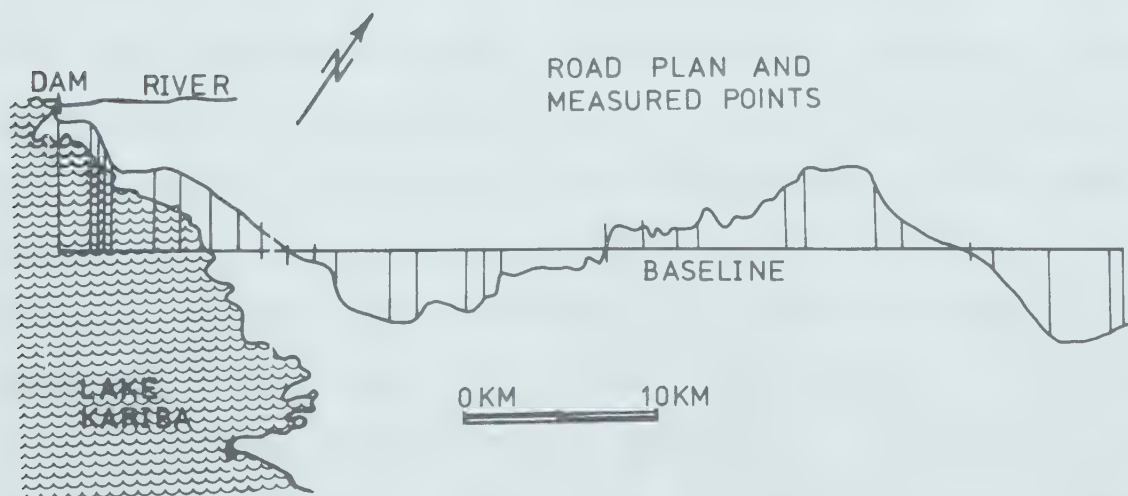
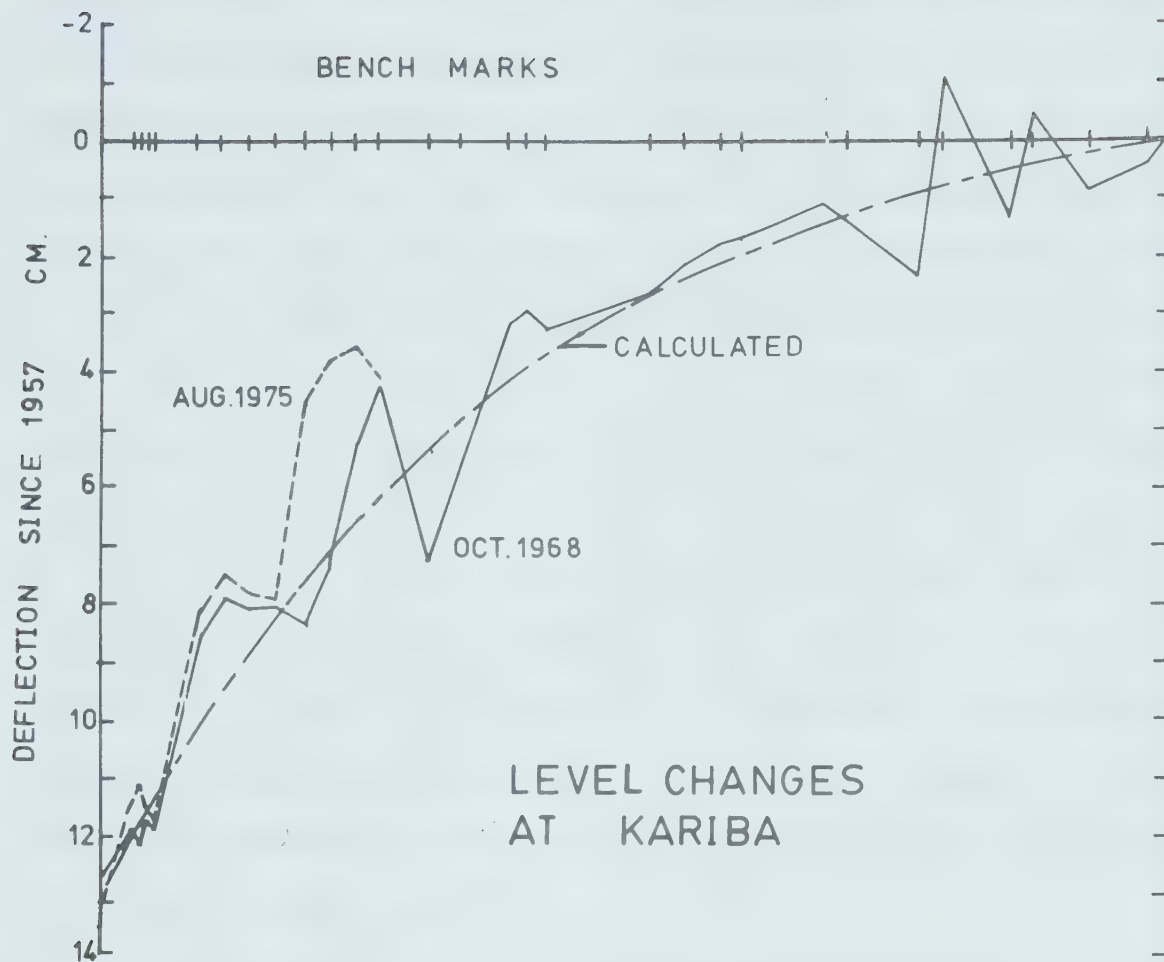
ν Poisson's Ratio

Y Young's Modulus

Kariba reservoir is about 200 km long, 25 km wide and is 80 metres deep. The largest vertical deflection at 3 km below the lake was 23 cm. The largest vertical stress, σ_1 , was about 8 bars under the deepest section of the lake. The maximum shear stress was about 2.1 bars again under the deepest part of the lake. There is little point in reproducing contours of these results at this stage. Later an alternate method will be developed for finding stress and displacement .

The elastic constants were taken from values published by Birch (1966). The values were $\nu=0.27$ and $Y=0.85$ Mbar which are consistent with a sound, intact rock. The displacements at Kariba were compared with road levelling done near the dam wall (Sleigh 1976). The results are shown in figure 2.1. They show an excellent agreement between the calculated and observed vertical deflection. The agreement confirms that analytic techniques can be applied to rock deflection over a scale of 10's of kilometers. The relelevelling has been repeated by Sleigh (1976) and little change is seen. Some deviation is noted in areas of Karroo sediment ; this is probably due to hydration.

Figure 2.1: Observed and calculated deflection measured along a roadbed near Kariba in Rhodesia. The calculated deflection was computed by the Gough and Gough (1970a) point force technique.
(Modified from Sleigh (1976))



The solutions obtained by summing the contribution of point forces has several advantages as well as disadvantages. As Gough and Gough showed in their 1976 analysis of Cabora Bassa, the point forces need not be equispaced. In sections of the lake which are long and thin, or, in which the depth changes rapidly, higher sampling rates may be made. The solution for the displacement (2.1) is of a $1/R$ form and is numerically indeterminate close to the point force. Gough and Gough (1970a) avoid these singularities by computing no closer than $4/3$ of the force separation. This is also justified since the approximation of the lake by point forces breaks down closer than this. The assumption of a flat surface and vertical loading is violated too close to the surface. The largest disadvantage of the technique, acknowledged by Gough and Gough, is the cost of computation. 14 minutes was required for a vertical section on an IBM 360-67.

The technique of summing point force contributions has been applied by Beck (1975) to Oroville in California. From the bathymetry, displacements and maximum shear stresses were computed. The largest shear stress was 3.4 bars under the deepest part of the lake. This value is larger than Kariba's maximum shear stress of 2.1 bars since Oroville is about twice as deep as Kariba. The maximum vertical displacement was estimated to be around 5.5 cm, again at the deepest lake section. Beck has extended the point force

solution to the surface by apparently trying to compute between the forces. He admits the deflection contours are seriously distorted by local effects. These distortions have been smoothed from the final results. These distortions could have been predicted during computation due to the $1/R$ singularity in displacement.

Another technique has been developed by Lee (1972). The Boussinesq problem was solved by a Fourier-Bessel expansion in cylindrical coordinates. The lake was approximated by a pattern of elemental loads, each shaped as sections of an annulus. The method is shown to be able to compute the displacements with the elastic parameters varying with depth. The expression for the vertical displacement is:

$$u(r, \theta, z) = \sum_{\text{elements}, i} \frac{T_i (1+2\nu) (1-\nu)}{\pi Y} \int_{A_i}^{B_i} [(V(b_i) - V(a_i)) + z^2 (W(b_i) - W(a_i))] d\alpha$$

where:

$$V(x) = [x^2 + r^2 - 2rx \cos(\theta - \alpha) + z^2]^{\frac{1}{2}} + r \cos(\theta - \alpha) \times \\ \times \ln \left[\left\{ \frac{x - r \cos(\theta - \alpha)}{(z^2 + r^2 \sin^2(\theta - \alpha))^{\frac{1}{2}}} \right\} * \left\{ \frac{z^2 + r^2 + x^2 - 2rx \cos(\theta - \alpha)}{z^2 + r^2 \sin^2(\theta - \alpha)} \right\}^{\frac{1}{2}} \right]$$

and:

$$W(x) = \frac{[xr \cos(\theta - \alpha) - z^2 - r^2]}{[z^2 + r^2 \sin^2(\theta - \alpha)] [x^2 + r^2 - 2rx \cos(\theta - \alpha) + z^2]^{\frac{1}{2}}}$$

$V(r, \theta, z)$: is the vertical displacement at (r, θ, z) relative to an established cylindrical coordinate origin.

T: is the average pressure over an area bounded by radii a and b and subtended between the angles A and B .

Y: is Young's Modulus and ν is Poisson's ratio.

The summation is taken over each of the elements used in the approximation of the lake load.

Lee did the computation by a five point Newton-Coates technique for Lake Gordon in Tasmania. The lake's shape was approximated by 51 elements and the computation was done at 598 points. No description is given of the treatment of singularities or the efficiency of the computation.

2.2 A Transform Solution of Boussinesq's Problem

For any material the conservation of forces and moments leads to the equilibrium equation:

$$F_i + \sigma_{ij,j} = 0 \quad i,j=1,2,3$$

where σ_{ij} is the stress component applied in the direction i to the plane whose normal is in the j direction. F_i are the body forces in the i direction. Normal index notation will be used with indices having values 1,2 or 3 unless otherwise specified. Repeated indices indicate summation over the index, and commas indicate differentiation with respect to the variable. There are six independent stresses due to the symmetry of the stress tensor, so:

$$\sigma_{ij} = \sigma_{ji}$$

For small deformations the material behaves elastically with stress linearly related to strain.

$$\sigma_{ij} = C_{ijkl} e_{kl}$$

The strains are defined by:

$$e_{ij} = \frac{1}{2} \left(\frac{\partial u_i}{\partial x_j} + \frac{\partial u_j}{\partial x_i} \right)$$

where u_i is the deformation in the i direction relative to a cartesian coordinate system $u(x_1, x_2, x_3)$.

The C_{ijkl} are constants of proportionality. The 21 independent constants can be reduced to 9 if the material has symmetry of properties around 3 mutually perpendicular axes. If the elastic properties are the same in all directions (isotropic) the number of elastic constants reduces to 2. In all the following work Poisson's ratio, ν , and Young's Modulus, Y , are taken as the measured elastic properties. For an isotropic elastic material the stress-strain relationship reduces to:

$$\sigma_{ij} = \frac{Y}{(1+\nu)} \left[\frac{\nu}{(1-2\nu)} \delta_{ij} e_{kk} + e_{ij} \right] \quad -2.2$$

To examine the stresses created by the application of a surface load to an elastic half space the equilibrium condition is differentiated to yield:

$$\nabla(\nabla \cdot \underline{u}) + (1-2\nu) \nabla^2 \underline{u} = 0 \quad -2.3$$

Landau and Lifshitz (1957 pp26-29) show that this equation can be reduced by replacing the displacement vector, \underline{u} , as:

$$\underline{u} = \underline{f} + \nabla \phi \quad -2.4$$

where \underline{f} is a harmonic vector $\nabla^2 \underline{f} = 0$. \underline{f} is partly re-

expressed in terms of another harmonic vector:

$$f_x = \frac{\partial g_x}{\partial z} \quad f_y = \frac{\partial g_y}{\partial z}$$

$$\nabla^2 g_x = 0 \quad \nabla^2 g_y = 0$$

Substituting into (2.2) yields:

$$\Phi = \frac{-z}{4(1-\nu)} \left(f_z + \frac{\partial g_x}{\partial x} + \frac{\partial g_y}{\partial y} \right) + \psi \quad -2.5$$

where ψ is another harmonic scalar. A Cartesian coordinate system has been chosen with z positive below the surface on which the forces are applied. For the complete description of the solution g_x, g_y, f_z and ψ are required. These are found from the boundary conditions at $z=0$. At the surface $\sigma_{iz} = -P_i$ where P_i are the applied forces in the x , y , and z directions. The negative sign is the normal convention to indicate that the surface is under compression. Tensional forces are positive.

Expressing u in terms of the four unknowns, and substituting into (2.2) yields the conditions at $z=0$:

$$\left. \frac{\partial^2 g_x}{\partial z^2} \right|_{z=0} + \left[\frac{\partial}{\partial x} \left\{ \frac{(1-2\nu)}{2(1-\nu)} f_z - \frac{1}{2(1-\nu)} \left(\frac{\partial g_x}{\partial x} + \frac{\partial g_y}{\partial y} \right) + 2 \frac{\partial \psi}{\partial z} \right\} \right] \Big|_{z=0}$$

$$= -2(1+\nu) P_x / Y$$

$$\left. \frac{\partial^2 g_y}{\partial z^2} \right|_{z=0} + \left[\frac{\partial}{\partial y} \left\{ \frac{(1-2\nu)}{2(1-\nu)} f_z - \frac{1}{2(1-\nu)} \left(\frac{\partial g_x}{\partial x} + \frac{\partial g_y}{\partial y} \right) + 2 \frac{\partial \psi}{\partial z} \right\} \right] \Big|_{z=0}$$

$$= -2(1+\nu) P_y / Y$$

$$\left[\frac{\partial}{\partial z} \left\{ f_z - \frac{\partial g_x}{\partial x} + 2 \frac{\partial \psi}{\partial z} \right\} \right] \bigg|_{z=0} = - \frac{2(1+\nu) P_z}{Y} \quad -2.6$$

A further condition is required to uniquely define the four unknowns. Landau and Lifshitz show that it is convenient and noncontradictory to set:

$$(1-2\nu) f_z - \left(\frac{\partial g_x}{\partial x} + \frac{\partial g_y}{\partial y} \right) + 4(1-\nu) \frac{\partial \psi}{\partial z} = 0 \quad -2.7$$

The first two relations of (2.6) become:

$$\frac{\partial^2 g_x}{\partial z^2} \bigg|_{z=0} = - \frac{2(1+\nu) P_x}{Y} \quad -2.8$$

$$\frac{\partial^2 g_y}{\partial z^2} \bigg|_{z=0} = - \frac{2(1+\nu) P_y}{Y}$$

Green's theorem is used for the solution of ψ and f_z . The theorem may be simply stated. If a function is harmonic, is zero at infinity, and has derivative $\partial f / \partial z$ at $z=0$, then:

$$f(x, y, z) = - \frac{1}{2\pi} \iint \frac{\partial F(x', y', z)}{\partial z} \bigg|_{z=0} \frac{dx' dy'}{R}$$

The integral is taken over the area of definition of f . R^2 is defined as $(x-x')^2 + (y-y')^2 + z^2$. Treating the load as a vertical force, P_z , or a free surface with $f_x = f_y = 0$ and

$\sigma_{xz} = \sigma_{yz} = 0$ then:

$$\frac{\partial \psi}{\partial z}(x, y, z) = - \frac{(1+\nu)(1-2\nu)}{2\pi Y} \iint \frac{P_z(x', y') \partial x' \partial y'}{[(x-x')^2 + (y-y')^2 + z^2]^{\frac{3}{2}}}$$

$$f_z(x, y, z) = \frac{2(1-\nu)(1+\nu)}{\pi Y} \iint \frac{P_z(x', y') \partial x' \partial y'}{[(x-x')^2 + (y-y')^2 + z^2]^{\frac{3}{2}}}$$

From the knowledge of $\frac{\partial \psi}{\partial z}$, $\frac{\partial \psi}{\partial x}$ and $\frac{\partial \psi}{\partial y}$ can be obtained by integrating $\frac{\partial \psi}{\partial z}$ over the variable z and then differentiating.

The solutions used by Gough and Gough (1970a) for the point force are easily obtainable at this stage by examining the z displacement due to a point force $F \cdot \delta(x') \cdot \delta(y')$ From equation (2.4):

$$\begin{aligned} u_z &= f_z + \frac{\partial \phi}{\partial z} \\ &= \frac{(3-4\nu)}{4(1-\nu)} f_z - \frac{z}{4(1-\nu)} \frac{\partial f_z}{\partial z} + \frac{\partial \psi}{\partial z} \end{aligned}$$

f_z and $\frac{\partial \psi}{\partial z}$ can be found from (2.9).

$$\frac{\partial \psi}{\partial z} = - \frac{(1+\nu)(1-2\nu)}{2\pi Y} \frac{P}{r}$$

$$f_z = \frac{2(1-\nu)(1+\nu)}{\pi Y} \frac{P}{r}$$

$$\frac{\partial f_z}{\partial z} = - \frac{2(1-\nu)(1+\nu)}{\pi Y}$$

Therefore:

$$u_z = \frac{F}{2\pi Y} \left[\frac{2(1-\nu^2)}{r} + \frac{z^2(1+\nu)}{r^3} \right]$$

This agrees with equation (2.1). Similar techniques are used in the determination of u, v . The integral (2.271-4, p86) of Gradshteyn and Ryzhik (1965) is necessary for these computations.

$$\int \frac{dz}{(x^2+y^2+z^2)^{\frac{1}{2}}} = \ln(z + (x^2+y^2+z^2)^{\frac{1}{2}})$$

The σ_{ij} stresses are found by differentiating.

For the lake , the surface load is continuous. Equation (2.9) can be solved using a Fourier Transform to remove the integration variables x', y' . Multiplying both sides of (2.9) of f_z by the transform variable and integrating over x, y gives:

$$\iint_{-\infty}^{\infty} f_z(x, y, z) e^{ipx} e^{iqy} dx dy = \frac{2(1-\nu)(1+\nu)}{\pi Y} \times \\ \times \int \frac{P(x', y') dx' dy' e^{ipx} e^{iqy}}{((x-x')^2 + (y-y')^2 + z^2)^{\frac{1}{2}}} dx dy$$

p and q are the Fourier transform variables, or wave numbers, for x and y . Using the substitutions:

$$\begin{aligned} x - x' &= r \cos \theta & y - y' &= r \sin \theta \\ p &= u \cos \phi & q &= u \sin \phi \end{aligned}$$

and the notation:

$$\begin{aligned} \tilde{g}(p, q, z) &= \iint_{-\infty}^{\infty} g(x, y, z) e^{ipx} e^{iqy} dx dy \\ g(x, y, z) &= \frac{1}{2\pi} \iint_{-\infty}^{\infty} \tilde{g}(p, q, z) e^{-ipx} e^{-iqy} dp dq \end{aligned}$$

the transformed equations become:

$$\begin{aligned} \tilde{f}_z &= \frac{2(1-\nu)(1+\nu)}{\pi Y} \iint_{-\infty}^{\infty} P(x', y') e^{ipx'} e^{iqy'} dx' dy' \\ &\int_0^{2\pi} \int_0^{\infty} \frac{e^{iru \cos(\theta-\phi)} r dr d\phi}{(r^2 + z^2)^{\frac{1}{2}}} \end{aligned}$$

Using Gradshteyn and Ryzhik (henceforth G.R.) (3.915, p482), (6.554, p682)

$$\int_0^{\pi} \cos(nx) e^{i\beta \cos x} dx = i^n \pi J_n(\beta) \quad (J_n \text{ is a Bessel function})$$

$$\int_0^{\infty} \frac{x J_0(xy) dx}{(x^2 + a^2)^{\frac{1}{2}}} = \frac{1}{y} e^{-ay} \quad (y > 0, \operatorname{Re} a > 0)$$

Solutions for f_z and ψ can be obtained:

$$\tilde{f}_z(p, q, z) = \frac{4(1-\nu)(1+\nu)}{Y} \frac{\tilde{P}(p, q)}{\sqrt{p^2 + q^2}} e^{-z\sqrt{p^2 + q^2}} \quad -2.10$$

$$\text{and} \quad \frac{\partial \tilde{\Psi}}{\partial z} = - \frac{(1+\nu)(1-2\nu)}{Y} \frac{\tilde{P}(p, q)}{\sqrt{p^2 + q^2}} e^{-z\sqrt{p^2 + q^2}}$$

$$\text{whence} \quad \tilde{\Psi}(p, q, z) = \frac{(1+\nu)(1-2\nu)}{Y} \frac{\tilde{P}(p, q)}{(p^2 + q^2)} e^{-z\sqrt{p^2 + q^2}} \quad -2.11$$

By using the transform of (2.4) and (2.5), the equation for the displacements can be found.

$$\tilde{u}_x(p, q, z) = \frac{(-ip)(1+\nu)}{Yk^2} [(1-2\nu) - zk] \tilde{P}(p, q) e^{-zk}$$

$$\tilde{u}_y(p, q, z) = \frac{(-iq)(1+\nu)}{Yk^2} [(1-2\nu) - zk] \tilde{P}(p, q) e^{-zk} \quad -2.12$$

$$\tilde{u}_z(p, q, z) = \frac{(1+\nu)}{Yk} [2(1-\nu) + zk] \tilde{P}(p, q) e^{-zk}$$

Where $k^2 = p^2 + q^2$. To compute the stresses, derivatives with respect to x, y and z are required. The z derivatives can all be done analytically, however the x and y derivatives are simplified by a property of Fourier transforms.

$$\frac{\partial \tilde{g}}{\partial x} = -ip \tilde{g}(p, q, z) \quad \text{and} \quad \frac{\partial^2 \tilde{g}}{\partial x^2} = -p^2 \tilde{g}(p, q, z)$$

It is tedious but routine to find:

$$\tilde{\sigma}_x(p, q, z) = \frac{1}{k^2} [-(p^2 + 2\nu q^2) + p^2 zk] \tilde{P}(p, q) e^{-zk}$$

$$\tilde{\sigma}_Y(p,q,z) = \frac{1}{k^2} [-(q^2 + 2\nu p^2) + q^2 zk] \tilde{P}(p,q) e^{-zk}$$

$$\tilde{\sigma}_Z(p,q,z) = - (1+zk) \tilde{P}(p,q) e^{-zk}$$

-2.13

$$\tau_{xy}(p,q,z) = \frac{pq}{k^2} [-(1-2\nu) + zk] \tilde{P}(p,q) e^{-zk}$$

$$\tilde{\tau}_{xz}(p,q,z) = - ipz \tilde{P}(p,q) e^{-zk}$$

$$\tilde{\tau}_{yz}(p,q,z) = - iqz \tilde{P}(p,q) e^{-zk}$$

The stresses and displacements can now be computed at a depth z . If we know the load $P(x,y)$ the $P(p,q)$ can be obtained by the fast Fourier transform (F.F.T) algorithm presented by Cooley and Tukey (1965). This algorithm is available at most large computing centres.

A singularity appears in the determination of the displacements. This difficulty exists for $p=q=0$. $P(0,0)$ corresponds to the integral of the load over the area transformed. It is the average load and in finite transforms is always non-zero. In order to avoid such computational singularities, we either subtract the D.C. level from the entire grid $P(x,y)$, before transforming, or do the inverse transforms in cylindrical coordinates. The first device is forced on us by our desire to use a F.F.T. algorithm. If the inverse transform is carried out in cylindrical coordinates, F.F.T. methods are not applicable. After inversion the D.C. contribution is added to the final

solution for the displacement.

The deflection and stresses due to a uniform square load can be derived from results in Love (1929). Love's solution can be computed at the surface if the edges of the square are avoided. The total solution can be found if the bounding area of the square is large relative to the size of the lake load. This should always be the case since it reduces to magnitude of the load on the square. For a rectangle of sides $2a$ by $2b$ centred at the origin of (x, y) each of the functions are evaluated four times due to the contribution of each edge of the rectangle.

$$f(x, y) = f(x+a, y+b) - f(x+a, y-b) + f(x-a, y-b) - f(x-a, y+b)$$

The displacements can be shown to be:

$$u = - \frac{(1+\nu)P}{2\pi Y} ((1-2\nu) \frac{\partial \chi}{\partial x} + z \frac{\partial V}{\partial x})$$

$$v = - \frac{(1+\nu)P}{2\pi Y} ((1-2\nu) \frac{\partial \chi}{\partial y} + z \frac{\partial V}{\partial y})$$

$$w = \frac{(1+\nu)P}{2\pi Y} (2(1-\nu)V - z \frac{\partial V}{\partial z})$$

The stresses are easily derivable from these:

$$\sigma_{xx} = \frac{P}{2\pi} (2\nu \frac{\partial V}{\partial z} - (1-2\nu) \frac{\partial^2 \chi}{\partial x^2} - z \frac{\partial^2 V}{\partial x^2})$$

$$\sigma_{yy} = \frac{P}{2\pi} (2\nu \frac{\partial V}{\partial z} - (1-2\nu) \frac{\partial^2 \chi}{\partial y^2} - z \frac{\partial^2 V}{\partial y^2})$$

$$\sigma_{zz} = \frac{P}{2\pi} (\frac{\partial V}{\partial z} - z \frac{\partial^2 V}{\partial z^2})$$

$$\sigma_{xz} = - \frac{Pz}{2\pi} \frac{\partial^2 V}{\partial x \partial z} \qquad \sigma_{yz} = - \frac{Pz}{2\pi} \frac{\partial^2 V}{\partial y \partial z}$$

$$\sigma_{xy} = - \frac{P}{2\pi} ((1-2\nu) \frac{\partial^2 \chi}{\partial x \partial y} + z \frac{\partial^2 V}{\partial x \partial y})$$

The potentials χ and V are:

$$\chi = \iiint \log(z+R) \, dx' dy'$$

$$V = \iiint \frac{dx' dy'}{R}$$

$$\text{where } R^2 = (x-x')^2 + (y-y')^2 + z^2$$

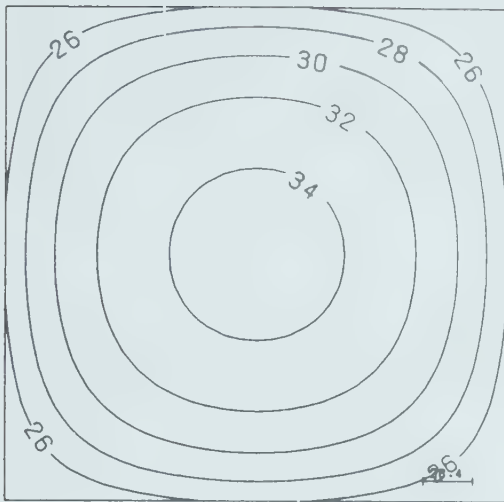
V may be shown from G.R. (2.261 p81, 2.266 p84, 2.267-1 p84) and partial integration to be

$$V = x \ln(y+r) + y \ln(x+r) - z \arcsin\left(\frac{z^2+y^2+yr}{(y+r)(y^2+z^2)^{\frac{1}{2}}}\right)$$

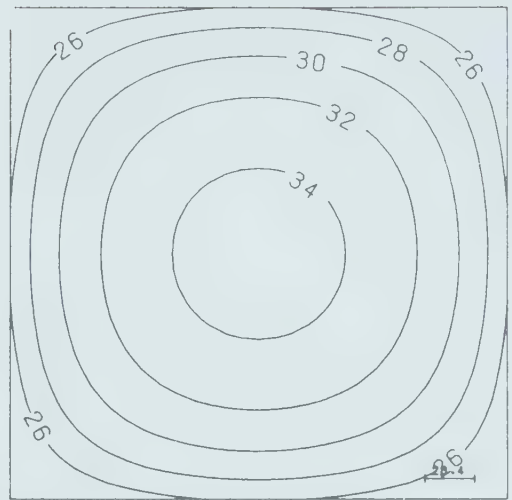
The remaining derivatives of V , can be calculated in a straightforward manner.

Figure 2.2 shows the vertical displacements below 1 bar pressure on a square of 284.16 km. This length had been chosen to agree with the Kariba results presented later. Figure 2.2 shows the computation at 0 km and at 13 km deep are only slightly different. This indicates the displacement changes slightly close to the surface. Figure 2.3 shows the stress 10 km below a rectangle on which is applied a one bar pressure. Figures 2.4 and 2.5 show displacements and stresses below a square with a side of 100 km. The same elastic parameters used by Gough and Gough (1970a) were chosen. The bar figure in the lower right of each of these diagrams is one tenth the length of the square. the length of the bar is given in kilometers.

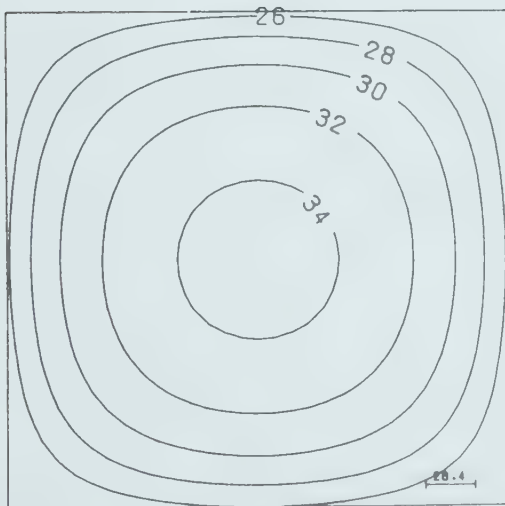
Figure 2.2: Vertical displacements at several depths below a 1 bar pressure applied over a square of side length 284 km. The elastic parameters of the halfspace were Poisson's ratio of 0.27 and Young's Modulus 0.85 Mbar. The equations derived by Love were used.



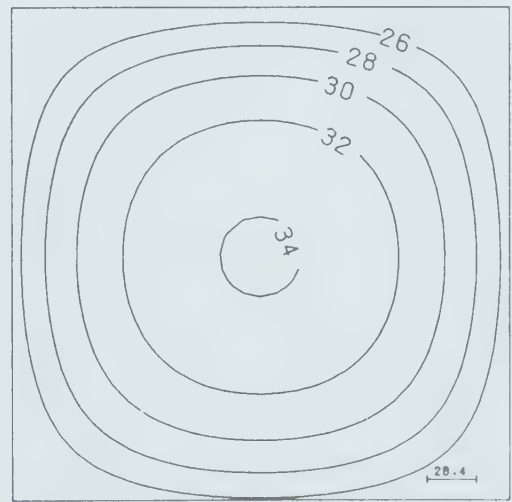
VERT. DISPLACEMENT (CM)
DEPTH= 0 WITH SIGMA=0.27 YOUNG=0.85MBAR



VERT. DISPLACEMENT (CM)
DEPTH= 3 WITH SIGMA=0.27 YOUNG=0.85MBAR

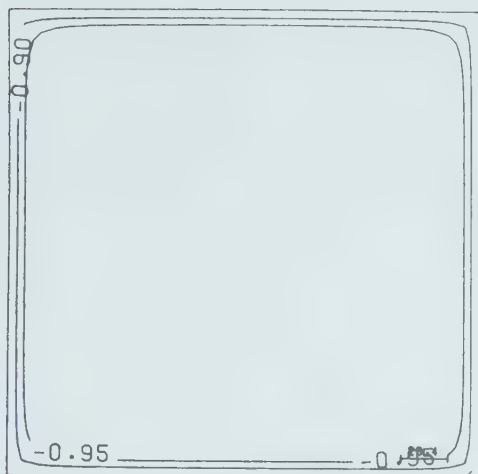


VERT. DISPLACEMENT (CM)
DEPTH= 13 WITH SIGMA=0.27 YOUNG=0.85MBAR

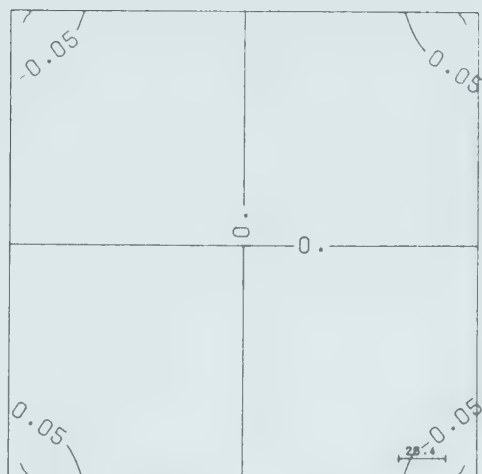


VERT. DISPLACEMENT (CM)
DEPTH= 30 WITH SIGMA=0.27 YOUNG=0.85MBAR

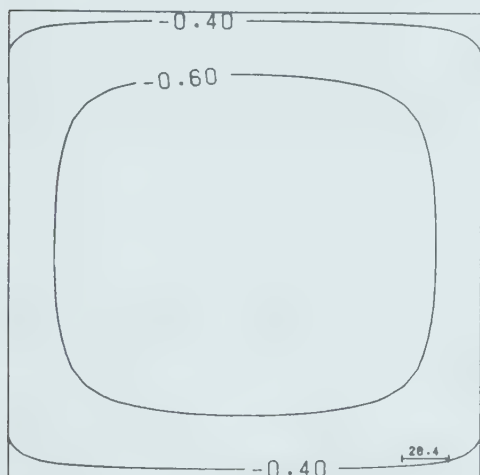
Figure 2.3: Stresses at 13 km below a unit pressure applied to a square of side 284 km.



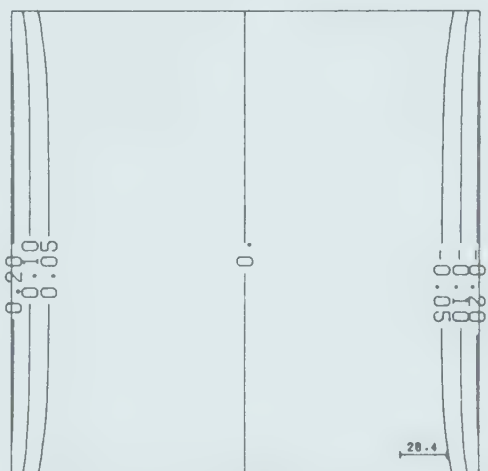
SIGZZ (BARS)
DEPTH= 13 WITH SIGMA=0.27 YOUNG=0.85MBAR



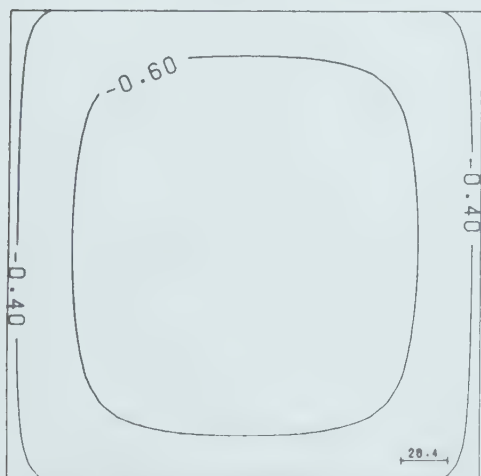
SIGXY (BARS)
DEPTH= 13 WITH SIGMA=0.27 YOUNG=0.85MBAR



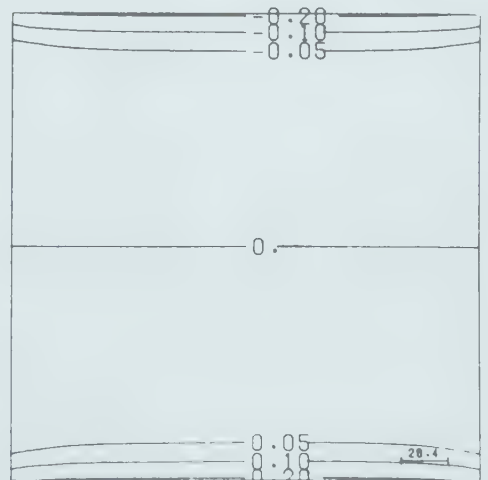
SIGXX (BARS)
DEPTH= 13 WITH SIGMA=0.27 YOUNG=0.85MBAR



SIGYZ (BARS)
DEPTH= 13 WITH SIGMA=0.27 YOUNG=0.85MBAR

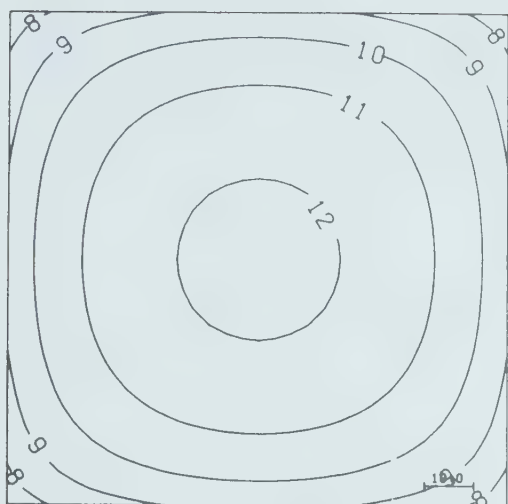


SIGYY (BARS)
DEPTH= 13 WITH SIGMA=0.27 YOUNG=0.85MBAR

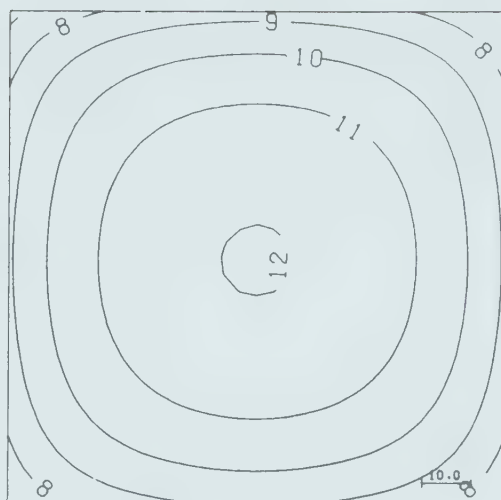


SIGXZ (BARS)
DEPTH= 13 WITH SIGMA=0.27 YOUNG=0.85MBAR

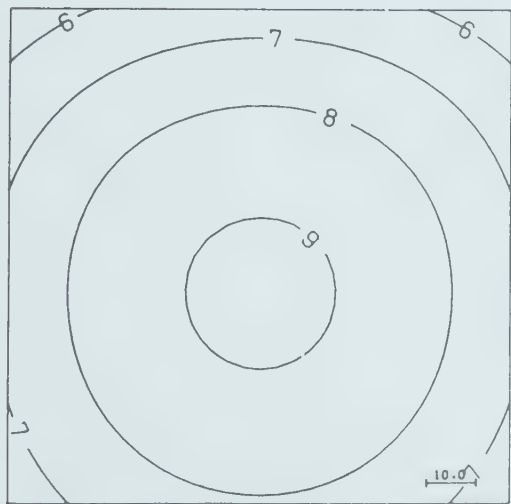
Figure 2.4: Vertical displacement at several depths below a unit pressure of 1 bar applied to a square with sides of 100 km.



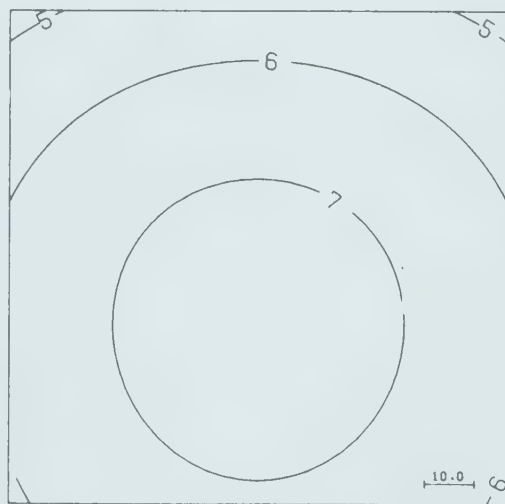
VERT. DISPLACEMENT (CM)
DEPTH= 0 WITH SIGMA=0.27 YOUNG=0.85MBAR



VERT. DISPLACEMENT (CM)
DEPTH= 10 WITH SIGMA=0.27 YOUNG=0.85MBAR

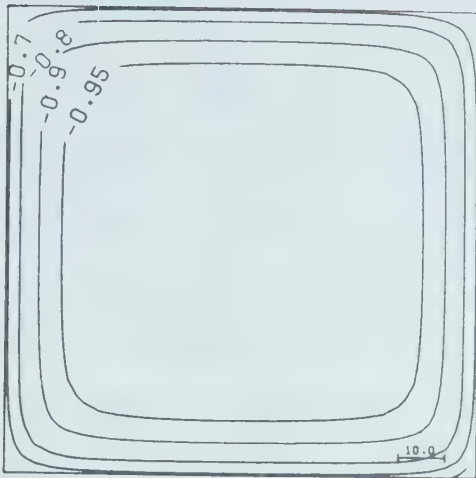


VERT. DISPLACEMENT (CM)
DEPTH= 50 WITH SIGMA=0.27 YOUNG=0.85MBAR



VERT. DISPLACEMENT (CM)
DEPTH= 75 WITH SIGMA=0.27 YOUNG=0.85MBAR

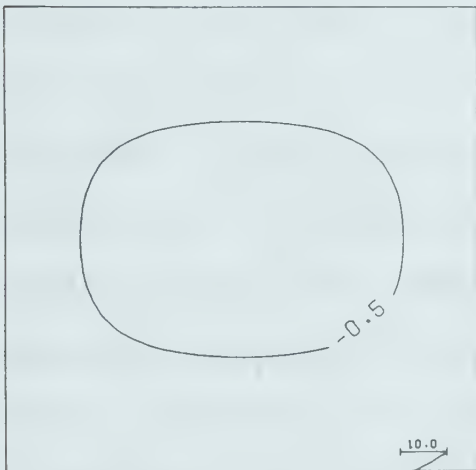
Figure 2.5: Stresses at 10 km below a square of side 100 km on which a unit pressure of 1 bar is applied. The solutions were obtained by the equations derived by Love.



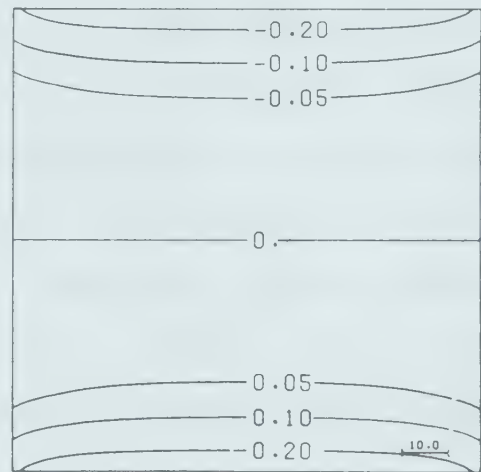
SIGZZ (BARS)
DEPTH= 10 WITH SIGMA=0.27 YOUNG=0.85MBAR



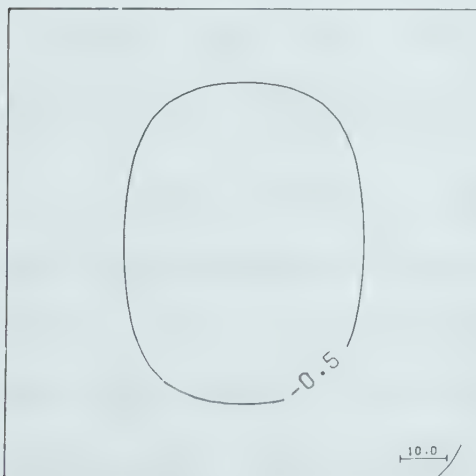
SIGXY (BARS)
DEPTH= 10 WITH SIGMA=0.27 YOUNG=0.85MBAR



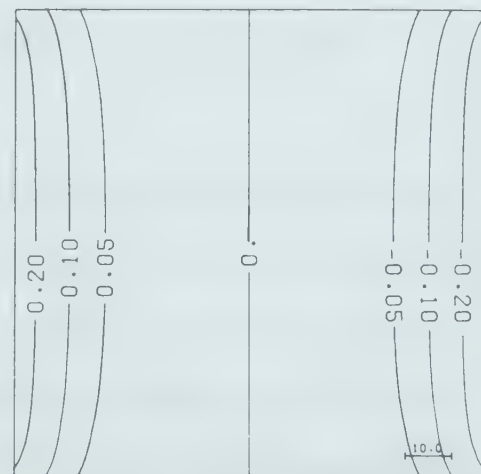
SIGXX (BARS)
DEPTH= 10 WITH SIGMA=0.27 YOUNG=0.85MBAR



SIGXZ (BARS)
DEPTH= 10 WITH SIGMA=0.27 YOUNG=0.85MBAR



SIGYY (BARS)
DEPTH= 10 WITH SIGMA=0.27 YOUNG=0.85MBAR



SIGYZ (BARS)
DEPTH= 10 WITH SIGMA=0.27 YOUNG=0.85MBAR

2.3 An example of Transform Techniques

The computation of the stress and displacement was undertaken for Lake Kariba. The point force magnitudes and positions obtained from the bathymetry were supplied to us by Dr. and Mrs. Gough. The pressures were the average depths over rectangles of 2.2x2.3 km. Over 1000 point forces were used. This data was placed onto a regular grid of up to 256x256 nodes. The 'D.C.' level of the load was removed and a two dimensional transform was taken using a library F.F.T. routine. The F.F.T. programme was a standard IBM routine 'HARM' supplied in their Scientific Subroutine Package. Singleton (1969) has published a listing and explanation of another F.F.T. programme. The transformed load was multiplied by the appropriate functions and the inverse transform was taken. A grid of 64x64 element was usually found adequate although larger grids can be handled efficiently. On the IBM 360/67 only a single stress component or displacement could be computed at one time for a 256x256 grid. The difficulty involved the storage of the 65536 source point forces.

On the Kariba example we found the results using the F.F.T. routines cost about 1/8 of what the Gough method cost (64x64 grid). If the accuracy criteria are relaxed to 5 per cent agreement, this fraction can become as small as 1/20 (32x32 grid). The loss of agreement is directly related to how frequently the lake is sampled by the grid nodes. There

are penalties when the grid is reduced. Transforming digitised data imprecisely on a limited grid may introduce aliased components of displacement and stress near sharp gradients of load, (see Kanasewich (1976)). It should be emphasised that routine processing and improved data can reduce these errors.

The displacements and eigenvalues of the stress matrix were computed at several depths. From the eigenvalues the maximum shear stress was calculated:

$$\tau_{\max} = \frac{\sigma_{\max} - \sigma_{\min}}{2}$$

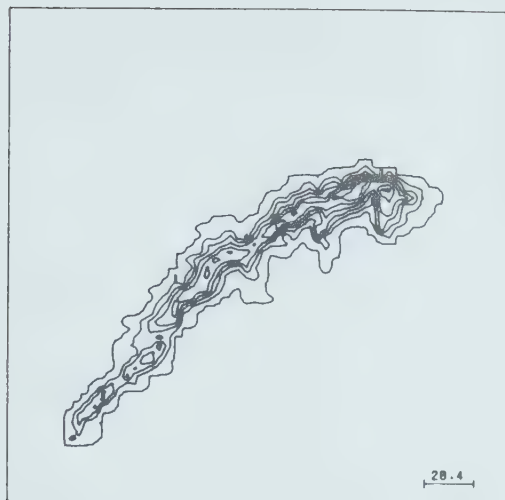
where σ_{\max} and σ_{\min} are the maximum and minimum eigenvalues of the stress matrix. The displacements, maximum shear stresses and shear planes at 0., 3., 13., and 30., Km are shown in figures 2.6, 2.7, 2.8. The derived stresses are everywhere within several per cent of the results of Gough and Gough (1970a). Since more points were computed for the contours the extra detail is probably real.

The deflection at 0. km, shown in figure 2.6, differs little from that of Gough and Gough at 3 km. This result reinforces the comparison between the computed and measured releveing data shown in figure 2.1.

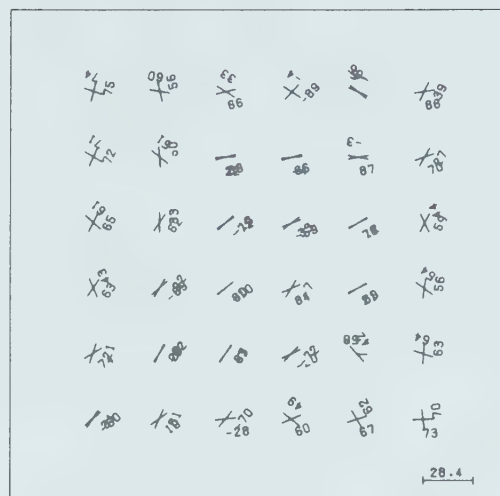
2.4 Generalisation to Regular Loads

The prime advantage of the transform technique is its

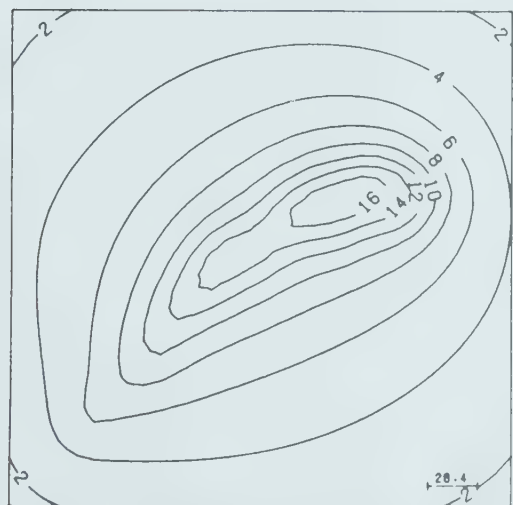
Figure 2.6: The maximum shear stress, vertical deflection and the planes along which the maximum shear stress acts are shown at 13 km below Lake Kariba. The position and bathymetry of the Lake are also shown. The two planes are each described by the azimuth of the symbol and the dip angles.



BATHYMETRY (M)
10M CONTOURS



SHEAR PLANES
DEPTH= 13 WITH SIGMA=0.27 YOUNG=0.85MBAR



VERT. DISPLACEMENT (CM)
DEPTH= 13 WITH SIGMA=0.27 YOUNG=0.85MBAR

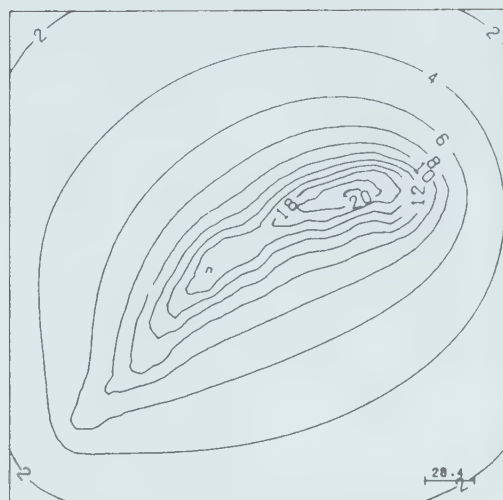


MAX. SHEAR STRESS (BARS)
DEPTH= 13 WITH SIGMA=0.27 YOUNG=0.85MBAR

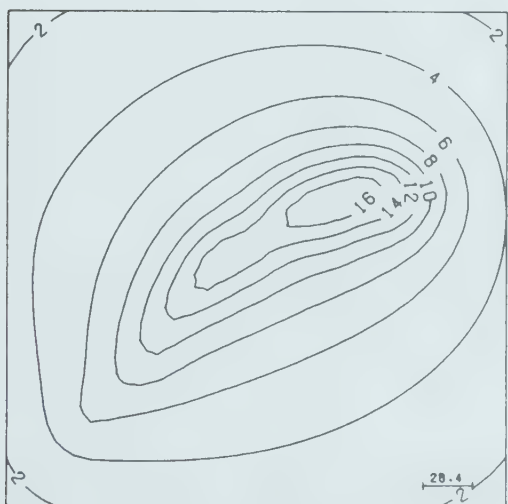
figure 2.7: Vertical deflections at several depths below Lake Kariba. The contours at 0 km depth are at 2 cm intervals.



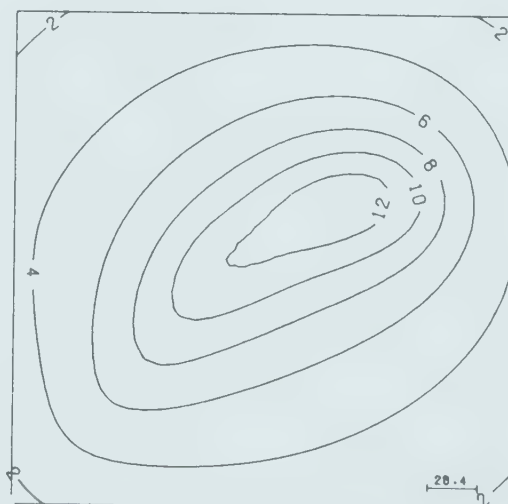
VERT. DISPLACEMENT (CM)
 DEPTH= 0 WITH SIGMA=0.27 YOUNG=0.85MBAR
 2. CM CONTOURS



VERT. DISPLACEMENT (CM)
 DEPTH= 3 WITH SIGMA=0.27 YOUNG=0.85MBAR

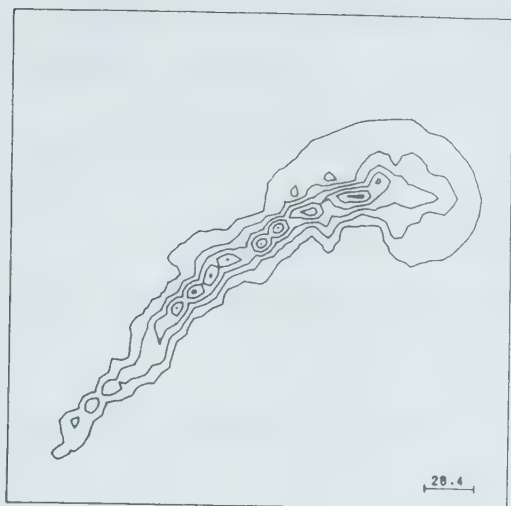


VERT. DISPLACEMENT (CM)
 DEPTH= 13 WITH SIGMA=0.27 YOUNG=0.85MBAR

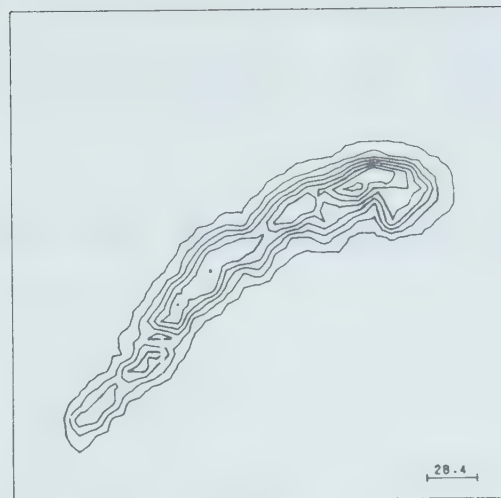


VERT. DISPLACEMENT (CM)
 DEPTH= 30 WITH SIGMA=0.27 YOUNG=0.85MBAR

Figure 2.8: The maximum shear stress at several depths below Lake Kariba



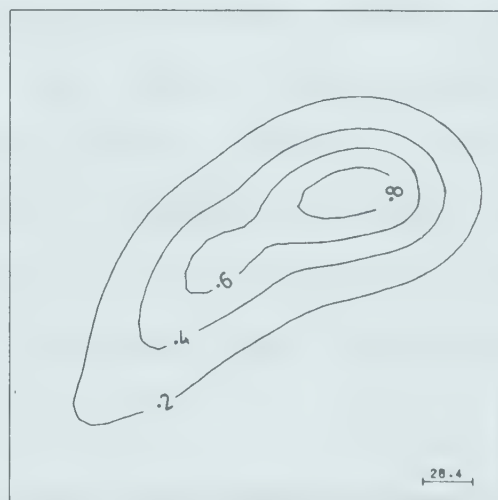
MAX. SHEAR STRESS (BARS)
 DEPTH= 0 WITH SIGMA=0.27 YOUNG=0.85MBAR
 0.2 BAR CONTOURS



MAX. SHEAR STRESS (BARS)
 DEPTH= 3 WITH SIGMA=0.27 YOUNG=0.85MBAR



MAX. SHEAR STRESS (BARS)
 DEPTH= 13 WITH SIGMA=0.27 YOUNG=0.85MBAR



MAX. SHEAR STRESS (BARS)
 DEPTH= 30 WITH SIGMA=0.27 YOUNG=0.85MBAR

ability to handle irregular shaped loads efficiently. In some circumstances a large computer may not be available and an analytic treatment is desired. The integrals involved are usually difficult to solve and little attention has been given to the method.

In some instances the reservoir may be approximated by one or more ellipsoids. The ellipsoid:

$$\left(\frac{x-x'}{a}\right)^2 + \left(\frac{y-y'}{b}\right)^2 + \left(\frac{z}{c}\right)^2 = 1$$

would transform to give the pressure:

$$\tilde{P}(p,q) = \frac{\rho g abc 2^{1/2} \pi^{3/2} J_{3/2}(\beta)}{\beta^{3/2}}$$

where $\beta^2 = (ap)^2 + (bq)^2$, ρ is the load density and $J_{3/2}$ is the Bessel function of order 3/2. A program was written to fit a small group of best fitting ellipsoids for Lake Kariba by least-squares methods. It was slow. For the most general ellipsoidal orientation the fitting alone required almost the same computing time as the complete solution by transform methods. This penalty may be acceptable in computers with small memories in which large transforms cannot be done.

The technique is also amenable to two dimensions. If the lake is straight, with the length about three or more times greater than the width, two dimensional analysis gives excellent results. The equations are easily obtained by setting $q=0$ in (2.12), (2.13).

2.5 Generalisation to a Layered Half Space

The generalisation to the layered half-space follows directly from the derivations in section 2.2. The extension is made by considering the boundary conditions at each layer. Equations (2.2) to (2.8) are applicable, but as f_x and f_y can no longer be neglected at each interface equation (2.9) no longer applies.

Each of the four unknowns ψ , f_z , g_x , g_y are transformed and are separated into two exponential components as follows:

$$\tilde{f}(p, q) = \iint_{-\infty}^{\infty} f(x, y) e^{i(px+qy)} dx dy$$

$$\tilde{g}_x = \tilde{g}_x^+ e^{-kz} + \tilde{g}_x^- e^{+kz}$$

$$\tilde{g}_y = \tilde{g}_y^+ e^{-kz} + \tilde{g}_y^- e^{+kz}$$

$$\tilde{f}_z = \tilde{f}_z^+ e^{-kz} + \tilde{f}_z^- e^{+kz}$$

From equation 2.7 it is easy to obtain:

$$\tilde{\psi}^{\pm} = \frac{+(1-2\nu)}{4(1-\nu)k} \tilde{f}_z^{\pm} \pm \frac{i}{4(1-\nu)k} (p\tilde{g}_x^{\pm} + q\tilde{g}_y^{\pm})$$

where the ψ^{\pm} form is assumed to follow directly from the definitions above. The p and q are the Fourier transform variables in x and y with $k^2=p^2+q^2$. The displacements can be obtained from the equation (2.4). The results can be summarized in matrix form:

$$\text{where} \quad [\tilde{u}]^{\pm} = [L]^{\pm} [\tilde{g}]^{\pm}$$

$$[\tilde{u}]^{\pm} = \begin{bmatrix} \tilde{u}_x^{\pm} \\ \tilde{u}_y^{\pm} \\ \tilde{u}_z^{\pm} \end{bmatrix} \quad [\tilde{g}]^{\pm} = \begin{bmatrix} \tilde{g}_x^{\pm} \\ \tilde{g}_y^{\pm} \\ \tilde{f}_z^{\pm} \end{bmatrix}$$

The complete solution for the displacements in matrix form is:

$$\begin{bmatrix} \tilde{u}_x \\ \tilde{u}_y \\ \tilde{u}_z \end{bmatrix} = [L]^+ [\tilde{g}]^+ e^{-kz} + [L]^- [\tilde{g}]^- e^{+kz}$$

where :

$$[L]^+ = \frac{1}{4(1-\nu)k} \times$$

$$\begin{bmatrix} p^2(zk+1) - 4(1-\nu)k^2 & pq(zk+1) & ip[zk - (1-2\nu)] \\ pq(zk+1) & q^2(zk+1) - 4k^2(1-\nu) & iq[zk - (1-2\nu)] \\ -ipk^2z & -iqzk^2 & k(2-2\nu + zk) \end{bmatrix}$$

and :

$$[L]^- = \frac{1}{4(1-\nu)k} \times$$

$$\begin{bmatrix} p^2(zk-1) + 4(1-\nu)k^2 & pq(zk-1) & ip[zk + (1-2\nu)] \\ pq(zk-1) & q^2(zk-1) + 4k^2(1-\nu) & iq[zk + (1-2\nu)] \\ +ipk^2z & +iqzk^2 & k(2-2\nu - zk) \end{bmatrix}$$

The expressions for the stresses can be obtained from the equation (2.2). Using the matrices $[L]^{\pm}$ above, and the

differentiation properties Fourier transformed variables, a similar matrix notation may be obtained for the stresses.

$$\tilde{\sigma}_{ij} = \tilde{\sigma}_{ij}^+ e^{-kz} + \tilde{\sigma}_{ij}^- e^{kz}$$

For convenience in the introduction of the boundary condition the six stress components are separated as follows:

$$[\tilde{\sigma}_z]^{\pm} = \begin{bmatrix} \tilde{\sigma}_{xz}^+ \\ \tilde{\sigma}_{yz}^+ \\ \tilde{\sigma}_{zz}^+ \end{bmatrix} = [M]^{\pm} \begin{bmatrix} \tilde{g}_x^+ \\ \tilde{g}_y^+ \\ \tilde{f}_z^+ \end{bmatrix}$$

$$[\tilde{\sigma}_x]^{\pm} = \begin{bmatrix} \tilde{\sigma}_{xx}^+ \\ \tilde{\sigma}_{yy}^+ \\ \tilde{\sigma}_{xy}^+ \end{bmatrix} = [N]^{\pm} \begin{bmatrix} \tilde{g}_x^+ \\ \tilde{g}_y^+ \\ \tilde{f}_z^+ \end{bmatrix}$$

If in M^{\pm} the upper sign corresponds to M^+ , and the lower to M^- then:

$$[M]^{\pm} = \frac{Y}{4(1+\nu)(1-2\nu)(1-\nu)} \quad .$$

$$\begin{bmatrix} (1-2\nu) [\bar{p}^2 zk + 2k^2 (1-\nu)] & \bar{p}(1-2\nu) pqzk & \bar{p}(1-2\nu) ipzk \\ \bar{p}(1-2\nu) pqzk & (1-2\nu) [\bar{q}^2 zk + 2k^2 (1-\nu)] & \bar{p}(1-2\nu) iqzk \\ ipk [\underline{+}(1-\nu)(zk-1) - \nu(zk+1)\bar{+}(1-\nu)] & iqk [\underline{+}(1-\nu)(zk-1) - \nu(zk+1)\bar{+}(1-\nu)] & -k(1-2\nu)(zk+1) \end{bmatrix}$$

and:

$$[N]^{\pm} = \frac{Y}{4(1+\nu)(1-\nu)k}$$

$$\begin{bmatrix} -ip[p^2(zk+1)+2k^2(\nu-2)] & -iq[p^2(zk+1)+2\nu k^2] & [p^2(zk+(1-2\nu))+2\nu q^2] \\ -ip[q^2(zk+1)+2\nu k^2] & -iq[q^2(zk+1)+2k^2(\nu-2)] & [q^2(zk+(1-2\nu))+2\nu p^2] \\ -iq[p^2(zk+1)+2(1-\nu)k^2] & -ip[q^2(zk+1)+2(1-\nu)k^2] & pq[zk+(1-2\nu)] \end{bmatrix}$$

The layered space identified in the figure 2.9 has N layers each with Young's Modulus and Poisson's Ratio Y, ν_i and depth at the top z_i . The N 'th layer is a half space. The matrix solutions for displacements and stresses at any depth z , in layer i , are written below.

$$[\tilde{u}]_{i,z} = [L^+ \ L^-]_{i,z} \begin{bmatrix} e^{-kz} & 0 \\ 0 & e^{kz} \end{bmatrix} \begin{bmatrix} \tilde{g}^+ \\ \tilde{g}^- \end{bmatrix}_i$$

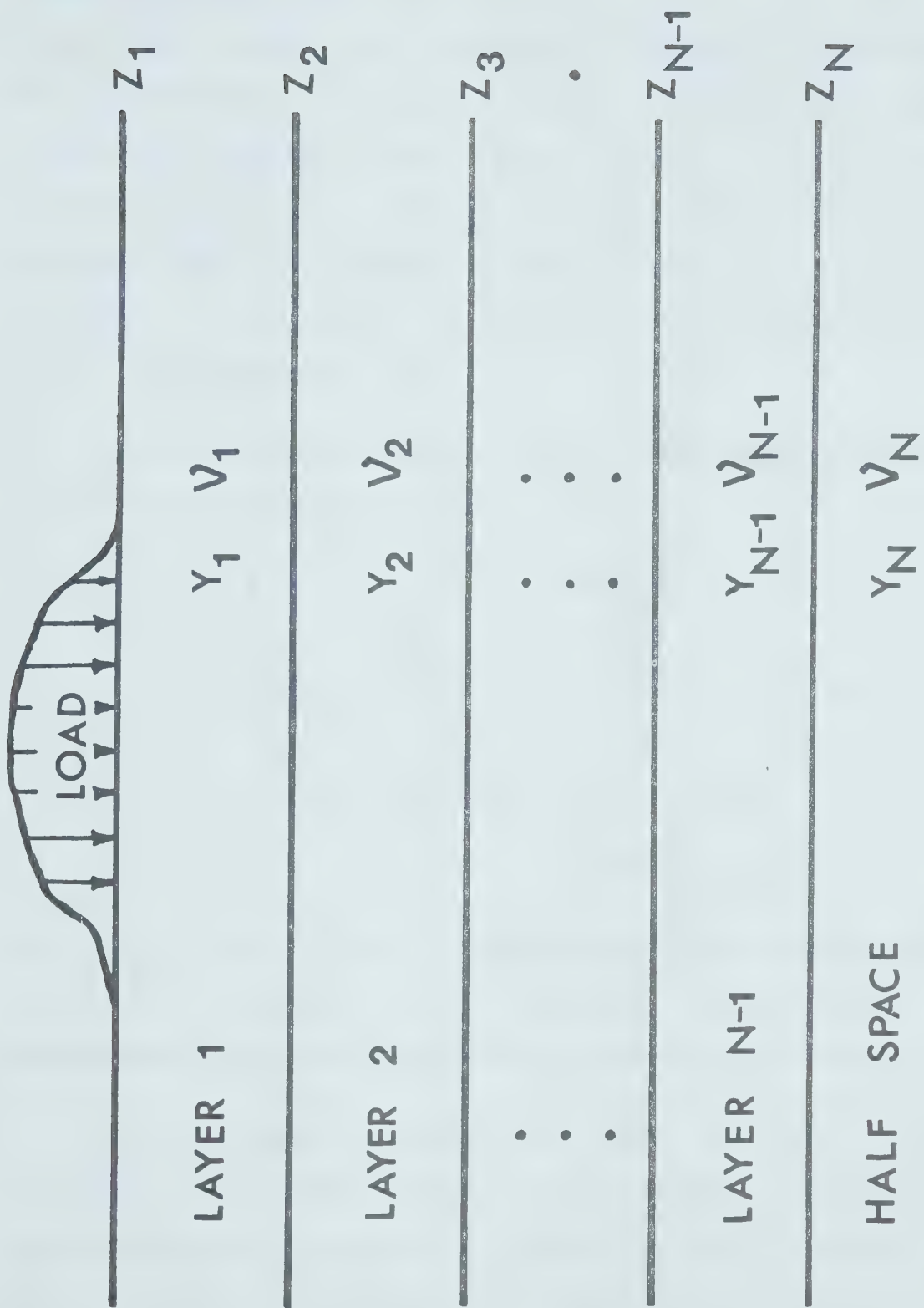
$$[\tilde{\sigma}_z]_{i,z} = [M^+ \ M^-]_{i,z} \begin{bmatrix} e^{-kz} & 0 \\ 0 & e^{kz} \end{bmatrix} \begin{bmatrix} \tilde{g}^+ \\ \tilde{g}^- \end{bmatrix}_i$$

$$[\tilde{\sigma}_x]_{i,z} = [N^+ \ N^-]_{i,z} \begin{bmatrix} e^{-kz} & 0 \\ 0 & e^{kz} \end{bmatrix} \begin{bmatrix} \tilde{g}^+ \\ \tilde{g}^- \end{bmatrix}_i$$

The notation $[]_{i,z}$ is introduced to indicate that computation is in the i layer at depth z below the free surface. The 1 is the 3×3 unitary matrix and 0 is the zero 3×3 matrix.

At each boundary there are 6 boundary conditions. The 3

Figure 2.9: Shows the configuration used for calculating the displacements and stresses in a layered half space. There are $N-1$ layers over a half space each with Young's modulus Y and Poisson's Ratio ν . The top of the layer i is at z_i with z_0 being the free surface on which the load is applied.



displacements are continuous if the layers are to stay welded together. The three stresses σ_{zz} , σ_{xz} , σ_{yz} must be continuous across each interface to ensure no acceleration of the interface. The top and bottom interfaces have special conditions imposed on them. The surface is free, so we conclude $\sigma_{xz} = \sigma_{yz} = 0$. The σ_{zz} is the applied load at the surface. Below the lowest interface lies a half space. To ensure the variables are bounded with increasing z , the $[\tilde{g}]_N^-$ are necessarily zero.

The boundary conditions allow the determination of $[\tilde{g}]_i^+$, $[\tilde{g}]_i^-$ in all the layers:

$$\begin{bmatrix} \tilde{g}^+ \\ \tilde{g}^- \end{bmatrix}_{i-1} = \begin{bmatrix} e^{kz_i} & 0 \\ 0 & e^{-kz_i} \end{bmatrix} \begin{bmatrix} M^+ & M^- \\ L^+ & L^- \end{bmatrix}_{i-1, z_i}^{-1}$$

$$\begin{bmatrix} M^+ & M^- \\ L^+ & L^- \end{bmatrix} \begin{bmatrix} e^{-kz_i} & 0 \\ 0 & e^{-kz_i} \end{bmatrix} \begin{bmatrix} \tilde{g}^+ \\ \tilde{g}^- \end{bmatrix}_i$$

The $[\tilde{g}]_N^- = 0$ and $[\tilde{g}]_N^+$ can be computed by chain application of the identity above to the top surface. Knowing $[\tilde{g}]_i^+$ the displacement and stresses can be calculated everywhere.

The complex matrices $[L]$, $[M]$, and $[N]$ can be separated into a real matrix, pre and post multiplied by complex diagonal matrices. The inversions can be found using real algebra routines. Caution must be taken to include the complex matrices when solving for the $[\sigma]$ matrix as this is

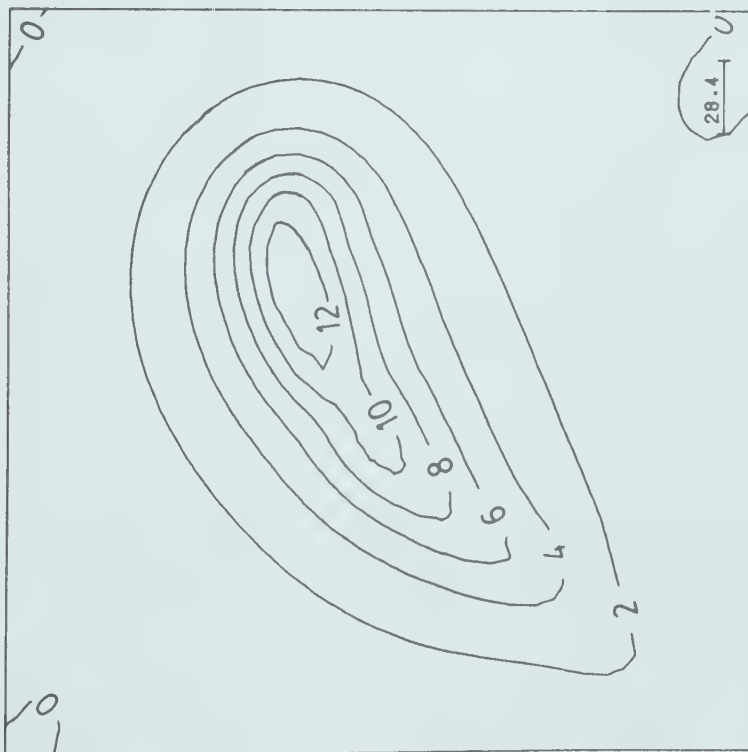
complex since the boundary conditions, \tilde{P} , are also complex.

Analytic inversions were attempted on the matrices L, M, N . These proved difficult to obtain and little simplification was achieved. In computation it was found more convenient to compute each of the matrices L, M, N and do the inversion numerically. The results obtained agreed well with the elastic case when the three layers were chosen to be the same. This is illustrated in figure 2.10, where the contribution of the square load has not been included. Figure 2.11 shows the results when three different layers were chosen. The technique was found to be unsatisfactory due to numeric instability in most of the models chosen.

A computation difficulty arises again for the zero wavelength component. Love's solution may be adapted into the layered model to remove the singularity if the average pressure over the grid is small. For a square much larger than the lake little difficulty will be experienced in the interpretation of the results. The solutions in the region of interest will only be slightly in error.

In this chapter the Boussinesq problem has been examined for elastic halfspace. The Fourier technique developed has been shown to be more efficient computationally and is able to be calculated at the surface. The theory was extended for the elastic layered half-space using Haskell-Thompson matrix techniques.

Figure 2.10: The vertical deflection is shown for the layered elastic halfspace (a). This agrees well with the solution found for the equivalent halfspace without interfaces. The effect of the average pressure has not been included in these diagrams so they differ in magnitude from the results shown in figure 2.7



VERT. DISPLACEMENT (CM)
DEPTH= 13KM

LAYER 1: Z 0. SIGMA 0.27, YOUNG 0.85MBAR
LAYER 2: Z 10. SIGMA 0.27, YOUNG 0.85MBAR
LAYER 3: Z 30. SIGMA 0.27, YOUNG 0.85MBAR

(a)



VERT. DISPLACEMENT (CM)
DEPTH= 13 WITH SIGMA=0.27 YOUNG=0.85MBAR

(b)

Figure 2.11: Vertical deflection below Lake Kariba found using the 3 layered half space with the parameters shown. The 'DC' level has not been included in this case.



VERT. DISPLACEMENT (CM)
DEPTH= 10KM

LAYER 1; Z 0, SIGMA 0.25, YOUNG 0.60MBAR
LAYER 2; Z 5, SIGMA 0.30, YOUNG 0.70MBAR
LAYER 3; Z 20, SIGMA 0.27, YOUNG 1.12MBAR

The model does not account for the effects of water, or allow for the concept of effective stress . These will be included by using the work of Biot (1940).

Chapter 3

Loading of a Reservoir on a Porous Elastic Fluid Filled Halfspace

The loading of reservoirs changes the pressure of the water contained in the rocks. Since reservoirs are built on rivers, groundwater is usually present and is observed by the presence of a watertable. The weight of the reservoir compresses the pore volumes and this effect must be included in any model of loading processes. The reservoir also allows water to enter the ground by leakage from the bottom raising the groundwater pressure. The modelling of a leaky reservoir on the porous elastic halfspace can be described by the concepts of effective stress and diffusion.

3.1 Biot's Consolidation Equations

Biot (1941 a,b,c) developed the basic equations governing the behaviour of solids containing fluids. The theory was developed for the study of consolidation of foundations in clay and sandy material but is sufficiently general that it can be applied to rock. Compaction of soils is described in articles by Hedberg (1936), Skempton (1970), and Marsal and Philipp (1970). A recent review article (Rice and Cleary 1976 a,b), concludes that recent work has not

greatly improved on the classic (Biot 1940a) and later works of Biot (1955, 1956a, 1973). This is the analysis which will be followed here. The extensive engineering literature concentrates on two-dimensional plane strain loads, and on problems with axial symmetry in three dimensions. Some of the recent applications include that by Nur and Booker (1972) and Booker (1974) to fault relaxation and by McNamee and Gibson to settlement (1960a, 1960b, 1957). A description of the solution of engineering problems by finite elements will be given in a later section, but it is apparent that very few analytic solutions exist. Biot's theory will be applied here to irregular loads which change with time in both shape and magnitude.

Hooke's equation of elasticity in the absence of fluid may be written as:

$$e_{ij} = \frac{(1+\nu)}{Y} \sigma_{ij} - \frac{\nu}{Y} \sigma_{kk} \delta_{ij} \quad -3.1$$

$$e_{ij} = \frac{1}{2} \left(\frac{\partial u_i}{\partial x_j} + \frac{\partial u_j}{\partial x_i} \right)$$

ν is Poisson's Ratio and Y is Young's modulus. The water pressure does not alter the shear components of stress but affects the rest equally. If σ is the water pressure, and H a parameter describing the effect of the pressure.

$$e_{ij} = \frac{(1+\nu)}{Y} \sigma_{ij} - \frac{\nu}{Y} \sigma_{kk} \delta_{ij} + \frac{\sigma}{3H} \delta_{ij} \quad -3.2$$

The sign convention used requires the water pressure to be positive with increased pressure and the stresses negative

in compression. Three assumptions have been made --

- (i) the material is isotropic
- (ii) a linear stress-strain relation exists
- (iii) the strains are small.

The amount of water in an element of volume is related to the six applied stresses and the fluid pressure. If the material is isotropic then the shear stresses cannot affect the water content. As there is symmetry of the material properties the contribution of each of the remaining stresses must be equal. In the first order theory Biot uses a linear dependence of the water content, θ , on the pressure and stresses.

$$\theta = \frac{1}{3H_1} (\sigma_{xx} + \sigma_{yy} + \sigma_{zz}) + \frac{p}{R} \quad -3.3$$

θ is defined as the increment of water volume per unit volume of the material. H_1 and R are two physical constants of the rock. If it is assumed that consolidation is a reversible process, it is possible to show that $H_1 = H$ by energy conservation arguments. The constant R allows for the inclusion of air with the water in the rock skeleton.

Equation (3.2) and (3.3) can be written in a more useful way as:

$$\sigma_{ij} = 2G (e_{ij} + (\eta-1)\epsilon \delta_{ij}) - \alpha p \quad -3.4$$

$$p = \alpha \epsilon + \frac{p}{Q} \quad -3.5$$

$$\text{where } \alpha = \frac{2(1+\nu)}{3(1-2\nu)H} \quad \frac{1}{Q} = \frac{1}{R} - \frac{\alpha}{H} \quad \eta = \frac{1-\nu}{1-2\nu} \quad G = \frac{Y}{2(1+\nu)}$$

$$\epsilon = \nabla \cdot \underline{u} = \frac{\partial u}{\partial x} + \frac{\partial v}{\partial y} + \frac{\partial w}{\partial z}$$

The four material constants G , ν , H and R and the derived constants α and Q need to be physically interpreted. G and ν are the equivalent elastic moduli of the solid skeleton in the absence of excess pressure. This condition can be established if experiments are conducted at a sufficiently slow rate to allow excess fluid to diffuse out of the rock. In order to interpret H and R consider the sample to be enclosed in a rubber jacket. In the absence of external stresses and with the pressure in the jacket reduced by $-\sigma$:

$$\dot{\theta} = -\frac{\dot{Q}}{R} \quad \epsilon = -\frac{\dot{Q}}{H}$$

where θ is the amount of fluid removed and ϵ is the change in the volume of the solid. The constants Q and α are meaningful when the solid is not saturated.

The constant α is the ratio of water volume squeezed out to the volume change of the solid if the latter is compressed while allowing the water to escape. The α of a saturated material is equal to 1., and for dry material it is 0. Irobe et. al. (1974) use α values between 0.83 and 0.98 in a description of the behavior of soils. Jaeger and Cook (1976) indicate that α has a value of one for rocks.

$1/Q$ is the measure of the amount of water which can be forced into the solid under pressure while the volume is

kept constant. A standard soil test affords a method of determining Q . A compressive load is applied through a porous slab to a laterally confined column of soil so that the water is allowed to drain away. The ratio of the axial strain to the applied load is equal to the "final compressibility coefficient". This is shown by Biot (1941a) to be

$$a = \frac{(1-2\nu)}{2G(1-\nu)}$$

If the test is repeated with the strain being measured before the water has had time to diffuse out of the solid, then the ratio of the strain to the applied load equals the "instantaneous compressibility".

$$a_i = \frac{a}{1 + \alpha^2 a Q}$$

Q can be determined from these conditions with a knowledge of α . Biot has shown that the initial compressive strain is large compared to the final compressive strain for soils. The ratio of instantaneous to final compressive strains is typically 0.01. On this basis Q is large, and several orders of magnitude larger than Young's modulus. Jaeger and Cook (1976) suggest that as the compressibility of rock-forming mineral is of the order of 0.1% per Kilobar, it is reasonable to neglect the volume change of minerals at laboratory pressures so that a Q value of infinity is suitable for rocks.

Rice and Cleary (1976a) modified the choice of derived

constants so they more closely resembled bulk moduli and have introduced the effective stress law of Nur and Byerlee (1971) rather than that of Terzaghi. The lack of information on any of the constants over scales of the size of lakes (10's of kilometers) is the largest single weakness of theoretical analysis. In the work of Rice and Cleary (1976b) on faults, the parameters may be monitored more closely, however, for lake analysis the simplest macro-parameters will be used. The notation of Biot will therefore be used throughout.

Equation (3.4) can be differentiated and simplified to yield the first of the basic equations required.

$$G(\nabla^2 u_i + (2\eta-1)\epsilon_{,i}) - \alpha\sigma_{,i} = 0 \quad -3.6$$

It is assumed the water's behaviour is governed by D'Arcy's Law where the fluid flow velocity is linearly proportional to the fluid pressure gradient. For an isotropic solid with coefficient of permeability K

$$V_i = -K \frac{\partial \theta}{\partial x_i} \quad -3.7$$

The assumption must be made that the flow is not turbulent, but its wide use in oil and hydrological studies implies this assumption is justified. If the water is incompressible, the increase of water content in an element of the solid equals the flow into it:

$$\frac{\partial \theta}{\partial t} = \frac{\partial V_x}{\partial x} + \frac{\partial V_y}{\partial y} + \frac{\partial V_z}{\partial z} \quad -3.8$$

Using (3.5), (3.7) and (3.8)

$$K \nabla^2 \epsilon = 0 \frac{\partial \epsilon}{\partial z} + \frac{1}{2} \frac{\partial^2 \epsilon}{\partial z^2} \quad -3.9$$

The Biot Consolidation Equations (3.6) and (3.9) fully describe the deformation of a fluid-filled elastic material due to an applied load.

3.2 Solution of the Boundary Value Problem

The equations (3.6) and (3.9) can be solved using the displacement functions of McNamee and Gibson (1960 a,b). Other solutions can be applied (see Rice and Cleary (1976a)) but are generally limited to two dimensions. Taking the divergence of the vector equation (3.6):

$$\nabla^2 (2\eta G \epsilon - \alpha \sigma) = 0$$

If S is a harmonic function ($\nabla^2 S = 0$) then,

$$2G\eta\epsilon - \alpha\sigma = -2G \frac{\partial S}{\partial z}$$

It can be shown that another scalar function E can be introduced which will satisfy this equation if

$$\begin{aligned} u &= - \frac{\partial E}{\partial x} + z \frac{\partial S}{\partial x} \\ v &= - \frac{\partial E}{\partial y} + z \frac{\partial S}{\partial y} \\ w &= - \frac{\partial E}{\partial z} + z \frac{\partial S}{\partial z} - S \\ \sigma &= \frac{2G}{\alpha} \left(\frac{\partial S}{\partial z} - \eta \nabla^2 E \right) \\ v_z &= -K \frac{2G}{\alpha} \left(\eta \frac{\partial \epsilon}{\partial z} + \frac{\partial^2 S}{\partial z^2} \right) \\ \epsilon &= - \nabla^2 E \end{aligned} \quad -3.10$$

Substitution of (3.10) into (3.9) and time scaling by $t' = tC$ leads to the two differential equations

$$\nabla^4 E = \frac{d}{dt} \nabla^2 E - 2a_1 \frac{d}{dt} \left(\frac{dS}{dz} \right) \quad -3.11$$

$$\nabla^2 S = 0 \quad -3.12$$

$$C = \frac{2G\eta KQ}{(\alpha^2 Q + 2G\eta)} \quad a_1 = \frac{G}{(\alpha^2 Q + 2G\eta)}$$

The time scale 'C' is linear in the permeability, κ , so one result may be examined for several permeabilities. For example the results computed at 1 year for a rock of 20 millidarcy ($20 \times 10^{-10} \text{cm/s}$) will be the same as a rock of 2 millidarcy computed at 10 years.

The equations (3.11), (3.12) are solved by Fourier transforming in the x and y variables and Laplace transforming in 't'. The notation used is:

$$\tilde{E}(p, q, z, t) = \int_{-\infty}^{\infty} \int_{-\infty}^{\infty} E(x, y, z, t) e^{i(px+qy)} dx dy$$

$$\hat{E}(p, q, z, s) = \int_0^{\infty} E(p, q, z, t) e^{-st} dt$$

Use is made of:

$$\frac{dE}{dt} = \tilde{E}(p, q, z, t=0) + sE(p, q, z, s)$$

$$L^{-1}(s\hat{f}(s)) = \tilde{f}(t=0) + \frac{d}{dt} \tilde{f}(p, q, z, t) \quad -3.13$$

$$L^{-1}(f(s) g(s)) = \int_0^t f(t-\tau) g(\tau) d\tau \equiv f(t) * g(t)$$

With $k^2 = p^2 + q^2$ (3.11) and (3.12) reduce to:

$$\left(-k^2 + \frac{d^2}{dz^2}\right) \left(-k^2 + \frac{d^2}{dz^2}\right) \hat{E} = \left(-k^2 + \frac{d^2}{dz^2}\right) (\hat{S}\hat{E} + \tilde{E}(t=0))$$

$$-2a_1 \frac{d}{dt} (S\hat{S} + \tilde{S}(t=0))$$

$$\left(-k^2 + \frac{d^2}{dz^2}\right) S = 0$$

The condition at $t=0$ corresponds to no initial compressibility and no excess pressure. This assumption is made on the basis that the results will reflect the effects of the anomalous load alone. If the initial stresses, fluid pressures and flow velocities were available they could be included at this stage. Body forces should be considered in this case as they will cause an increase in the lithostatic and hydrostatic pressures with depth. Other initial conditions could be incorporated into the mathematics if required at this stage. Since the compression $\tilde{\epsilon} = -\nabla^2 \tilde{E}$, then at $t=0$:

$$\left(-k^2 + \frac{d^2}{dz^2}\right) E(t=0) = 0$$

With the zero initial pressure condition this requires:

$$\frac{d}{dz} S(t=0) = 0$$

The equations simplify to:

$$\left(-\mu^2 + \frac{d^2}{dz^2}\right) \left(-k^2 + \frac{d^2}{dz^2}\right) \hat{E} = -2a_1 S \frac{d}{dz} \hat{S}$$

$$\left(-k^2 + \frac{d^2}{dz^2}\right) \hat{S} = 0$$

with $\mu^2 = k^2 + S$. The solutions must be bounded at infinity so, by the Method of Variations (Butkov 1968, p126)

$$\hat{E} = Ae^{-kz} + Be^{-\mu z} + a_1 z Ce^{-kz}$$

$$S = C_0 e^{-kz} \quad -3.14$$

A, B, C can be determined from the boundary conditions. They may depend on p, q and s but are independent of z.

At the free surface, $z=0$, $\hat{\sigma}_{xz} = \hat{\sigma}_{yz} = 0$ reduces to:

$$kA = -\mu B + C a_1 \quad -3.15$$

The surface $\hat{\sigma}_{zz}$ must equal the weight of the water and is represented by the compressive load - $\hat{T}(p, q, 0, S)$.

$$-\frac{\hat{T}}{2G} = k(\mu - k)B + Ck(1 - a_1)$$

The third condition involves the volume of flow at the bottom of the reservoir or the fluid pressure. Since the fluid pressure is easier to monitor by test wells over a large area this was chosen to be the surface boundary condition. Water losses could not be ignored since leakage can be significant. At the Tel-Yeruham reservoir in Israel, losses ranged from 10 to 30cm/day over an area of 390,000 square metres at the 50m high water mark (Aisenstein et.al. (1957)). From (3.10) :

$$\frac{\alpha P}{2G} = -(\mu^2 - k^2)B + (2a_1\eta - 1)kC$$

The A, B, C can be solved giving the equations:

$$B = -\frac{(a_4 \hat{T} + \alpha P)}{2G\eta(\mu + \lambda)(\mu - k)} = \frac{\hat{\Gamma}}{2G\eta(\mu + \lambda)(\mu - k)}$$

$$C = \frac{1}{(2a_1\eta - 1)k} \left(\frac{\alpha P}{2G} + \eta(\mu^2 - k^2)B \right) \quad -3.17$$

$$kA = -\mu B + a_1 C$$

$$\text{where } \hat{\Gamma} = -(a_4 \hat{T} + \alpha \hat{P}) \quad , \quad \lambda = \frac{(\eta + a_4)^k}{\eta} \quad , \quad a_4 = \frac{(2a_1 \eta - 1)}{(1 - a_1)}$$

From the equation (3.17), (3.4), (3.10) and (3.14) it is possible to compute the stresses, displacements and excess pressure at any depth at any time.

3.3 Excess Fluid Pressure

Substituting for \hat{E} and \hat{S} into equation (3.10) gives:

$$\frac{\alpha \hat{\sigma}}{2G} = Ck(2a_1 \eta - 1)e^{-kz} - \eta B(\mu^2 - k^2)e^{-z}$$

$$\alpha \hat{\sigma} = \alpha \hat{P}e^{-kz} + \left(\frac{e^{-kz}}{(\mu + \lambda)(\mu - k)} - \frac{e^{-\mu z}}{(\mu + \lambda)(\mu - k)} \right) s \hat{\Gamma}$$

The terms may be broken into suitable parts by partial fractions and the initial values set to zero.

$$\alpha \hat{\sigma} = \alpha \hat{P}e^{-kz} + \frac{1}{(\lambda + k)} \left(\frac{e^{-\mu z}}{(\mu + \lambda)} - \frac{e^{-\mu z}}{(\mu - k)} - \frac{e^{-kz}}{(\mu + \lambda)} + \frac{e^{-kz}}{(\mu - k)} \right) s \hat{\Gamma}$$

The inverse Laplace transforms were all obtained from the tables of Roberts and Kaufman (1966). The necessary transforms are listed below. Equations (p257,5) and (p224,23) were rederived since they were contradictory in the small z limit.

$g(s)$	$g(t)$	Ref(R.K.)
$\frac{1}{s^{\frac{1}{2}} + a}$	$\frac{1}{(\pi t)^{\frac{1}{2}}} - ae^{a^2 t} \text{Erfc}(at^{\frac{1}{2}})$	(p211,49)
$\frac{e^{-zs^{\frac{1}{2}}}}{s^{\frac{1}{2}} + a}$	$\frac{\exp(-z^2/4t)}{(\pi t)^{\frac{1}{2}}} - ae^{a^2 t + az} \text{Erfc}\left(\frac{z}{2t^{\frac{1}{2}}} + at^{\frac{1}{2}}\right)$	(p247,26)
$\frac{1}{(s^{\frac{1}{2}} + a)^2}$	$(2a^2 t + 1)e^{a^2 t} \text{Erfc}(at^{\frac{1}{2}}) - 2at^{\frac{1}{2}}\pi^{-\frac{1}{2}}$	(p224,23)

$$\frac{e^{-zs^{\frac{1}{2}}}}{(s^{\frac{1}{2}}+a)^2} \quad (2a^2t+az+1)e^{az+a^2t}\text{Erfc}\left(\frac{z}{2t^{\frac{1}{2}}}+at^{\frac{1}{2}}\right) - 2at^{\frac{1}{2}}\pi^{-\frac{1}{2}}\exp(-a^2/4t) \quad (\text{p257,5})$$

$$f(s+a) \quad e^{-k^2t} L^{-1}(f(s)) \quad (\text{p169,3})$$

Using (3.13) it is routine to show:

$$\alpha\hat{o} = \alpha\hat{p}e^{-kz} + \frac{d}{dt}(\tilde{\Gamma}) *$$

$$\frac{e^{-kz}}{\lambda+k} \left[\lambda e^{(\lambda^2-k^2)t} (\text{Erfc}(\lambda t^{\frac{1}{2}}) - e^{(\lambda+k)z} \text{Erfc}\left(\frac{z}{2t^{\frac{1}{2}}} + \lambda t^{\frac{1}{2}}\right)) + \right. \\ \left. + k (\text{Erfc}(-kt^{\frac{1}{2}}) - \text{Erfc}\left(\frac{z}{2t^{\frac{1}{2}}} - kt^{\frac{1}{2}}\right)) \right] \quad -3.18$$

From the surface load and pressure at time t , $\tilde{\Gamma}$ can be calculated by taking the Fourier transform at known times. A linear interpolation was used to calculate the wavelength contribution at times intermediate between those available. Spline interpolation was attempted, but proved less successful in treating rapid water-level changes. Numerically unrealistic results due to overshoots were found in the time derivatives in these instances.

The convolution integration was done using a Gaussian Quadrature integration technique (Ralston 1965). The time interval was sampled for orders 10, 15 and 25 of the Legendre Polynomials. Rather than increase the order of integration to improve accuracy, it was found that excellent accuracy consistent with low cost could be obtained by interval integration. Since the derivatives are constant between the known depth-time values, each of these intervals was

integrated with up to a 10th order polynomial. This has the advantage that a small sample interval was used where the functions change most rapidly.

Heaviside loading, or rapid filling is easily incorporated into the analysis. If the lake fills at an infinite rate to the depth described by $\tilde{\Gamma}$, and is held at that pressure for all times greater than $t=0$ then:

$$\frac{d}{dt} \hat{\Gamma} = \delta(t) \tilde{\Gamma}(t=0)$$

$$\int_0^t \frac{d}{dt} \tilde{\Gamma}(t-\tau) f(\tau) d\tau = \tilde{\Gamma}(0) f(t)$$

In the event of rapid filling the convolution becomes a simple multiplication of the $\tilde{\Gamma}$ (just after filling) with the function evaluated at time t .

3.4 Displacement

The vertical displacement can be found from:

$$\hat{W} = - \frac{\partial \hat{E}}{\partial z} + z \frac{\partial S}{\partial z} - \hat{S}$$

$$\hat{W} = \mu B (e^{-kz} - e^{-\mu z}) + C(-kz(1-a_1)-1)e^{-kz}$$

Expanding the B. C terms from (3.17)

$$\hat{W} = \frac{\mu \hat{\Gamma} (e^{-kz} - e^{-\mu z})}{2G\eta(\mu+\lambda)(\mu-k)} + \frac{a_3}{k} \left(\frac{\alpha \hat{P}}{2G} + \frac{(\mu^2 - k^2) \hat{\Gamma}}{2G(\mu+\lambda)(\mu-k)} \right) e^{-kz}$$

$$\text{where } a_3 = \frac{-zk(1-a_1) - 1}{(2a_1\eta - 1)}$$

This expression may be expanded by partial fractions and the inverse Laplace transforms taken from those tabulated earlier.

$$\begin{aligned}
2\tilde{G}\tilde{W} = & \frac{a_3 \alpha \tilde{P} e^{-kz}}{k} + \frac{d}{dt}(\tilde{\Gamma}) * \frac{e^{-kz}}{\eta} \times \\
& \left\{ \frac{\lambda^2 e^{(\lambda^2 - k^2)t}}{(\lambda^2 - k^2)(\lambda + k)} \left[\text{Erfc}(\lambda t^{\frac{1}{2}}) - e^{(\lambda + k)z} \text{Erfc}\left(\frac{z}{2t^{\frac{1}{2}}} + \lambda t^{\frac{1}{2}}\right) \right] \right. \\
& - \frac{1}{4(\lambda - k)} \left[\text{Erfc}(kt^{\frac{1}{2}}) - e^{2kz} \text{Erfc}\left(\frac{z}{2t^{\frac{1}{2}}} + kt^{\frac{1}{2}}\right) \right] \\
& - \frac{(\lambda - k)}{4(\lambda + k)^2} \left[\text{Erfc}(-kt^{\frac{1}{2}}) - \text{Erfc}\left(\frac{z}{2t^{\frac{1}{2}}} - kt^{\frac{1}{2}}\right) \right] \\
& + \frac{1}{2(\lambda + k)} \left[-(2k^2 t + 1) \text{Erfc}(-kt^{\frac{1}{2}}) + (2k^2 t - kz + 1) \text{Erfc}\left(\frac{z}{2t^{\frac{1}{2}}} - kt^{\frac{1}{2}}\right) \right. \\
& \quad \left. - 2kt^{\frac{1}{2}} \pi^{-\frac{1}{2}} e^{-k^2 t} (1 - e^{-z^2/4t + kz}) \right] \\
& \left. + \frac{\eta a_3}{k(\lambda + k)} \left[\lambda \text{Erfc}(\lambda t^{\frac{1}{2}}) + k \text{Erfc}(kt^{\frac{1}{2}}) \right] \right\} \quad -3.19
\end{aligned}$$

3.5 Effective Stress

The effective stresses are obtained in a similar way . The boundary constants A, B and C are substituted into equation (3.10), the stress-strain relation for effective stress. Expansion by partial fractions and use of the known Laplace transforms leads to the required results. It can be shown that:

$$\begin{aligned}
\tilde{\sigma}_{zz} = & a_5 \alpha \tilde{P} e^{-kz} + \frac{d}{dt}(\tilde{\Gamma}) * \frac{e^{-kz}}{\eta} \times \\
& - \left\{ \frac{\lambda e^{(\lambda^2 - k^2)t}}{(\lambda^2 - k^2)(\lambda + k)} \left[(\lambda^2 + (\eta - 1)(\lambda^2 - k^2)) e^{(\lambda + k)z} \text{Erfc}\left(\frac{z}{2t^{\frac{1}{2}}} + \lambda t^{\frac{1}{2}}\right) \right. \right. \\
& \quad \left. \left. + (\lambda k - \eta a_5(\lambda^2 - k^2)) \text{Erfc}(\lambda t^{\frac{1}{2}}) \right] \right\}
\end{aligned}$$

$$\begin{aligned}
& + \frac{k}{4(\lambda+k)} \left[e^{2kz} \operatorname{Erfc}\left(\frac{z}{2t^{\frac{1}{2}}} + kt^{\frac{1}{2}}\right) + \operatorname{Erfc}(kt^{\frac{1}{2}}) \right] \\
& + \frac{k}{4(\lambda+k)^2} \left[-(3\lambda+k) - 4(\eta-1)(\lambda+k) \operatorname{Erfc}\left(\frac{z}{2t^{\frac{1}{2}}} - kt^{\frac{1}{2}}\right) + \right. \\
& \quad \left. ((\lambda-k) + 4a_5\eta(\lambda+k)) \operatorname{Erfc}(-kt^{\frac{1}{2}}) \right] \\
& + \frac{k}{2(\lambda+k)} \left[(2k^2t+1) \operatorname{Erfc}(-kt^{\frac{1}{2}}) - (2k^2t-kz+1) \operatorname{Erfc}\left(\frac{z}{2t^{\frac{1}{2}}} - kt^{\frac{1}{2}}\right) \right. \\
& \quad \left. + 2kt^{\frac{1}{2}} \pi^{-\frac{1}{2}} e^{-k^2t} (1 - e^{-z^2/4t+kz}) \right] \}
\end{aligned}$$

-3.20

where

$$a_5 = \frac{2a_1\eta - a_1 + kz(1-a_1)}{(2a_1\eta-1)}$$

$$\begin{aligned}
\tilde{\sigma}_{xx} &= a_6 \alpha \tilde{p} e^{-kz} + \frac{d}{dt}(\tilde{\Gamma}) * \frac{e^{-kz}}{\eta} \times \\
& \left\{ \frac{\lambda e^{(\lambda^2-k^2)t}}{\lambda+k} \left[(a_6\eta + \frac{p^2\lambda}{k(\lambda^2-k^2)}) \operatorname{Erfc}(\lambda t^{\frac{1}{2}}) + \left(\frac{p^2}{\lambda^2-k^2} - (\eta-1) \right) \right. \right. \\
& \quad \left. \left. e^{(\lambda+k)z} \operatorname{Erfc}\left(\frac{z}{2t^{\frac{1}{2}}} + \lambda t^{\frac{1}{2}}\right) \right] \right. \\
& - \frac{p^2}{4k(\lambda-k)} \left[e^{2kz} \operatorname{Erfc}\left(\frac{z}{2t^{\frac{1}{2}}} + kt^{\frac{1}{2}}\right) + \operatorname{Erfc}(kt^{\frac{1}{2}}) \right] \\
& + \frac{1}{4k(\lambda+k)} \left[(4k^2a_6\eta - \frac{p^2(\lambda-k)}{(\lambda+k)}) \operatorname{Erfc}(-kt^{\frac{1}{2}}) + \left(-\frac{p^2(3k+\lambda)}{(k+\lambda)} - \right. \right. \\
& \quad \left. \left. 4k^2(\eta-1) \right) \operatorname{Erfc}\left(\frac{z}{2t^{\frac{1}{2}}} - kt^{\frac{1}{2}}\right) \right] \\
& + \frac{p^2}{2k(\lambda+k)} \left[(2k^2t-kz+1) \operatorname{Erfc}\left(\frac{z}{2t^{\frac{1}{2}}} - kt^{\frac{1}{2}}\right) - (2k^2t+1) \operatorname{Erfc}(-kt^{\frac{1}{2}}) + \right. \\
& \quad \left. 2kt^{\frac{1}{2}} \pi^{-\frac{1}{2}} e^{-k^2t} (e^{-z^2/4t+kz} - 1) \right] \}
\end{aligned}$$

-3.21

$$a_6 = \frac{(p^2(zk(a_1-1)+a_1) + (\eta-1)2a_1k^2)}{(2a_1\eta-1)k^2}$$

The expression for σ_{yy} can be obtained by replacing all occurrences of p with q in 3.21.

$$\begin{aligned}\tilde{\sigma}_{xy} = & - \frac{pq a_8 \alpha \tilde{p} e^{-kz}}{k^2} - \frac{d}{dt} \tilde{\Gamma} * \frac{pq e^{-kz}}{k^2 \eta} \times \\ & \left\{ \frac{\lambda e^{(\lambda^2 - k^2)t}}{\lambda + k} \left[(a_8 \eta - \frac{\lambda k}{(\lambda^2 - k^2)}) \operatorname{Erfc}(\lambda t^{\frac{1}{2}}) - \frac{k^2}{(\lambda^2 - k^2)} e^{(\lambda + k)z} \right. \right. \\ & \quad \left. \left. \operatorname{Erfc}(\frac{z}{2t^{\frac{1}{2}}} + \lambda t^{\frac{1}{2}}) \right] \right. \\ & + \frac{k}{4(\lambda - k)} [\operatorname{Erfc}(kt^{\frac{1}{2}}) + e^{2kz} \operatorname{Erfc}(\frac{z}{2t^{\frac{1}{2}}} + kt^{\frac{1}{2}})] \\ & + \frac{k}{4(\lambda + k)^2} [((4a_8 \eta (\lambda + k) + (\lambda - k)) \operatorname{Erfc}(-kt^{\frac{1}{2}}) + (3k + \lambda) \\ & \quad \left. \operatorname{Erfc}(\frac{z}{2t^{\frac{1}{2}}} - kt^{\frac{1}{2}})] \right. \\ & + \frac{k}{2(\lambda + k)} [(2k^2 t + 1) \operatorname{Erfc}(-kt^{\frac{1}{2}}) - (2k^2 t - kz + 1) \operatorname{Erfc}(\frac{z}{2t^{\frac{1}{2}}} - kt^{\frac{1}{2}}) \\ & \quad \left. + 2kt^{\frac{1}{2}} \pi^{-\frac{1}{2}} e^{-k^2 t} (1 - e^{-z^2/4t + kz})] \right\} - 3.22\end{aligned}$$

where

$$a_8 = \frac{[zk(1 - a_1) - a_1]}{(2a_1 \eta - 1)}$$

$$\begin{aligned}\hat{\sigma}_{xz} = & - \frac{ip \alpha a_9 p e^{-kz}}{k} - \frac{ip}{k\eta} \frac{d}{dt} \tilde{\Gamma} * e^{-kz} \times \\ & \left\{ - \frac{\lambda^2 k e^{(\lambda^2 - k^2)t}}{(\lambda^2 - k^2)(\lambda + k)} [\operatorname{Erfc}(\frac{z}{2t^{\frac{1}{2}}} + \lambda t^{\frac{1}{2}}) e^{(\lambda + k)z} - \operatorname{Erfc}(\lambda t^{\frac{1}{2}})] \right. \\ & + \frac{k}{4(\lambda - k)} [\operatorname{Erfc}(\frac{z}{2t^{\frac{1}{2}}} + kt^{\frac{1}{2}}) e^{2kz} - \operatorname{Erfc}(kt^{\frac{1}{2}})] \\ & + \frac{k(\lambda - k)}{4(\lambda + k)^2} [\operatorname{Erfc}(\frac{z}{2t^{\frac{1}{2}}} - kt^{\frac{1}{2}}) - \operatorname{Erfc}(-kt^{\frac{1}{2}})] \\ & + \frac{k}{2(k + \lambda)} [(2k^2 t - kz + 1) \operatorname{Erfc}(\frac{z}{2t^{\frac{1}{2}}} - kt^{\frac{1}{2}}) - (2k^2 t + 1) \operatorname{Erfc}(-kt^{\frac{1}{2}}) \\ & \quad \left. + 2kt^{\frac{1}{2}} \pi^{-\frac{1}{2}} e^{-k^2 t} (e^{-z^2/4t - k^2 t} - 1)] \right\}\end{aligned}$$

$$+ \frac{a_9 \eta}{(\lambda+k)} [k \operatorname{Erfc}(-kt^{\frac{1}{2}}) + \lambda e^{(\lambda^2-k^2)t} \operatorname{Erfc}(\lambda t^{\frac{1}{2}})] \} \quad -3.23$$

where
$$a_9 = \frac{zk(a_1-1)}{(2a_1\eta-1)}$$

σ_{yz} can be obtained by replacing p with q in the above equation.

3.6 Vertical Flow Velocity

The flow velocity used in D'Arcy's Law was defined in equation (3.7). It is of interest to know its surface value since it could have been used as one of the surface boundary conditions. Substituting into (3.10) the values of A, B, and C leads to:

$$\begin{aligned} \frac{V_z \alpha}{K} = & -\alpha k P e^{-kz} + \frac{d}{dt} \tilde{r} * \frac{e^{-kz}}{\eta} \times \\ & \left\{ \frac{k^2}{\lambda+k} \left[\operatorname{Erfc}\left(\frac{z}{2t^{\frac{1}{2}}} - kt^{\frac{1}{2}}\right) - \operatorname{Erfc}(-kt^{\frac{1}{2}}) \right] \right. \\ & - \frac{\lambda e^{(\lambda^2-k^2)t}}{\lambda+k} \left[\lambda e^{(\lambda+k)z} \operatorname{Erfc}\left(\frac{z}{2t^{\frac{1}{2}}} + \lambda t^{\frac{1}{2}}\right) + k \operatorname{Erfc}(\lambda t^{\frac{1}{2}}) \right] \\ & \left. + \pi^{-\frac{1}{2}} t^{-\frac{1}{2}} e^{-z^2/4t+kz-k^2t} \right\} \quad -3.24 \end{aligned}$$

where K is the permeability of the rock matrix constituting the half-space.

3.7 Examples of Heaviside Loading in Two Dimensions

To illustrate an application of the equations (3.18) to (3.24), a two dimensional cross-section of Lake Kariba, 54m deep, will be analysed. The two dimensional analysis was used only for simplicity in representing the results and is

obtained by setting $q=0$. It should be emphasised that the technique is general, and some three dimensional examples will be given later. To avoid complications arising from a time dependent history of filling and emptying Heaviside loading will be used. This may be interpreted as a rapid filling to maximum depth. The elastic parameters of the drained sample were the same as those used earlier with Poisson's Ratio 0.27 and Young's Modulus 0.85 Mbar. The other two parameters Q and α were unknown for the rock so it was assumed that it behaves as what Biot calls a 'Saturated Clay', and which Jaeger and Cook (1976) indicate applies to rocks under laboratory conditions.

$$Q = \infty$$

$$\alpha = 1$$

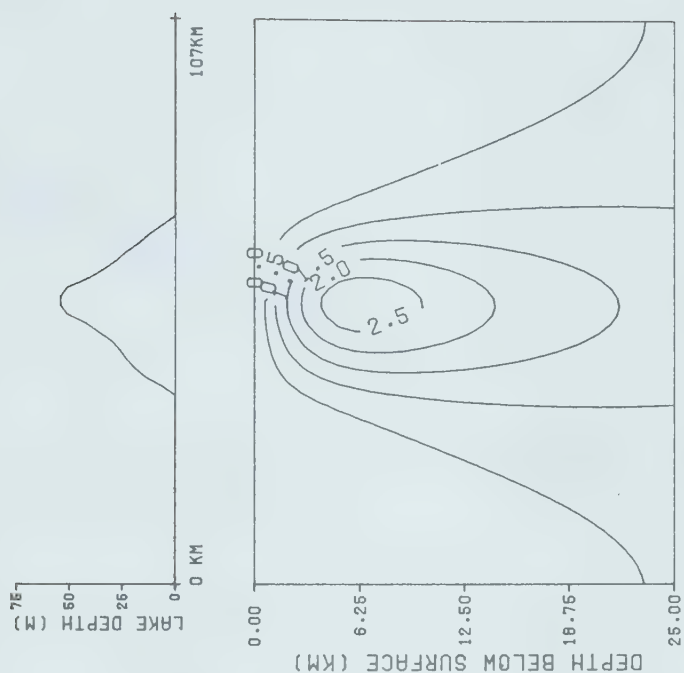
No data was available for the permeability in this region so a value of 2 millidarcy with a water viscosity of 0.01 Poise was chosen and is consistent with the chosen elastic constants. This value corresponds to a sound rock of low permeability. Scholz et.al.(1973) has estimated a permeability of 2 millidarcy from precursors time scales assuming diffusion through a solid matrix. This permeability could change by several orders of magnitude if the material is extensively fractured, but at the depths of 1-10 km where the seismic energy is thought to be released, these fractures are probably not a major factor in bulk fluid transfer since they will be closed by the weight of the overburden. The permeability of sound rock is most likely to describe the diffusion, but it should be emphasised that the

behaviour of aquifers or major faulting has not been included in the model and these may seriously distort the diffusion results.

The pressure at the surface was also unknown. The filling of the reservoir changes the water table but at this stage the amount of this change over a large area is unknown. The literature has not provided a guide to the solution of the question and a physical argument must be used. If the filling of the reservoir does not alter the water table and the surface pressure is zero at all times. Examples are given of the pressure and displacement in 3.1a, 3.1b. The load in this case is equivalent to a lake being filled with the water in the lake separated from the water in the rock. This would be the case if the lake bottom was sealed or the lake was a block of ice. This has been designated as zero coupling to indicate that the water table has not changed.

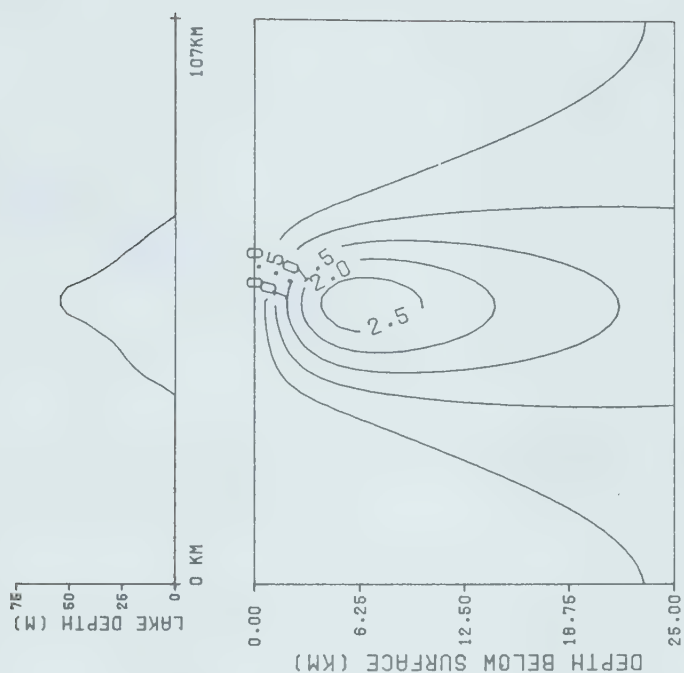
Figures 3.1c, 3.1d show the results at various times along an axis directly below the centre of the lake. Notice that the displacement increases at all points with time after an initial elastic compression. This consolidation is analogous to the behaviour of a loaded wet sponge. There is a certain amount of initial compression and then a settling as the water flows out of the sponge. The pressure variations are particularly interesting. The surface pressure has been forced by the boundary conditions to be

Figure 3.1: For the permeable fluid filled half space (a) shows the vertical deflection and (b) the pressures below a two dimensional load applied to the surface 1 year after loading. The excess pore pressure at the surface is zero at all times. The maximum deflection and excess pore pressure under this load are shown as functions of the depth below the surface and time in figures c, d, e, f. The half space has a Young's Modulus of 0.85 Mbar, Poisson's Ratio of 0.27 and a permeability of 2 millidarcy.



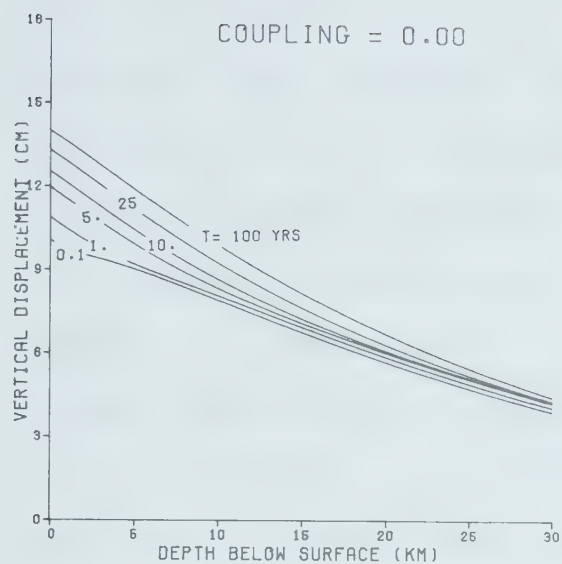
VERTICAL DISPLACEMENT (CM) AT 1.0 YRS
 YOUNG= 0.85MB SIGMA= 0.27
 PERM = 2.00MD COUPLING = 0.00
 ALPHA = 1.00 Q = 1.0E+34

(a)

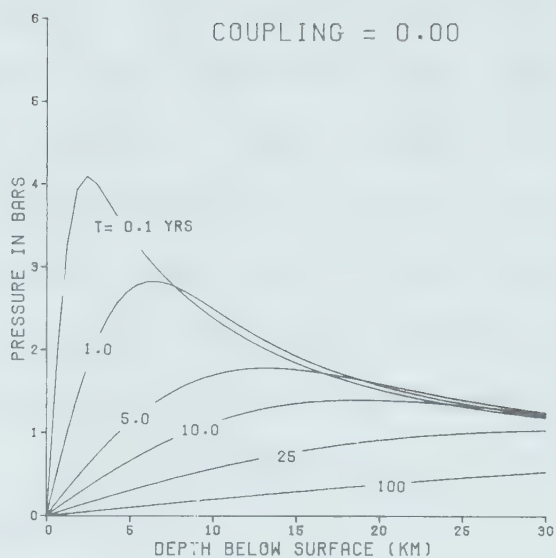


EXCESS PRESSURE (BARS) AT 1.0 YRS
 YOUNG= 0.85MB SIGMA= 0.27
 PERM = 2.00MD COUPLING = 0.00
 ALPHA = 1.00 Q = 1.0E+34

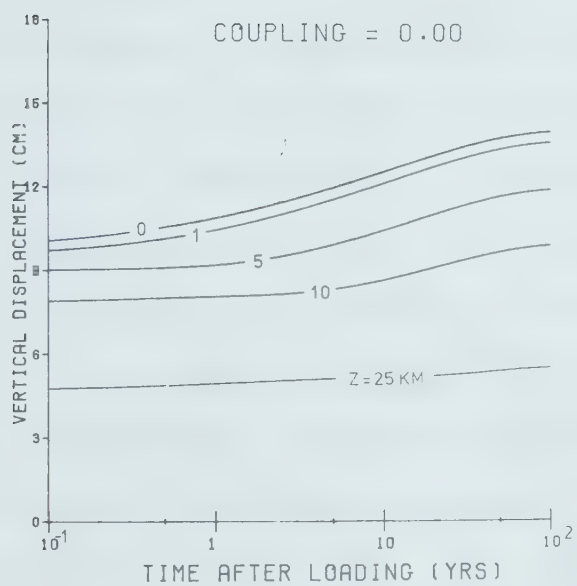
(b)



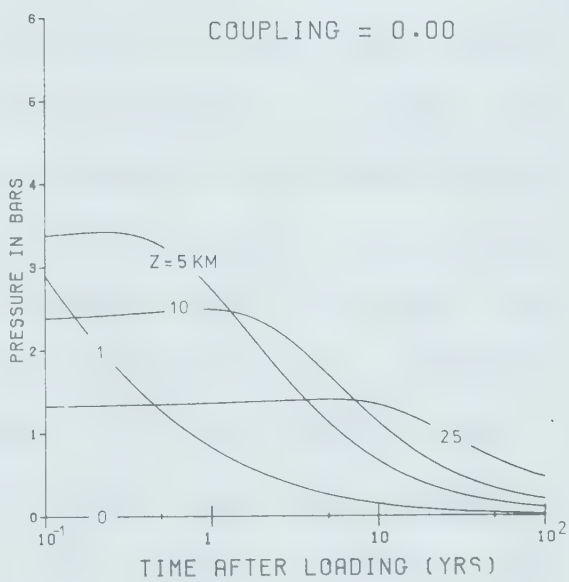
(c)



(d)



(e)



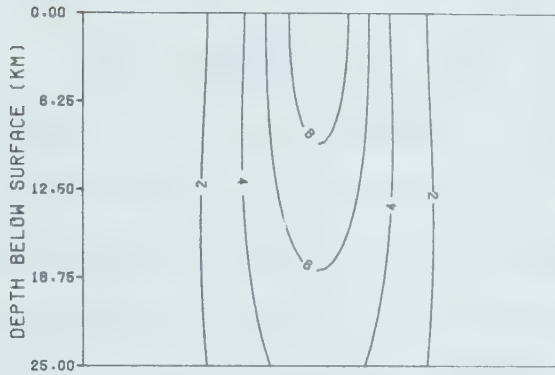
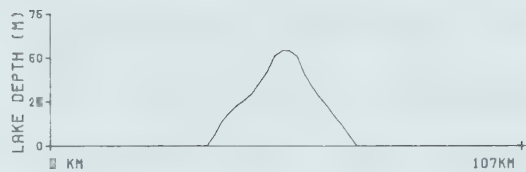
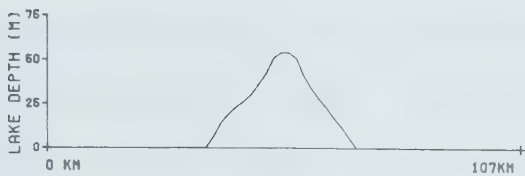
(f)

zero, but everywhere else the pressure rises. The loading has compressed the pores and the pressure of the water has risen to oppose the compression. The smaller pressure increases at greater depths is expected since the compressive effect of the load decreases with depth. The pressure gradients cause flow of the water in a manner that will reduce the gradients and this is indicated by the lower pressures at later times. The displacements and pressures at several depths below the surface are plotted as functions of time in figures 3.1e, 3.1f. The consolidation of the reservoir is clearly seen in figure 3.1e.

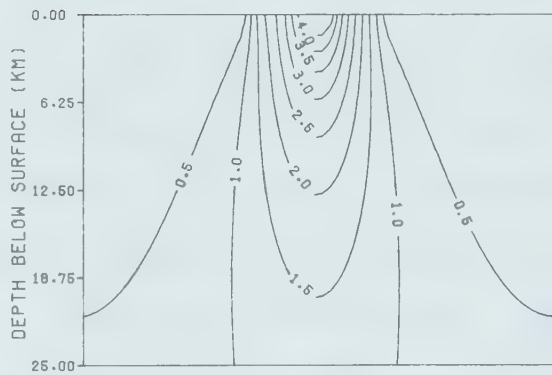
A second possible condition that may be imposed on the surface pressure is that in which the water pressure rises everywhere to equal that at the bottom of the lake. This is the expected condition for the application of a water load and is designated as 'full coupling' of the fluids in the rock and in the lake. This is indicated by the unit coupling on the diagrams. In this case figures 3.2a, 3.2b show there is no time variation of either the pressure or settlement. The pressure gradients established are such that the flow of water in the rock is governed by the rate of change of strain rather than the rate of change of pressure in a normal diffusion equation for the material constants chosen. This is seen from equation (3.9).

In this problem the pressure increase was expected to be delayed some time behind the pressure increase at the

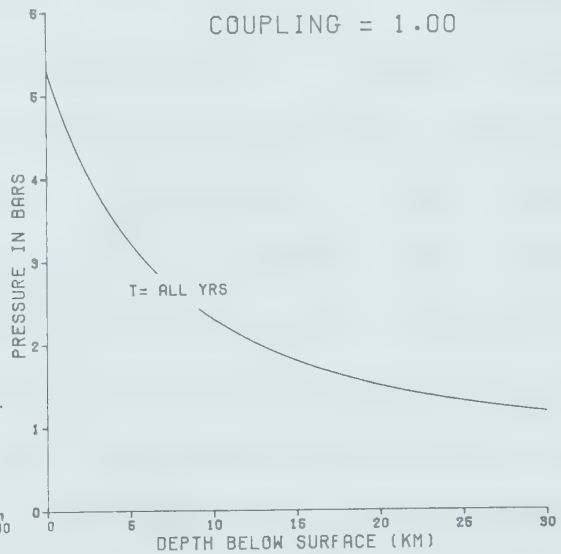
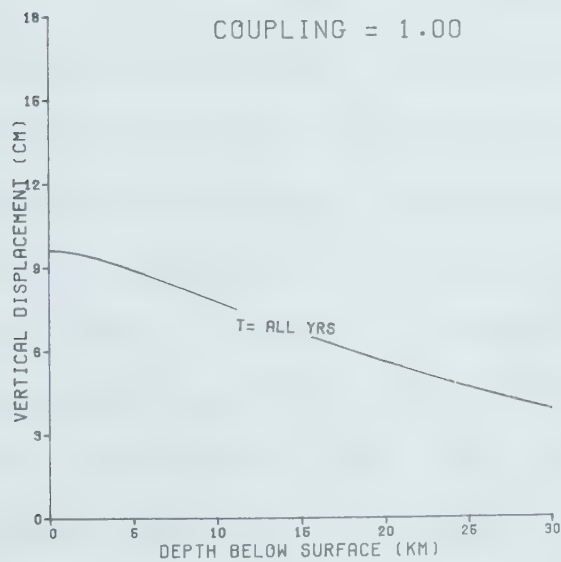
Figure 3.2: For the same half space and load as in figure 3.1, the excess pore pressure and deflection are plotted against depth for the surface boundary condition that the pressure is the same as the applied compressive load. Notice in this case there is no time variation.



VERTICAL DISPLACEMENT (CM) AT 1.00 YRS
 YOUNG= 0.85MB SIGMA= 0.27
 PERM = 2.00MD COUPLING = 1.00
 ALPHA = 1.00 Q = 1.0E+34



EXCESS PRESSURE (BARS) AT 1.00 YRS
 YOUNG= 0.85MB SIGMA= 0.27
 PERM = 2.00MD COUPLING = 1.00
 ALPHA = 1.00 Q = 1.0E+34



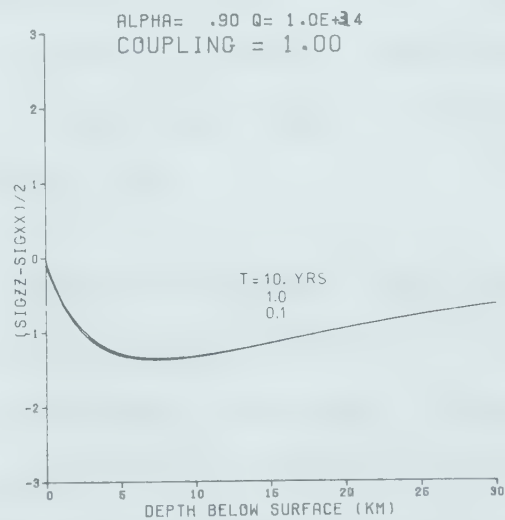
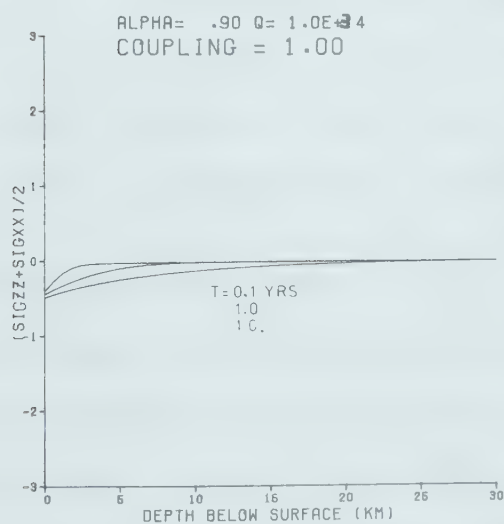
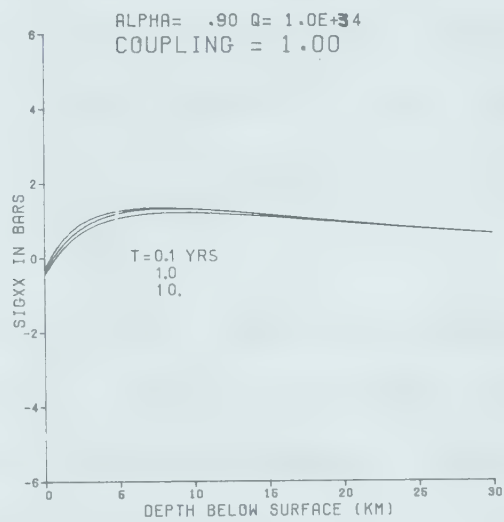
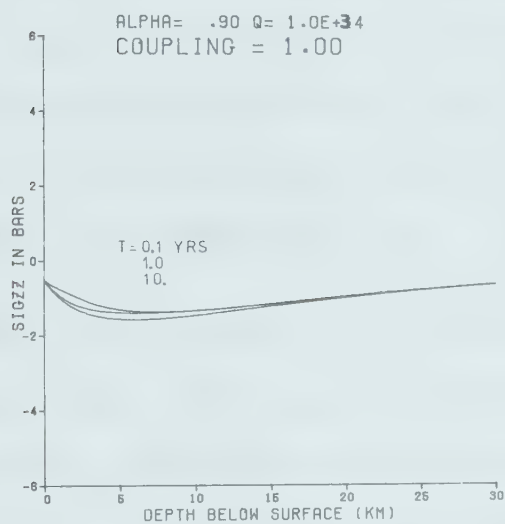
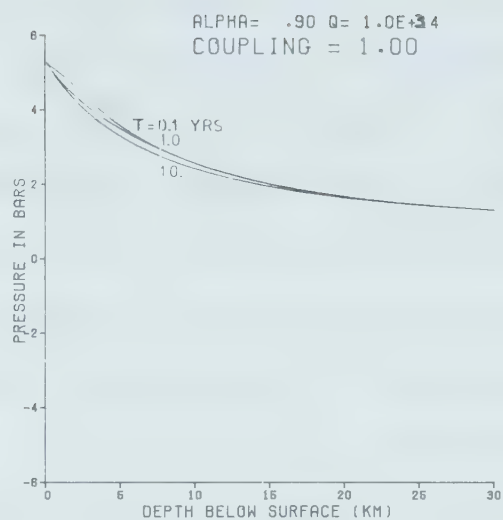
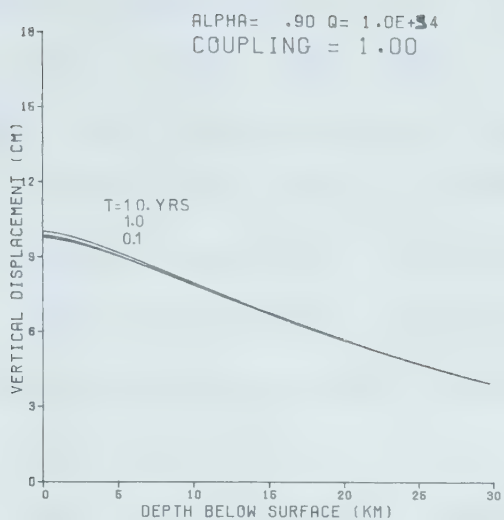
surface . For this reason it is necessary to examine the assumptions made. The consolidation at Kariba was small, and as the elastic constants appear to give a reasonable agreement between the calculated and observed deflection so the constants seem reasonable. The three fluid parameters chosen for the calculation are the permeability, α , and Q .

The permeability only alters the time scale, so to expand the time effects a low permeability has been chosen. Increasing the permeability would only force the fluid equilibrium to be established earlier. It should be appreciated that if the rock is fractured extensively, the fluid may move through the fissures.

The second parameter α relates to the rock saturation. It is reasonable to assume that rocks are relatively saturated so that α , lies between 0.9 and 1. A larger value of α decreases the time required for equilibrium, however, if α is too small the pressure may increase in the manner shown by figure 3.1. This is called the Mandel-Cryer effect and the anomalous pressures may be larger than the applied pressure (see Schiffman et. al. (1969)). For large Q , noticeable time lags can be seen for α of 0.9. The consolidation in this case is very small and is illustrated in figure 3.3.

The other parameter that may be varied is Q . This has been specified in terms of the initial (undrained) and final

Figure 3.3: The displacement, excess pressure, and stresses directly below the two dimensional lake section at several times. The elastic constants were the same, but Q and α have been reduced to illustrate that time delays by diffusion are possible.

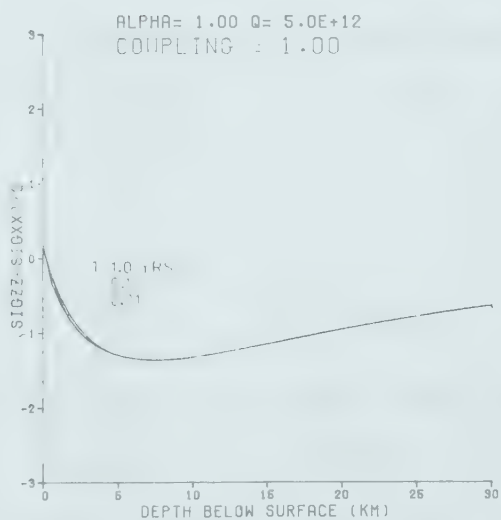
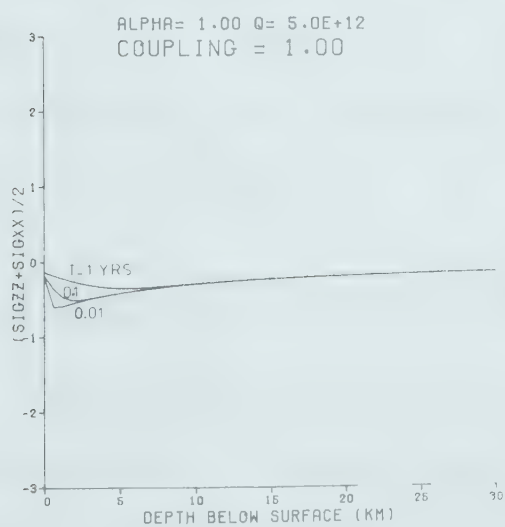
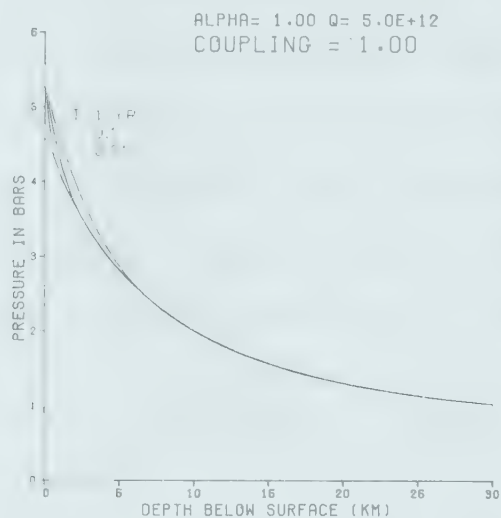
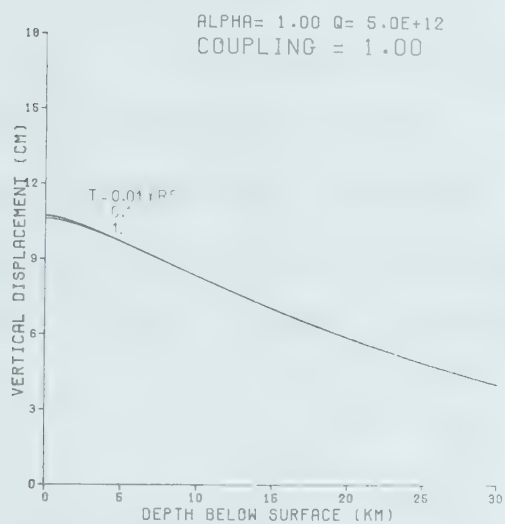
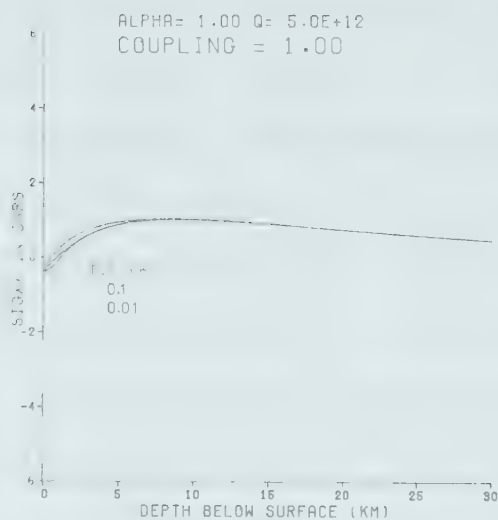
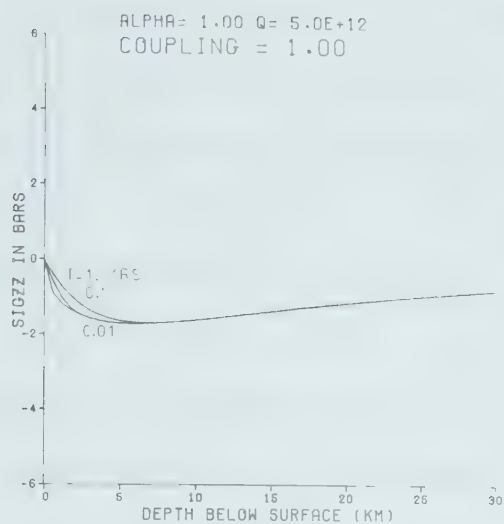


(drained) compressibilities. In the laboratory results quoted by Jaeger and Cook, a rock with high compressive strength will consolidate by the movement of water. The final compressive state is almost entirely a result of the water volume change. For this case Q is infinite with the final equilibrium being established instantaneously. Figure 3.4 illustrates that lowering the Q value leads to diffusion and a time lag. In the geometry of figure 3.2 detectable time lags at 0.1 years requires that Q be about 10 times larger than Young's Modulus. This implies that the initial to final compressibility be in the ratio of 1/10. The surface consolidation would still be smaller than the accuracy of releveing data.

The literature on Q and α for rocks is limited. Hendron (1969) presents the results of compression tests on drained and undrained black shales. From the Young's Modulus found, it is possible to conclude that Q is of the same order of magnitude as the drained Young's Modulus. Computation with a Q five times larger than Young's Modulus leads to the results shown in figure 3.4.

With the variation of the elastic and fluid parameters of the rock a large range of results can be obtained. A lot of work should be done to determine these parameters before the numeric results are emphasised. The calculations made here will concentrate on the behaviour, rather than the magnitude, of the rock stresses.

Figure 3.4: The displacement, excess pressure, and stresses below the two dimensional lake in a fully saturated rock. The elastic conditions have remained unchanged, but Q has been reduced to illustrate that pressure increases with time are possible with a different choice of fluid parameters.



Another approach to the problem is to assume that the surface boundary conditions are poorly chosen. If the surface is heavily fracture, inhomogeneous, and geologically variable, then the problem should be initialised at some depth just below the surface. At this point the vertical load is still similar to the applied load but the water pressure is assumed smaller than the full head. The boundary pressure would probably extend beyond the edges of the lake, but for simplicity is assumed to be of the same shape but smaller by a factor of 0.25 than the applied load. This is assume to be 0.25 coupling, to imply that the load lies somewhere between the block of ice and the fully connected water solution. In the absence of other values Q and α were chosen to be ∞ and 1 respectively. The theoretical $\tilde{\Gamma}$ now becomes

$$\tilde{\Gamma} = -(a_4 \hat{T} + \alpha \hat{P}) = -\left(\frac{(2a_1\eta-1)}{(1-a_1)} + 0.25\alpha\right)\hat{T}$$

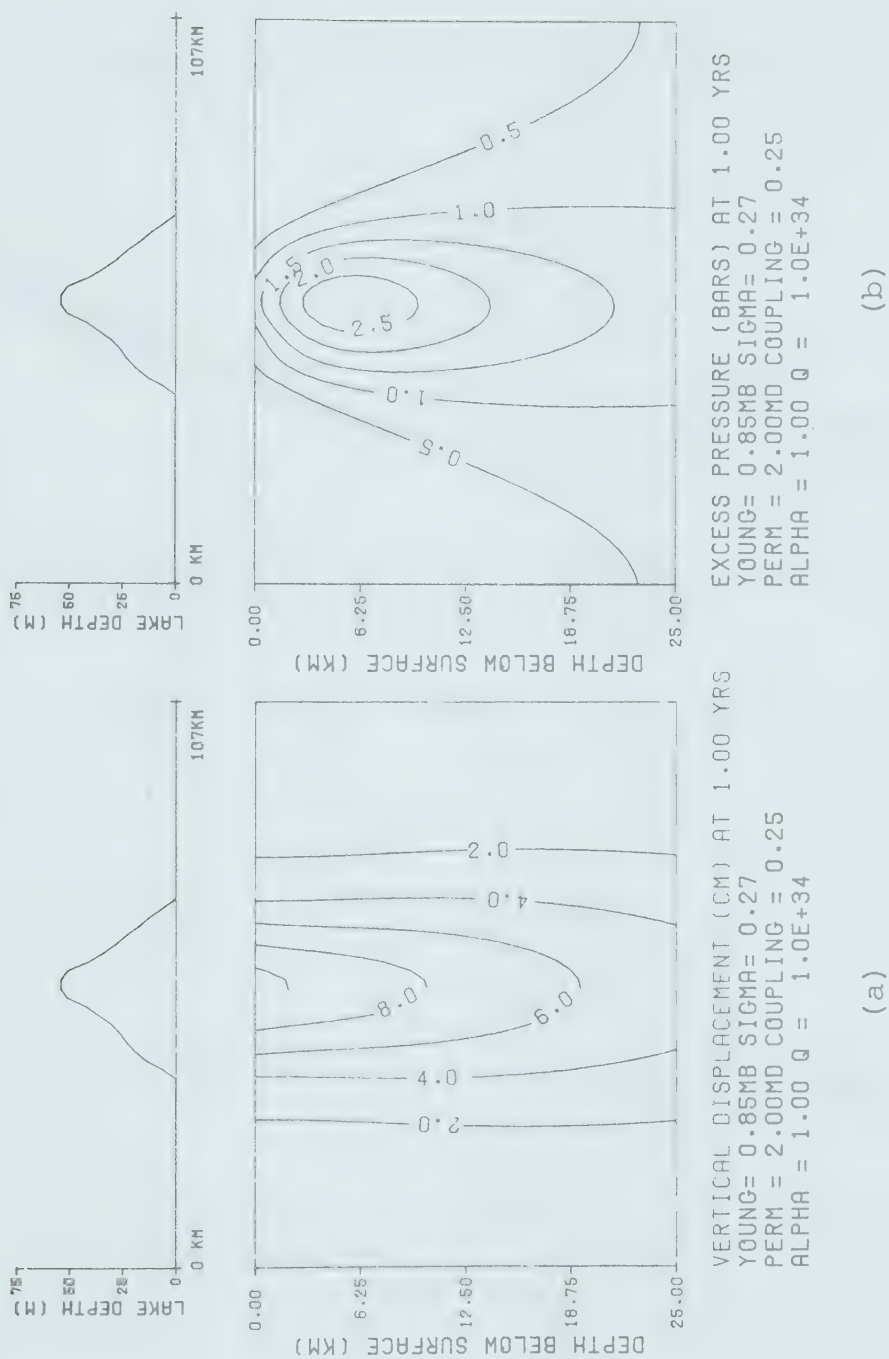
where $a = 0$ for $Q = \infty$ $\alpha = 1$

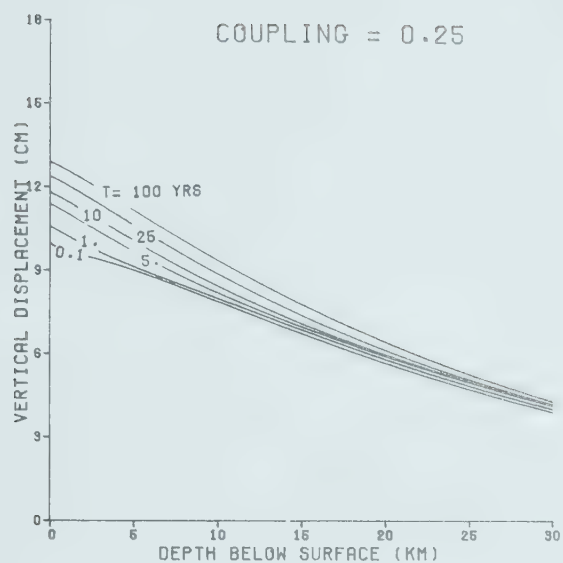
Figure 3.5 summarizes the pressure and displacement variation with 0.25 coupling. The settling is smaller than with zero coupling.

3.8 Examples of Time Dependent Loading

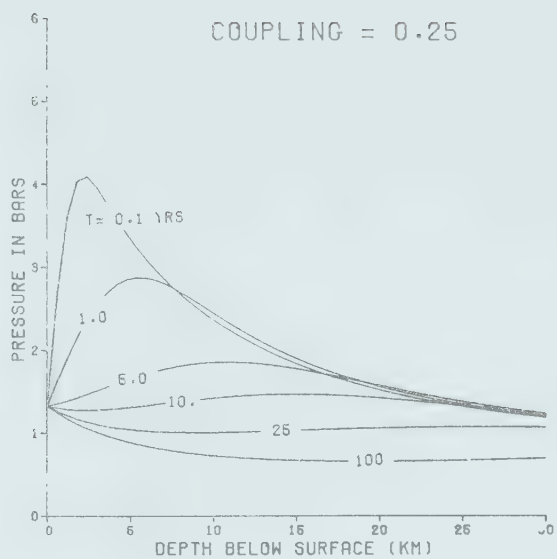
The equations (3.18) to (3.24) were analysed using time convolution. A typical loading history was modelled and is shown in figure 3.6. The water depth relates to the lake cross-section shown in the two dimensional sections of

Figure 3.5: The excess pore pressure and displacement are plotted for a permeable half space with Young's Modulus 0.85 Mbar and Poisson's Ratio 0.27 and permeability of 2 millidarcy for the situation where the water table has increased by 0.25 of the depth of the lake. Figures c, d, e, f show the variations of the maximum deflection and excess pressure as functions of depth and time.

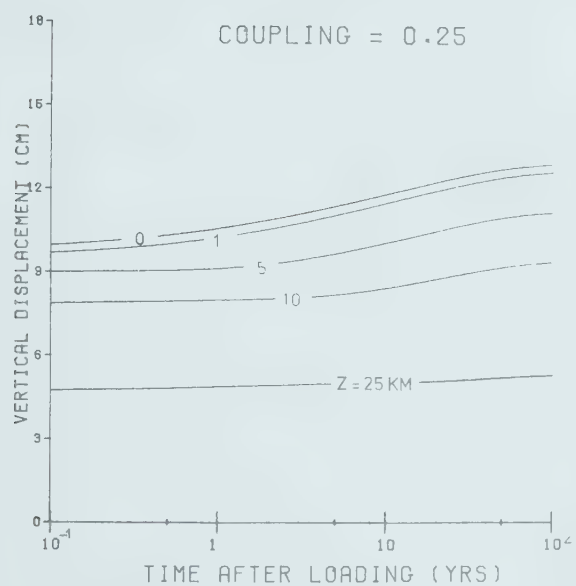




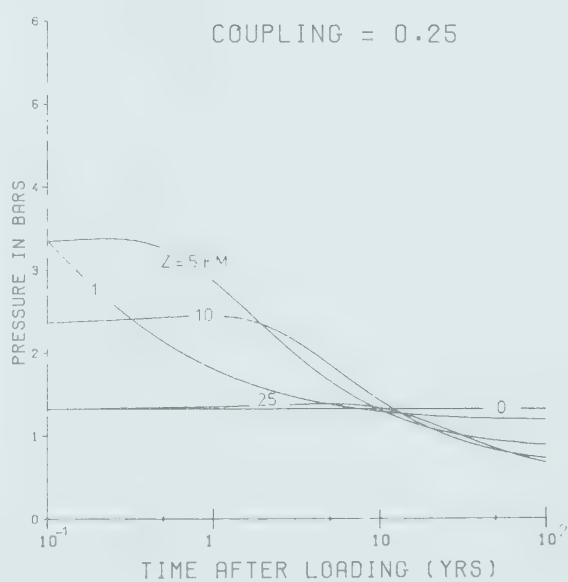
(c)



(d)

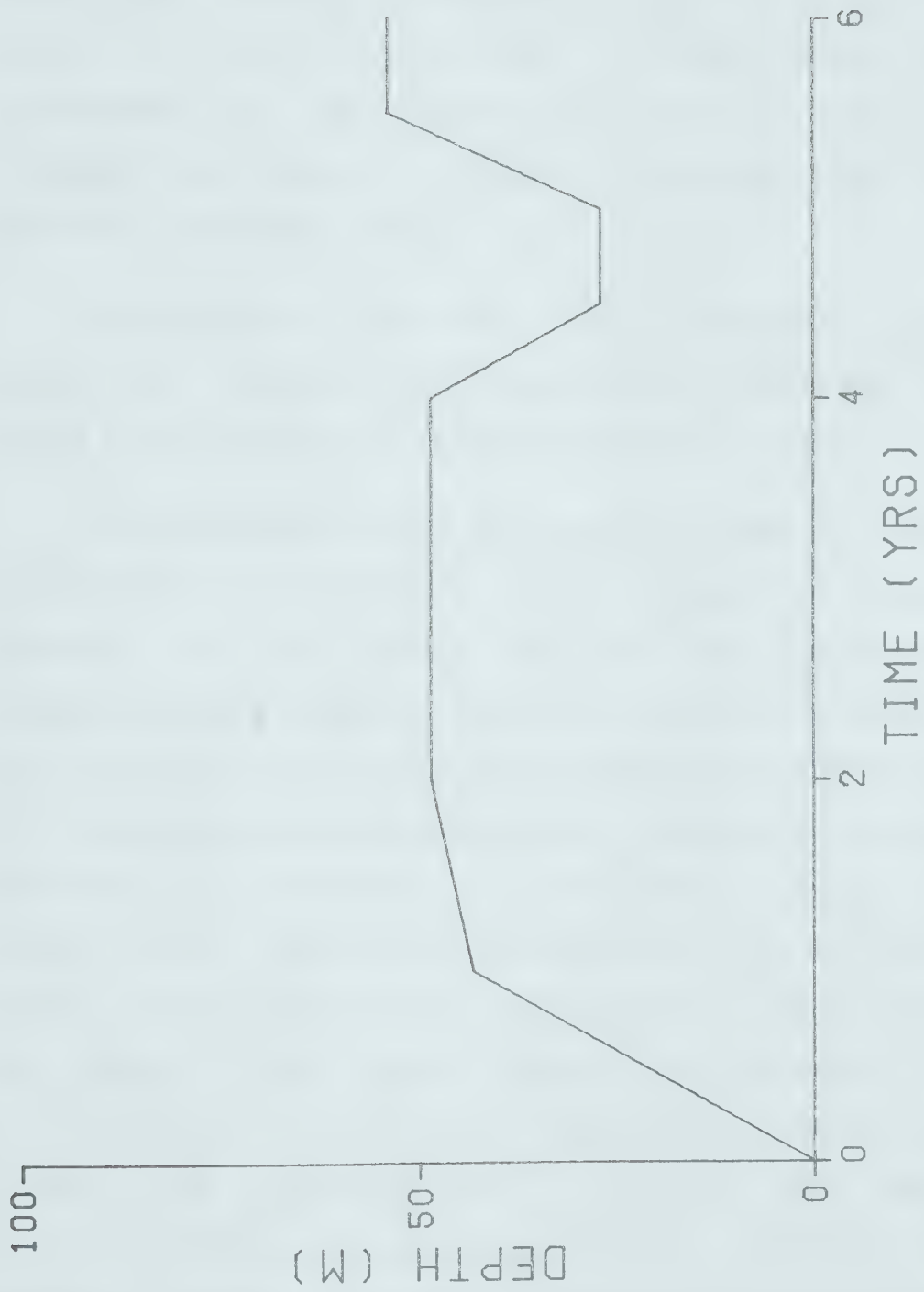


(e)



(f)

Figure 3.6: Plot of a hypothetical depth filled as a percentage of the maximum depth against time for the two dimensional lake section shown earlier. The drawdown starts at 4 years at 90% full, drops to 50% at 4.5 years, and from 5.0 years rises to be 100% full at 5.5 years. This filling history will be used with other lake sections later.

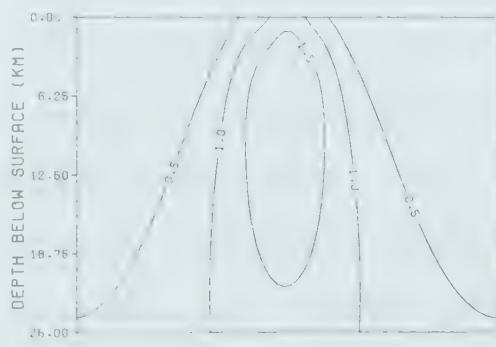
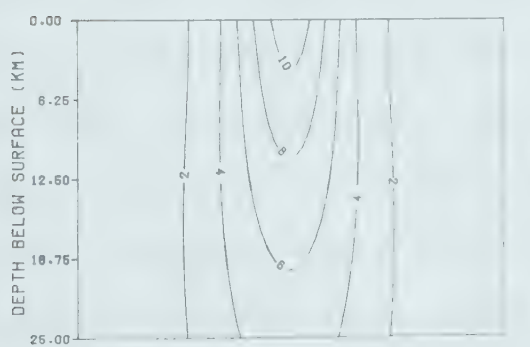
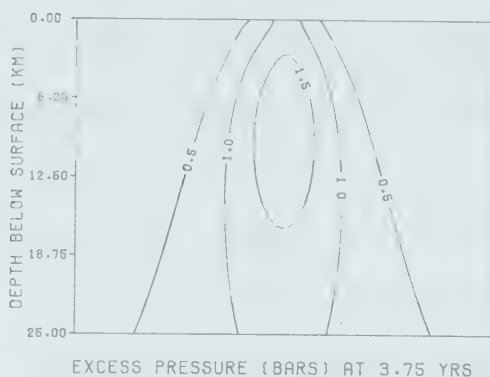
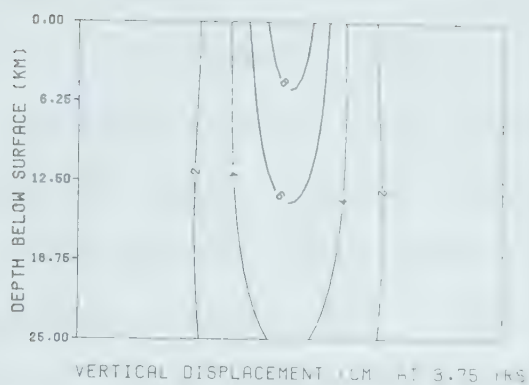


figures 3.1,3.2. This same filling history , although to different depths, will be used in the other examples at Kariba, Nurek, and Oroville. This variation of the water depth was meant to illustrate a typical drawdown situation where the lake is drained for a short period for dam inspection and then rapidly refilled. There was a similar drawdown just before the seismic activity began at Lake Oroville (Marlette 1975).

To examine the effective stress just before, during and after the drawdown, plots showing variations with time and depth were made for the loading history in figure 3.6.

The figure 3.7 shows the cross sections of pressure and displacement at 3.75, 4.75 and 6.5 years at Kariba. The pressure at 3.75 years is less than that determined in the earlier results shown in figure 3.5. This is a result of the slow loading of the lake which allows for the fluid pressure to dissipate as filling progresses. Instability is difficult to define, and relative Mohr circle positions were used to decide when an area is least stable. If at any time a Mohr circle lies to the left of its position at another time, or is larger and hence closer to a failure envelope, instability is suggested. The stresses produced by the lake loading are relatively small, only a few bars, and must of course be added to pre-existing tectonic stresses of up to several hundred bars before the Mohr circle is meaningful. If the σ_x and σ_z are the principal tectonic stresses then

Figure 3.7: Cross-sections below the reservoir at 3.75, 4.75 and 6.5 years showing the excess pressure and consolidation. The parameters used are shown on each diagram and they were all computed for 0.25 coupling.



VERTICAL DISPLACEMENT (CM) AT 6.50 YRS
 YOUNG= 0.85MB SIGMA= 0.27
 PERM = 2.00MD COUPLING = 0.25
 ALPHA = 1.00 Q = 1.0E+34

EXCESS PRESSURE (BARS) AT 6.50 YRS
 YOUNG= 0.85MB SIGMA= 0.27
 PERM = 2.00MD COUPLING = 0.25
 ALPHA = 1.00 Q = 1.0E+34

at Kariba where dip-slip faulting occurred σ_z will equal the weight of the rock and σ_x must be less than σ_z . A review of the state of the stress in the earth was published by Haimson (1975). It appears that the horizontal stresses may exceed the vertical at shallow depths (1 km) but are less than lithostatic below 1.5 km. The ratio of horizontal to vertical stress being eventually about 0.6. These conclusions were broadly applicable to southern Africa and the United States. It of course does not apply to thrust environments where the largest stress must be horizontal. There is little reason to expect these observations, which are averaged over large areas, to apply to a particular place. At each dam site under investigation an attempt to determine the local tectonic stresses should be made.

Figure 3.8 shows the variations of stress, pressure, and displacement as functions of time at a point centred under the load at depths of 3., 6., and 12. km. The sum of the stresses indicates how the Mohr circle moves to the left and right and the difference is a guide to its radius change. The Mohr circle position and radius change with time and will be examined in a later section. Figure 3.9 shows the changes of variables with depth at times just before (3.75 years), during (4.75 years), and after the lake drawdown (6.5 years). The rebound is more than expected but reloading is sufficient to consolidate the material more than that observed before the drawdown. A different loading history is



Figure 3.8: The variation of the vertical displacement, pressure, and stress in the Z and X direction, and their sum and difference are plotted at 3, 6, and 12 km. The displacement (a) illustrates how the unloading relieves a lot of the consolidation and this is reflected in the pressure low in (b). The pressure increases initially but as the rate of loading decreases the pressure falls as the fluid diffuses away. The changes in the effective stresses (negative in compression) were smaller than anticipated. Notice the change in the sum of the stresses occurs later than the major change in the difference.

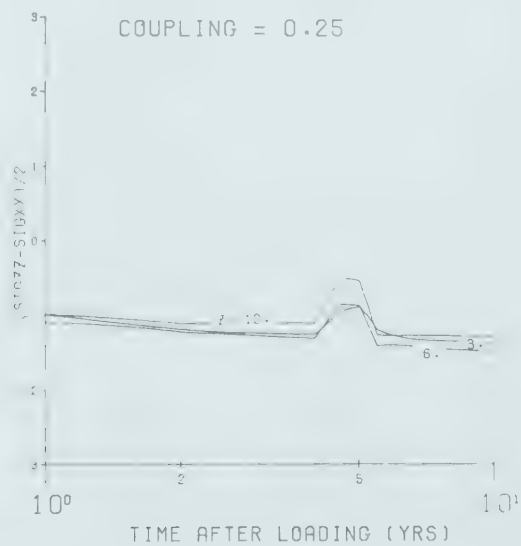
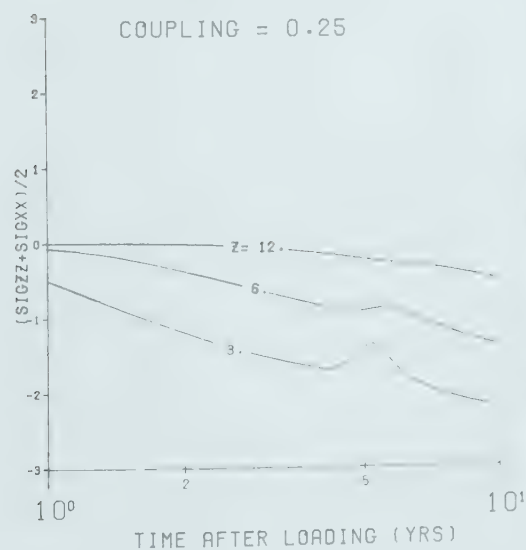
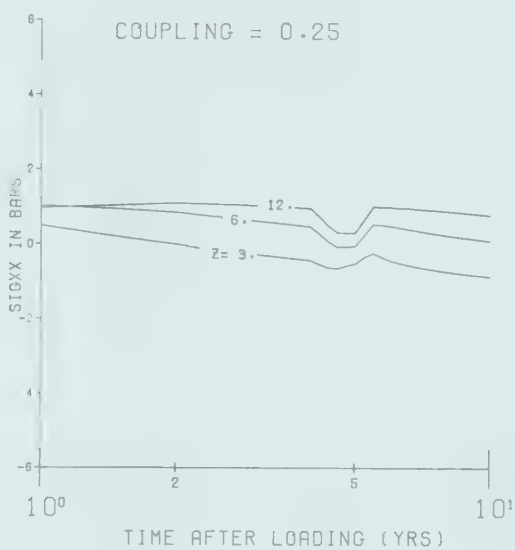
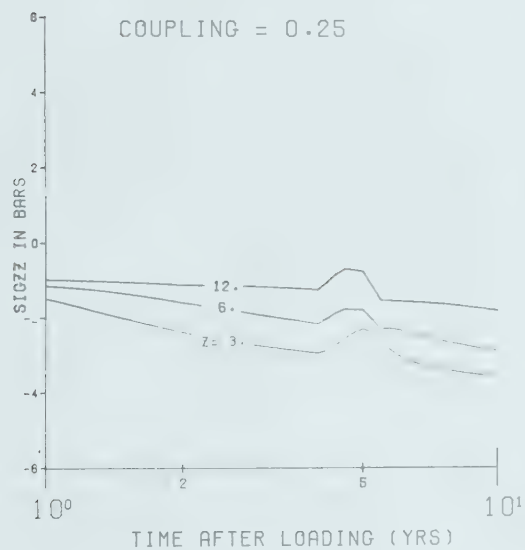
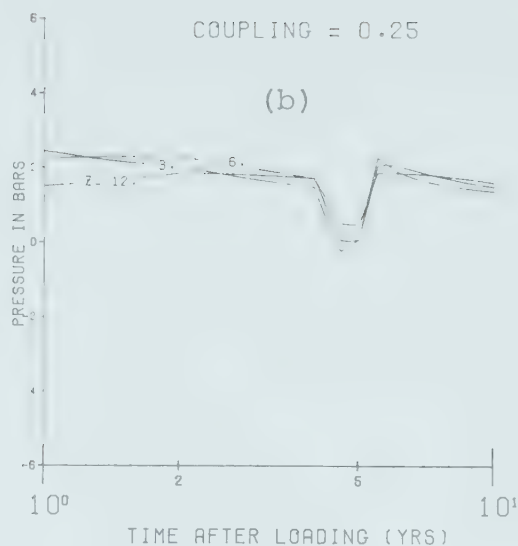
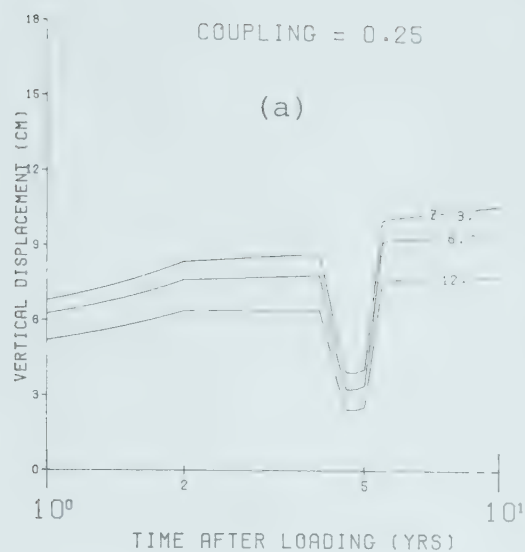
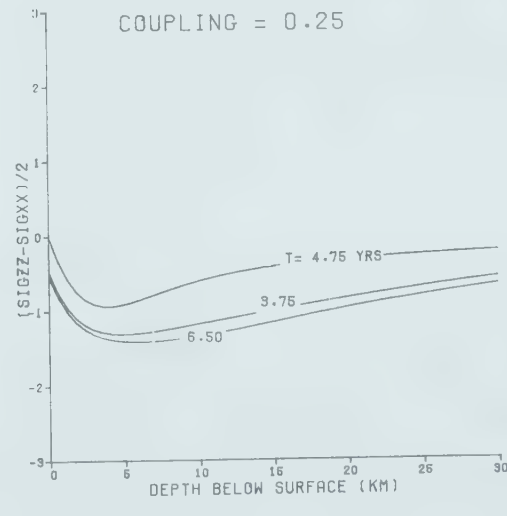
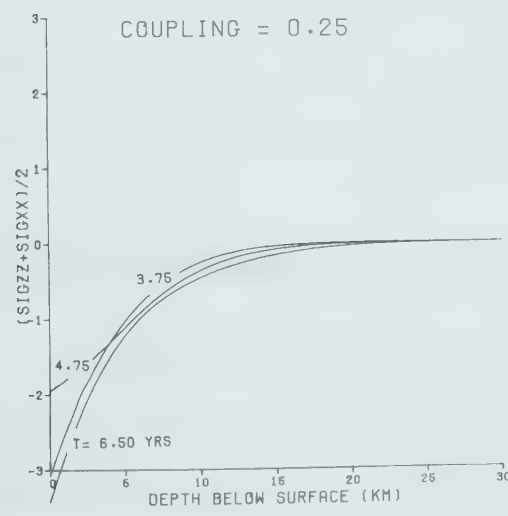
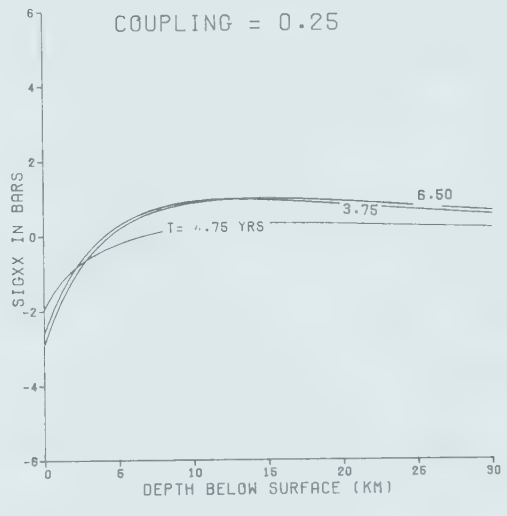
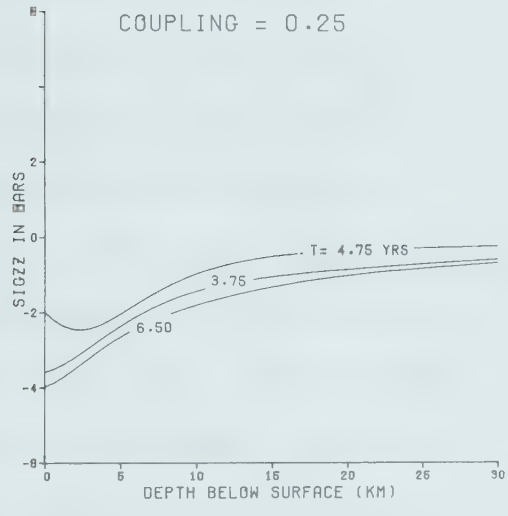
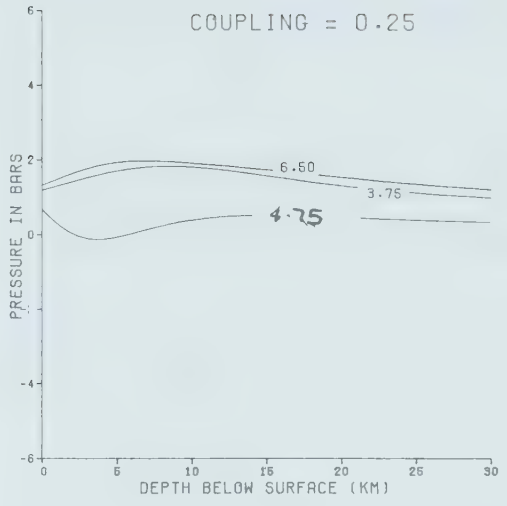
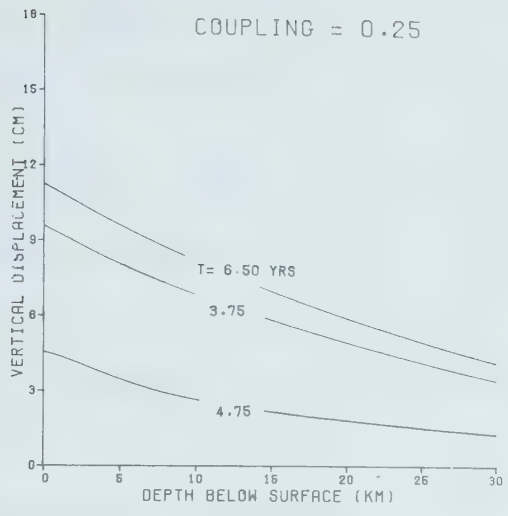


Figure 3.9: Changes in displacement, excess pressure and effective stresses are plotted for different times as functions of depth. The values chosen for the constants agree with those used in figure 3.7. The loading history was shown in Figure 3.6.



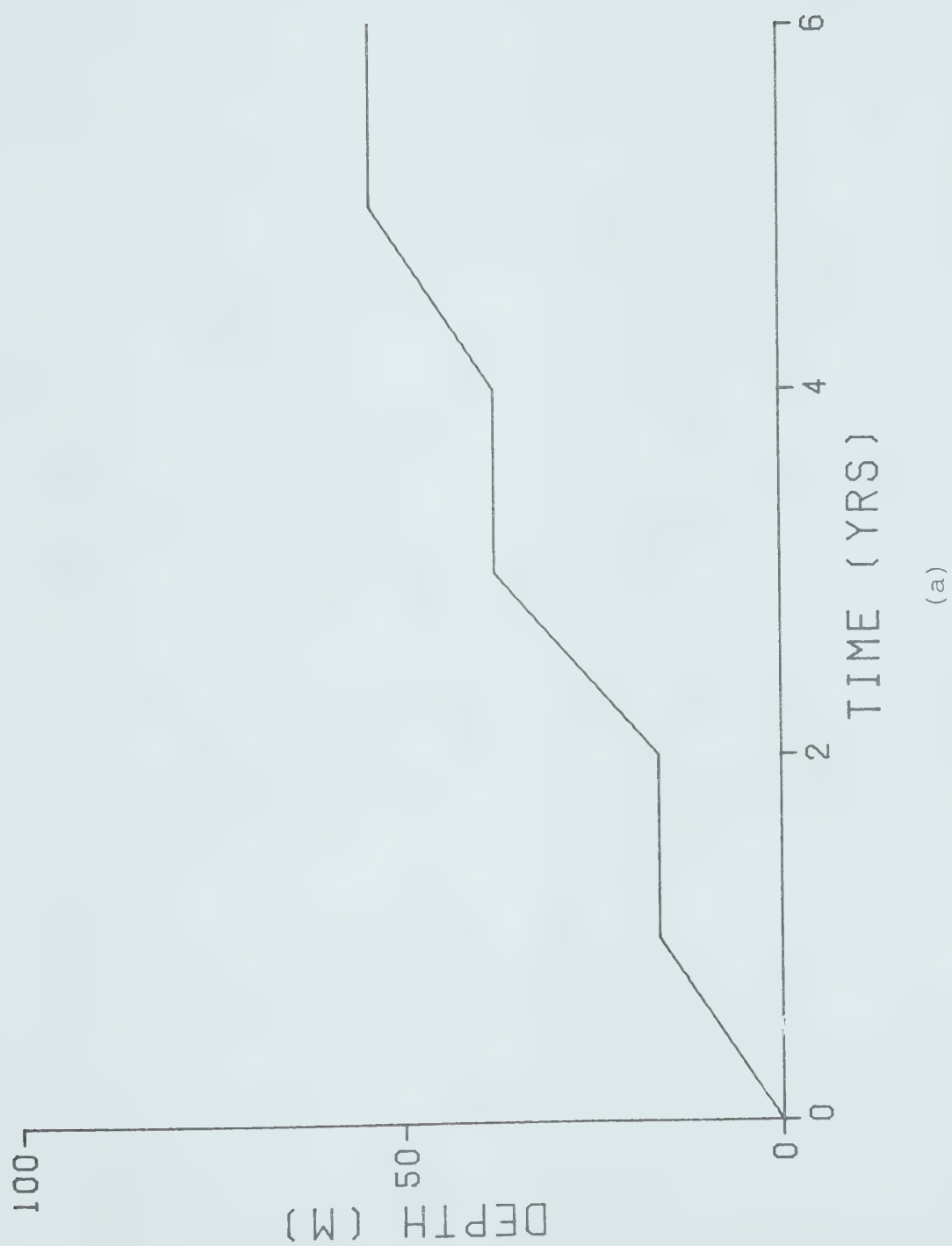
used for the Figure 3.10. The change of rate of filling has little effect on the centre of the Mohr circle, but the radius follows the level changes.

Three dimensional sections can be analysed and an example is shown in Figure 3.11. This shows the pressure, displacement, and effective stress at 5.5 years after filling using the filling history of figure 3.4. It is felt that the apparently noisy results are real since similar results were observed at higher orders of integration in two dimensions. The stresses are difficult to interpret in three dimensions, so an analysis of the physical behaviour will be done for two dimensional cross-sections only. The figure 3.11 indicates that the same results will generally be applicable. A similar analysis was repeated for lakes Nurek and Oroville. The results are shown in figures 3.12, 3.13. In each of these cases the filling history was the same, but the depth of fill varied in each case. The bathymetries are given with the lake depths being found by the technique of triangular interpolation outlined in section 5.1.4.

3.9 Layered Porous Elastic Half-Space

To allow for the variation of parameters with depth two approaches are possible. A functional dependence, perhaps exponential, may be introduced and the derivations found analytically. Substitutions must be made into the expressions already derived and similar processes followed.

Figure 3.10: Displacement, excess pressure, and effective stress for the loading rate shown (a). The changes in filling rate are only slightly seen in the movement of the centre of the Mohr circle.



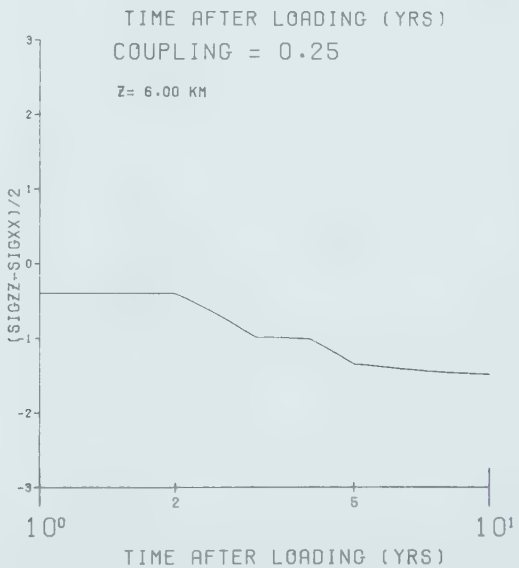
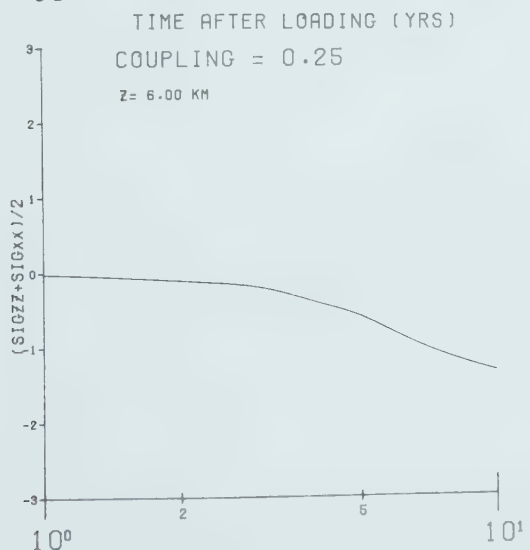
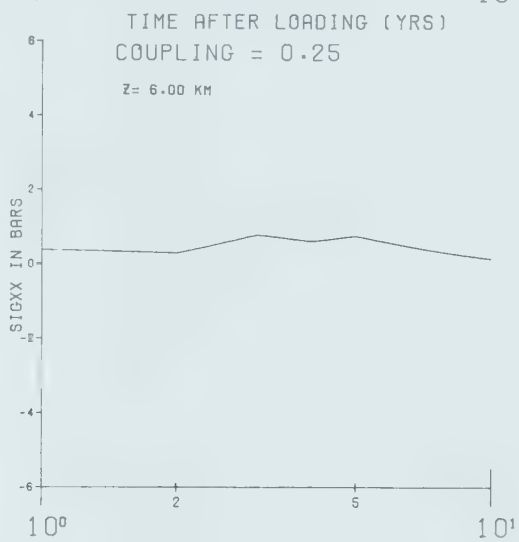
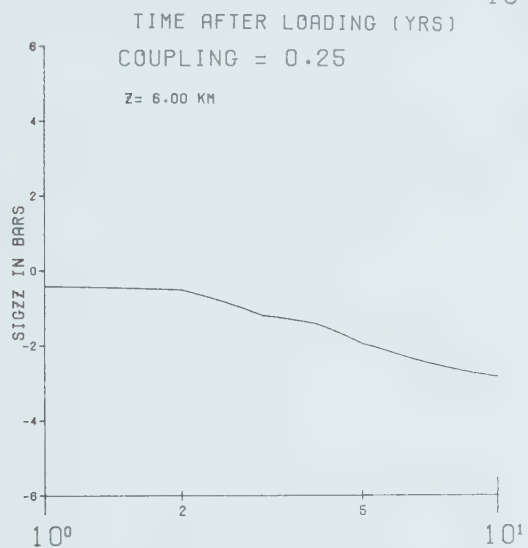
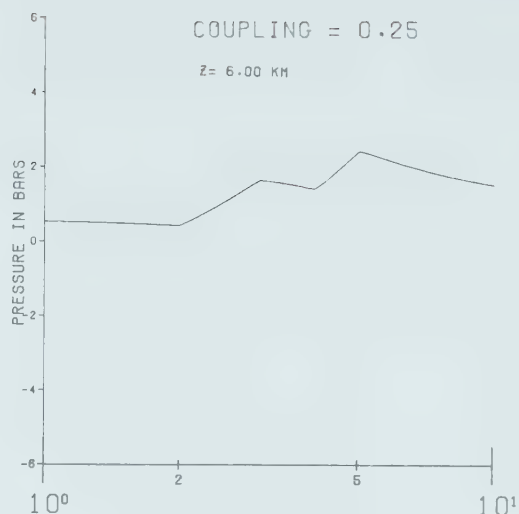
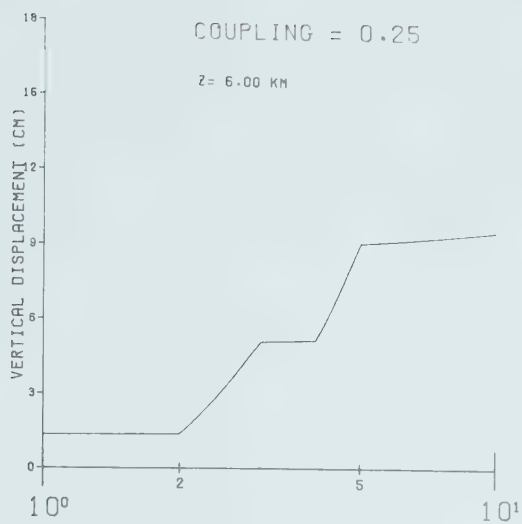


Figure 3.11: Three dimensional analysis below Lake
Kariba at 5.5 years.



VERT. DISPLACEMENT (CM) AT 5.5 YRS



EXCESS PRESSURE (BARS) AT 5.5 YRS



MAX PRIN. STRESS (BARS) AT 5.50 YRS



MIN PRIN. STRESS (BARS) AT 5.50 YRS

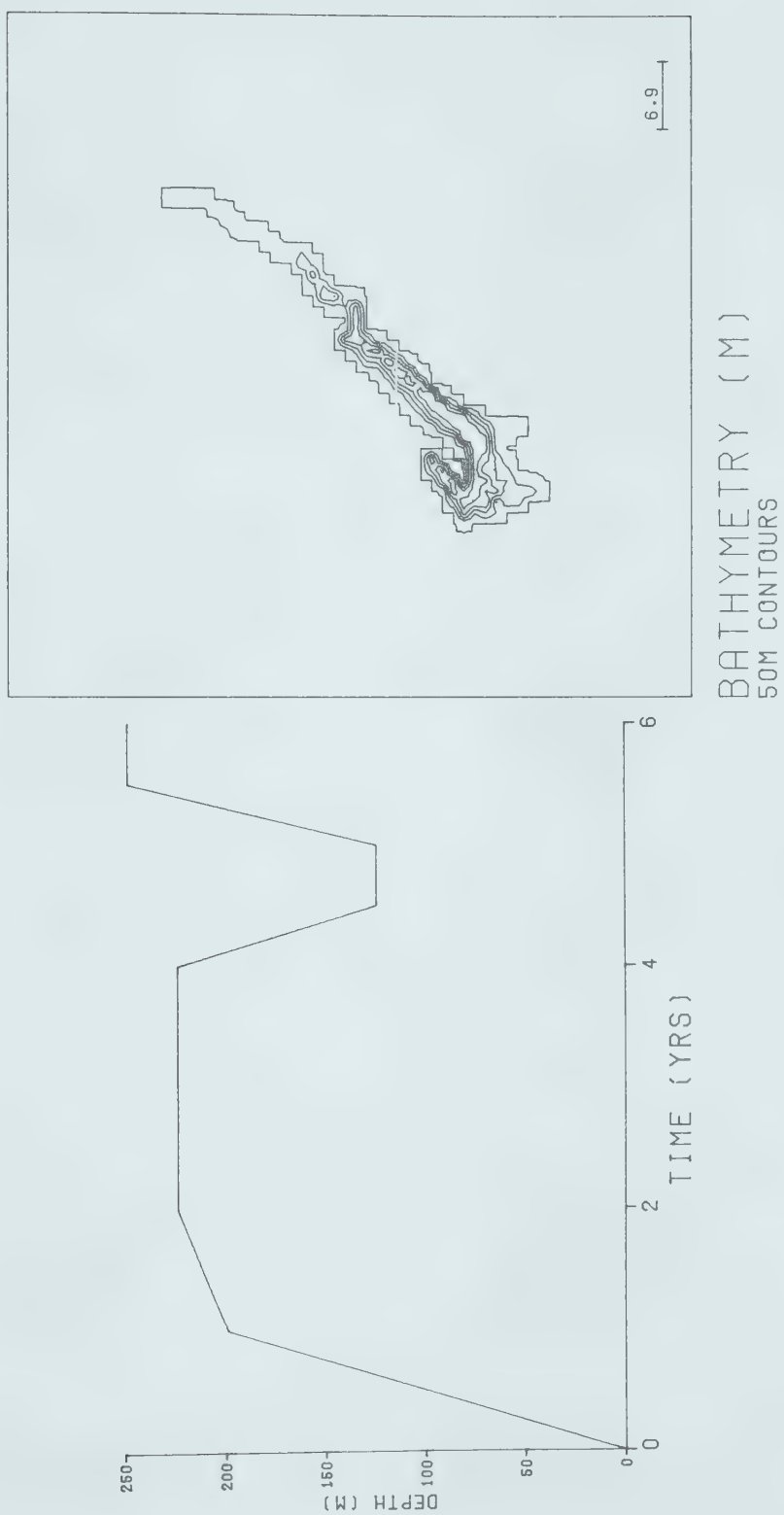


(MAX+MIN)/2 PRIN. STRESS AT 5.50 YRS
 YOUNG= 0.85MB SIGMA= 0.27
 PERM = 2.00MD COUPLING = 0.25
 ALPHA= 1.0 Q= 1.0E+34 DEP 6KM



MAXIMUM SHEAR STRESS AT 5.50 YRS
 YOUNG= 0.85MB SIGMA= 0.27
 PERM = 2.00MD COUPLING = 0.25
 ALPHA= 1.0 Q= 1.0E+34 DEP 6KM

Figure 3.12: Three dimensional analysis below Lake
Nurek at 5.5 years.





VERT. DISPLACEMENT (CM) AT 5.5 YRS



EXCESS PRESSURE (BARS) AT 5.5 YRS



MAX PRIN. STRESS (BARS) AT 5.50 YRS



MIN PRIN. STRESS (BARS) AT 5.50 YRS

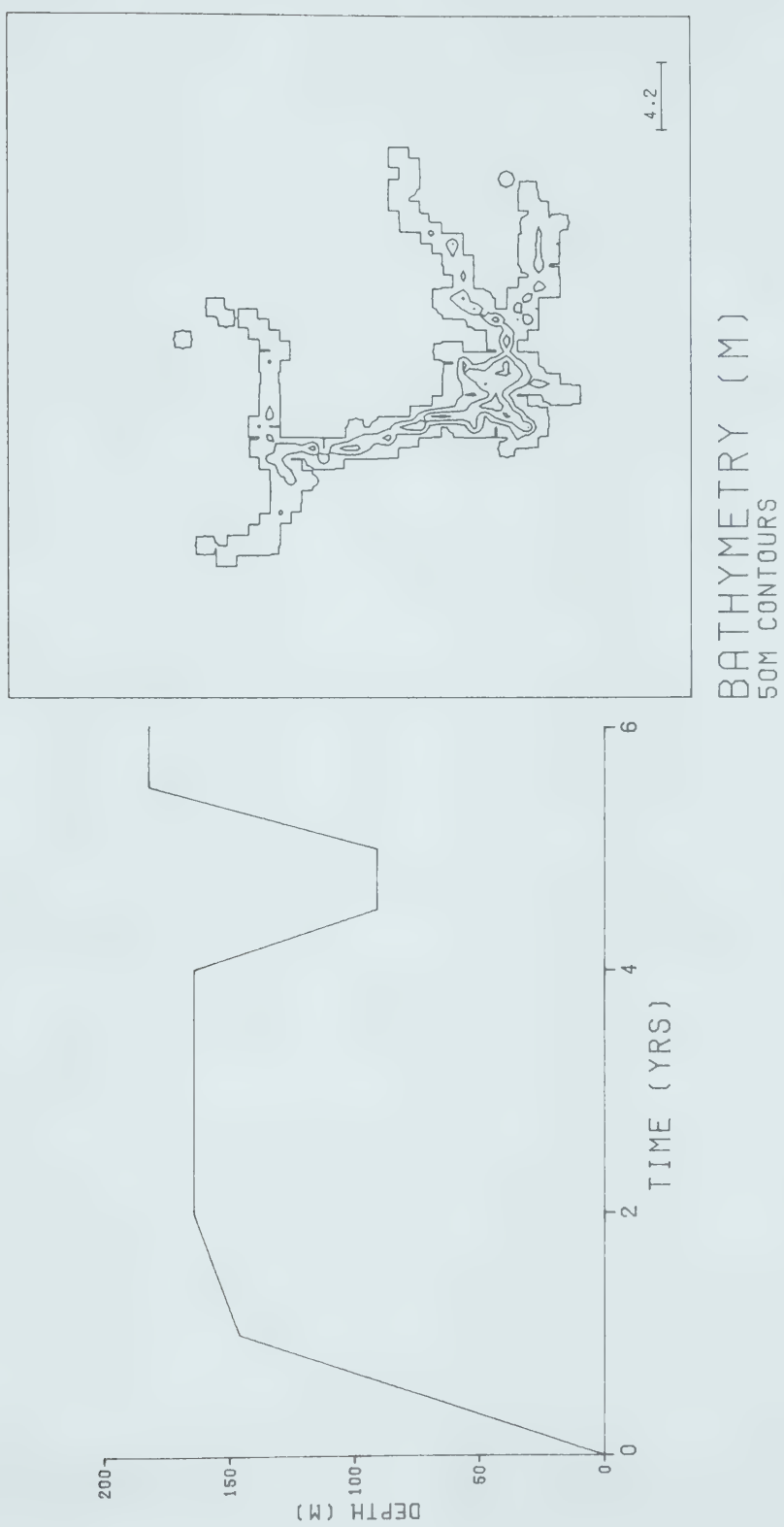


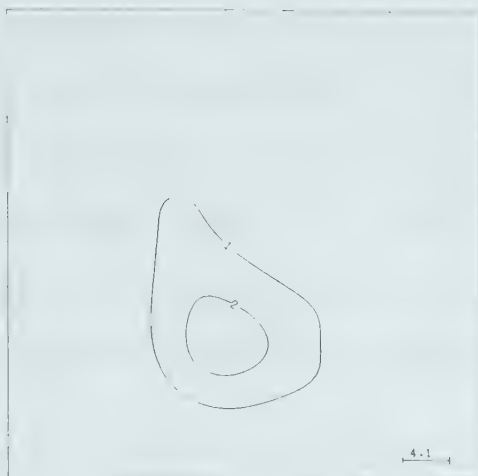
(MAX+MIN)/2 PRIN. STRESS AT 5.50 YRS
 YOUNG= 0.85MB SIGMA= 0.27
 PERM = 2.00MD COUPLING = 0.25
 ALPHA= 1.0 Q= 1.0E+34 DEP 3KM



MAXIMUM SHEAR STRESS AT 5.50 YRS
 YOUNG= 0.85MB SIGMA= 0.27
 PERM = 2.00MD COUPLING = 0.25
 ALPHA= 1.0 Q= 1.0E+34 DEP 3KM

Figure 3.13: Three dimensional analysis below Lake Oroville at 5.5 years. The excess pore pressure, vertical deflection, and effective stress are shown. The loading history of figure 3.6 was used for the calculation.





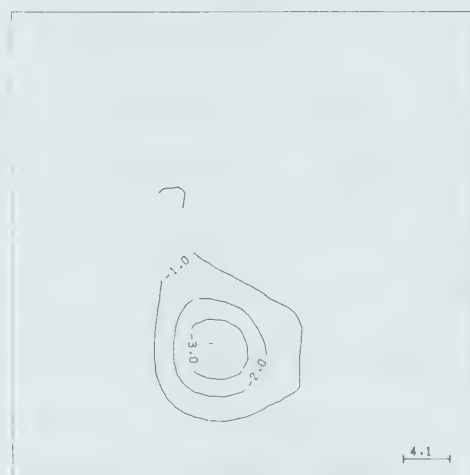
VERT. DISPLACEMENT (CM) AT 5.5 YRS



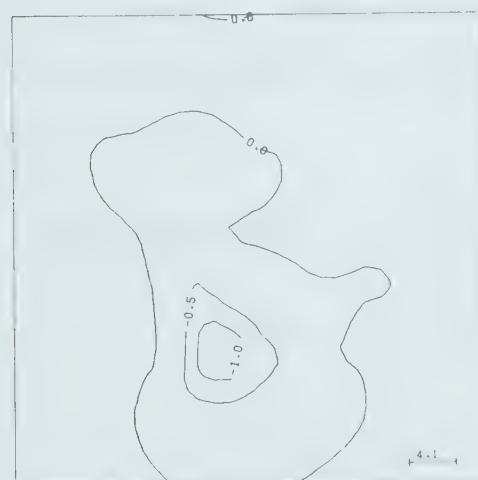
EXCESS PRESSURE (BARS) AT 5.5 YRS



MAX PRIN. STRESS (BARS) AT 5.5 YRS



MIN PRIN. STRESS (BARS) AT 5.5 YRS



(MAX+MIN)/2 PRIN. STRESS AT 5.5 YRS
 YOUNG= 0.85MB SIGMA= 0.27
 PERM = 2.00MD COUPLING = 0.25
 ALPHA= 1.0 Q= 1.0E+34 DEP 3KM



MAXIMUM SHEAR STRESS AT 5.50 YRS
 YOUNG= 0.85MB SIGMA= 0.27
 PERM = 2.00MD COUPLING = 0.25
 ALPHA= 1.0 Q= 1.0E+34 DEP 3KM

The algebra will become even more confused than it was in the work shown above. Another approach models the halfspace as a series of layers, each with different elastic and fluid properties. This is often a good approximation to sedimentary basins, and if there are a sufficient number of thin layers reasonable parameter variations may be modelled.

The treatment is analogous to that presented earlier for the elastic case with each interface having six boundary conditions. The continuity of displacements u, v, w reduce to two conditions which requires the interfaces to stay together. Continuity of the three stresses σ_{iz} again reduces to two conditions which prevents acceleration of the interface. Two other constraints are required. The pressure of the water must be continuous across an interface and the amount of water flowing out the bottom of a layer, V_z , must equal the amount flowing in the top of the layer below it. The time scaling introduced earlier depended on permeability and cannot be used here with each layer having a different permeability.

The equations (3.11) and (3.12) apply at any point.

$$\bar{c} \nabla^4 E = \frac{d}{dt} (\nabla^2 E) - 2a_1 \frac{d}{dt} \left(\frac{ds}{dz} \right)$$

$$\nabla^2 S = 0$$

$$c = \frac{2G\eta KQ}{(\alpha^2 Q + 2G\eta)}$$

$$a_1 = \frac{G}{(\alpha^2 Q + 2G\eta)}$$

Taking the Fourier and Laplace transforms reduces the

equation to:

$$(-\mu^2 + \frac{d^2}{dz^2})(-k^2 + \frac{d^2}{dz^2})\hat{E} = -2a_1s \frac{d\hat{S}}{dz}$$

$$(-k^2 + \frac{d^2}{dz^2})\hat{S} = 0$$

where

$$\mu^2 = k^2 + \frac{S}{C}$$

Solving the differential equations leads to the expanded form:

$$\hat{E} = A^+e^{-kz} + A^-e^{kz} + B^+e^{-\mu z} + B^-e^{\mu z} + a_1C^+ze^{-kz} + a_1C^-ze^{kz}$$

$$\hat{S} = C^+e^{-kz} + C^-e^{kz}$$

The six unknown constants A^+ , A^- , B^+ , B^- , C^+ and C^- are determined from the continuity conditions at each interface. Substituting into equation (3.10) leads to the matrix equation:

$$\begin{bmatrix} \sigma \\ \sigma_{zz} \\ \sigma_{xz} \\ u \\ v \\ V_z \end{bmatrix} = \begin{bmatrix} C_f & 0 \\ 0 & C_g \end{bmatrix} \begin{bmatrix} f^+ & f^- \\ g^+ & g^- \end{bmatrix} \begin{bmatrix} e^z & 0 \\ 0 & e^{+z} \end{bmatrix} \begin{bmatrix} A^+ \\ B^+ \\ C^+ \\ A^- \\ B^- \\ C^- \end{bmatrix}$$

$$\text{or } [\sigma] = [C][M][P][A]$$

-3.25

where

$$C_f = \begin{bmatrix} 2G/\alpha & 0 & 0 \\ 0 & 2G & 0 \\ 0 & 0 & 2G \end{bmatrix}$$

$$C_g = \begin{bmatrix} 1 & 0 & 0 \\ 0 & 1 & 0 \\ 0 & 0 & -\frac{2KG}{\alpha} \end{bmatrix}$$

$$e^{-z} = \begin{bmatrix} e^{-kz} & 0 & 0 \\ 0 & e^{-\mu z} & 0 \\ 0 & 0 & e^{-kz} \end{bmatrix}$$

$$e^{+z} = \begin{bmatrix} e^{kz} & 0 & 0 \\ 0 & e^{\mu z} & 0 \\ 0 & 0 & e^{kz} \end{bmatrix}$$

$$f_{\pm}^{\pm} = \begin{bmatrix} 0 & [-\eta(\mu^2 - k^2)] & \pm a_0 k \\ -k^2 & [-\mu^2 - (\eta - 1)(\mu^2 - k^2)] & \pm a_3^+ k \\ \mp ipk & \mp ip\mu & -ipa_2^+ \end{bmatrix}$$

$$g_{\pm}^{\pm} = \begin{bmatrix} ip & ip & ipz(a_1 - 1) \\ \pm k & \pm \mu & (a_2^+ - 1) \\ 0 & \pm \eta \mu (\mu^2 - k^2) & -k^2 a_0 \end{bmatrix}$$

$$a_0 = (2a_1\eta - 1)$$

$$a_3^+ = 2a_1\eta \pm zk(a_1 - 1)$$

$$a_2^+ = \pm zk(a_1 - 1) - a_1$$

and 0 is the 3x3 zero matrix.

The stresses are determined from the matrix equation:

$$[\sigma] = 2G[h^+ \quad h^-] \begin{bmatrix} e^{-z} & 0 \\ 0 & e^z \end{bmatrix} [A]$$

$$h^+ = \begin{bmatrix} p^2 & [p^2 - (\eta-1)(\mu^2 - k^2)] & [p^2 z(a_1-1) + 2a_1(\eta-1)k] \\ q^2 & [q^2 - (\eta-1)(\mu^2 - k^2)] & [q^2 z(a_1-1) + 2a_1(\eta-1)k] \\ -k^2 & [-\mu^2 - (\eta-1)(\mu^2 - k^2)] & [2a_1\eta + kz(1-a_1)] \\ \bar{i}pk & \bar{i}p\mu & -ip(+zk(a_1-1) - a_1) \\ \bar{i}qk & \bar{i}q\mu & -iq(+zk(a_1-1) - a_1) \\ pq & pq & pq z(a_1-1) \end{bmatrix}$$

$$[\sigma]^T = [\sigma_{xx} \quad \sigma_{yy} \quad \sigma_{zz} \quad \sigma_{xz} \quad \sigma_{yz} \quad \sigma_{xy}]$$

Continuity at the i interface at depth z below the surface, separating the i and $i-1$ layers requires:

$$[C]_i [M]_{i,z_i} [P(z_i)] [A]_i = [C]_{i-1} [M]_{i-1,z_i} [P(z_i)] [A]_{i-1}$$

or

$$[A]_{i-1} = [P(z_i)]^{-1} [M]_{i-1,z_i}^{-1} [C]_{i-1}^{-1} [C]_i [M]_{i,z_i} [P(z_i)] [A]_i$$

-3.27

The notation of figure 2.9 has been used here. Below the lowest interface (N) lies a halfspace and the boundedness of values requires A_N^- , B_N^- and C_N^- to be zero. The top surface has specified values of excess pressure, $\hat{\sigma}$, the normal load $\hat{\sigma}_z$ and $\hat{\sigma}_{xz} = 0$. The three remaining unknown constants can be evaluated from:

$$\begin{bmatrix} \hat{P} \\ \hat{T} \\ 0 \end{bmatrix} = [C]_1 [M]_{1,z=0} [P(0)] [A]_1 \quad -3.28$$

$$A_N^- = B_N^- = C_N^- = 0 \quad -3.29$$

The equations (3.27), (3.28), (3.29) are sufficient to calculate the A_i^\pm , B_i^\pm , C_i^\pm in all the layers ($i=1,2,\dots,N$) and (3.25) and (3.26) suffice to compute the stresses and displacements everywhere.

The inverse Laplace transforms are difficult to do in this layered model. The inverse matrices $[M]_{i,z}^{-1}$ can be found analytically in terms of μ and when post multiplied by $[M]_{i,z}$ in the next layer leads to functions for which the inverse Laplace transforms are known. After several attempts, efforts to find simplified inverses were discontinued. There are algebra routines (REDUCE2, ALTRAN, FORMAC) available which can do this type of tedious manipulation but they were not used. It is sufficient to conclude that $[A]$ in an upper layer may be connected to $[A]$ in other layers by a series of convolution integrals. The convolutions become derivatives when a bottom layer is connected with a top layer. This series of time convolutions and derivatives indicate the results at any time and place depend on the behaviour at all other layers and times.

The numeric instability inherent in the required computation indicated the results would always be suspect. The analysis is adaptable, but other methods are probably more useful for this type of problem. The finite element technique will be described in the next chapter.

Chapter 4

Extension and Improvements of the Work

The theoretical description given in Chapter 3 is only a first attempt to describe the behaviour of water filled material. Various extensions can be made to the theory to allow for changes in the various parameters which depend on stress. Assumptions have also been made which, though unnecessary, simplify the model representation.

The stresses which are computed are only the anomalous stresses applied to the 'neutral' background with the initial stresses, hydrologic conditions and the gravitational forces being ignored. These are easily substituted into the equations but were omitted to avoid confusing the output results. In any application requiring the absolute stress levels these of course should be considered.

4.1 Pressure Dependent Effective Stress Laws

The simple, or conventional effective stress law was defined in section 1.3 with $\alpha=1$ being used in the equation

$$\sigma_{\text{effective}} = \sigma_{\text{applied}} + \alpha P$$

where P is the fluid pressure. For large changes of stress α is found to be pressure dependent. Terzaghi argued that

$\alpha = \eta$, where η is the porosity, however, his experimental results showed that α was close to one. Handin et.al. (1963) extended these experiments to different pressures and rock types and showed α is usually one except for very low porosities. Brace and Martin (1968) try to explain this to be a result of the applied strain rate. Brace and Martin also report a pressure drop (dilation) just before failure. Hubbert and Rubey (1959) attempted to prove that $\alpha = 1$, but Nur and Byerlee (1971) show this argument is not valid for low porosities. Skempton (1961) and Geertsma (1971) proposed a model which was verified by Nur and Byerlee (1971) in which

$$\alpha = 1 - \beta/\beta_s \quad -4.1$$

where β is the bulk modulus of the porous rock and β_s is the bulk modulus of the rock grains. Usually β/β_s is small, but β is strongly dependent on pressure. Empirically they suggest a linear dependence:

$$\beta = \beta_0 (P_c - P_w) \quad -4.2$$

where P_w is the water pressure and P_c the confining pressure. Knutson and Bohor (1963) show the variation of bulk modulus for several rock types over a wide pressure range. Changes of more than 100% are observed for Weber Sandstone with a pressure change of 1000 bars.

Moreland (1972) approached the problem of defining the pressure and stress as the average over several grains. This work on the Theory of Interacting Continua (TINC) derived

the form of (4.1) by a first order simplification. Garg and Nur (1973) compared each of the models and concluded that while the conventional stress law ($\alpha = 1$) overcorrects for the pore pressure effect, the TINC and (4.1) underestimates the effect. They suggest the underestimation may be a result of strain rate used. They also show that the conventional stress law best describes the material strength but is the poorest in describing deformation.

This study is mainly concerned with fracturing and the conventional stress law ($\alpha = 1$) was used. If the application is directed more towards deformation the equations 4.1 and 4.2 should be used.

4.2 Variation of Permeability

The existence of fractures reflects the water transferring capability of rocks. If an earthquake occurs in a certain region it will introduce new fractures and may change the drainage pattern of the area. Water may also be transmitted by diffusion through the rock, so the permeability and fracture frequency must be considered.

Little information is available about effective permeabilities on the large scales of 10's of kilometers, however both aperture aspect and permeabilities are stress dependent. Snow (1970) describes fracture frequency and aperture width at depths of about 25-100m. In most cases,

both the frequency and permeability (which depends on the aperture) decrease with depth. Fatt (1953) has shown that the permeability decreases with increasing pressure in hydraulically tested samples. For rocks taken from oil-gas reservoirs, the permeability was observed to decrease by as much as 30% upon application of 300 bar confining pressures. The rocks he tested had high permeabilities initially: between 100 and 250 millidarcy. Morgenstern and Guther (1974) interpret experimental results on dry samples slightly differently. The permeability was certainly found to decrease with pressure, it decreased rapidly initially and less rapidly at higher stresses. In most cases the permeability of sandstone was reduced by less than 50 per cent over substantial pressure ranges. Coals, granites and gneisses had larger reductions attributable to changes in the secondary structure of the materials, Guther (1972) found that the function

$$K = \frac{A}{(J + T)^N}$$

embraces much of the experimental data. He defines the average principal stress

$$J = \frac{1}{3}[\sigma_v(1+2R_o) + (1+\nu)(\Delta\sigma_h + \Delta\sigma_v)]$$

where σ_v , σ_h , $\Delta\sigma_v$, $\Delta\sigma_h$ are the horizontal and vertical effective stresses and the changes in the stresses respectively. R_o is the ratio of horizontal to vertical effective stress. ν is Poisson's Ratio. 'A' is a constant adjusted to match the permeability at zero effective stress.

The values of T and N are found from experiments. For rocks showing a strong dependence of permeability with stress, the best approximation for the samples tested was $N=3.0$ $T=20$ psi (2.8 bars). Weak dependence gave $N=2.0$, $T=40$ psi. These values will depend on the rocks used but indicate the typical magnitudes. It should be mentioned the fit of this function was shown only in the 1 to 25 bar range.

Gangi (1976) has derived a permeability-pressure law using arguments of Hertz compression of spherical granular material. The permeability variation with pressure is given by

$$K(p) = K_0 \left(1 - C_0 \left[\frac{(P+P_i)^{2/3}}{P_0} \right]^2 \right)$$

where K_0 is the initial permeability of the loose grain packing, C_0 is a packing constant (of the order of 4), P_i is the "equivalent pressure due to the cementation and deformation of the grains since there is some deformation even at zero pressure. P_0 is the effective elastic modulus of the grains defined by

$$P_0 = 4\beta_s (1-2\nu) (1-\nu^2)$$

where β_s is the grain's bulk modulus and ν is Poisson's Ratio.

Gangi (1976) also derived the permeability-pressure relation for a "bed of nails" model. In this case two flat layers are separated by small, column like, asperities. The functional dependence is $K(p) = K_0 (1 - (P/P_1)^m)^3$

where K_0 is the zero pressure permeability, P_1 is the effective modulus of the asperities defined by

$$P_1 = E A_r/A \ll E$$

and A_r/A is the fraction of the fracture face covered with the asperities (generally this is small). 'm' is a constant ($0 < m < 1$) which characterises the distribution function of the asperity lengths. Gangi was able to obtain a good fit to the experimentally determined permeability of a 200 millidarcy sample between 0 and 700 bars.

4.3 Finite Element Analysis

In geologically realistic problems the earth is rarely homogeneous or isotropic. There are always rock type changes, fracturing and large variation of parameters. The largest single disadvantage to the theory outlined is its inability to handle lateral variations of parameters - and this includes inclined faulting. One way to solve these problems uses the technique known as 'Finite Element Analysis'. In this, the space is divided into elements and the behaviour within the element is found by a variational analysis with the value at the nodes either being specified or computed. The determination of unknown nodal values is done by solving a matrix equation. Within each element interpolation is done by polynomial expansion, usually of orders one to four.

Finite element analysis is not often used simply because a three dimensional problem requires a prohibitively large matrix inversion. Problems with axial symmetry or with two dimensions are quite solveable using this method. The time dependence is another difficulty since linear time stepping introduces numeric noise.

For completeness a description will be given of the development necessary for finite element analysis of Biot's Consolidation Equations. The coupling of transform techniques with F.E.M. for solutions of the equations near the surface shows great promise. Near surface fracturing, rock changes and topography could be solved by the F.E.M. and below this the analysis could be done by transforms since the property changes are more gradual.

The literature on the F.E.M. technique being used in consolidation problems is indeed extensive. A selection of the literature is given in the Bibliography with the works of Hwang, Irobe, Valliappan and Zienkiewicz being noteworthy. The notation and description by Irobe et.al. (1974) will be followed since it describes unsaturated soils.

4.3.1 Variational Equation

The basic equations are:

(a) the equilibrium equation

$$\sigma_{ij} + \rho_l F_i = 0$$

where σ_{ij} is the stress and ρ_1 the density of the saturated soil. F_i are body force components with gravity being the significant force.

(b) the constitutive equation

$$\sigma_{ij} + \alpha_{ij}P = C_{ijkl} e_{kl}$$

where the u_i are displacement components of the solid. Ghaboussi and Wilson (1973) show that the introduction of two elastic matrices will describe a compressible fluid model. The α_{ij} is a second order symmetric tensor and are the 21 elastic moduli of the solid. 'P' is the excess pore pressure.

(c) Strain displacement equation

$$e_{ij} = \frac{1}{2}(u_{i,j} + u_{j,i})$$

(d) the generalised D'Arcy's equation

$$\dot{V}_i = \dot{U}_i - \dot{u}_i = -K_{ij}(P_{,j} + \rho_2 F_j) \quad -4.3 \quad -4.3$$

where V_i is the component of fluid flow volume, K_{ij} is the permeability tensor, ρ_2 the mass density of the water. U_i is the component of fluid displacement and u_i the displacement component of the solid. The inflow volume $-V_{i,i}$ is composed of air void, volume change and solid deformation. If the Biot notation is again used, $1/Q$ is a measure of the amount of water that can be pressed into the solid while the volume is kept constant. Then:

$$- \dot{V}_{i,i} = \frac{1}{Q} \dot{P} + \alpha_{ij} R_{ij} \quad -4.4$$

Two invariants must be used in a variational solution to this problem. The first invariant is defined:

$$\Psi = \int \frac{1}{2}(C_{ijkl} e_{kl} e_{ij} + P/Q) dv$$

and it may be referred to as the elastic consolidation potential. If the initial conditions are all zero:

$$u_i = 0 = U_i \quad p_{ij} + \rho_2 F_j = 0$$

then (4.4) may be rearranged:

$$p = -Q(V_{i,i} + \frac{1}{2}\alpha_{ij}(u_{i,j} + u_{j,i})) \quad -4.5$$

If Ω plays the role of the dissipation function, then its variation is given by

$$\delta\Omega = \int \lambda_{ij} \dot{V}_j \delta V_i dv$$

where λ_{ij} is the flow resistivity tensor equal to the inverse of the permeability tensor. The variation equation must also satisfy the boundary condition and the total variation for the problem becomes

$$\begin{aligned} \delta\Psi + \delta\Omega = & \int \rho_1 F_i \delta u_i dv - \int \rho_2 F_i \delta V_i dv \\ & + \int (T_i \delta u_i - P_O \delta V n_i) ds \end{aligned} \quad -4.6$$

where T_i and P_O are the surface tractions and pressure acting on the surface with outward normal .

4.3.2 Finite Element Description

If the space below the load is divided into elements and the value at any point is described in terms of a polynomial expansion of the nodal values, then the displacements and inflow volumes may be expressed in the matrix form.

$$\{u\} = [N] \{u\}^* \quad -4.7$$

$$\{V\} = [N] \{V\}^* \quad -4.8$$

where the notation $\{ \}$ is used for column matrices, $\langle \rangle$ for row matrices and $[]$ for rectangular matrices. The $[N]$ are the shape functions for the elements chosen and $\{ \}^*$ implies that the array contains values of nodal points.

The strain matrix can be obtained from the derivative of (4.7)

$$\{e\} = [B] \{U\}^* \quad -4.9$$

where $[B]$ is obtained from $[N]$ and the equation (4.3). The pressure is determined from (4.5), (4.7) and (4.9).

$$P = -Q(\langle 1 \rangle [B_1] \{V\}^* + \langle \Lambda \rangle [B] \{u\}^*)$$

where $\langle 1 \rangle = \langle 1, 1, \dots, 1 \rangle$ and $\langle \rangle = \langle \alpha_{11}, \dots, \alpha_{31} \rangle$. The $[B_1]$ matrix is required for contraction of the indices in the $\{ \}^*$. The six components of equation (4.6) may be written in matrix form:

$$\delta \Psi = \{ \delta u \}^{*T} [B]^T [D]^T \{ u \}^* dv$$

$$+ Q \int \{ u \}^{*T} ([B]^T \{ \Lambda \} \langle \Lambda \rangle [B] \{ u \}^* + [B]^T \{ \Lambda \} \langle 1 \rangle [B_1] \{ V \}^*) dv$$

$$+ Q \int \{ \delta V \}^{*T} ([B_1]^T \{ 1 \} \langle \Lambda \rangle [B] \{ u \}^* + [B_1]^T \{ 1 \} \langle 1 \rangle [B_1] \{ V \}^*) dv \quad -4.10$$

$$\delta \Omega = \int \{ \delta V \}^{*T} [N]^T [D_V] [N] \{ \dot{V} \} dv \quad -4.11$$

where $[D]$ and $[D_V]$ are the elastic and flow resistivity matrices for the elements, and

$$\int \rho_1 F_i \delta u_i dv = \int \{ u \}^{*T} [N]^T \{ P_1 \} dv \quad -4.12$$

$$\int \rho_2 F_i \delta V_i dv = \int \{ V \}^{*T} [N]^T \{ P_2 \} dv \quad -4.13$$

$$\int T_i \delta u_i ds = \{u\}^{*T} \{F\}^* \quad -4.14$$

$$\int P_o \delta V_i n_i ds = \{\delta V\}^{*T} [H] \{P_o\}^* = \{\delta V\}^{*T} \{G\}^* \quad -4.15$$

where $\{P_j\}$ is the column vector of the body force $\rho_j F_i$, $\{F\}^*$ is the column vector of the equivalent nodal point loads, $[H]$ is the matrix derived by the integral of the product of the interpolation functions of inflow volume and pore pressure along the boundary, and $\{P_o\}^*$ are pore pressures at the nodal points.

Since the variations of u and v are arbitrary then substitution of (4.10) to (4.15) into (4.6) leads to the two equations describing the equilibrium equation and the flow equation

$$\{F\}^* = ([K] + [L_o])\{u\}^* + [L_1]\{V\}^* - \{F_1\}^* \quad -4.16$$

$$- \{G\}^* = [L_2]\{u\}^* + [L_3]\{V\}^* + [M]\{\dot{V}\}^* - \{F_2\}^* \quad -4.17$$

where $[K] = \int [B]^T [D] [B] dv$

$$[L_o] = Q \int [B]^T \{\Lambda\} \langle \Lambda \rangle [B] dv$$

$$[L_1] = Q \int [B]^T \{\Lambda\} \langle 1 \rangle [B] dv$$

$$[L_2] = Q \int [B]^T \{1\} \langle \Lambda \rangle [B] dv$$

$$[L_3] = Q \int [B_1]^T \{1\} \langle 1 \rangle [B_1] dv \quad -4.18$$

$$[M] = \int [N]^T [D_v] [N] dv$$

$$\{F_1\}^* = \int [N]^T \{P_1\} dv$$

$$\{F_2\}^* = \int [N]^T \{P_2\} dv$$

It is assumed by Irobe et.al. that the v changes linearly over small time intervals Δ so that $\{\dot{v}\}^*$ evaluated at time t may be expressed as:

$$\begin{aligned} \{\dot{V}\}_t^* &= \frac{2}{\Delta} \{\dot{V}\}_t^* - \left(\frac{2}{\Delta}\right) \{V\}_{t-\Delta}^* + \{\dot{V}\}_{t-\Delta}^* \\ &= \frac{2}{\Delta} \{V\}_t^* - \{G\}_{t-\Delta} \end{aligned}$$

Equations (2.16), (2.17) may be combined in the matrix form

$$\begin{bmatrix} F \\ -G \end{bmatrix}_t^* + \begin{bmatrix} F_1 \\ F_2 \end{bmatrix}_t^* + \begin{bmatrix} 0 \\ G_V \end{bmatrix}_{t-\Delta}^* = \begin{bmatrix} k_{11} & k_{12} \\ k_{12} & k_{22} \end{bmatrix} \begin{bmatrix} U \\ V \end{bmatrix}_t^*$$

where

$$[k_{11}] = [k] + [L_0]$$

$$[k_{12}] = [L_1]$$

$$[k_{21}] = [L_2]$$

$$[k_{22}] = [L_3] + \frac{2}{\Delta} [M]$$

This equation can be solved by time stepping as it has a recurring form. This time stepping is numerically poor and may diverge. Other techniques using time convolutions (see Hwang et.al. 1972) avoid some of these difficulties. The earlier analysis showed that the time dependence usually involves error functions, however published results using time stepping agree well with analytic solutions in two dimensions.

4.3.3 Possible Elements in Three Dimensions

In three dimensional problems several element shapes are possible. Zienkiewicz (1971) describes these elements and indicates that the choice will depend eventually on the problem. Since there is no symmetry in the lake problems the choice would be limited to the tetrahedron and the brick element. The number of nodes chosen will also depend on the order of polynomial the interpolation will use. In general, polynomial order will be one less than the number of nodes along the element edge. Examples of elements are given in figures 4.1 and 4.2.

The tetrahedral element shape functions are best described in terms of volume coordinates. These coordinates have values between 0 and 1 and are equivalent to the normalised perpendicular height above a particular side. There are of course four coordinates for the four corners and heights. In figure 4.1d the coordinate L_1 is defined by:

$$L_1 = \frac{\text{Volume}(P234)}{\text{Volume}(1234)}$$

For the cubic tetrahedron (4.1c) the shape function for each of the node types is:

Corner Nodes

$$N_1 = \frac{1}{2} (3L_1 - 1) (3L_1 - 2) L_1$$

Midside Nodes

$$N_5 = \frac{9}{2} L_1 L_2 (3L_1 - 1)$$

Mid-face Nodes

$$N_{18} = 27 L_1 L_2 L_3$$

figure 4.1: The tetrahedral finite element family with the required nodes for (a) linear, (b) quadratic, and (c) cubic interpolation. The volume coordinate, with values between 0 and 1 is defined as the ratio of the volume (P234) to volume (1234).

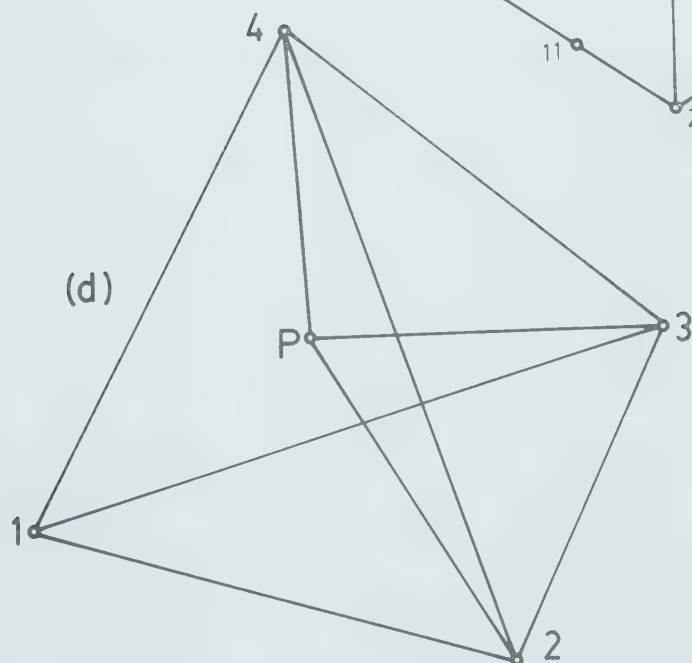
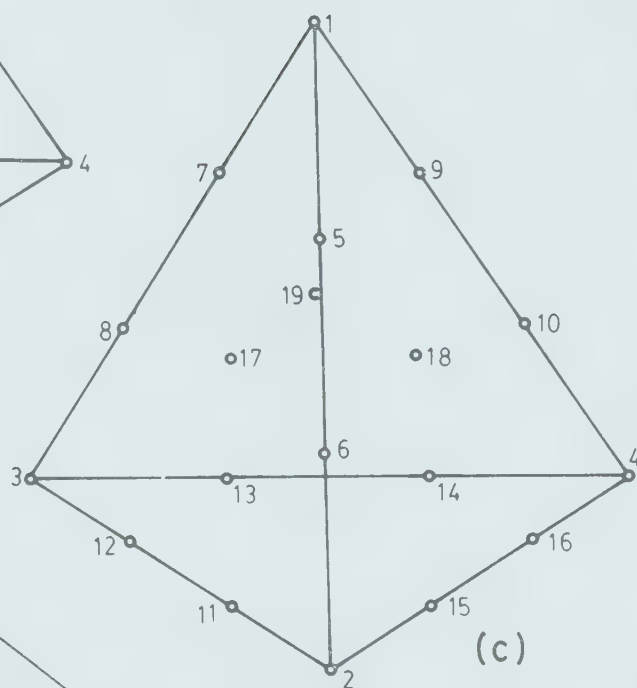
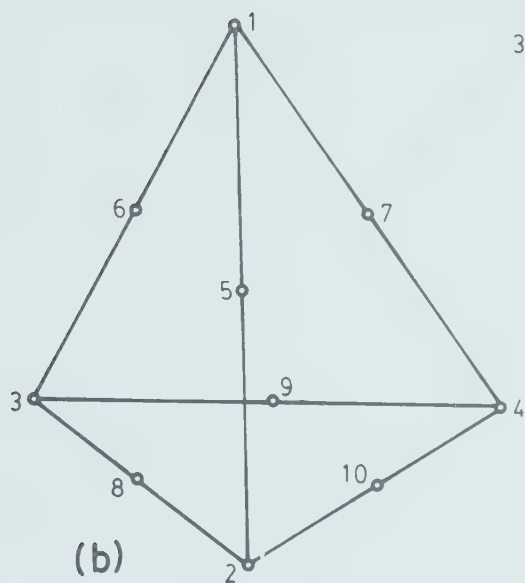
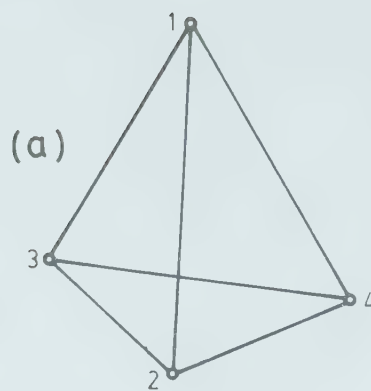
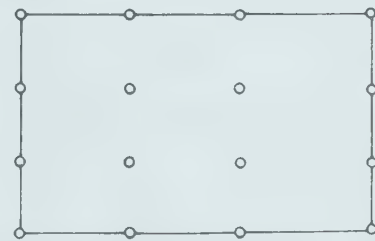
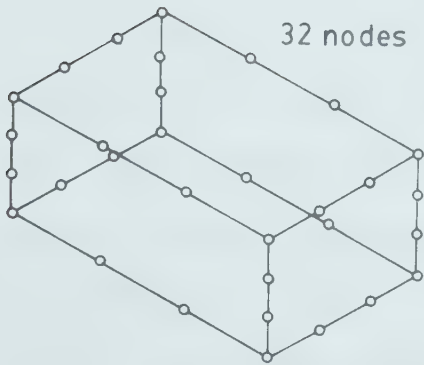
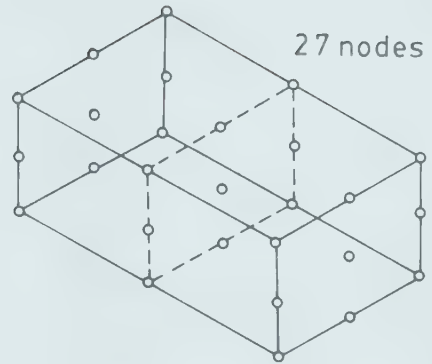
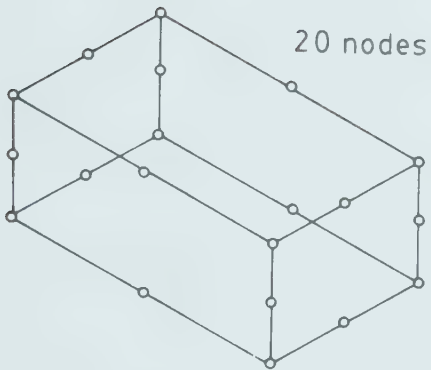
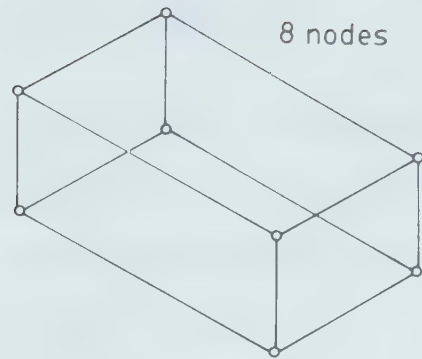
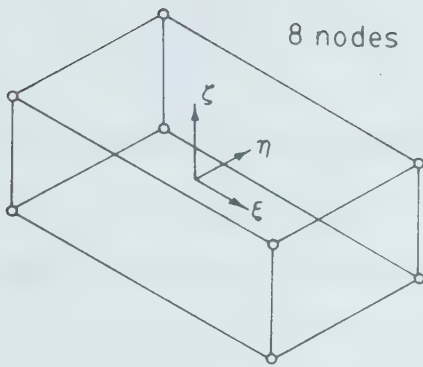


figure 4.2: Nodal points for the 'brick' elements. The serendipity elements (a), and the Lagrangian elements (b) are shown for linear, quadratic, and cubic interpolation. Notice the large number of internal nodes required for the Lagrangian elements.



SERENDIPITY
ELEMENTS

(a)

LAGRANGE
ELEMENTS

(b)

The integration formula required in the integrations of (4.18) is

$$\iiint_{\text{element}} L_1^a L_2^b L_3^c L_4^d dx dy dz = \frac{a!b!c!d!}{(a+b+c+d+3)!} 6V$$

The matrix form of equation (4.7) can be written immediately with this knowledge of the shape functions N . Since all the nodes there are three displacement components specified:

$$\begin{bmatrix} u \\ v \\ w \end{bmatrix} = [IN_1, IN_2, \dots, IN_j] \begin{bmatrix} u_1 \\ v_1 \\ w_1 \\ \vdots \\ \vdots \\ u_j \\ v_j \\ w_j \end{bmatrix} = [N]\{u\}^*$$

where $I = \begin{bmatrix} 1 & 0 & 0 \\ 0 & 1 & 0 \\ 0 & 0 & 1 \end{bmatrix}$

In the case of rectangular prisms two shape functions are usually chosen. The coordinate axis, shown in figure 4.2a, is centred in the middle of the brick with the bricks edges having coordinate values of ± 1 . The cubic 'serendipity' elements require nodes only along the edges and the polynomial expansion is incomplete. This is still satisfactory since the F.E.M. usually only requires continuity of the boundary values and the first derivatives.

The shape functions are derived in terms of the coordinate axis given in figure 4.2a. As an example a cubic

element has 32 nodes and the shape functions are given by:

Corner Nodes

$$N_i = \frac{1}{64} (1+\xi_0) (1+\eta_0) (1+\zeta_0) [9(\xi^2 + \eta^2 + \zeta^2) - 19]$$

Mid-side Nodes

$$\xi_i = \pm \frac{1}{3} \quad \eta_i = \pm \frac{1}{3} \quad \zeta_i = \pm 1$$

$$N_i = \frac{9}{64} (1+\xi^2) (1+\eta_0) (1+\zeta_0) (1+\zeta_i)$$

where

$$\xi_0 = \xi \xi_i \quad \eta_0 = \eta \eta_i \quad \zeta_0 = \zeta \zeta_i$$

These forms were introduced to allow for \pm signs in the general formula. The other shape functions useful for brick elements involve products of Lagrangian polynomials which can be written

$$L_i^n(x) = \frac{(x-x_1)(x-x_2)(x-x_3) \dots (x-x_n)}{(x_i-x_1)(x_i-x_2)(x_i-x_3) \dots (x_i-x_n)}$$

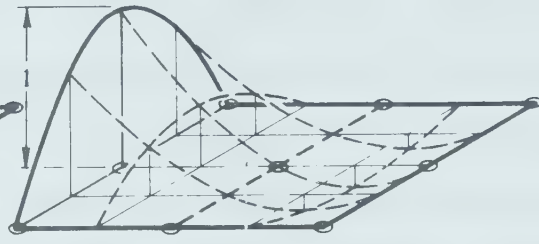
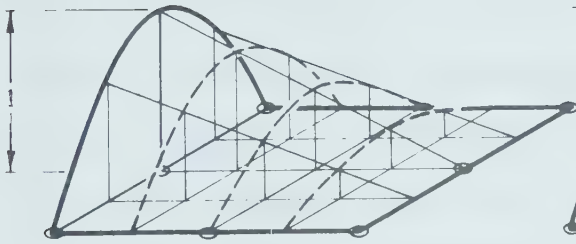
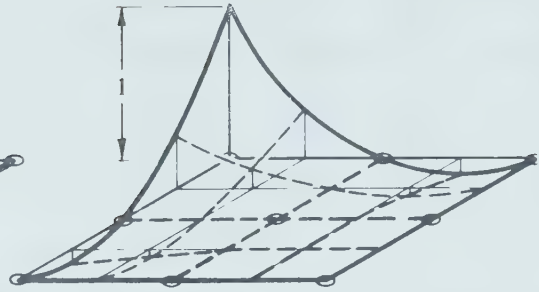
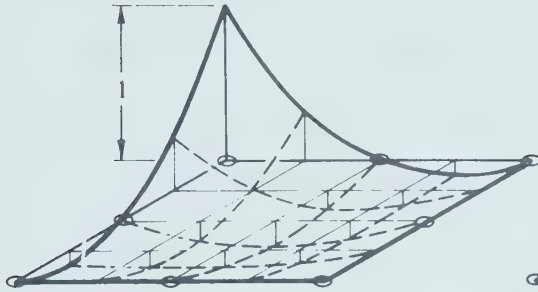
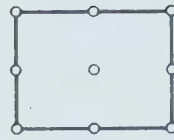
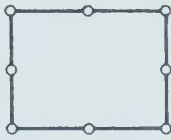
This is clearly equal to one at the point x_i and is zero at all other x_j . The shape functions in three dimensions are products of those in one dimension:

$$N_{ij\ell} = L_i^n(\xi) L_j^m(\eta) L_\ell^k(\zeta)$$

The Lagrangian family is unlimited and is easy to generate, however it is limited by the large number of internal nodes. The higher order polynomials also exhibit poor curve fitting properties.

The Lagrangian and Serendipity elements in two and three dimensions are shown in figure 4.2. The quadratic shape functions in two dimensions are shown in figure 4.3.

figure 4.3: The two dimensional quartic shape functions for the serendipity (a), and Lagrangian (b) elements.



(a)

(b)

4.4 An Introduction to Statistical Prediction

A large amount of statistical analysis is done in an attempt to predict earthquakes and determine seismic risk by examining the seismicity of a region. This approach is of particular interest in areas such as Kremasta (see figure 1.3) where it is difficult to determine whether a certain earthquake is related to the filling of a reservoir, or is part of the natural sequence. Oroville (see figure 1.7) is a case where there may have been a change in the pattern of earthquakes. The event in 1975 occurred in an apparently quiet area, and the decision should be made whether this fell within the scatter of the normal tectonic events or whether it reflects a change in the seismicity. The answer to this question is relevant to other dams in the area. If there had been an induced change in the seismicity with a delay after filling, then it may happen again. If the Oroville earthquake was of natural origin, then other dams will have different behaviour depending on their proximity to tectonic lineaments.

In an attempt to answer questions of this type a review of the literature was made. At this stage no attempt has been made to apply the techniques described below to real lake situations and their inclusion is for completeness and as a guide to future work.

The usual work on seismicity is described in a paper by

McGuire (1976) and involves the determination of seismic risk and maximum intensity for state building codes. The area under study is divided into regions each with similar seismic and geological features. It is necessary to determine the magnitude of an earthquake which may occur with a specified probability. The events are assumed to be Poisson distributed when aftershocks are removed from the sequence. The size of successive events are assumed independent and the number of events are exponentially related to the intensity. McGuire (1976) gives a description of the algebra required, and shows how the uncertainty of the parameters affects the statistics.

Possibly a more suitable statistical approach is that proposed by Knopoff, Vere-Jones, Keilis-Borok and others using stochastic processes which are reviewed by Knopoff (1971). In this 1971 review of the Markov process, a model is suggested in which the energy of a certain area is increased at a constant rate and released by sudden drops so that an energy balance is achieved. A typical energy buildup and release resembles an irregular sawtooth pattern. The probabilities can be specified so that the larger the energy at a certain time, the more likely there is of a large earthquake occurring. Spatial as well as temporal changes should be included in this model for it to be applicable in a particular region.

A third method of predicting earthquakes has recently

been suggested by Gasperini et.al. (1976). From the Italian data they used they were able to predict that a 'large' earthquake would occur within six years of a swarm in the same region. The definition of a swarm is based on the number of events in one year and a certain area, exceeding the average of the data available up to that time. They predicted 14 of 20 earthquakes using this method. The events they missed were the smallest of their defined mainshocks, and mostly occurred before 1920. Two events which followed on successive years after other mainshocks were also missed. They do, however, compare this technique with the model in which the swarm and after-shock occur independently. The six year period would vary between regions but is too long to be of use as a predictive tool.

Each of these three techniques suffers from similar problems which limit their use in the prediction of earthquakes at dams. In each, the prediction is based on past experience - they are learning processes. The loading of the reservoir changes the stress pattern, albeit by a small amount, but enough to question the applicability of the statistics after filling. The second difficulty is in the determining of two dimensional probability functions. The probability function must take account of the fact that most earthquakes occur near pre-existing faults, so seismic lineaments must be given a high weighting. Allowance must also be made for a normal spread in the epicentres, and the

uncertainty in determining the hypocentre. However the major limitation of these statistics is their lack of resolution. It is felt that the use of statistics will never be sufficient to decide whether an earthquake will occur with the resolution of 10's of kilometers , and less than a year necessary for design considerations or cause-effect considerations.

Statistical research is an excellent field of endeavour since the present techniques seem unable to solve the statistical questions raised at dam sites. This work would also be relevant to nuclear-site studies where, thus far, most of the work has concentrated on the detection of microevents and seismic lineaments.

Chapter 5

Data Analysis and Interpretation

5.1 Conversion of Bathymetry to Regular Grid

A considerable amount of effort was required to reduce a contour map of a lake bottom into a form useable by the transform programmes. Three techniques can be used to convert randomly distributed data to a regular grid.

5.1.1 Manual Integration

Dr. and Mrs. Gough reduced the contour map of Kariba by dividing the map into over 1000 squares. The average pressure within the square was found by estimating what fraction lay between the existing contour levels. The benefit of this procedure is that good control may be had at ridges and saddle points and areas usually subject to different interpretations. The process is obviously very time consuming and an alternate method was sought.

5.1.2 Digitising

In an attempt to increase the speed of the data reduction a new approach was used. The data was digitised at available contour levels and interpolation programmes used

to find the value at a given point. At Oroville, seven levels each 100 feet apart were digitised while at Nurek, 6 contours were used with 50 m separation since that contour map was less detailed. The Oroville digitising rate was 0.1 inches, however, for reasons outlined later, some sections were redone at 0.05 inches when greater detail was desired. The number of points (x,y,z) produced by the digitising was very large - over 16,000 at Oroville. The large scale Nurek map was digitised with a separation of 0.05 inches everywhere, but as it was a smaller map, the data points numbered only about 8000.

Several difficulties were experienced in the digitising which, although easy to correct, are inconvenient. The digitising is usually done in several sessions and great care should be taken in resetting the origin. The error was usually one digitising unit, (0.05 or 0.1 inches) since the nearest unit is recorded by the machine. Plotting the results as an overlay usually makes the error obvious and corrections easy. The digitised data is usually stored in files, 96 for Oroville, and difficulties arose in identifying which file belonged to which contour and where on the map it belonged. Eventually each file had to be plotted to identify its value and position. The procedure finally adopted was the use of a file identifier using the first x and y. The x was given a number like 1.03 to mark it as the third file of map one and the y value was set equal

to the contour value. The contour value was entered as a large negative number, e.g. -1000, when the operator was unsure of the contour.

This procedure worked well at Nurek which was digitised later, and hopefully the comments may save confusion if someone else uses this approach. Two methods are possible to reduce this digitised data into a regular grid.

5.1.3 Weighted Distance Techniques

The weighted distance method is a commonly used technique in determining the value at a given point. The data suite is searched for the six, or sometimes eight or more, nearest neighbours to the desired point with each contributing to the value depending on how far they are away.

There are three disadvantages to this method. The first is that the fall-off distance-weighting functions have to be chosen and these will vary with the application. Potential functions fall off as $1/r^2$ with distance, while others fall as $1/r^3$ or $1/r$, but often the choice is quite arbitrary. The second disadvantage is that it is possible for the near neighbours, say six, all to lie on one side of the required point, and the value will be biased toward those values while a seventh neighbour on the other side contributes nothing. This poor choice of neighbour distribution can lead

to misleading results. The greatest disadvantage to the 'near neighbour' method lies in the cost of determining the neighbours. In truly random data each search point requires all the data points to be scanned. The Oroville data was fitted to a 256x256 regular grid and needed 65536 near neighbour searches of the 16000 data points. This method was considered unacceptable based on an estimate of the computer time necessary to extract the regular grid.

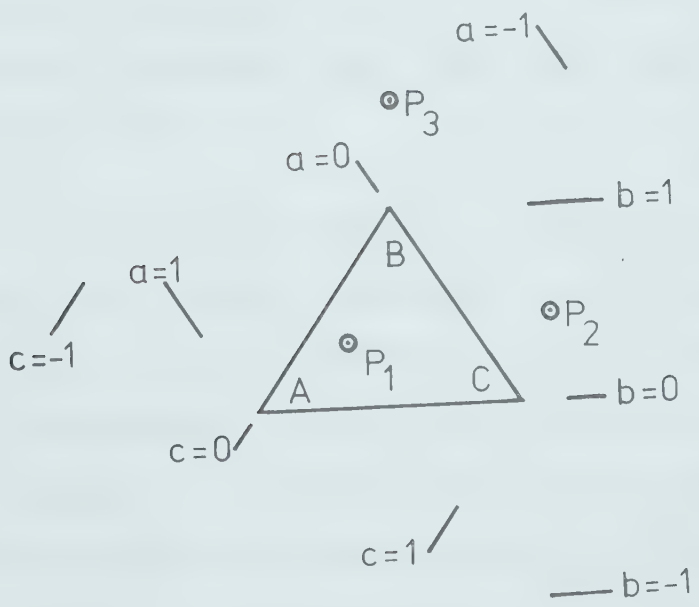
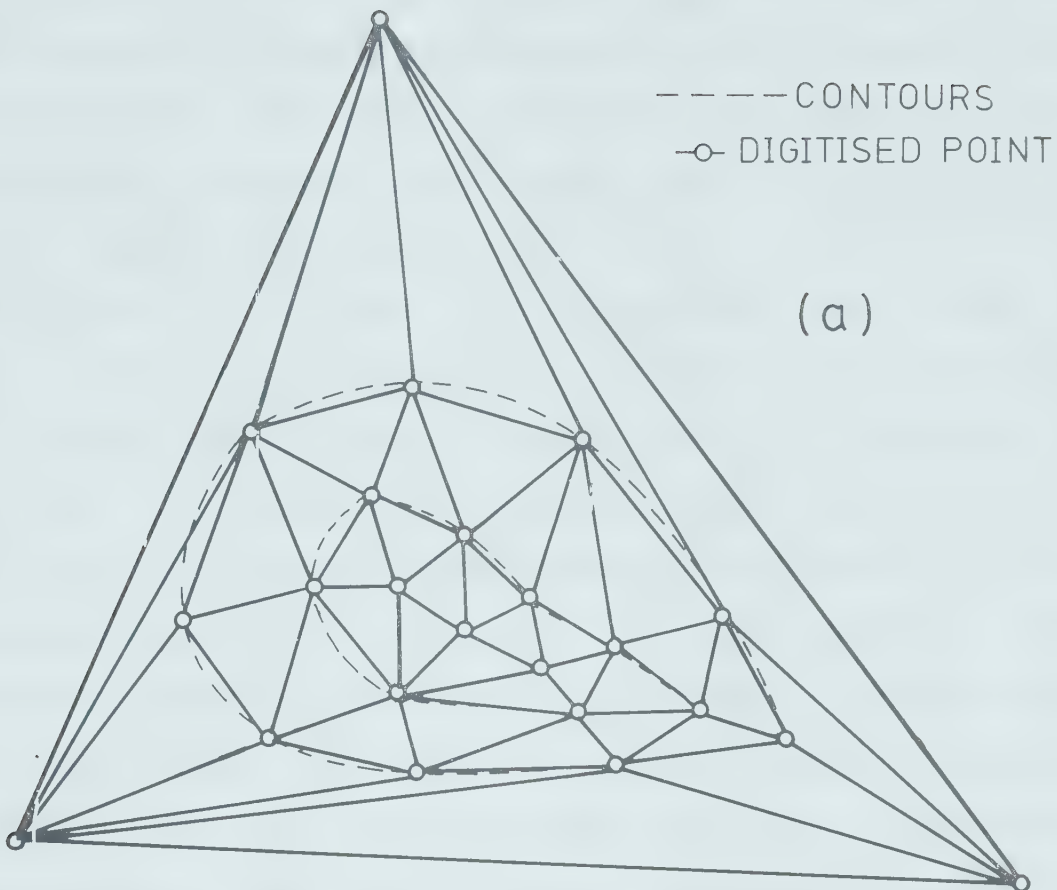
5.1.4 Irregular Triangular Interpolation

An alternative to the weighted distance method is to use triangular elements (Gold et.al. 1977). The random data is connected to form triangles, each being as near to equilateral as possible and with no overlaps. A universal triangle was used to enclose the data and specify the values at a large distance from the data. A typical triangular network is shown in figure 5.1a.

The choice of the digitising interval caused some difficulties since the resolution at any point was limited by the sampling rate. Spurs and valleys were poorly interpolated until extra contours were inserted at crests and valleys. At Oroville the data separation also had to be reduced when the contours were close together.

There are two advantages to this method over the weighted distance method. The first is that interpolation is

figure 5.1: A typical triangular net that would be set up by the interpolation programme. The co-ordinates used are shown in (b). The three co-ordinates will all be positive and between zero and one only if the point is internal to the triangles.



	a	b	c
P_1	0.5	0.3	0.3
P_2	-0.5	0.5	0.9
P_3	-0.3	1.5	-0.2

(b)

always done by three points spaced around the desired point. The number of weighting points could be increased as it is possible to know which triangles are adjacent to a particular triangle since they share two mutual points. These neighbouring triangles are used if continuity of the derivative is desired as in contouring applications. The main advantage to triangulation is that searching for points is ordered and a directed search is used to determine the triangle in which a particular point lies. This is made possible by triangular coordinates which indicate by their magnitude on which side of a triangle the point lies. A negative coordinate, see figure 5.1, for a certain point indicates that the point is behind a side. The adjacent triangle to this side is then used to determine new coordinates. Only when all three triangular coordinates are positive and between zero and one is a certain point within that triangle. The coordinates are then used as weighting functions.

The interpolation is linear along each side and is the way one would probably do the problem manually - a line would be drawn joining each of the points and linear interpolation used along it. If a , b , and c are the triangular coordinates for a point, p , and A , B and C the value at the triangle corners the weighted valued at p is:

$$Z(p) = aA + bB + cC$$

Gold (1977) estimates the triangular interpolation is at

least three times faster than the weighted distance method and has the added advantage of ensuring a good interpolation distribution.

In the data used it was found that a lot of digitising could be omitted where the contours were equally spaced and parallel. Eventually about a third of the data was removed without any loss of accuracy. Some extra contours at crests and valleys were added to increase the detail in certain regions.

As a guide to the cost of the method statistics were kept for each subset of the Oroville data. In the case of set 4 (right section of the map) there were 2550 points of digitised data, with a further 748 points added by the programme to avoid poor interpolation when contours are close together. This was done by bisecting data points along the contour until the difference between points was less than the distance between contours.

Searches were made for the values of 5358 regularly spaced points in this triangular net. The triangular arrangement requires optimisation for the triangular net so that better interpolation is possible. For this reason the data was inserted in sections (actually digitised files) and optimised after each insert. The results and costs are summarised in table 5.1.

The data obtained agreed when checked manually and the

TABLE 5.1TRIANGULATION COST AND STATISTICS

File Number	No. of data points	Insert time (cpu)	No. of optimisa- tions	Total No. of triangle switches	Time for insertion & optimi- sation (cpu)
1	1289	.293	32	6216	2.106
2	577	.138	8	2199	.826
3	114	.025	4	288	.184
4	95	.018	7	316	.249
5	15	.005	3	23	.079
6	258	.051	7	718	.404
7	122	.026	4	221	.197
8	80	.018	5	174	.203
	<u>2550</u>	<u>.574</u>	<u>70</u>	<u>10155</u>	<u>4.246</u>

Number of points computed, inserted and
optimised by the programme

748	90	2450	0.940
<u>3298</u>	<u>160</u>	<u>12605</u>	<u>5.186</u>

TOTALS

Searching for 5358 regular grid points	10.027
Time to write results	.222
Entering data defining the problem	.002
Time to read, insert and optimise data triangulation	<u>5.186</u>
	(cpu) <u>15.437</u>

At deferred priority on an AMDAHL-470 this
reflects a cost of approximately \$4.50.

technique was considered a great improvement over the manual method. The regular grids of Nurek and Oroville were used to compute the stresses and deflections at several times using the filling history of figure 3.6. The results are shown in figures 3.12 and 3.13.

5.2 Discussion of Results

The objective of this work was to see how the fluid filled elastic material behaved under the influence of a surface load which varied both in shape and time. It is apparent from the figures presented that this can be done efficiently at any depth and time and with any loading history. The algebra can be solved in three dimensions for simple homogeneous material.

There has been a large amount of numeric information produced and presented, but to be meaningful it must be summarised into a more concise form. For this reason the figure 3.9, showing stresses and pressure as functions of time at several depths, will be analysed in detail since it contains all the relevant information. The pressure and displacements follow curves predictable from the assumptions of the model.

The displacement becomes larger as the load increases and continues to increase, even though the load is kept constant, until it reaches a final value at a later time. In

this model the water saturates the rock and, as the fluid flows away from the compressed zone, consolidation is possible even with no load changes. The initial settling in response to the load is a result of the elastic compression of the rock fabric. During the unloading there is a rebound since the load is less. Consolidation is observed during the unloaded period. Reapplying the load increases the displacement with consolidation continuing beyond the refilling time. The rate of settling decreases noticeably several years after the refill.

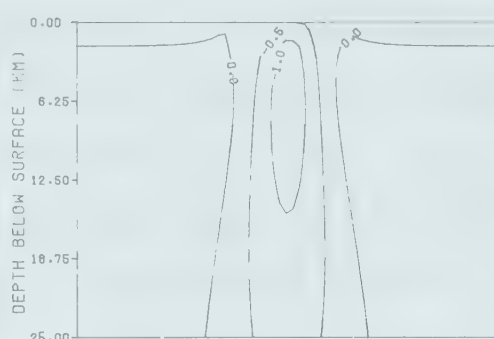
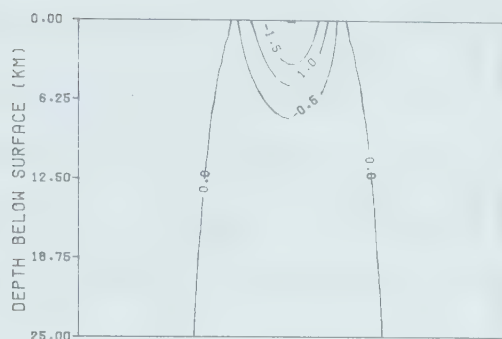
The pressure distribution is quite surprising since 'lobes' are observed at depth below the lake. This is noticed both in two and three dimensions. These regions of increased pressure are due to the rock and pores being compressed, and hence, the pressure in the pores is increased. The fluid cannot immediately escape from the pores since the motion is limited by the diffusion constant. The lateral extent of the lobes is governed by the fall-off of stress with the distance from the source. The top of the lobe depends on the pressure boundary condition. The coupling choice of 0.25 causes smoother fall-off than the zero surface pressure condition often used in engineering applications which makes the lobes even more prominent (see figure 3.1). If the loading is Heaviside, the lobes decrease in amplitude as the fluid diffuses away, however, when the lake depth is being varied, the behaviour is more complex.

This is seen in figures 3.8 and 3.9 in which the pressure is plotted below the centre of the lake at different depths and times. For the loading history chosen (figure 3.6) the pressure is seen to decrease while the water depth is held constant as expected by the diffusion process, but during loading the pressure depends on how fast the load is applied and how rapidly the pressure can diffuse away. This indicates how dependent the calculations are on the rate of loading and the rock parameters. Without an adequate knowledge of each at a particular dam site there is little value in using calculations of this type for earthquake prediction.

The centre of the Mohr circle and the maximum shear stress at several times after filling started are shown in figure 5.2. Notice that the maximum shear stress occurs between 6 and 12 km deep and has a magnitude of over 1.0 bar except during the unload cycle. The radius of the Mohr circle is a measure of the instability of the region. There is a close similarity in the figure 5.2 and the distribution of aftershocks determined at Koyna shown in figure 1.9. This suggests the model may provide a guide to the position of unstable regions, however the locations of aftershocks at other lakes must be known before this can be confirmed.

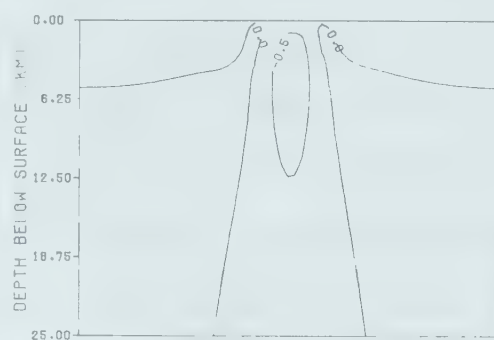
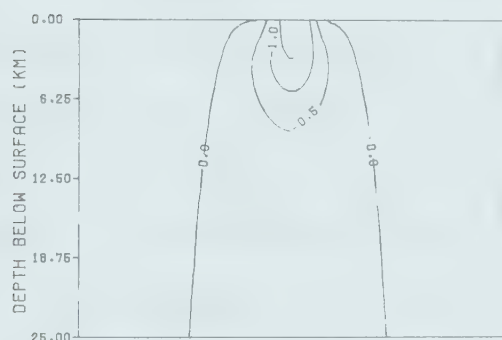
The Mohr circle centre should be considered as important as the radius, since if two circles have the same shear stress, the centre position decides instability. For

Figure 5.2: Radius and centre of the Mohr circle for the loading of the lake shown in figure 3.4. The values are plotted as functions of depth at various stages of loading and unloading. The shear stresses are a maximum between 6. and 12 km deep directly below the lake.



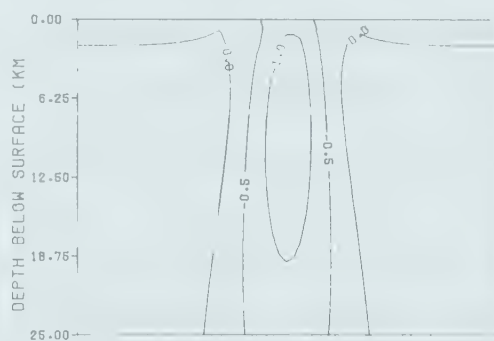
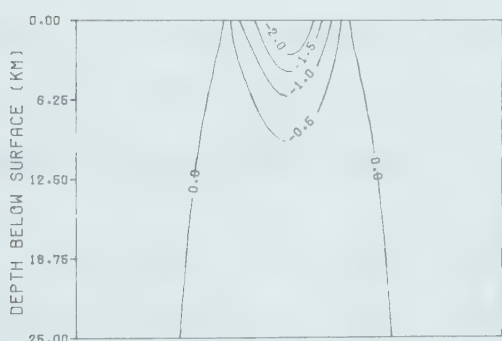
(SIGXX+SIGZZ)/2 (BARS) AT 3.75 YRS

(SIGZZ-SIGXX)/2 (BARS) AT 3.75 YRS



(SIGXX+SIGZZ)/2 (BARS) AT 4.75 YRS

(SIGZZ-SIGXX)/2 (BARS) AT 4.75 YRS



(SIGXX+SIGZZ)/2 (BARS) AT 6.50 YRS
 YOUNG= 0.85MB SIGMA= 0.27
 PERM = 2.00MD COUPLING = 0.25
 ALPHA = 1.00 Q = 1.0E+34

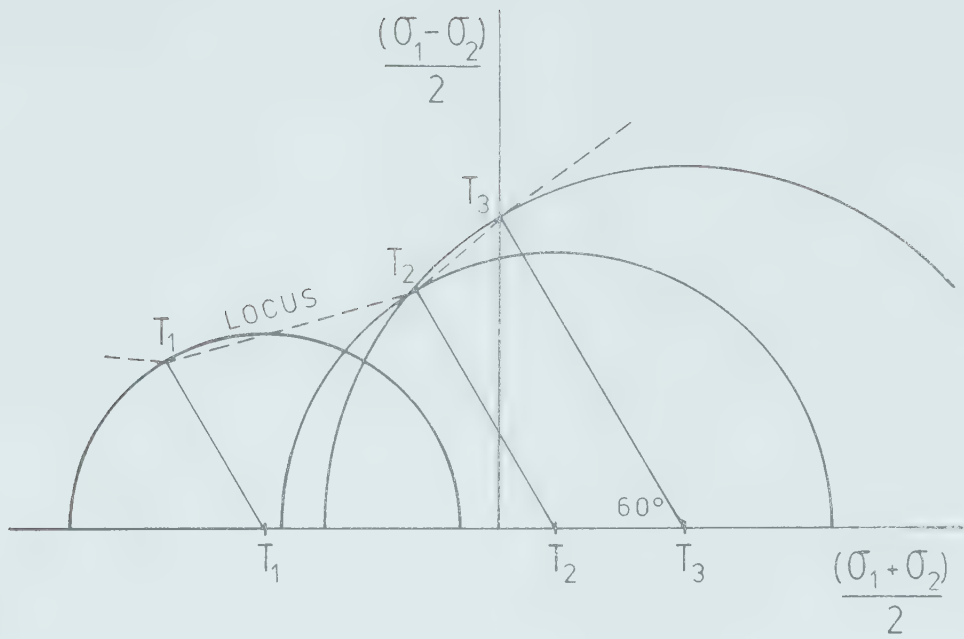
(SIGZZ-SIGXX)/2 (BARS) AT 6.50 YRS
 YOUNG= 0.85MB SIGMA= 0.27
 PERM = 2.00MD COUPLING = 0.25
 ALPHA = 1.00 Q = 1.0E+34

this reason the locus of the point on the Mohr circle at which a line inclined at 30° is tangent, is plotted to see relative instability. The Mohr circle for any particular point can be reconstructed by projecting a line back at 60° to the positive stress axis. In these diagrams compressive stresses are positive so the figures are consistent with figure 1.11. Figure 5.3a indicates how the locus at different times was traced and 5.3b shows what is meant by the measure of instability for a certain Mohr circle.

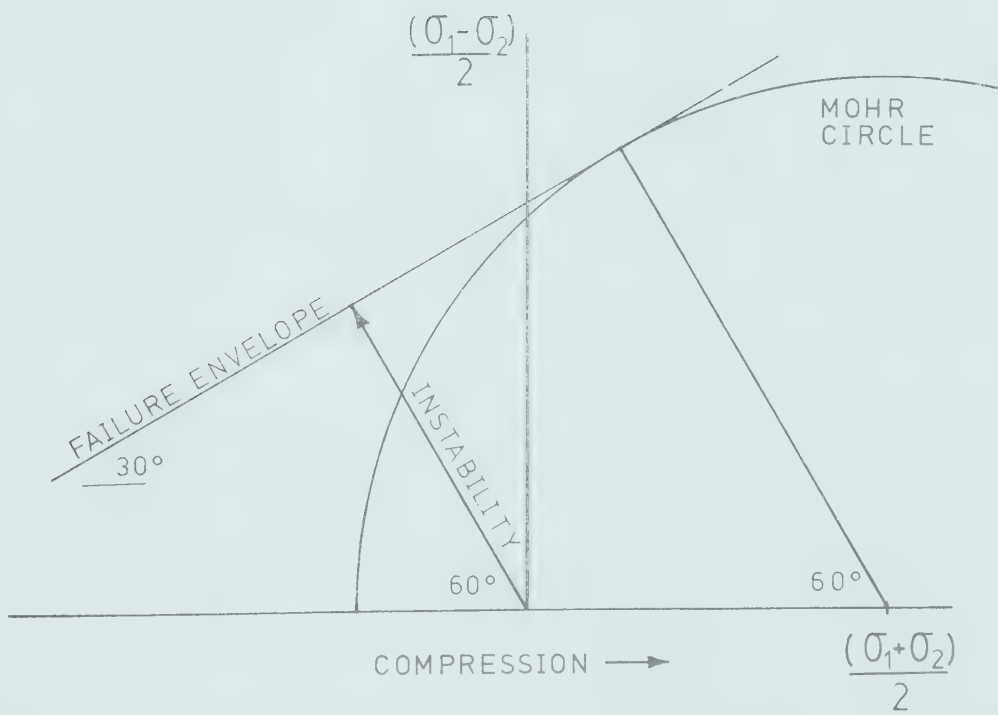
Since tectonic stresses are present the origins of all these diagrams represents the tangent point for the tectonic stresses, and motions of the total Mohr circle are all relative to this point. The larger the instability, the larger is the deviation from the initial stressed condition, and supposedly, the area is more likely to fail. It is necessary to assume that the area is highly prestressed and close to failure with the anomalous stresses acting as triggers. The locus diagrams will differ depending on the assumed stress environment and faulting mechanism expected.

The loci of four points were plotted at each of the depths of 3, 6 and 12 km. Below 12 km most effects decrease and need not be shown since the stresses are always larger elsewhere. Four positions '1', '2', '3' and '4' were examined at each of the depths with position 1 directly under the lake and '4' off to the side. These positions are shown in the figure 5.4. The loci of the 12 selected points

Figure 5.3: The method of determining the locus of the Mohr circle with increasing time is shown in (a). The "instability" measure is shown as a projection of the Mohr circle onto a line at 60° centered on the initial prestressed condition. The larger the instability the larger the triggering force available at that time and place.

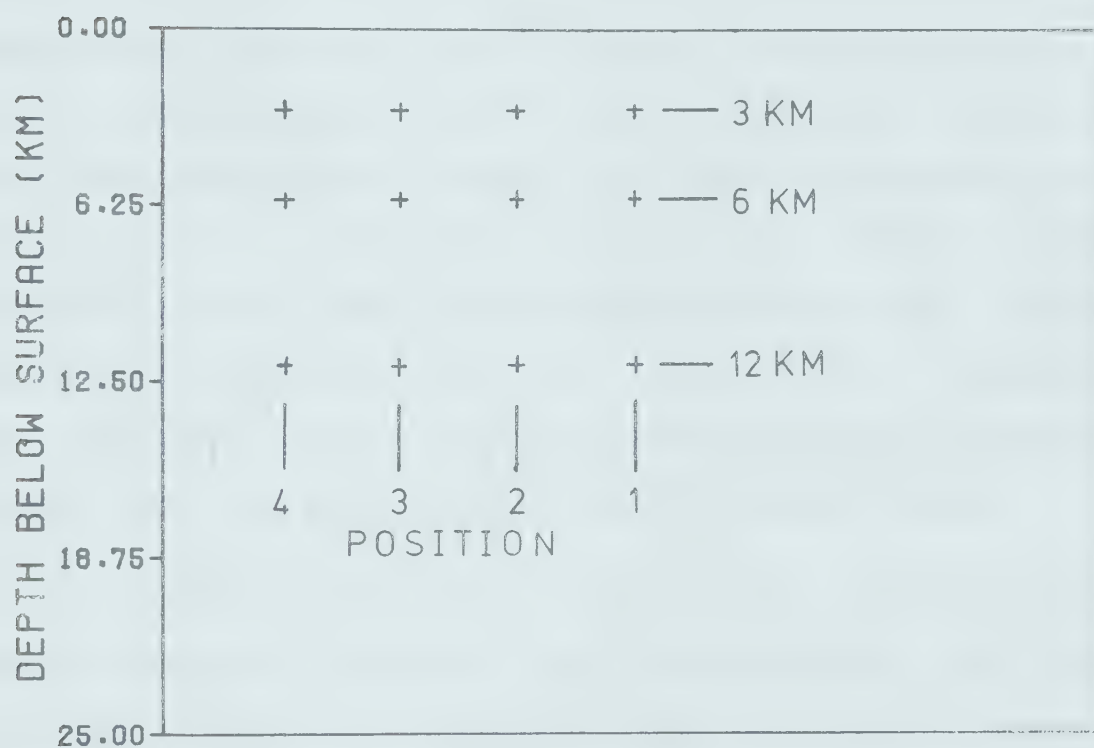
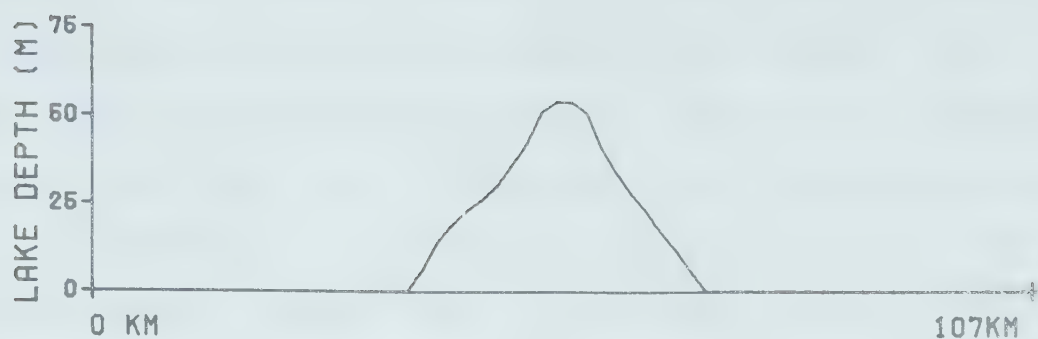


(a)



(b)

Figure 5.4: Positions for which the loci of the Mohr circle were plotted in figure 5.5. Position 1 is directly under the lake and 4 is offset by about 40 km from the centre.

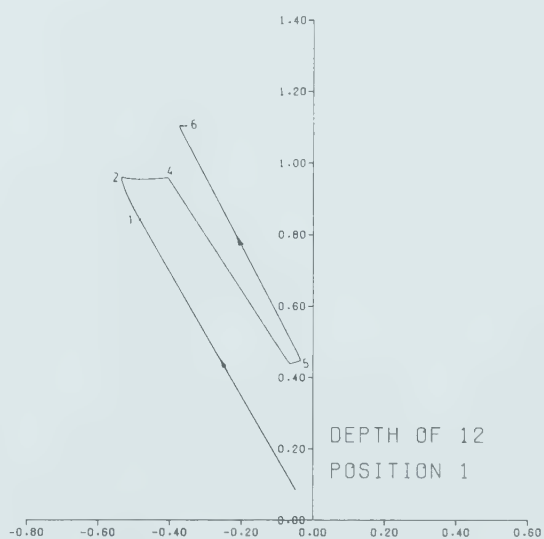
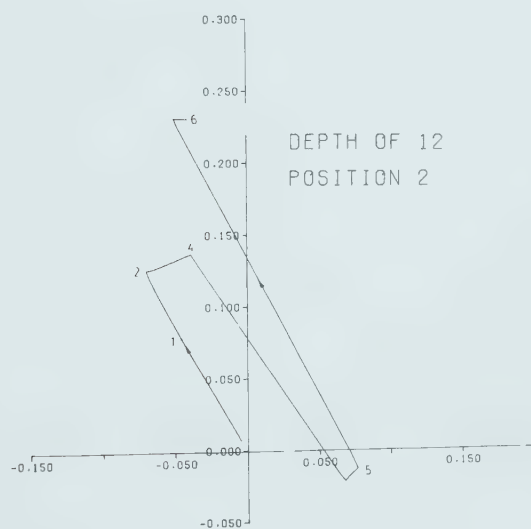
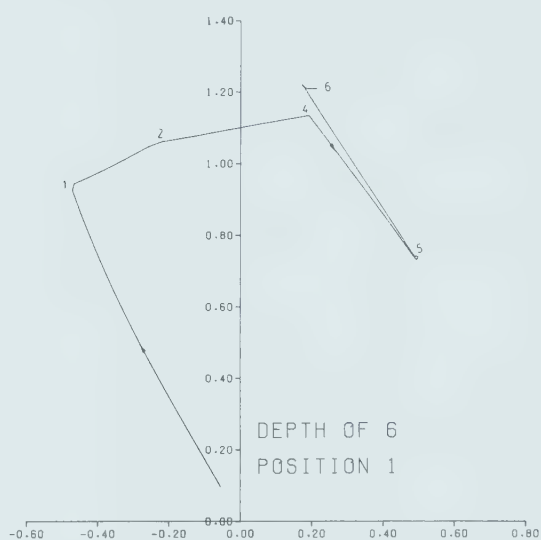
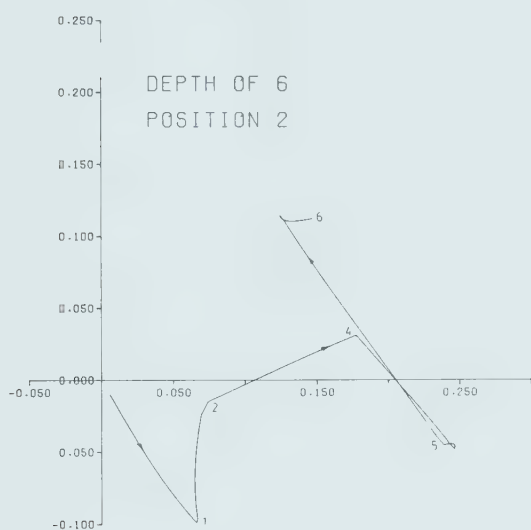
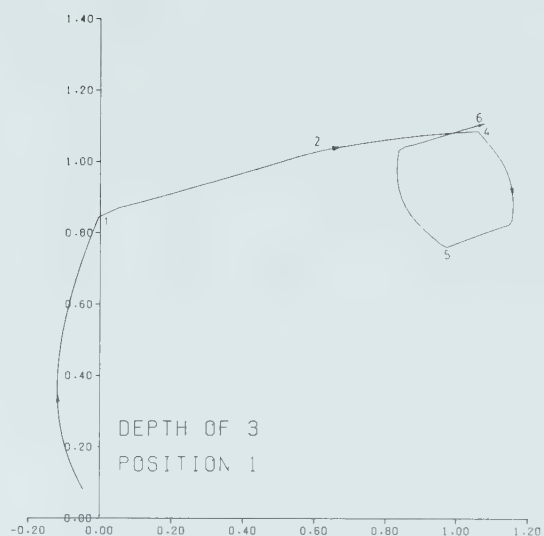
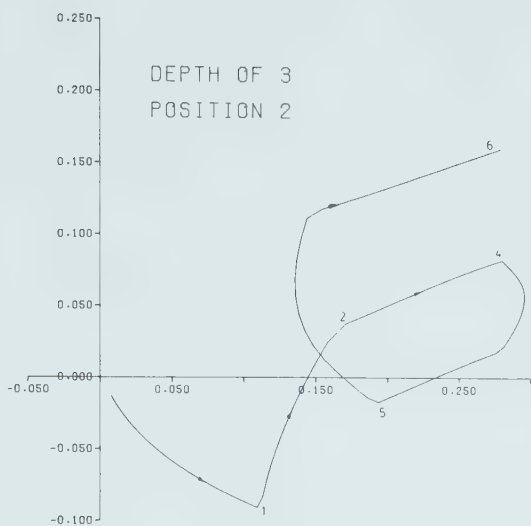


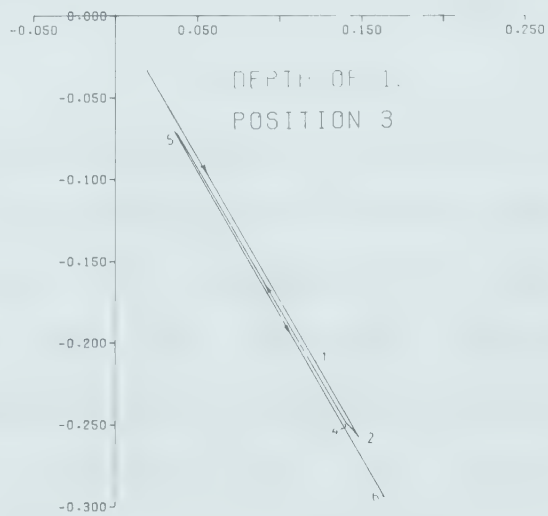
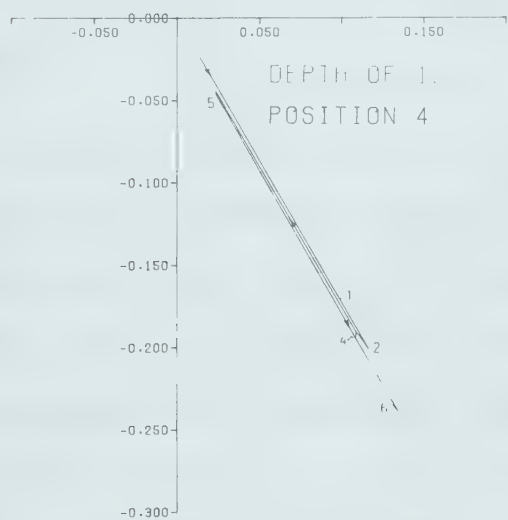
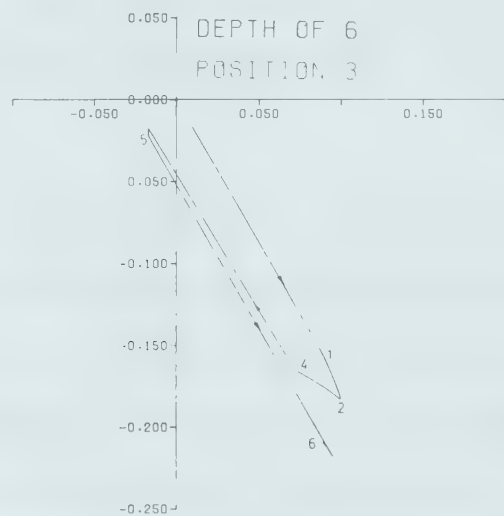
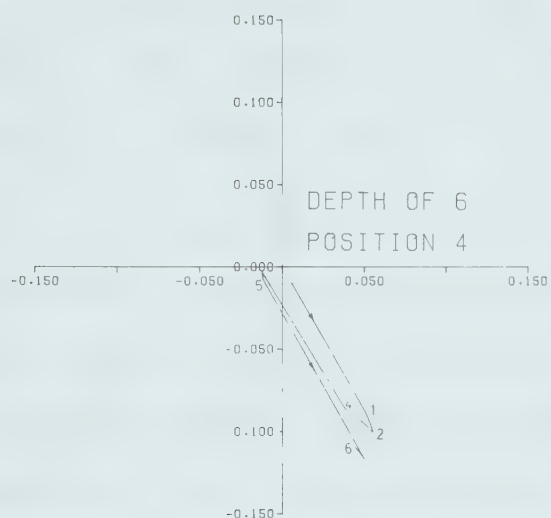
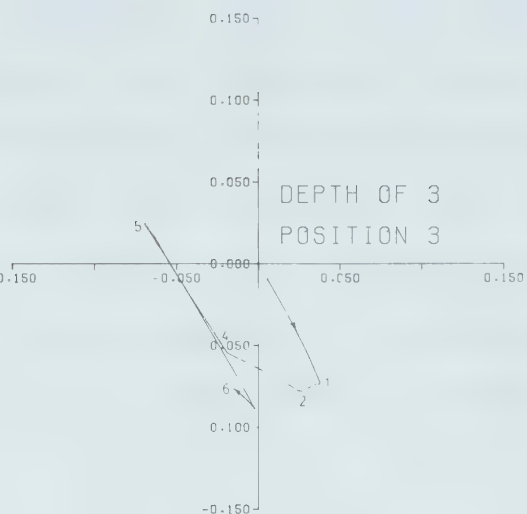
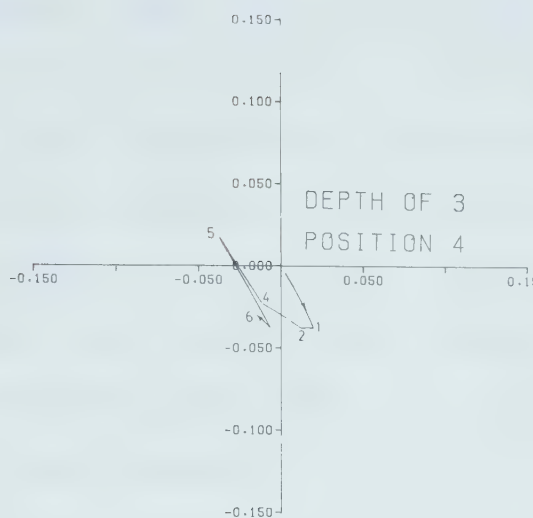
are shown in figure 5.5 and several of the paths are very unusual. These loci are for the normal faulting stress convention. The detail is felt to be real since the curves were generated using two time intervals (0.1-4.yrs and 4.-6.yrs), each sampled at 51 log-spaced points. A zero radius indicates that the X and Z components of the stress are equal and movement to the left and right is mostly a result of fluid pressure changes as illustrated by the simple models of figure 1.11. Since the pressure increases during compressions resulting from the loading, then diffusion will always move the circle towards the stabilising direction. This does not however prevent the radius of the Mohr circle becoming larger as time progresses, but the general result observed is that after the refilling perturbation, the rock is always more stable. The figure 5.5 attempts to summarize most of the results of the research since it shows the seismic risk at particular regions for various times.

At 1 year the most unstable region is at six kilometers depth immediately below the lake. The instability is about 1.2 bars above the tectonic level and, depending on the sensitivity of the area, may trigger an earthquake.

At 2 years, at the end of the first filling, the most unstable position is at 12 km directly below the lake, with all other regions having a level of instability less than this. This position at two years is more unstable than it was at one year. The stresses at two years, at depth 12 km

Figure 5.5: Loci of the Mohr circle for the points indicated in figure 5.4. The closer a point is to a line $y = \tan(30^\circ) * x + C$ the more unstable is the region during the initial filling. At some positions instability is at 1 while at others it is at 2 years. Often the largest instability occurs at 5.5 (after the refill). The water level followed the history shown in figure 3.4.





below the lake are just slightly larger than those experienced earlier at 6 km one year after filling started. If an event hadn't occurred at one year and 6 km deep then it may happen at 12 km and 2 years. The stresses at the positions 2, 3, and 4 are much smaller than directly under the lake and failure most probably will be initiated directly under the lake at position 1 where the instability is much larger.

Between two and four years while the lake's depth is being kept constant the region stabilises as the high pressures diffuse away.

It is possible to conclude that the initial filling is associated with an unstable period. This is consistent with the figure 1.10. Both Vajont and Kremasta had onset of seismicity during the first loading. Unfortunately the exact positions of epicentres are unknown and it is impossible to check if they lay directly under the deepest section of the lakes.

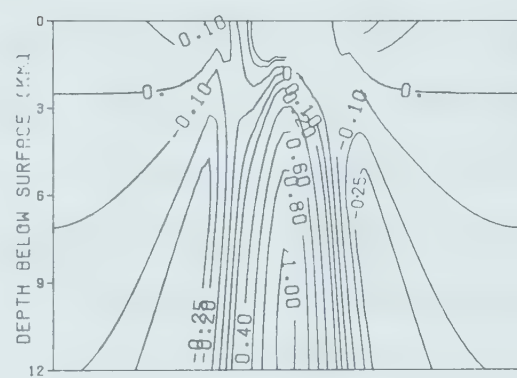
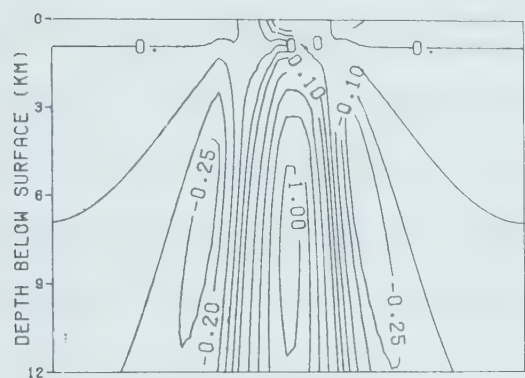
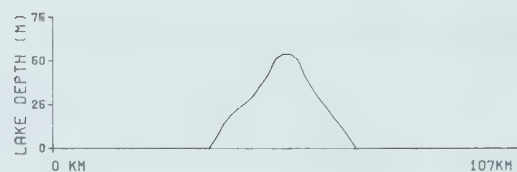
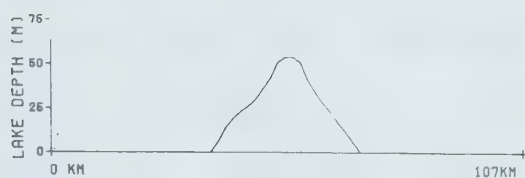
The next period of the lake history involves an emptying, followed later by a refilling to 10 % deeper than earlier. This type of history was included to see what connection it has, if any, with the possible delayed earthquake at Oroville which occurred just after a refill such as this.

At the 3 and 6 km depths below the lake the anomalous

stresses at 5.5 years are less than those experienced at an earlier time. It must be concluded that these areas would not have earthquakes since they were stressed to a higher level at an earlier time. At 12 km below the lake an interesting result is observed. The stresses after refilling are larger than at any previous time or position. If no earthquakes had occurred to relieve stresses, the refilling is the time at which earthquakes are most likely to happen. After unloads and reloads a marked increase in the seismicity is observed, always starting after the water depth starts to increase. The calculations agree with this observation. The timing of the event at Oroville could perhaps have been predicted from this model, however, the off-set must be explained on geological grounds as the off-set is larger than predicted. The diagrams showing loci have been plotted with a stress sign convention consistent with the normal faulting observed at Oroville.

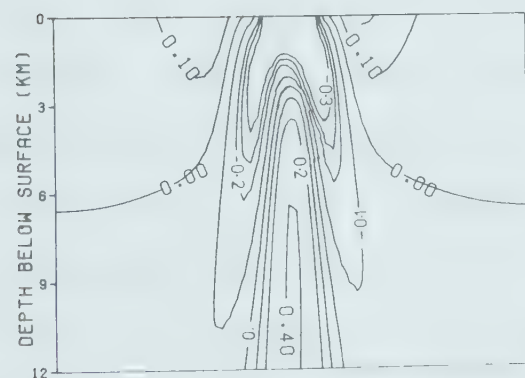
The stresses are always largest immediately under the lake, but on the assumption that this area will have an earthquake which will release the locally stored strains, the question becomes which area to the sides are most unstable? To determine this, the 'instability' has been plotted at different times on figure 5.6. It is apparent that there is a zone where the x and z effective stresses are equal. To either side of the central area are regions with negative instability - these areas are more stable than

Figure 5.6: Instability (see figure 5.4) at different times during the loading. The results are shown to 12 km depth with instabilities (stabilised zones) having values less than zero not being contoured.

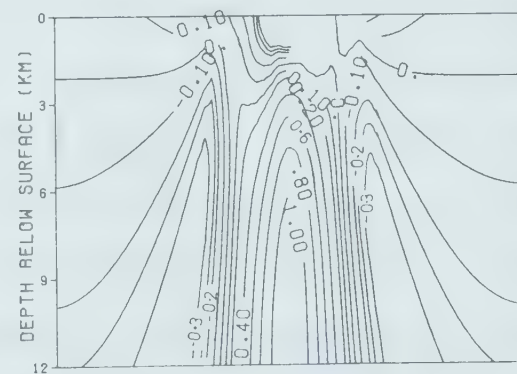


INSTABILITY AT 60 DEG AT 1.00 YRS

INSTABILITY AT 60 DEG AT 4.00 YRS



INSTABILITY AT 60 DEG AT 4.50 YRS
 YOUNG= 0.85MB SIGMA= 0.27
 PERM = 2.00MD COUPLING = 0.25
 ALPHA = 1.00 Q = 1.0E+34



INSTABILITY AT 60 DEG AT 5.50 YRS
 YOUNG= 0.85MB SIGMA= 0.27
 PERM = 2.00MD COUPLING = 0.25
 ALPHA = 1.00 Q = 1.0E+34

before filling.

Locus were redrawn using the stress convention in a thrust faulting environment with the vertical stress being smaller than the horizontal. The same stress values were used to determine the locus shown in figure 5.7. It can be seen that the conclusions discussed above no longer apply. The initial filling leads to instability only off to the sides of the lake. The instability levels are very small and if failure did not occur during the initial filling, then it would appear unlikely to happen later. From the figure 5.6 it appears that the instability may be large at shallow depths at the end of the down-draw in a thrust environment.

To illustrate the effect of changing the fluid parameters, a normal faulting locus plot was made using three time intervals (0.01-4yrs, 4-6yrs, 6.-25yrs) using $\alpha=1$ and Q of 5.Mbar. This is shown in figure 5.8. Again the largest instability is at five years or later for the locus found. The movement of the circle to the left indicates that the pressure is increasing with time so the effective stresses are decreasing. The results at 25 years are very close to the final locus position. This illustrates that the conclusions can vary considerably if the fluid parameters are uncertain.

5.3 Concluding Remarks

Figure 5.7: Instability at 6. km below the two dimensional lake in a thrust environment. The largest instability now occurs off to the side of the lake

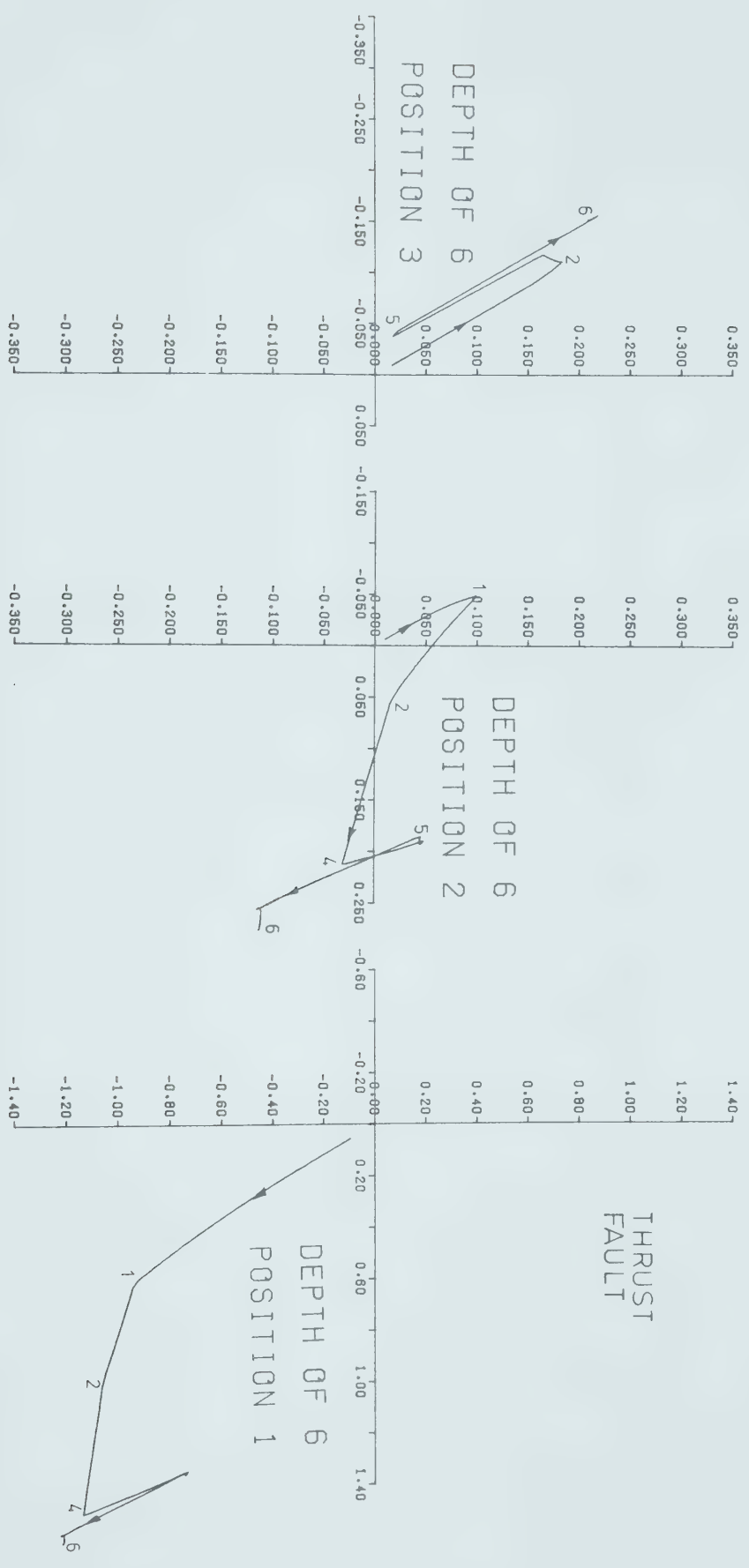
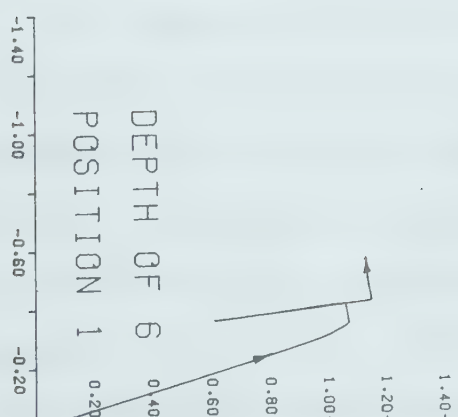
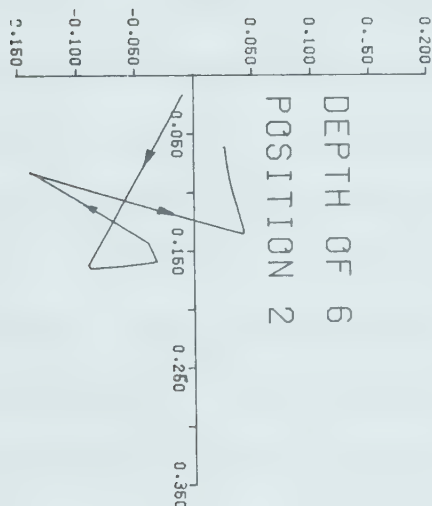
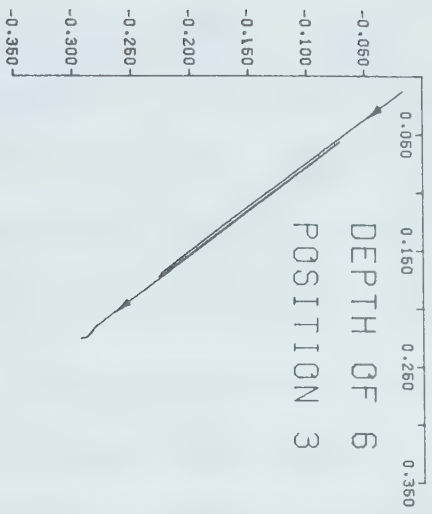
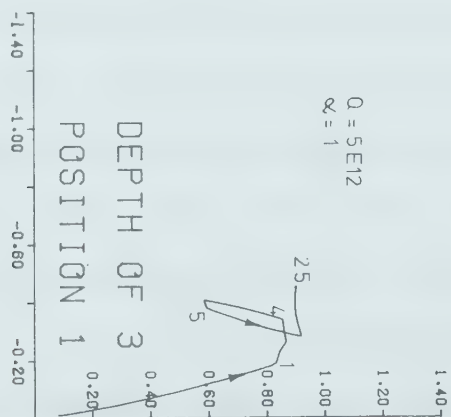
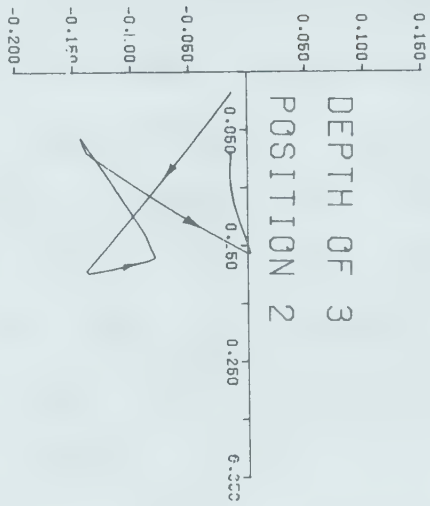
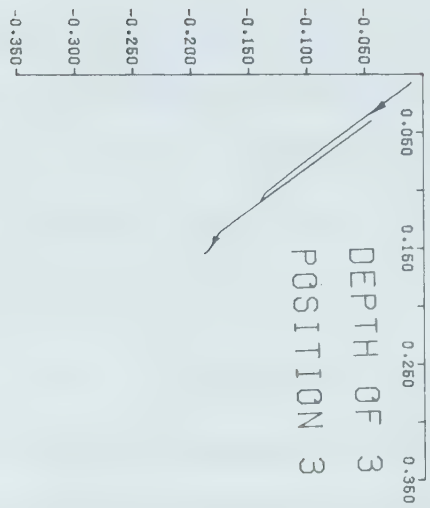


Figure 5.8: Instability in a normal faulting area with the Q reduced so that the diffusion may take place. The coupling is one in this case. The result differs considerably from those shown earlier.



It appears that the model can explain many of the observed seismic effects at reservoirs. The stresses, pore pressures and displacement functions each have terms depending on the convolution of the rate of change of water level, on the water depth, and on a diffusion time. The instability during initial loading and again during an unload-reload situation is encouraging.

Application of this work to a particular reservoir in detail has been avoided for three reasons. Firstly, not enough is known about the geologic and elastic behaviour of the rocks; secondly, nothing is known about the initial stresses and hydrology; and finally, the epicentral positions and depths are usually inaccurately known. This leads to the question of future research. How can the results and conclusions made here be tested? Several experiments can be made to check the results, however, each is expensive and are major projects.

Of utmost importance is a test to find the amount of triggering stresses needed to open fractures in the reservoir area and this could be done by hydrofracturing at a deep test hole near the site. The test hole could also provide geological samples, insitu permeability results and information on the water table, both top and bottom. A seismic velocity and resistivity log down the hole would also be useful. The resistivity log could be used to monitor changes in the water table cheaply and easily during and

after filling. Several shallow holes could be drilled around the test site, again to monitor water table changes, but also as source holes in diffusion studies over long distances so that a 'bulk permeability' is obtained.

It is important that the hydrology and fluid parameters be known. This is not a simple task over the large scales discussed here. Regional hydrology would have to be obtained if initial conditions are to be imposed on the fluid behaviour of the rock. A guide to the rock parameters may be obtained by modelling the behaviour of similar reservoirs in the region.

A promising line of predictive research lies in the monitoring of the delay time of a seismic signal over a fixed baseline. If sufficient acoustic energy can be pumped into the ground, it may be possible to pass the waves beneath the reservoir at several kilometers depth. Since the material properties are stress dependent, an increase of the stress is thought by some researchers (Reasonberg and Aki, 1974) to change the velocity sufficiently so that one bar stress changes may be detected with good seismic timing. The amount of delay is uncertain, but if it is sufficient, insitu stresses could be continuously monitored. The seismic energy could perhaps be obtained from construction blasts. Strain meters may also be useful in monitoring strain accumulation. Eventually an extensive study will have to be done into the depths and lateral migrations of earthquakes

at dams so that models of the type presented here can be compared. Hopefully, some of the data being collected now will be soon available. The research groups at Nurek and Lamont are currently obtaining good seismic locations. In any event, an array of seismometers should be placed at all new dam sites to monitor any activity that occurs.

Although the mathematical calculations done here are gratifyingly close to what little observational data exists, the reader is cautioned that application of mathematical models to real problems in earth science is more of an uncertain art than an unambiguous science. Mathematical modelling like this work indicates trends, and provides quantitative measures which can make the weight of evidence for, or against, seismic risk at a dam site far more convincing. It is not by itself sufficient evidence, but it is an essential component of the evidence.

Bibliography

- Acton, F.S.; 1970. Numerical methods that usually work. Harper & Row.
- Aisenstein, B., Yevnin, A., and Saidoff, I.; 1957. Reducing water losses from storage reservoirs in Israel: Blanketing of Tel-Yeruham Reservoir. Proc. Fourth Inter. Conf. on Soil Mech. and Foundation Engineering. Vol 1 and 2.
- Beck, J.L.; 1975. Weight induced stresses and the recent seismicity at Lake Oroville, California. Submitted to J. Geoph. Res.
- Biot, M.A.; 1941a. General theory for three dimensional consolidation. J. App. Phys., 12, 155-164.
- Biot, M.A.; 1941b. Consolidation settlement under a rectangular load distribution. J. App. Phys., 12, 426-430.
- Biot, M.A.; 1941c. Consolidation settlement of a soil with an impervious top surface. J. App. Phys., 12, 578-581.
- Biot, M.A.; 1956. General Solutions of the equations of elasticity and consolidation for a porous material. J. Appl. Mech., 78, 91-96.
- Biot, M.A.; 1973. Nonlinear and semilinear rheology of porous solids. J. Geophy. Res., 78, 4924-4937.
- Biot, M.A., and Clingan, F.M.; 1955. Theory of elasticity and consolidation for a porous anisotropic solid. J. App. Phys., 26, 182-185.
- Birch, F.; 1966. Compressibility; Elastic Constants. in Handbook of Physical Constants, Geol. Soc. Am. Memoir 97.
- Booker, J.R.; 1974. Time dependent strain following faulting of a porous medium. J.G.R., 79, 2037-2044.
- Brace, W.F.; 1974. Experimental studies of seismic behavior of rocks under crustal conditions. Engin. Geology, 8, 109-127.
- Brace, W.F., and Martin, R.J.; 1968. A test of effective stress law for crystalline rocks of low porosity. Int. J. Rock Mech. Miner. Sci., 5, 415.
- Bufe, C.G., Lester, F.W., Lahr, K.M., Lahr, J.C., Seekins,

- L.C., and Hanks, T.C.; 1976. Oroville earthquakes: Normal faulting in the Sierra Nevada Foothills. *Science*, 192, 72-74.
- Butkov, E.; 1968. Mathematical Physics. Addison Wesley, London, pp 735.
- Comninakis, P., Drakopoulos, J., Moumoulidis, G. and Papazachos, B.C.; 1968. Foreshock Sequences of the Kremasta earthquake and their relation to the water loading of the Kremasta artificial lake. *Ann. Geofis. (Rome)*, 21, 39-71.
- Cooley, J.W. and Tukey, J.W.; 1965. An algorithm for the machine calculation of complex Fourier Series. *Math Comp.*, 19, 297-301.
- Crochet, M.J., and Naghdi, P.M.; 1966. On constitutive equations for flow through an elastic solid. *Inter. Jour. Eng. Science*, 4, 383-401.
- Farrell, W.E.; 1972. Deformation of the earth by surface loads. *Review of Geophysics and Space Physics*, 10, 761-797.
- Fatt, I.; 1953. The effect of overburden pressure on relative permeability. *Jcur. Petroleum Technology Note* 194, 1, 15-16.
- Galanopoulos, A.G.; 1967. The influence of the fluctuation of Marathon lake elevation on local earthquake activity in the Attica Basin area. *Ann. Geol. Pays. Hell.*, 18, 281-306.
- Gangi, A.F.; 1976. Variation of whole and fracture porous rock permeability with confining pressure. *Engineering Geology*, in press.
- Garg, S.K. and Nur, A.; 1973. Effective Stress laws for fluid saturated porous rocks. *J. Geoph. Res.*, 78, 26, 5911-5921.
- Geertsma, J.; 1957. The effect of fluid pressure decline on the volumetric changes of porous rocks. *Trans. AIME*, 210, 331.
- Ghaboussi, J., and Wilson, E.L.; 1973. Flow of compressible fluid in porous elastic media. *Inter. Jour. Num. methods in Engineering*, 5, 419-442.
- Gibson, R.E. and McNamee, J.; 1957. The consolidation settlement of a load uniformly distributed over a rectangular area. 4th Inter. Conference on Soil

Mech. and Foundation Engineering 1957 Vol. 1.

- Gold, C.M., Charters, T.D., and Ramsden, J.; 1977. Automated contour mapping using triangular element data structures and an interpolant over each irregular triangular domain. Submitted to Fourth Ann. Conf. on Comp. Graphics, Inter. Techniques, and Image Processing. ASC/SIGGRAPH July, 1977.
- Gough, D.I. and Gough, W.I.; 1970a. Stress and Deflection in the lithosphere near lake Kariba - I. Geophys. J.R. Ast. Soc., 21, 65-78.
- Gough, D.I. and Gough, W.I.; 1976. Incremental Stresses near the Cabora Bassa Gorges. Engineering Geology, in press.
- Gough, D.I. and Gough, W.I.; 1970b. Load Induced Earthquakes at Lake Kariba - II. Geophys. J.R. Ast. Soc., 21, 79-101.
- Gough, D.I.; 1976. Induced seismicity. UNESCO Report for publication as a chapter in a book.
- Gradshteyn, I.S. and Ryzhik, I.M.; 1965. Table of integrals Series and Products. Academic Press New York. pp 1086.
- Gubin, I.E.; 1969. Koyna Earthquake of 1967. Bull Inst Seism Earthquake Eng., 6, 45-62.
- Guha, S.K., Gosavi, P.D., Agarwal, S.P., Padale, J.G., and Marwadi, S.C.; 1974. Case Histories of some artificial crustal disturbances. Engineering Geology, 8, 59-77.
- Guha, S.K., Gosavi, P.D., Nand, K., Padale, J.G., and Marwadi, S.C.; 1974. Koyna earthquakes. Central Water and Power Research Station, Khadakwasla, Poona - 24, India.
- Gupta, H.K., Rastogi, B.K; 1976. Dams and Earthquakes. Elsevier, Amsterdam. pp 229.
- Guther, H.; 1972. Some problems in non-homogeneous seepage. MSc thesis, University of Alberta. (Unpublished).
- Hagiwara, T. and Ohtake, M.; 1972. Seismic activity associated with the filling of the reservoir behind Kurobe Dam, Japan, 1963-1970. Tectonophysics, 15, 241-254.
- Haimson, B.C.; 1957. Proc. 14 Symp. Rock Mech., p 689.

- Haimson, B.C.; 1975. The state of stress in the Earth's crust. Reviews of Geophysics and Space Physics, 13, 350-352.
- Handin, J., Hager, R.V., Friedman, M. and Feather, J.N.; 1963. Experimental deformation of sedimentary rocks under confining pressure: pore pressure tests. Bull. Am. Ass. Petrol. Geol., 47, 717-755.
- Healey, J.H., Rubey, W.W., Griggs, D.T., and Raleigh, C.B.; 1968. The Denver earthquakes. Science, 161, 1301-1310
- Hedberg, H.D.; 1936. Gravitational compaction of clays and shales. Amer. Jour. of Science, 31, 16-287
- Hubbert, M.K. and Rubey, W.W.; 1959. Role of fluid pressure in mechanics of overthrust faulting: 1 and 2. Bull. Geol. Soc. Amer., 70, 115-166.
- Hubbert, M.K. and Willis, D.G.; 1957. Mechanics of Hydraulic Fracturing. Trans. A.I.M.E., 210, 153-168.
- Hwang, C.T., Morgenstern, N.R., and Murray, D.W.; 1970. On solutions of plane strain consolidation problems by finite element methods. Can. Geotechnical Jour., 8, 109-118.
- Hwang, C.T., Morgenstern, N.R., and Murray, D.W.; 1972. Application of the finite element method to consolidation problems. Symp. on Applic. of finite element methods to problems in Geotechnical Engineering, Mississippi, 2, 739-764.
- I.C.O.L.D.; 1973. World Register of Dams. International Commissions on Large Dams, Paris. pp 998.
- Irobe, M., Akagi, T., and Itoh, H.; 1974. Finite element analysis of consolidation of unsaturated soil. Finite Elem Methods in Flow Problems, Ed. J.T. Oden, univ. of Alabama. 757-767.
- Jacob, K.H., Armbruster, J., Seeber, L., and Pennington, W.; 1976. Tarbela Reservoir, Pakistan: a Region of compressional tectonics with reduced seismicity upon initial filling. In press, Engineering geology.
- Jaeger, J.C., and Cook, N.G.W.; 1976. Fundamentals of Rock Mechanics, Wiley, New York, 2nd Edition pp585.
- Kagan, Y., and Knopoff, L.; 1976. Statistical search for

nonrandom features of the seismicity of strong earthquakes. *Phys. Earth and Plan. Int.*, 12, 291-318.

Kanasewich, E.R.; 1976. Time Sequence Analysis in Geophysics, 2.Ed. University of Alberta Press, Edmonton.

Keilis-Borok, V.I., Konrod, Y.L., and Molchan, G.M.; 1974. Algorithm for the estimation of seismic risk. Available from M.I.T. Civil Engineering Internal Study report 46.

Kemeny, J.G., Mirkil, H., Snell, J.L., and Thompson, G.L.; 1959. Finite mathematical Structures. Prentice-Hall, Englewood Cliffs N.J., U.S.A.

King, Chi-Yu, and Knopoff, L.; 1968. Stress drop in earthquakes. *BSSA*, 58, 249-257.

King, Chi-Yu, and Knopoff, L.; 1969. A magnitude-energy relation for large earthquakes. *BSSA*, 59, 269-273.

Knopoff, L.; 1971. A stochastic Model for the occurrence of main sequence earthquakes. *Reviews of Geophysics and Space Phys.*, 9, 175-188.

Knutson, C.F. and Bohor, B.F.; 1963. Reservoir rock behavior under moderate confining pressure. In Rock Mechanics edited by C. Fairhurst.

Landau, L.D. and Lifshitz, E.M.; 1959. Theory of Elasticity. Addison and Wesley.

Langston, C.A.; 1976. A body wave inversion of the Koyna, India, earthquake of December 10, 1967, and some implications for body wave focal mechanisms. *J. Geoph. Res.*, 81, 2517-2529.

Lee, T.; 1972. A method for computing the deformation of the crust caused by the filling of large lakes. *BSSA*, 62, 1597-1610.

Love, A.E.H.; 1929. The stress produced in a semi-infinite solid by pressure on part of the boundary. *Trans. Roy. Soc., A*, 228, 377-420.

Marlette, J.W.; 1975. Personal Communication. Division of Design and Construction, Department of Water Resources, Sacramento, California.

Marsal, D., and Phillip, W.; 1970. Compaction of sediments. *Bull. Geol. Inst. of Upsala*, 2:7, 59-66.

- McGuire, R.K.; 1976. Methodology for incorporating parameter uncertainties into seismic hazard analysis for low risk design intensities. Paper presented at Inter. Symp. on Earthquake Structural Engineering. St. Louis 1976. Preprint provided from U.S.G.S. Denver.
- McNamee, J. and Gibson, R.E.; 1960a. Displacement functions and Linear transforms applied to diffusion through porous elastic media. Quart. Jour. Mech. App. Math., 13, 98-111.
- McNamee, J. and Gibson, R.E.; 1960b. Plane strain and axially symmetric problems of the consolidation of of a semi-infinite clay stratum. Quart. Jour. Mech. and Applied Math., 13, 210-227.
- Moreland, L.W.; 1972. A simple constitutive theory for a fluid-saturated porous solid. J. Geophy. Res., 77, 890-900.
- Morgenstern, N.; 1962. A relation between hydraulic fracture pressures and tectonic stresses. Geoph. Pura App., 52, 104-114.
- Morgenstern, N.R. and Guthrie, H.; 1972. Seepage into an excavation in a medium possessing stress dependent permeability. Proc. of Symp. on Flow through Fractured Rock. German Soc. Soil and Rock Mech. Stuttgart.
- Nur, A. and Booker, J.R.; 1972. Aftershocks caused by pore fluid flow. Science, 175, 885-887.
- Nur, A. and Eyerlee, J.; 1971. An exact effective stress law for elastic deformation of rock with fluids. J. Geoph. Res., 76, 26, 6414-6419.
- Nyland, E., and Withers, R.J.; 1976. A fast method for computing load induced stress in the Earth. Geophys. J.R. Ast. Soc., 44, 689-698.
- Papazachos, B.C.; 1974. On the relation between certain artificial lakes and the associated seismic sequences. Engineering Geology, 8, 39-48.
- Raleigh, C.B., Healey, J.H. and Bredehoeft, J.D.; 1975. An experiment on Earthquake control at Rangely, Colorado. Science, 191, 1230-1237.
- Ralston, A.; 1965. A first course in numerical analysis. McGraw Hill.

- Reasonberg, P., and Aki, K.; 1974. A precise, continuous measurement of seismic velocity for measuring in-situ stress. J. Geoph. Res., 79, 399-406.
- Rice, J.R. and Cleary, M.P.; 1976. Some basic stress diffusion solutions for fluid-saturated elastic porous media with compressible constituents. Reviews of Geophysics and Space Phys., 14, 227-242.
- Rice, J.R. and Simons, D.A.; 1976. The stabilization of spreading shear faults by coupled deformation diffusion effects in fluid infiltrated porous materials. J. Geoph. Res., 81, 5322-5334.
- Richter, C.F.; 1958. Elementary Seismology Freeman and Company, San Francisco. pp 768.
- Roberts, G.E. and Kaufman, H.; 1966. Table of Laplace transforms. W.B. Saunders, London pp 367.
- Robinson, L.H.; 1959. The effect of pore and confining pressure on the failure process in sedimentary rock. Col. School of Mines Quart., 54, 3, 177-199.
- Rothé, J.P.; 1970. Seismic Artificiels. Tectonophysics, 9, 215-238.
- Rothé, J.P.; 1973. A Geophysical report. In W.C. Ackerman, G.F. White and E.B. Worthington (Editors). "Man Made Lakes: Their problems and Environmental Effects.
- Sandu, R.S., and Wilson, F.L.; 1969. Finite element analysis of seepage in elastic media. Proc. ASCE, EM95, 641-652.
- Schiffman, R.L., Chen, A.T.F., and Jordan, J.C.; 1969. An analysis of consolidation theories. A.S.C.E., SM95, 285-312.
- Scholz, C.H., Sykes, L.R., and Aggarwal, Y.P.; 1973. Earthquake prediction: a physical basis. Science, 181, 803-810.
- Simpson, D.W.; 1976. Seismicity changes associated with reservoir loading. Proc. First Symp. on Induced Seismicity Engineering Geology: 10, 123-150.
- Singleton, R.C.; 1969. An algorithm for computing the mixed radix Fast Fourier transform. IEEE trans on Audio and Electroacoustics, 17, 93-103.

- Skempton, A.W.; 1961. Effective Stress in Soils, concrete and rocks. In Conference on Pore Pressure and Suction in Soils, Butterworth, London.
- Skempton, A.W.; 1970. The consolidation of clays by gravitational compaction. Q. Jour. Geol. Soc. London, 125, 373-411.
- Sleigh, R.W.; 1976. Investigation of crustal deformation following the imposition of a large mass of water. Geophys. J.R. Astr. Soc. (1976), 47, 531-533.
- Snow, D.T.; 1970. The frequency and Apertures of fractures of fractures in rock. Int. J. Rock. Mech. Min. Sci, 7, 23-40.
- Sykes, L.R.; 1967. Mechanism of earthquakes and the nature of faulting on mid-oceanic ridges. JGR, 72, 2131-2153.
- Sykes, L.R.; 1970. Seismicity of the Indian Ocean and possible nascent island arc between Ceylon and Australia. J. Geoph. Res., 75, 5041-5055.
- Terzaghi, K.Van; 1923. Die Berechnung der Durchlässigkeitsziffer des Tores aus dem Verlauf der hydrodynamischer Spannungserscheinungen. In german in Sitzungsber Akad. Wiss. Wier. Math. Naturwiss kl. Abt 2A, 132, 105.
- Timoshenko, S.P. and Goodier; J.N., 1970. Theory of Elasticity 3rd Edition. McGraw-Hill, New York, pp567.
- Valliappan, S., Lee, I.K., and Boonlvahohr, P.; 1974. Finite element analysis of consolidation problem. In Finite Element Methods in Flow Problems, Ed. by J.T. Oden, Univ. of Alabama, 741-755.
- Vere-Jones, D.; 1966. A Markov model for aftershock Occurrence. Pure and Applied Geophys., 63, 31-42.
- Vere-Jones, D.; 1970. Stochastic Models for earthquake occurrence. J. Royal Stat. Soc., B21, 1-45.
- Withers, R.J., and Nyland, E.; 1976. Theory for the rapid solution of ground subsidence near reservoirs on layered and porous media. Eng. Geol., 10, 169-186.
- Yokoo, Y., Yamagata, K., and Nagaoka, H.; 1971. Variational principles for consolidation. Soils and Foundations, 11, 25-58.

Zienkiewicz, O., Mayer, P., and Cheung, Y.K.; 1966. Solution of anisotropic seepage by finite elements. Proc. ASCE, 92, 111-120.

Zienkiewicz, O.C.F.; 1971. The finite element method in engineering Science. McGraw Hill, London. pp. 521.

B30179